ISTANBUL TECHNICAL UNIVERSITY ★ INSTITUTE OF SCIENCE AND TECHNOLOGY

THE EFFECTS OF CURRENT CONVEYOR NON-IDEALITIES ON THE PERFORMANCE OF ACTIVE FILTERS AND NOVEL CURRENT CONVEYOR STRUCTURES SUITABLE FOR CONTINUOUS-TIME FILTERS

Ph.D. Thesis

Nil TARIM, M.Sc

Date of Submission : 21 August 1998

Date of Defence Examination : 22 December 1998

Supervisor (Chairman) : Prof. Dr. Hakan Kuntman

Members of the Examining Committee : Prof. Dr. Uğur Çilingiroğlu

Prof. Dr. Cevdet Acar

Prof. Dr. Atilla Ataman

Prof. Dr. Avni Morgül

DECEMBER 1998

İSTANBUL TEKNİK ÜNİVERSİTESİ ★ FEN BİLİMLERİ ENSTİTÜSÜ

AKIM TAŞIYICININ AKTİF OLMAMASININ AKTİF FİLTRELER ÜZERİNDEKİ ETKİLERİNİN İNCELENMESİ VE YENİ AKIM TAŞIYICI YAPILARININ ELDE EDİLMESİ

DOKTORA TEZİ

Y. Müh. Nil TARIM

Tezin Enstitüye Verildiği Tarih : 21 Ağustos 1998
Tezin Savunulduğu Tarih : 22 Aralık 1998

Tez Danışmanı : Prof. Dr. Hakan Kuntman
Diğer Jüri Üyeleri : Prof. Dr. Uğur Çilingiroğlu
Prof. Dr. Cevdet Acar
Prof. Dr. Atilla Ataman
Prof. Dr. Avni Morgül

ARALIK 1998

PREFACE

Hope to be a guiding light for the others...

August 1998 Nil Tarım

CONTENTS

Page No

PREFACE ii

LIST OF FIGURES v

LIST OF TABLES xiv

SUMMARY xv

ÖZET xvi

CHAPTER 1 INTRODUCTION 1

CHAPTER 2 CURRENT CONVEYOR NON-IDEALITIES 7

2.1 The Current Conveyor Macromodel 7
2.2 Behavior of Ideal and Non-Ideal Current Conveyors 8
2.3 Macromodel Development 10
2.4 Comparison with Semiconductor Device-Level Models 13
2.5 Parameter Determination 19

CHAPTER 3 STUDIES ON THE PERFORMANCE CHARACTERISTICS OF VARIOUS CURRENT CONVEYOR TOPOLOGIES 23

3.1 Performance Characteristics of Current Conveyor 1 24
3.2 Performance Characteristics of Current Conveyor 2 25
3.3 Performance Characteristics of Current Conveyor 3 30
3.4 Performance Characteristics of Current Conveyor 4 31
3.5 Performance Characteristics of Current Conveyor 5 35
3.6 Performance Characteristics of Current Conveyor 6 36
3.7 Performance Characteristics of Current Conveyor 7 38
3.8 Performance Characteristics of Current Conveyor 8 40

CHAPTER 4 THE EFFECTS OF CURRENT CONVEYOR NON-IDEALITIES ON A VOLTAGE-MODE ACTIVE FILTER 44

4.1 The Effects of Current Conveyor Non-Idealities on Filter Characteristics 45
4.1.1 The effect of r_X 48
4.1.2 The effect of Y_Z 50
4.1.3 The effect of k_I (k_V) 57
4.1.4 The effect of Y_Y 59
4.2 The Filter Performance for Various Current Conveyor Circuits 64

CHAPTER 5 THE EFFECTS OF CURRENT CONVEYOR NON-IDEALITIES ON A CURRENT-MODE ACTIVE FILTER 77

5.1 The Effects of Current Conveyor Non-Idealities on Filter Characteristics 77
5.1.1 The effect of r_X 80
5.1.2 The effect of Y_Z 82
5.1.3 The effect of k_I 84
5.1.4 The effect of k_V 88
5.1.5 The effect of Y_Y 92
5.2 The Filter Performance for Various Current Conveyor Circuits 99

CHAPTER 6 NOVEL CURRENT CONVEYOR STRUCTURES SUITABLE FOR CONTINUOUS-TIME ACTIVE FILTERS 112

6.1 Performance Characteristics of Current Conveyor 1n 112
6.2 Performance Characteristics of Current Conveyor 2n 115
6.3 Performance Characteristics of Current Conveyor 3n 117
6.4 Performance Characteristics of Current Conveyor 4n 119
6.5 Performance Characteristics of Current Conveyor 5n 124
6.6 Performance Characteristics of Current Conveyor 6n 125
6.7 The Voltage-Mode Filter Performance for the Proposed Current Conveyors 129
6.8 The Current-Mode Filter Performance for the Proposed Current Conveyors 138
6.9 Discussions on the Current Conveyor Performances 139

CHAPTER 7 CONCLUSION 149

REFERENCES 152

APPENDIX A 156

BIOGRAPHY 164

LIST OF FIGURES

Page No

Figure 2.1 a) Block diagram of the current conveyor b) The non-ideal current conveyor c) A detailed circuit of the non-ideal current conveyor d) Proposed macromodel 11

Figure 2.2 Circuit examples for CMOS realization of current conveyors a) Non-inverting type current conveyor b) Inverting type current conveyor 14

Figure 2.3 Dc transfer characteristics obtained from SPICE simulations: a) Plots of V_X against V_Y for $R_X = \infty$ b) Plots of V_Z against V_Y for $R_Z = \infty$ c) Plots of I_X against V_Y for $R_X = 0$ 16

Figure 2.4 Frequency responses of a) Voltage gains v_x / v_y and v_z / v_y b) Currents i_z and i_x 17

Figure 2.5 Frequency responses of a) the impedance of terminal x, Z_X b) the impedance of terminal y, Z_Y, c) the impedance of terminal z, Z_Z 18

Figure 2.6 An example of a second order lowpass active filter 20

Figure 2.7 a) Simulated frequency response of the filter b) Transient analysis results of the filter 20

Figure 3.1 a) Circuit diagram of current conveyor 1 b) Inverting type current conveyor derived from a) 25

Figure 3.2 Device characteristics of current conveyor 1 a) $V_X = V_X(V_Y)$ for $R_X = \infty$ b) $V_Z = V_Z(V_Y)$ for $R_Z = \infty$ c) $I_X = I_X(V_Y)$ for $R_X = 0$ d) $I_X = I_X(V_Y)$, $I_Z = I_Z(V_Y)$ for $R_X = R_Z = 1\ k\Omega$ e) The frequency responses of v_x / v_y and i_z / i_x for $R_X = R_Z = 10\ k\Omega$ f) The frequency response of Z_X g) The frequency response of Z_Y h) The frequency response of Z_Z 26

Figure 3.3 a) Circuit diagram of current conveyor 2 b) Inverting type current conveyor derived from a) 28

Figure 3.4 Device characteristics of current conveyor 2
a) $V_X = V_X(V_Y)$ for $R_X = \infty$ b) $V_Z = V_Z(V_Y)$ for $R_Z = \infty$ c) $I_X = I_X(V_Y)$ for $R_X = 0$ d) $I_X = I_X(V_Y)$, $I_Z = I_Z(V_Y)$ for $R_X = R_Z = 1$ kΩ e) The frequency responses of v_x/v_y and i_z/i_x for $R_X = R_Z = 10$ kΩ f) The frequency response of Z_X g) The frequency response of Z_Y h) The frequency response of Z_Z 29

Figure 3.5 a) Circuit diagram of current conveyor 3 b) Inverting type current conveyor derived from a) 30

Figure 3.6 Device characteristics of current conveyor 3
a) $V_X = V_X(V_Y)$ for $R_X = \infty$ b) $V_Z = V_Z(V_Y)$ for $R_Z = \infty$ c) $I_X = I_X(V_Y)$ for $R_X = 0$ d) $I_X = I_X(V_Y)$, $I_Z = I_Z(V_Y)$ for $R_X = R_Z = 1$ kΩ e) The frequency responses of v_x/v_y and i_z/i_x for $R_X = R_Z = 10$ kΩ f) The frequency response of Z_X g) The frequency response of Z_Y h) The frequency response of Z_Z 32

Figure 3.7 a) Circuit diagram of current conveyor 4 b) Inverting type current conveyor derived from a) 33

Figure 3.8 Device characteristics of current conveyor 4
a) $V_X = V_X(V_Y)$ for $R_X = \infty$ b) $V_Z = V_Z(V_Y)$ for $R_Z = \infty$ c) $I_X = I_X(V_Y)$ for $R_X = 0$ d) $I_X = I_X(V_Y)$, $I_Z = I_Z(V_Y)$ for $R_X = R_Z = 1$ kΩ e) The frequency responses of v_x/v_y and i_z/i_x for $R_X = R_Z = 10$ kΩ f) The frequency response of Z_X g) The frequency response of Z_Y h) The frequency response of Z_Z 34

Figure 3.9 Circuit diagram of current conveyor 5 36

Figure 3.10 Device characteristics of current conveyor 5
a) $V_X = V_X(V_Y)$ for $R_X = \infty$ b) $V_Z = V_Z(V_Y)$ for $R_Z = \infty$ c) $I_X = I_X(V_Y)$ for $R_X = 0$ d) $I_X = I_X(V_Y)$, $I_Z = I_Z(V_Y)$ for $R_X = R_Z = 1$k e) The frequency responses of v_x/v_y and i_z/i_x for $R_X = R_Z = 10$ kΩ f) The frequency response of Z_X g) The frequency response of Z_Y h) The frequency response of Z_Z 37

Figure 3.11 a) Circuit diagram of current conveyor 6 b) Inverting type current conveyor derived from a) 38

Figure 3.12 Device characteristics of current conveyor 6
a) $V_X = V_X(V_Y)$ for $R_X = \infty$ b) $V_Z = V_Z(V_Y)$ for $R_Z = \infty$ c) $I_X = I_X(V_Y)$ for $R_X = 0$ d) $I_X = I_X(V_Y)$, $I_Z = I_Z(V_Y)$ for $R_X = R_Z = 1$ kΩ e) The frequency responses of v_x/v_y and i_z/i_x for $R_X = R_Z = 10$ kΩ f) The frequency response of Z_X g) The frequency response of Z_Y h) The frequency response of Z_Z 39

Figure 3.13 Circuit diagram of current conveyor 7 40

Figure 3.14 Device characteristics of current conveyor 7 a) $V_X = V_X(V_Y)$ for $R_X = \infty$ b) $V_Z = V_Z(V_Y)$ for $R_Z = \infty$ c) $I_X = I_X(V_Y)$ for $R_X = 0$ d) $I_X = I_X(V_Y)$, $I_Z = I_Z(V_Y)$ for $R_X = R_Z = 10$ kΩ e) The frequency responses of v_x/v_y and i_z/i_x for $R_X = R_Z = 10$ kΩ f) The frequency response of Z_X g) The frequency response of Z_Y h) The frequency response of Z_Z 41

Figure 3.15 a) Circuit diagram of current conveyor 8 b) Inverting type current conveyor derived from a) 42

Figure 3.16 Device characteristics of current conveyor 8 a) $V_X = V_X(V_Y)$ for $R_X = \infty$ b) $V_Z = V_Z(V_Y)$ for $R_Z = \infty$ c) $I_X = I_X(V_Y)$ for $R_X = 0$ d) $I_X = I_X(V_Y)$, $I_Z = I_Z(V_Y)$ for $R_X = R_Z = 1$ kΩ e) The frequency responses of v_x/v_y and i_z/i_x for $R_X = R_Z = 10$ kΩ f) The frequency response of Z_X g) The frequency response of Z_Y h) The frequency response of Z_Z 43

Figure 4.1 A voltage-mode biquadratic filter configuration 45

Figure 4.2 The effect of r_X on filter characteristics a) Bandpass filter of $f_O = 10$ kHz b) Bandpass filter of $f_O = 10$ MHz c) Lowpass filter of $f_O = 10$ kHz d) Lowpass filter of $f_O = 10$ MHz e) Highpass filter of $f_O = 10$ kHz f) Highpass filter of $f_O = 10$ MHz 51

Figure 4.3 The effect of r_Z and C_Z on the bandpass filter characteristics a) and b) $f_O = 10$ kHz c) and d) $f_O = 100$ kHz e) and f) $f_O = 1$ MHz g) and h) $f_O = 10$ MHz 54

Figure 4.4 The effect of r_Z and C_Z on the lowpass filter characteristics a) and b) $f_O = 10$ kHz c) and d) $f_O = 100$ kHz e) and f) $f_O = 1$ MHz g) and h) $f_O = 10$ MHz 55

Figure 4.5 The effect of r_Z and C_Z on the highpass filter characteristics a) and b) $f_O = 10$ kHz c) and d) $f_O = 100$ kHz e) and f) $f_O = 1$ MHz g) and h) $f_O = 10$ MHz 56

Figure 4.6 The effect of k_I (k_V) on the filter characteristics 60

Figure 4.7 The effect of r_Y and C_Y on the bandpass filter characteristics a) and b) $f_O = 10$ kHz c) and d) $f_O = 100$ kHz e) and f) $f_O = 1$ MHz g) and h) $f_O = 10$ MHz 61

Figure 4.8 The effect of r_Y and C_Y on the lowpass filter characteristics a) and b) $f_O = 10$ kHz c) and d) $f_O = 100$ kHz e) and f) $f_O = 1$ MHz g) and h) $f_O = 10$ MHz 62

Figure 4.9 The effect of r_Y and C_Y on the highpass filter characteristics a) and b) f_O =10 kHz c) and d) f_O =100 kHz e) and f) f_O =1 MHz g) and h) f_O =10 MHz 63

Figure 4.10 The bandpass filter performance for CC1-CC4 at four different resonant frequencies of a) and e) f_O = 10 kHz b) and f) f_O = 100 kHz c) and g) f_O = 1 MHz d) and h) f_O = 10 MHz 68

Figure 4.11 The bandpass filter performance for CC5-CC8 at four different resonant frequencies of a) and e) f_O = 10 kHz b) and f) f_O = 100 kHz c) and g) f_O = 1 MHz d) and h) f_O = 10 MHz 69

Figure 4.12 The lowpass filter performance for CC1-CC4 at four different cutoff frequencies of a) and e) f_O = 10 kHz b) and f) f_O = 100 kHz c) and g) f_O = 1 MHz d) and h) f_O = 10 MHz 70

Figure 4.13 The lowpass filter performance for CC5-CC8 at four different cutoff frequencies of a) and e) f_O = 10 kHz b) and f) f_O = 100 kHz c) and g) f_O = 1 MHz d) and h) f_O = 10 MHz 71

Figure 4.14 The highpass filter performance for CC1-CC4 at four different cutoff frequencies of a) and e) f_O = 10 kHz b) and f) f_O = 100 kHz c) and g) f_O = 1 MHz d) and h) f_O = 10 MHz 72

Figure 4.15 The highpass filter performance for CC5-CC8 at four different cutoff frequencies of a) and e) f_O = 10 kHz b) and f) f_O = 100 kHz c) and g) f_O = 1 MHz d) and h) f_O = 10 MHz 73

Figure 4.16 The large-signal behavior of the bandpass filter for various current conveyors a) CC1 b) CC2 c) CC4 d) CC5 e) CC6 f) CC7 g) CC8 74

Figure 4.17 The large-signal behavior of the lowpass filter for various current conveyors a) CC1 b) CC2 c) CC4 d) CC5 e) CC6 f) CC7 g) CC8 75

Figure 4.18 The large-signal behavior of the highpass filter for various current conveyors a) CC1 b) CC2 c) CC4 d) CC5 e) CC6 f) CC7 g) CC8 76

Figure 5.1 Current-mode filter configurations a) The circuit configuration for realizing a bandpass filter transfer function b) The circuit configuration for realizing highpass and lowpass filter transfer functions 79

Figure 5.2 The effect of r_X on filter characteristics a) Bandpass filter of f_O =10 kHz b) Bandpass filter of f_O =10 MHz c) Lowpass filter of f_O =10 kHz d) Lowpass filter of f_O =10 MHz e) Highpass filter of f_O =10 kHz f) Highpass filter of f_O =10 MHz 83

Figure 5.3 The effect of r_Z and C_Z on the bandpass filter characteristics a) and b) f_O =10 kHz c) and d) f_O =100 kHz e) and f) f_O =1 MHz g) and h) f_O =10 MHz 85

Figure 5.4 The effect of r_Z and C_Z on the lowpass filter characteristics a) and b) f_O =10 kHz c) and d) f_O =100 kHz e) and f) f_O =1 MHz g) and h) f_O =10 MHz 86

Figure 5.5 The effect of r_Z and C_Z on the highpass filter characteristics a) and b) f_O =10 kHz c) and d) f_O =100 kHz e) and f) f_O =1 MHz g) and h) f_O =10 MHz 87

Figure 5.6 The effect of k_I on the filter characteristics 90

Figure 5.7 The effect of k_V on the filter characteristics 93

Figure 5.8 The effect of r_Y and C_Y on the bandpass filter characteristics a) and b) f_O =10 kHz c) and d) f_O =100 kHz e) and f) f_O =1 MHz g) and h) f_O =10 MHz 96

Figure 5.9 The effect of r_Y and C_Y on the lowpass filter characteristics a) and b) f_O =10 kHz c) and d) f_O =100 kHz e) and f) f_O =1 MHz g) and h) f_O =10 MHz 97

Figure 5.10 The effect of r_Y and C_Y on the highpass filter characteristics a) and b) f_O =10 kHz c) and d) f_O =100 kHz e) and f) f_O =1 MHz g) and h) f_O =10 MHz 98

Figure 5.11 The bandpass filter performance for CC1-CC4 at four different resonant frequencies of a) and e) f_O = 10 kHz b) and f) f_O = 100 kHz c) and g) f_O = 1 MHz d) and h) f_O = 10 MHz 103

Figure 5.12 The bandpass filter performance for CC5-CC8 at four different resonant frequencies of a) and e) f_O = 10 kHz b) and f) f_O = 100 kHz c) and g) f_O = 1 MHz d) and h) f_O = 10 MHz 104

Figure 5.13 The lowpass filter performance for CC1-CC4 at four different cutoff frequencies of a) and e) f_O = 10 kHz b) and f) f_O = 100 kHz c) and g) f_O = 1 MHz d) and h) f_O = 10 MHz 105

Figure 5.14 The lowpass filter performance for CC5-CC8 at four different cutoff frequencies of a) and e) f_O = 10 kHz b) and f) f_O = 100 kHz c) and g) f_O = 1 MHz d) and h) f_O = 10 MHz 106

Figure 5.15 The highpass filter performance for CC1-CC4 at four different cutoff frequencies of a) and e) $f_O = 10$ kHz b) and f) $f_O = 100$ kHz c) and g) $f_O = 1$ MHz d) and h) $f_O = 10$ MHz 107

Figure 5.16 The highpass filter performance for CC5-CC8 at four different cutoff frequencies of a) and e) $f_O = 10$ kHz b) and f) $f_O = 100$ kHz c) and g) $f_O = 1$ MHz d) and h) $f_O = 10$ MHz 108

Figure 5.17 The large-signal behavior of the bandpass filter for various current conveyors a) CC1 b) CC2 c) CC3 d) CC4 e) CC5 f) CC6 g) CC7 h) CC8 109

Figure 5.18 The large-signal behavior of the lowpass filter for various current conveyors a) CC1 b) CC2 c) CC3 d) CC4 e) CC5 f) CC6 g) CC7 h) CC8 110

Figure 5.19 The large-signal behavior of the highpass filter for various current conveyors a) CC1 b) CC2 c) CC3 d) CC4 e) CC5 f) CC6 g) CC7 h) CC8 111

Figure 6.1 a) Circuit diagram of current conveyor 1n b) Two-output mirror based on the modified Wilson current mirror 113

Figure 6.2 Device characteristics of current conveyor 1n a) $V_X = V_X(V_Y)$ for $R_X = \infty$ b) $V_Z = V_Z(V_Y)$ for $R_Z = \infty$ c) $I_X = I_X(V_Y)$ for $R_X = 0$ d) $I_X = I_X(V_Y)$, $I_Z = I_Z(V_Y)$ for $R_X = R_Z = 10$ kΩ e) The frequency responses of v_x/v_y and i_z/i_x for $R_X = R_Z = 10$ kΩ f) The frequency response of Z_X g) The frequency response of Z_Y h) The frequency response of Z_Z 114

Figure 6.3 Circuit diagram of current conveyor 2n 117

Figure 6.4 Device characteristics of current conveyor 2n a) $V_X = V_X(V_Y)$ for $R_X = \infty$ b) $V_Z = V_Z(V_Y)$ for $R_Z = \infty$ c) $I_X = I_X(V_Y)$ for $R_X = 0$ d) $I_X = I_X(V_Y)$, $I_Z = I_Z(V_Y)$ for $R_X = R_Z = 10$ kΩ e) The frequency responses of v_x/v_y and i_z/i_x for $R_X = R_Z = 10$ kΩ f) The frequency response of Z_X g) The frequency response of Z_Y h) The frequency response of Z_Z 118

Figure 6.5 Circuit diagram of current conveyor 3n 119

Figure 6.6 Device characteristics of current conveyor 3n
a) $V_X = V_X(V_Y)$ for $R_X = \infty$ b) $V_Z = V_Z(V_Y)$ for $R_Z = \infty$ c) $I_X = I_X(V_Y)$ for $R_X = 0$ d) $I_X = I_X(V_Y)$, $I_Z = I_Z(V_Y)$ for $R_X = R_Z = 1$ kΩ e) The frequency responses of v_x/v_y and i_z/i_x for $R_X = R_Z = 10$ kΩ f) The frequency response of Z_X g) The frequency response of Z_Y h) The frequency response of Z_Z 120

Figure 6.7 a) Circuit diagram of current conveyor 4n b) Inverting type current conveyor derived from a) 121

Figure 6.8 Circuit diagram of operational amplifier 1 121

Figure 6.9 Device characteristics of operational amplifier 1
a) Dc voltage transfer characteristic b) The unity gain frequency response of the output voltage 122

Figure 6.10 Device characteristics of current conveyor 4n
a) $V_X = V_X(V_Y)$ for $R_X = \infty$ b) $V_Z = V_Z(V_Y)$ for $R_Z = \infty$ c) $I_X = I_X(V_Y)$ for $R_X = 0$ d) $I_X = I_X(V_Y)$, $I_Z = I_Z(V_Y)$ for $R_X = R_Z = 1$ kΩ e) The frequency responses of v_x/v_y and i_z/i_x for $R_X = R_Z = 10$ kΩ f) The frequency response of Z_X g) The frequency response of Z_Y h) The frequency response of Z_Z 123

Figure 6.11 a) Circuit diagram of current conveyor 5n b) Inverting type current conveyor derived from a) 124

Figure 6.12 Device characteristics of current conveyor 5n
a) $V_X = V_X(V_Y)$ for $R_X = \infty$ b) $V_Z = V_Z(V_Y)$ for $R_Z = \infty$ c) $I_X = I_X(V_Y)$ for $R_X = 0$ d) $I_X = I_X(V_Y)$, $I_Z = I_Z(V_Y)$ for $R_X = R_Z = 10$ kΩ e) The frequency responses of v_x/v_y and i_z/i_x for $R_X = R_Z = 10$ kΩ f) The frequency response of Z_X g) The frequency response of Z_Y h) The frequency response of Z_Z 126

Figure 6.13 a) Circuit diagram of current conveyor 6n b) Inverting type current conveyor derived from a) 127

Figure 6.14 Device characteristics of current conveyor 6n
a) $V_X = V_X(V_Y)$ for $R_X = \infty$ b) $V_Z = V_Z(V_Y)$ for $R_Z = \infty$ c) $I_X = I_X(V_Y)$ for $R_X = 0$ d) $I_X = I_X(V_Y)$, $I_Z = I_Z(V_Y)$ for $R_X = R_Z = 1$ kΩ e) The frequency responses of v_x/v_y and i_z/i_x for $R_X = R_Z = 10$ kΩ f) The frequency response of Z_X g) The frequency response of Z_Y h) The frequency response of Z_Z 128

Figure 6.15 The voltage-mode bandpass filter performance for CC1N-CC4N at four different resonant frequencies of a) and e) f_O = 10 kHz b) and f) f_O = 100 kHz c) and g) f_O = 1 MHz d) and h) f_O = 10 MHz 130

Figure 6.16 The voltage-mode bandpass filter performance for CC5N-CC6N at four different resonant frequencies of a) and e) f_O = 10 kHz b) and f) f_O = 100 kHz c) and g) f_O = 1 MHz d) and h) f_O = 10 MHz 131

Figure 6.17 The voltage-mode lowpass filter performance for CC1N-CC4N at four different resonant frequencies of a) and e) f_O = 10 kHz b) and f) f_O = 100 kHz c) and g) f_O = 1 MHz d) and h) f_O = 10 MHz 132

Figure 6.18 The voltage-mode lowpass filter performance for CC5N-CC6N at four different resonant frequencies of a) and e) f_O = 10 kHz b) and f) f_O = 100 kHz c) and g) f_O = 1 MHz d) and h) f_O = 10 MHz 133

Figure 6.19 The voltage-mode highpass filter performance for CC1N-CC4N at four different resonant frequencies of a) and e) f_O = 10 kHz b) and f) f_O = 100 kHz c) and g) f_O = 1 MHz d) and h) f_O = 10 MHz 134

Figure 6.20 The voltage-mode highpass filter performance for CC5N-CC6N at four different resonant frequencies of a) and e) f_O = 10 kHz b) and f) f_O = 100 kHz c) and g) f_O = 1 MHz d) and h) f_O = 10 MHz 135

Figure 6.21 The large-signal behavior of the bandpass and lowpass filters for various current conveyors a) BP-CC2N b) BP-CC3N c) BP-CC4N d) BP-CC5N e) LP-CC2N f) LP-CC3N g) LP-CC4N 136

Figure 6.22 The large-signal behavior of the highpass filter for various current conveyors a) CC2N b) CC3N c) CC4N d) CC5N 137

Figure 6.23 The current-mode bandpass filter performance for CC1N-CC4N at four different resonant frequencies of a) and e) f_O = 10 kHz b) and f) f_O = 100 kHz c) and g) f_O = 1 MHz d) and h) f_O = 10 MHz 140

Figure 6.24 The current-mode bandpass filter performance for CC5N-CC6N at four different resonant frequencies of a) and e) f_O = 10 kHz b) and f) f_O = 100 kHz c) and g) f_O = 1 MHz d) and h) f_O = 10 MHz 141

Figure 6.25 The current-mode lowpass filter performance for CC1N-CC4N at four different resonant frequencies of a) and e) f_O = 10 kHz b) and f) f_O = 100 kHz c) and g) f_O = 1 MHz d) and h) f_O = 10 MHz 142

Figure 6.26 The current-mode lowpass filter performance for CC5N-CC6N at four different resonant frequencies of a) and e) f_O = 10 kHz b) and f) f_O = 100 kHz c) and g) f_O = 1 MHz d) and h) f_O = 10 MHz 143

Figure 6.27 The current-mode highpass filter performance for CC1N-CC4N at four different resonant frequencies of a) and e) f_O = 10 kHz b) and f) f_O = 100 kHz c) and g) f_O = 1 MHz d) and h) f_O = 10 MHz 144

Figure 6.28 The current-mode highpass filter performance for CC5N-CC6N at four different resonant frequencies of a) and e) f_O = 10 kHz b) and f) f_O = 100 kHz c) and g) f_O = 1 MHz d) and h) f_O = 10 MHz 145

Figure 6.29 The large-signal behavior of the bandpass filter for various current conveyors a) CC1N b) CC2N c) CC3N d) CC4N e) CC5N f) CC6N 146

Figure 6.30 The large-signal behavior of the lowpass filter for various current conveyors a) CC1N b) CC2N c) CC3N d) CC4N e) CC5N f) CC6N 147

Figure 6.31 The large-signal behavior of the highpass filter for various current conveyors a) CC1N b) CC2N c) CC3N d) CC4N e) CC5N f) CC6N 148

LIST OF TABLES

Page No

Table 2.1 Macromodel parameters (* for inverting current conveyor $k_I = -1$) 14

Table 2.2 Computer times in seconds needed for SPICE simulations 22

Table 2.3 Equations to calculate the macromodel parameters 22

Table 3.1 Characteristic values of various current conveyors 27

Table 4.1 Limits of non-ideality terms for a deviation of 10% in filter parameters 59

Table 4.2 The maximum input signal amplitude for various current conveyors 67

Table 5.1 Limits of non-ideality terms for a deviation of 10% in filter parameters 99

Table 5.2 The maximum input signal amplitude for various current conveyors 102

Table 6.1 Characteristic values of the proposed current conveyors 116

Table 6.2 Characteristic values of operational amplifiers OA1 and OA2 122

Table 6.3 The maximum input signal amplitude for example current conveyors 129

Table 6.4 The maximum input signal amplitude for example current conveyors 138

SUMMARY

The current conveyor is one of the most versatile active elements which can potentially provide the high accuracy, wide bandwidth, low input impedance and high output impedance characteristics needed for many current domain signal processing applications. Since its first proposal in 1968 and its reformulation named as the second generation current conveyor in 1970 this circuit element continues to receive a great deal of attention and find numerous applications. This growing interest to current-mode approach, has led us to focus on this basic building block of current-mode design, and its widely used application of active filters. In active filters, the performance of the active element plays an important role in the overall performance of the filter, besides the filter configuration itself. It is obvious that the non-idealities of the current conveyor will result in deviations in filter parameters such as the cutoff frequency, quality factor and filter gain. Therefore the derivation of analytical expressions for the deviations in the filter parameters in terms of current conveyor non-idealities may be of vital importance. This will enable one to realize the effect of each non-ideality term on the filter parameters and help design or choose a suitable current conveyor configuration for a specified filter performance.

After an introduction in Chapter 1, Chapter 2 starts with a complete macromodel, which fully represents both the small and large-signal behavior of the current conveyor, which is especially suitable for the simulation of active filter applications. Results show that the simple and yet accurate model provides a relative amount of simulation speedup. The studies made on eight current conveyor configurations found in literature are given in Chapter 3. Both bipolar and MOS structures, as well as one of the commercially available current conveyors, namely the AD844 circuit has been covered and compared results of the current conveyor performance characteristics are given. In Chapter 4 and 5, provided that a certain filter configuration is given, we will investigate the effects of current conveyor non-idealities on both voltage and current-mode active filter examples, and derive analytical expressions for the filter parameter deviations in terms of non-ideality terms. We will determine the requirements for the current conveyor non-ideality terms in order to obtain a specified filter performance. The filter configurations chosen, actually represent certain classes of active filters, which enables us to generalize the results obtained. A comparable demonstration of the filter transfer function and large-signal behavior for each current conveyor will be given. Simulations including three types of filters, namely, the bandpass, lowpass and highpass filters, confirm the analytical expressions obtained. In Chapter 6, current conveyors suitable for continuous-time filter applications will be proposed, taking the results obtained previously under consideration. Performance characteristics of the current conveyors and comparable demonstration of the voltage and current-mode filter performances will be given. The results show that acceptable performance has been obtained for the filters.

ÖZET

AKIM TAŞIYICININ İDEAL OLMAMASININ AKTİF FİLTRELER ÜZERİNDEKİ ETKİLERİNİN İNCELENMESİ VE YENİ AKIM TAŞIYICI YAPILARININ ELDE EDİLMESİ

709, ayrık elemanların performansını yakalayabilen ilk monolitik kuvvetlendirici devresi olarak ortaya çıktı. LM 101 tümdevresi bundan sonraki ilk kayda değer aşamadır. Genel olarak 709 ile aynı özelliklere sahip olup bazı uygulama sorunlarını ortadan kaldırmıştır. İşlemsel kuvvetlendiricinin tümdevre olarak ortaya çıkması ve kabul görmesi sonucu 1960'lı yıllar boyunca lineer analog tümdevre uygulamaları büyük bir ilerleme kaydetmiştir. Bunun sonucu olarak, ayrık benzerleri kadar, hatta daha iyi performanslı tümdevre işlemsel kuvvetlendirici tasarımları, daha ekonomik fiyatlarla ortaya çıkmıştır. Maliyet, 1965'te 70$'dan 1970'te 2$'dan daha az bir rakama inmiştir. O zamandan beri, işlemsel kuvvetlendirici tümdevreleri, piyasada üretilen ürünler içerisinde en fazla kullanılan lineer elemanlar olmuşlardır. Analog/sayısal ve sayısal/analog çeviriciler, gerilim referans kaynakları, analog çarpma devreleri, dalga şekillendirici devreler, osilatörler ve dalga üreteçleri gibi pek çok alanda uygulama imkanı bulmuşlardır. İşaret işlemenin gerilim değişkenleri aracılığıyla düşünülmesi alışkanlığının sonucu olarak, gerilim kuvvetlendiricileri, gerilim integratörleri, gerilim transfer fonksiyonu gerçekleyen filtreler gibi gerilim modlu işaret işleme devreleri ortaya çıkmıştır. Bugün, yüksek kaliteli işlemsel kuvvetlendirici devreleri 0.1$ mertebelerinde maliyete sahiptir. Bunun sonucu olarak, yapısından kaynaklanan yükselme eğimi - kazanç bant genişliği ikilemine rağmen, kullanışlı olması, işlemsel kuvvetlendiriciyi gerilim modlu tasarımların vazgeçilmez elemanlarından birisi yapmıştır.

Aynı dönemlerde, bu gelişmelere paralel olarak tümdevre tasarımında da önemli aşamalar kaydedilmiştir. İşlemsel kuvvetlendiricinin ortaya çıkıp yaygın bir hal almaya başladığı dönemlerde, analog devre tasarımı, çoğunlukla bipolar ve hibrit teknolojileriyle gerçekleştirilmekteydi. 1980'lerin başlarında NMOS teknolojisi ortaya çıktı; ancak eşlenik elemanların olmaması, CMOS teknolojisini, sayısal olduğu kadar analog tasarımlar için de temel üretim teknolojisi haline getirdi. Son on yılda, tasarımcıya bipolar ve MOS teknolojilerinin avantajlarını birleştirme olanağı sağlayan BiCMOS teknolojisi ortaya çıkmıştır. Bu şekilde, bugünün yüksek performanslı, çok geniş ölçekli tümleştirilmiş, analog ve sayısal devre tasarımları mümkün hale gelebilmektedir. Öte yandan, henüz nispeten pahalı ve

az rastlanılır olmasına rağmen GaAs teknolojisi, bazı ticari olmayan tasarımlarda kullanılmaktadır.

Son dönemde, elektronik devre tasarımı, yüksek performanslı işlemsel kuvvetlendiricilere her zamankinden daha çok ihtiyaç duymuştur. Bazı alışılmadık yöntemlerle elemanın çalışma frekansının yükseltilmesi amacı doğrultusunda çalışmalar yapılmıştır. Bu arada, işaretlerin işlendikleri ortamın empedans seviyesinin, yeni ortaya çıkan teknolojilerin olanaklarından hakkıyla yararlanabilmek açısından önem taşıdığı fark edilmiştir. Ayrıca, bugünün en yaygın teknolojisi olan CMOS teknolojisi, mikronaltı boyutlara inmekte ve 3.3 V ve 1.8 V standartlarının ortaya çıkmalarında görüldüğü gibi düşük besleme gerilimlerine eğilim göstermektedir. Bu faktörler, yüksek lineerlikte ve geniş dinamik aralıklı gerilim modlu devrelerin tasarımını zorlaştırdığından, gerilim yerine akımın temel işaret ortamı olduğu düşük empedanslı analog devreler dikkat çekmeye başlamışlardır. Bu tür akım modlu devreler, düşük empedanslı düğümlerdeki düşük gerilim salınımları nedeniyle, düşük besleme gerilimlerinde çalışabilmektedirler. Bu sayede, küçük işaret geçiş frekansına yakın geniş bantlı frekans cevapları elde edilebilmektedir.

Bütün bu gelişmelerin doğal sonucu olarak, gerilim modlu devrelerin temel elemanı olan işlemsel kuvvetlendirici yerine akım modlu devrelere ait bir temel işlem bloğu ihtiyacı ortaya çıkmaktadır. Buna yönelik çalışmalar yirmi yıldır sürmektedir. Ses bandının üzerindeki frekanslarda çalışan tümdevre aktif RC filtrelerin tasarımına yönelik çalışmalar, önceleri ilgiyi işlemsel geçiş kuvvetlendiricisine yöneltmiştir. İşlemsel kuvvetlendirici giriş katının çekirdeğini oluşturduğu bu eleman, bir gerilim kontrollü akım kaynağı olarak düşünülebilir. Daha sonraki dönemlerde en önemli rakiplerden akım geribeslemeli kuvvetlendirici ve akım taşıyıcı ortaya çıkmış ve tümdevre olarak piyasaya sürülmüşlerdir. Bugünün aktif elemanları, kuvvetlendirmeyi sağlamak üzere empedans dönüşümü yaparak işareti ileten, kontrollü çıkış akımına sahip geçiş iletkenliği elemanları olarak düşünülebilir. Bunun sonucu olarak, pek çok işaret işleme dalında, gerilim modlu devreler yerlerini akım modlu tasarımlara bırakmaktadırlar. Dinamik akım aynaları, analog/sayısal çeviriciler, anahtarlamalı MOS işaret işleme devreleri, analog hesaplama ve nöral devreler, şu anda uygulama alanı buldukları tasarım örneklerinden sadece bazılarıdır. Yüksek hızlı GaAs devrelerdeki son gelişmeler, akım modlu devrelerin uygulama alanlarını mikrodalga ve optik haberleşmeye kadar genişletmiştir. Görünen o ki, monolitik işlemsel kuvvetlendirici elemanı yeni ve gelişmiş şekillerde ortaya çıkmaya devam edecektir.

Bu yeni yapılar arasında akım taşıyıcı, potansiyel olarak pek çok akım modlu işaret işleme uygulamasının gerektirdiği yüksek doğruluk ve bant genişliği, düşük giriş empedansı ve yüksek çıkış empedansı karakteristiklerini sağlayacak yetenektedir. 1968'de ilk ortaya atılması ve 1970'te yeniden formüle edilerek ikinci kuşak akım taşıyıcı olarak adlandırılmasından beri bu eleman oldukça dikkat çekmiş ve sayısız uygulamada rol almıştır. İşlemsel esneklik ve basitliği nedeniyle akım taşıyıcıyı akım modlu devrelerin temel işlem bloğu olarak düşünmek yerinde olur. Oysa yüksek performanslı devre örnekleri sadece son on yılda ortaya çıkmış ve akım taşıyıcıların; aktif filtreler, kuvvetlendiriciler, osilatörler ve imitans simulatörleri gibi klasik işlemsel kuvvetlendirici uygulamalarında bu elemana meydan okumasına olanak sağlamışlardır.

Akım modlu devrelere gösterilen bu ilginin bir sonucu olarak bu çalışmada, akım taşıyıcı elemanı ve en çok uygulama alanı bulduğu alanlardan biri olan aktif filtreler ele alınmıştır. Aktif filtreler, adından da anlaşılacağı üzere yapısında aktif eleman bulunduran devrelerdir. Tipik olarak, böyle bir filtrede aktif eleman, indüktans elemanının işlevini görmek üzere devreye konur. İndüktans elemanının yokluğu, frekans seçici devrelerin tasarımında önemli bir eksikliktir. Pek çok uygulamada bu eksiklik, geleneksel aktif RC filtre tasarım teknikleri kullanılarak giderilebilir. İndüktans elemanına gereksinim göstermeyecek şekilde frekans seçici devre tasarlamak amacıyla direnç, kondansatör ve lineer geribesleme çevrimleri içinde kazanç blokları kullanılır.

İlk ortaya çıkışlarından itibaren aktif filtreler çeşitli derecelere varan oranlarda tümleştirilmişlerdir. Son yıllarda, çok yüksek kaliteli ve tamamen tümleştirilmiş aktif filtreler tasarlanmasına olanak sağlayan mikroelektronik teknolojileri, filtre mimarileri ve tasarım teknikleri ortaya çıkmıştır. Bu gelişmeler sonucunda, önemli alt bloklardan birini aktif filtrelerin oluşturduğu, tek kırmık üzerinde hem analog hem sayısal sistemlerin bulunduğu devreler tasarlanabilmiştir. Bilgi tanıma ve ses/veri iletimi, bu tür filtrelere en fazla gereksinim gösteren uygulama alanlarıdır. Çoğu tümleştirilmiş filtre, düşük güç harcaması, analog ve sayısal işlem bloklarını beraber aynı kırmıkta bulundurabilme ve ideale yakın kondansatör ve analog anahtar elemanı oluşturabilme özelliklerine sahip CMOS teknolojisiyle gerçekleştirilmektedir. Özellikle yüksek frekanslarda çalışan sürekli zaman filtreleri, bipolar ve CMOS teknolojileri kullanılarak tasarlanmaktadırlar.

Bu çalışmada aktif eleman olarak akım taşıyıcıyı kullanan aktif filtreler ele alınmıştır. İyi bir filtre performansının sağlanabilmesi için, iyi tasarlanmış bir filtre yapısının yanısıra, kullanılacak akım taşıyıcı da önemli bir rol oynar. İdeale yakın eleman karakteristikleri, belirli bir filtre yapısından en iyi performansın alınmasını sağlar. Açıktır ki, akım taşıyıcının ideal olmaması; filtre kesim frekansı, kalite faktörü ve filtre kazancı gibi filtre parametrelerinde ideal değerlerden sapmalar oluşturacak ve filtre karakteristiklerini etkileyecektir. Bu nedenle, filtre parametrelerindeki bağıl değişimlerin akım taşıyıcıyı karakterize eden büyüklüklere bağlı olarak incelenmesi ve gerekirse analitik bağıntıların çıkarılması önemlidir. Bu şekilde, filtre parametrelerinin hangi akım taşıyıcı karakteristik değerlerine ne şekilde bağlı olduğu bulunabilir ve öngörülecek herhangi bir filtre performansını sağlamak üzere tasarlanacak ya da seçilecek akım taşıyıcının hangi özellikleri sağlaması gerektiği belirlenebilir.

Doğaldır ki, herhangi bir eleman üzerinde ve onun kullanımına dayalı olarak yapılacak çalışmalar, o elemanın davranışına mümkün olan en iyi ölçüde hakim olmayı gerektirir. Hem bu amaca yönelik olarak hem de yapılacak bazı simülasyonların yapılmasına getireceği kolaylık açısından, çalışmaya, akım taşıyıcının hem lineer hem de lineer olmayan davranışını modelleyen bir makromodel geliştirilerek başlanmıştır. Şekil 1'de görülen model, özellikle aktif filtrelerin simülasyonunda büyük kolaylıklar sağlamakta, analizler oldukça yakın doğrulukla çok daha kısa sürede tamamlanabilmektedir.

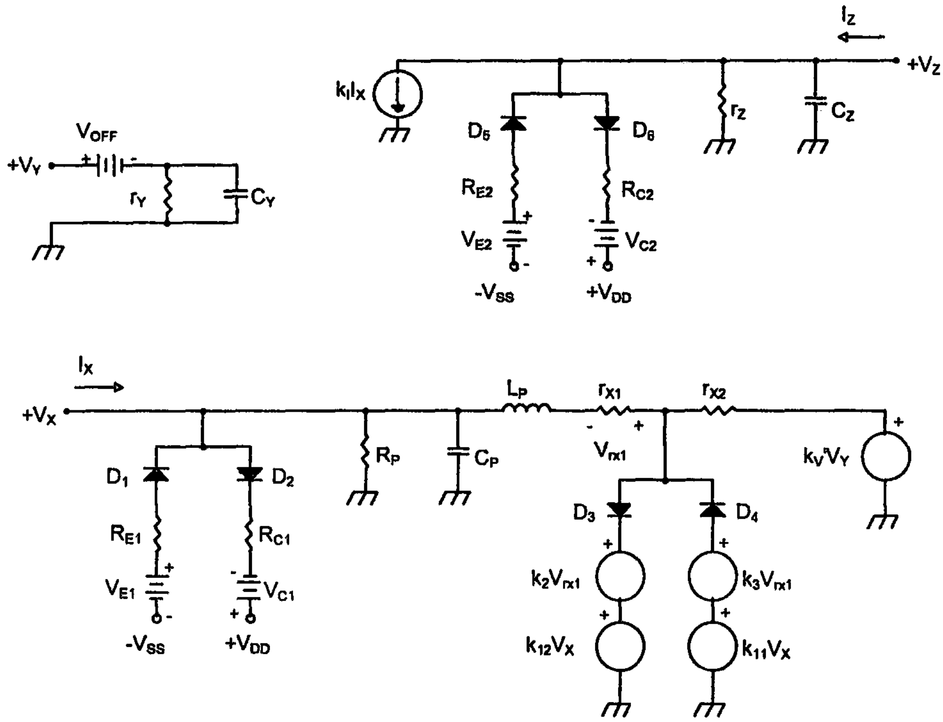

Şekil 1 Akım taşıyıcı için önerilen makromodel

Yapılan çalışmada, literatürde bulunan devreler arasından sekiz tanesi seçilerek eleman karakterizasyonları yapılmıştır. Bu şekilde hem akım taşıyıcının yakından tanınması amaçlanmış hem de çeşitli devrelerin performanslarının karşılaştırılması olanağı sağlanmıştır.

Akım taşıyıcının ideal olmamasının filtre parametreleri ve karakteristikleri üzerindeki etkilerini incelemek üzere gerilim ve akım transfer fonksiyonu sağlayan iki adet filtre yapısı seçilmiştir. Bu devreler Şekil 2 ve 3'te verilmiştir. Ancak bu seçim yapılırken, bu devrelerin belli grup filtre yapılarını temsil etmelerine dikkat edilmiş, böylece elde edilecek sonuçların bu özellikteki tüm filtrelere uygulanabilir olması sağlanmıştır. Her iki filtre devresi için, akım taşıyıcıyı karakterize eden büyüklüklerin tek başlarına filtre transfer fonksiyonlarına nasıl etki ettikleri ve yeni durumdaki filtre parametre değerleri analitik olarak çıkarılmıştır. Yapılan analizler; bant geçiren, alçak geçiren ve yüksek geçiren olmak üzere üç türde filtre yapısını kapsamış ve filtre parametrelerinde önceden öngörülen bağıl değişimlerin sağlanabilmesi için akım taşıyıcıyı karakterize eden büyüklüklerin sağlaması gereken koşullar çıkarılmıştır. Çalışmada, akım taşıyıcıyı karakterize eden büyüklükler olarak; x ucundan görülen direnç, y ve z noktalarındaki empedanslar ve akım ile gerilim transfer oranları seçilmiştir. Bütün bu büyüklükler en genel halde frekansa bağlı olup analizlerde bu durum dikkate alınmıştır.

Analitik bağıntıların elde edilmesinden sonra, elde edilen sonuçların doğrulanması ve performansların sergilenmesi açısından, daha önce incelenen sekiz akım taşıyıcı devresi için filtrelerin transfer fonksiyonları ve büyük işaret davranışları elde edilmiştir. Bu şekilde, belli özellikteki akım taşıyıcıların hangi tür ve hangi modda çalışan filtreleri ne şekilde etkiledikleri gözlemlenmiştir.

Bütün bu incelemeler doğrultusunda, yapılan çalışmanın son aşamasını, elde edilen sonuçları dikkate alan yeni akım taşıyıcı yapılarının önerilmesi oluşturmuştur. Bu yapıların eleman karakteristikleri çıkarılmış ve daha önce incelenen iki filtrenin üç türü üzerindeki performansları incelenmiştir. Elde edilen sonuçlar, bu yapıların aktif filtre uygulamalarında kullanılmalarının uygunluğunu doğrulamaktadır.

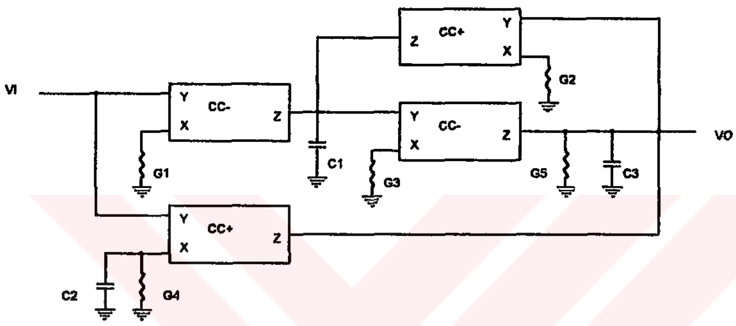

Şekil 2 Gerilim modunda çalışan filtre yapısı

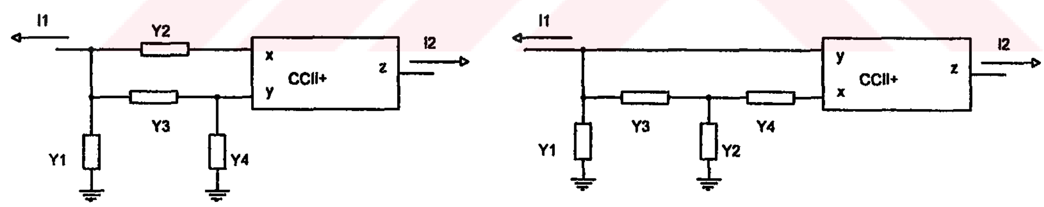

a) b)

Şekil 3 Akım modunda çalışan filtre yapısı
a) Bant geçiren filtre yapısı b) Yüksek ve alçak geçiren filtre yapısı

CHAPTER 1

INTRODUCTION

The 709 was the first monolithic operational amplifier circuit which approached discrete designs in general performance and usefulness [1]. The LM101, announced in 1967, was the next major advance in monolithic amplifiers [2]. It had essentially the same specifications as the 709, but eliminated most of the application problems. The late 1960s experienced a tremendous growth in the application of linear analog integrated circuits, due largely to the development and acceptance of the integrated operational amplifier. This gave boost to many operational amplifier designs providing circuit performance as good as, or even better than, discrete component realizations, at a cost lower than that of individual components. Prices dropped from $70 in 1965 to less than $2 in 1970. Since then, the integrated circuit operational amplifier has been the most widely used of all linear circuits in production. It has found application in virtually every analog area such as analog/digital and digital/analog convertors, voltage reference sources, analog multipliers, waveshaping circuits, oscillators and waveform generators. It has become customary to think of signal processing in terms of voltage variables which has resulted in voltage signal processing circuits such as voltage amplifiers, voltage integrators, filters which realize voltage transfer functions, etc. Today, high quality operational amplifiers can be obtained at price levels on the order of $0.1. As a result, despite its inherent limitations, namely slew-rate and gain-bandwidth tradeoff, the versatility of the operational amplifier has made it a ubiquitous element of voltage-mode design, present in most electronic systems and in many integrated circuits.

This same period has experienced some major developments in integrated circuit design as well. During the time the operational amplifier had emerged and had become a popular component, analog circuit design was mostly done in bipolar and hybrid technologies. In the 1980s, analog design techniques were initially developed around NMOS technology. However, limited performances due to lack of complimentary devices made CMOS the principal technology for digital as well as analog designs. In the last decade, we have seen the BiCMOS technology, which allows the designer to use both bipolar and MOS devices to their best advantage. This gives the opportunity to design today's high performance mixed analog and digital very large scale integrated circuits and systems. Moreover, the GaAs fabrication technology has been used in some non-commercial designs, which still remains to be relatively expensive and unavailable.

In the last decade, innovative electronic circuit design has suffered from high performance operational amplifiers more than ever. Some researchers have been trying, by means of clever and rather unconventional design techniques, to push the limits of classical operational amplifiers looking forward to increasing their frequency of operation. Meanwhile, it has been recognized that the impedance level of the signal handling environment is of fundamental importance in order to obtain many of the benefits promised by new technologies. Moreover, scaling/reliability considerations are driving the currently dominant CMOS process technology towards submicron feature sizes and low power supply voltages as evidenced by the 3.3 V and 1.8 V standards. Since these factors make it considerably more difficult to design voltage-mode circuits with high linearity and wide dynamic range, the class of low impedance analog circuits wherein current rather than voltage is the primary signal medium, is receiving considerable attention as an alternative to conventional high impedance analog circuitry. Such current-mode circuits can operate with low power supply voltages because of the small voltage swings associated with the low impedance nodes. Wideband frequency responses approaching the small-signal transition frequency also result from the low impedance characteristics of current-mode circuits.

Since the operational amplifier is the basic circuit in voltage-mode design, it follows that an analogous building block is needed for current-mode applications. Efforts toward this objective span more than two decades. The recent attention given to the realization of integrated active RC filters at frequencies above the audio band had initially focused the interest on the operational conductance amplifier (OTA). This component of which the operational amplifier input stage forms the core of it, can be considered as a voltage controlled current source. The next stages has faced the most important competitors; the current feedback amplifier [3] and the current conveyor [4] are now commercially available as integrated circuits. Nowadays, active devices are regarded as transconductance elements with a controlled output current, carrying signals by impedance transformation to achieve amplification. Consequently, current-mode circuits in which current is the active variable rather than voltage, have started to replace voltage-mode configurations in many branches of signal processing. They have been introduced to main areas such as dynamic current mirrors, analog/digital convertors, switched signal processing in MOS, analog computing and neural networks. Recent developments in high speed GaAs circuits have extended the scope of current-mode circuits to microwave and optical communications. The trend shows that the monolithic operational amplifier will continue to evolve in new and improved forms.

Among these, the current conveyor can potentially provide the high accuracy, wide bandwidth, low input impedance and high output impedance characteristics needed for many current domain signal processing applications. Since its first proposal in 1968 [5], and its reformulation named as the second generation current conveyor in 1970 [6], this circuit element continues to receive a great deal of attention and find numerous applications. It would be appropiate to consider the current conveyor as being the basic building block of current-mode design, due to its favorable balance of operational flexibility and simplicity, giving it a similar role of the operational amplifier in voltage-mode operation. However, high performance implementations have emerged only in the last decade, and has enabled current conveyors to challenge traditional voltage operational amplifier applications such as active filters, amplifiers, oscillators and immitance simulators

[6-18]. Up to date reviews concerning the current conveyor and its applications have been made available by various authors [19-23].

This growing interest to current-mode approach, has led us to focus on this basic building block of current-mode design, the current conveyor, and its widely used application of active filters. The term active filter refers to a filter that incorporates active devices in its schematic. Typically, in such a filter, active circuits replace the function of inductors. The lack of inductors is a serious disadvantage in the design of frequency selective integrated circuits. In many applications, this drawback can be overcome by the use of conventional active RC filter techniques. In designing active RC filters, one uses a combination of resistors, capacitors and gain blocks in linear feedback loops to obtain the desired frequency selectivity without the need for inductors.

Historically, active filters have been implemented with various degrees of integration. In recent years, the microelectronic technologies, filter architectures and design techniques have emerged that allow the realization of very high quality fully integrated active filters. The developments have resulted in the implementation of single chip mixed analog/digital systems of which the integrated active filter forms one of the several important subsystems. Information acquisition and voice/data telecommunications are among the areas of highest demand for such filter circuits. Most integrated filters are implemented in CMOS due to the advantages of low power dissipation, the ability to mix analog and digital subsystems on the same die and the near ideal quality of such components as capacitors and analog switches. Some filters, particularly high frequency continuous-time filters, have been realized in bipolar and in CMOS. The BiCMOS technology, combining CMOS and bipolar transistors, is being used for some high-peformance analog systems. However, given the relative simplicity of the CMOS process, CMOS continues to be the dominant fabrication technology.

In this study, active filters using the current conveyor as the active component, will be covered. In active filters, the performance of the active element, of which here the current conveyor is of our concern, plays an important role in the overall performance of the filter, besides the filter configuration itself. Device characteristics close to ideal case, help provide the best performance for a certain filter configuration. It is obvious that the non-idealities of the current conveyor will result in deviations in filter parameters such as the cutoff frequency, quality factor and filter gain, and affect the filter characteristics. Therefore the derivation of analytical expressions for the deviations in the filter parameters in terms of current conveyor non-idealities may be of vital importance. This will enable one to realize the effect of each non-ideality term on the filter parameters and help design or choose a suitable current conveyor configuration for a specified filter performance.

We believe that for studies on a certain circuit element and any application based on this device, an improved understanding of the element is essential. Therefore, Chapter 2 starts with a complete macromodel, which fully represents both the small and large-signal behavior of the current conveyor, which is especially suitable for the simulation of active filter applications [24-32]. results show that the simple and yet accurate model provides a relative amount of simulation speedup.

The studies made on eight current conveyor configurations found in literature are given in Chapter 3 [8-16]. Both bipolar and MOS structures, as well as one of the commercially available current conveyors, namely the AD844 circuit has been covered and compared results of the current conveyor performance characteristics are given.

In active filters, as mentioned before, the performance of the active element plays an important role in the overall performance of the filter, besides the filter configuration itself. In Chapter 4 and 5, provided that a certain filter configuration is given, we will investigate the effects of current conveyor non-idealities on both voltage and current-mode active filter examples [17,18], and derive analytical expressions for the filter parameter deviations in terms of non-ideality terms. This will enable us to determine the requirements for the current conveyor non-ideality terms in order to obtain a specified filter performance. The filter configurations chosen, actually represent certain classes of active filters, which enables us to generalize the results obtained. A comparable demonstration of the filter transfer function and large-signal behavior for each current conveyor circuit studied in Chapter 3 will be given. Simulations including three types of filters, namely, the bandpass, lowpass and highpass filters, confirm the analytical expressions obtained.

In Chapter 6, a number of current conveyor structures suitable for continuous-time active filter applications will be proposed, taking the results obtained previously under consideration. Performance characteristics of the current conveyors and comparable demonstration of the voltage and current-mode filter performances will be given.

CHAPTER 2

CURRENT CONVEYOR NON-IDEALITIES

The vast amount of studies in literature, which explain the behavior of the operational amplifier in a simplified and understandable manner, has played an important role in the wide usage of this component. For a long time, voltage-mode design has dominated in analog circuitry, due to the simple behavioral modeling of the operational amplifier. The trend towards current-mode design techniques, thus requires an improved understanding of its related building blocks, of which here the current conveyor is of our concern. Macromodels are widely used for the investigation and modeling of the non-idealities of electronic components such as operational amplifiers and OTAs. This study aims to investigate the effects of current conveyor non-idealities on certain filter structures and to develop new current conveyor configurations in order to reduce these effects. So, in this chapter we will investigate and specify the current conveyor non-idealities and develop a complete macromodel, which will fully represent both the small and large-signal behavior of the current conveyor. The next section describes a simple and accurate non-linear current conveyor macromodel which will be used for introducing the non-idealities of a current conveyor into the filter transfer functions in Chapters 4 and 5, and will enable us to obtain analytical expressions for the filter parameter deviations in terms of non-ideality terms.

2.1 THE CURRENT CONVEYOR MACROMODEL

Integrated circuit simulators have proven to be useful tools for integrated circuit design engineers. With the increasing popularity of VLSI systems, the demand for simplified but still accurate models that handle analog circuit blocks is continuously growing to combine as much accuracy as possible with a maximum simulation speedup. Resorting to macromodels instead of device-level models is a widely used strategy which allows the designer to reduce the high computation time when simulating complex systems [24-26].

Contrary to operational amplifier and OTA applications where non-linear macromodels of different complexity and accuracy levels are available, there are only few linear and non-linear equivalent models for current conveyors [27-32]. In this study, we aim to fulfill the needs for a simple and accurate current conveyor macromodel which is especially suitable for the simulation of active filter applications.

2.2 BEHAVIOR OF IDEAL AND NON-IDEAL CURRENT CONVEYORS

As mentioned earlier, it would be appropiate to consider the current conveyor as being the basic building block of current-mode design, due to its favorable balance of operational flexibility and simplicity, giving it a similar role of the operational amplifier in voltage-mode operation. After its first proposal in 1968 [5] named as the first generation current conveyor (CCI), the second generation current conveyor (CCII), which is proved to be by far the more useful of two types, was introduced in 1970 [6]. A block diagram is given in Fig. 2.1a, and the behavior of the ideal current conveyor is characterized by

$$\begin{pmatrix} I_Y \\ V_X \\ I_Z \end{pmatrix} = \begin{pmatrix} 0 & 0 & 0 \\ 1 & 0 & 0 \\ 0 & \pm 1 & 0 \end{pmatrix} . \begin{pmatrix} V_Y \\ I_X \\ V_Z \end{pmatrix} \tag{2.1}$$

The device relies upon the ability to act as a voltage buffer between its inputs and the ability to convey current between two ports which show extremely different impedance levels. The output current I_Z depends only on the current at terminal x. This current may be injected directly at x, or may be produced by the copy of the input voltage V_Y which will appear across the impedance connected at terminal x. No current is drawn from terminal y. The ± sign indicates whether the element is of non-inverting (CCII+) or inverting type (CCII-), which has the conventional meaning as the output current I_Z flowing the same or the opposite direction of the input current I_X, respectively.

However, the behavior of an actual current conveyor differs from the ideal case and can be represented by the following equations in the linear region;

$$\begin{pmatrix} I_Y \\ V_X \\ I_Z \end{pmatrix} = \begin{pmatrix} Y_Y(s) & 0 & 0 \\ k_V(s) & Z_X(s) & 0 \\ 0 & \pm k_I(s) & Y_Z(s) \end{pmatrix} \cdot \begin{pmatrix} V_Y \\ I_X \\ V_Z \end{pmatrix} \tag{2.2}$$

where Z_X is the impedance of terminal x, Y_Y and Y_Z are the admittances of terminal y and z, respectively. k_V is the voltage transfer ratio from terminal y to x, and k_I is the current transfer ratio from terminal x to z.

Comparison of Eqs. 2.1 and 2.2 yields that, in contrary to the ideal case where $Z_X = 0$, $Y_Y = 0$ and $Y_Z = 0$, the actual current conveyor shows non-zero values for these parameters. k_V and k_I also differ from the ideal case which results in values other than 1 and ± 1, respectively. In general case, all of these parameters are frequency dependent. Furthermore, the boundaries of the linear operation region of the current conveyor is determined by the voltage and current limitings at terminals x and z. Eq. 2.2 represents the current conveyor in the linear operating region. However, the physical component is non-linear and behaves linearly only if the conditions of

$$\begin{aligned} I_{Xmin} &\leq |i_X(t)| \leq I_{Xmax} \\ V_{Xmin} &\leq |v_X(t)| \leq V_{Xmax} \\ V_{Zmin} &\leq |v_Z(t)| \leq V_{Zmax} \end{aligned} \tag{2.3}$$

are satisfied; where I_{Xmin}, I_{Xmax}, V_{Xmin}, V_{Xmax}, V_{Zmin} and V_{Zmax} denote the maximum and minimum current and voltage values of terminal x and voltage values of terminal z, respectively.

It can be easily observed that the macromodel to be derived must represent the conditions described above as accurately as possible.

Fig. 2.1b depicts the non-ideal current conveyor represented by Eq. 2.2. A detailed circuit of this representation is given in Fig. 2.1c where $k_V' = \frac{Z_P}{Z_P + Z_S} k_V$, $Z_P=R_P // (1/sC_P)$, $Z_S=sL_P+r_X$ and $Z_X=Z_P // Z_S$.

2.3 MACROMODEL DEVELOPMENT

The proposed macromodel for the current conveyor is shown in Fig. 2.1c. With a proper choice of model parameters and elements, the non-linear equivalent circuit represents the circuit behavior for non-linear dc, ac and large signal transient responses of the current conveyor accurately. The macromodel consists of nine resistors, three capacitors, one inductor, one dependent current and five dependent voltage sources, five independent voltage sources and six diodes. The derived macromodel is subdivided into three sections, namely, the input stage (terminal y), the intermediate stage (terminal x) and the output stage (terminal z).

The input impedance at y is represented by the resistor r_Y and the capacitor C_Y. The independent voltage source V_{OFF} is introduced for the modeling of the offset voltage. The input impedance at x is represented by the resistors r_{X1}, r_{X2}, R_P, the inductor L_P and the capacitor C_P, where $r_X = r_{X1} + r_{X2}$. In conventional models derived for the current conveyor, the impedance at terminal x is represented by a simple lowpass RC circuit [27]. However, the behavior of an actual current conveyor differs from this simple model and shows a second order character. An accurate representation of this second order character is very important, because it is the primary factor which determines the frequency response of the current conveyor. This is achieved by the use of a novel approximation introducing the inductor L_p which forms a resonant circuit with the capacitor C_P. The resistors R_p and r_X are intended to adjust the bandwidth of the resonant circuit. The voltage dependent voltage source $k_V'(s).V_Y$ reflects the input voltage V_Y to terminal x.

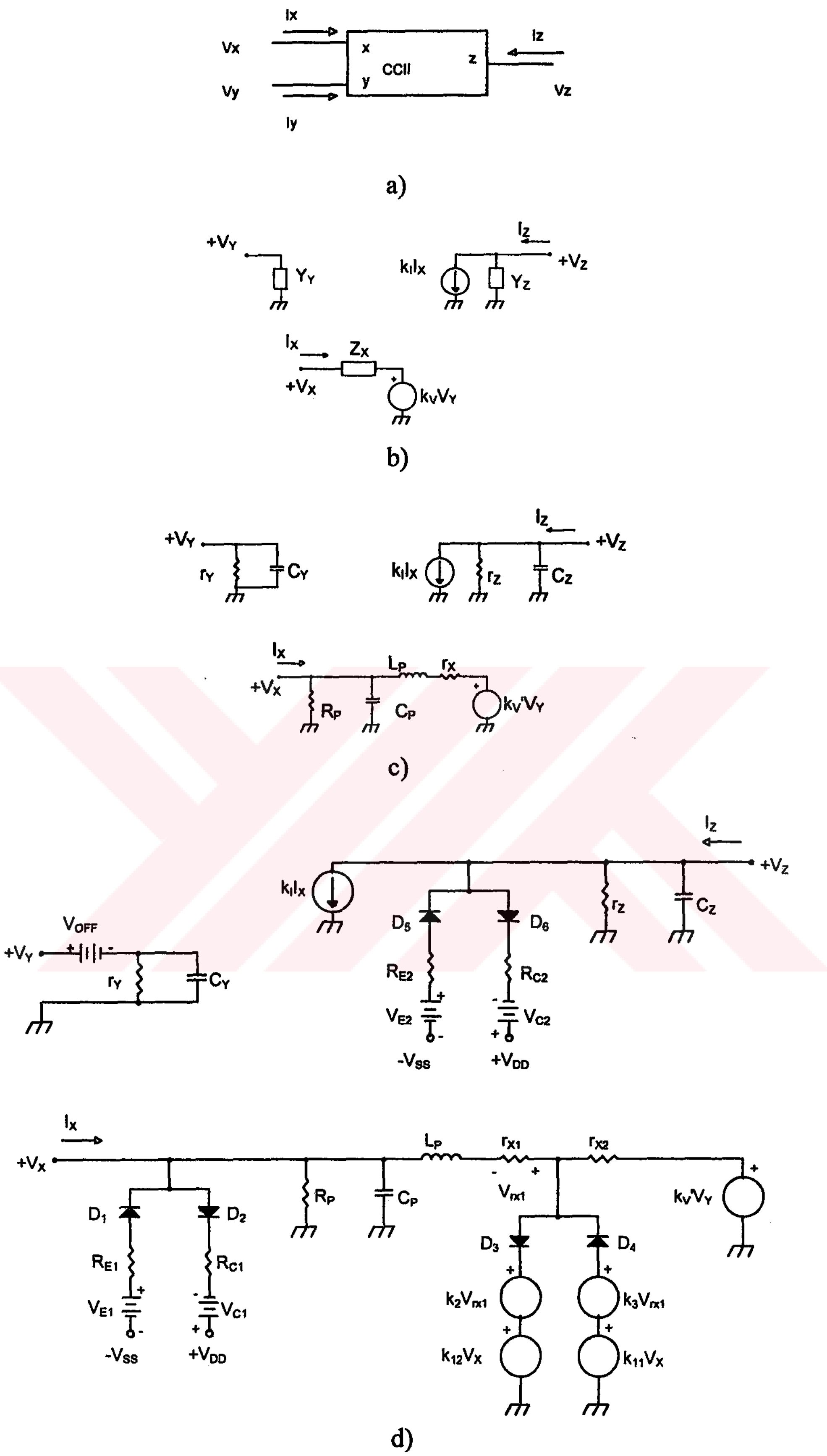

Figure 2.1 a) Block diagram of the current conveyor b) The non-ideal current conveyor c) A detailed circuit of the non-ideal current conveyor d) Proposed macromodel for current conveyor

The macromodel yields the impedance Z_X as

$$Z_X(s) = \frac{1}{C_P} \frac{s + \frac{r_X}{L_P}}{s^2 + s\left(\frac{C_P R_P r_X}{C_P L_P R_P} + \frac{L_P}{C_P L_P R_P}\right) + \frac{r_X + R_P}{C_P L_P R_P}} \tag{2.4}$$

which can be rewritten as

$$Z_X(s) = \frac{1}{C_P} \frac{s + w_Z}{s^2 + s\frac{w_P}{Q_P} + w_P{}^2} \tag{2.5}$$

where $w_Z = \frac{r_X}{L_P}$, $w_P = \sqrt{\frac{r_X + R_P}{C_P L_P R_P}}$ and $Q_P = \frac{\sqrt{C_P L_P R_P (r_X + R_P)}}{C_P R_P r_X + L_P}$.

The transfer function $H(s) = V_X/V_Y$ is given by

$$H(s) = H(0) \frac{\frac{R_E + r_X}{C_P L_P R_E}}{s^2 + s\left(\frac{C_P R_E r_X}{C_P L_P R_E} + \frac{L_P}{C_P L_P R_E}\right) + \frac{R_E + r_X}{C_P L_P R_E}} \tag{2.6}$$

where $H(0) = k_V \frac{R_E}{R_E + r_X}$ and $R_E = R_P // R_X$, R_X denoting the external resistor.

The non-linearity of the current conveyor caused by the voltage and current limiting at terminal x is modeled by introducing additional elements.

The voltage swing is limited by the voltage source-resistor-diode combinations V_{C1}, D_2, R_{C1} and V_{E1}, D_1, R_{E1} [26]. To represent the current limiting, the voltage dependent voltage sources $k_{11}V_X$, $k_{12}V_X$, k_2V_{rx1}, k_3V_{rx1} and the diodes D_3, D_4 are incorporated to the circuit where V_{rx1} is the voltage across the resistor r_{X1}. In contrary to conventional macromodels for operational amplifiers, where a single dependent voltage source is used to sense a short-circuit at the output, two separate dependent voltage sources $k_{11}V_X$ and $k_{12}V_X$ are introduced into the new model to provide flexibility in representing the non-linear current limiting behavior of terminal x for both short-circuited and resistive loaded operating conditions, where in case of a single dependent voltage source, as used in conventional operational amplifier macromodels, the error increases.

The output impedance at z is modeled by the resistor r_Z and the capacitor C_Z. The current controlled current source $I_1 = k_I(s).I_X$ produces a current output at z which is proportional to the current I_X. The output voltage excursion is limited by the voltage source-resistor-diode combinations V_{C2}, D_6, R_{C2} and V_{E2}, D_5, R_{E2} [26].

The resistors R_{C1}, R_{E1}, R_{C2} and R_{E2} are newly introduced resistive elements to the circuit model which adjust the slope of the dc voltage transfer characteristics $V_X = V_X(V_Y)$ and $V_Z = V_Z(V_Y)$ at the boundaries of the linear operating region by using a piecewise linear approximation and which are not represented in the conventional macromodels for operational amplifiers [24,25].

Although piecewise linear approximations find a place in conventional macromodel methodology, it is not being used in current operational amplifier models [24-25]. It has been proved in a recent study that the use of piecewise linear approximation techniques is necessary and improves the characteristics [26]. The same technique has been also used in this study.

2.4. COMPARISON WITH SEMICONDUCTOR DEVICE-LEVEL MODELS

The accuracy of the current conveyor macromodel is demonstrated by comparing the simulated current conveyor characteristics with simulation results obtained from the semiconductor device model. The non-inverting current conveyor topology shown in Fig. 2.2a was chosen for the demonstration [7]. The SPICE device model parameters and dimensions for the NMOS and PMOS transistors are given in Appendix A. The macromodel parameters of the derived macromodel were determined from SPICE simulations using device models and are given in Table 2.1. The supply voltages were taken as ±10V.

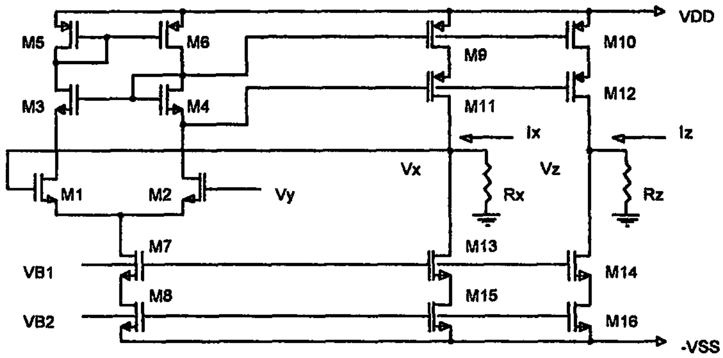

a)

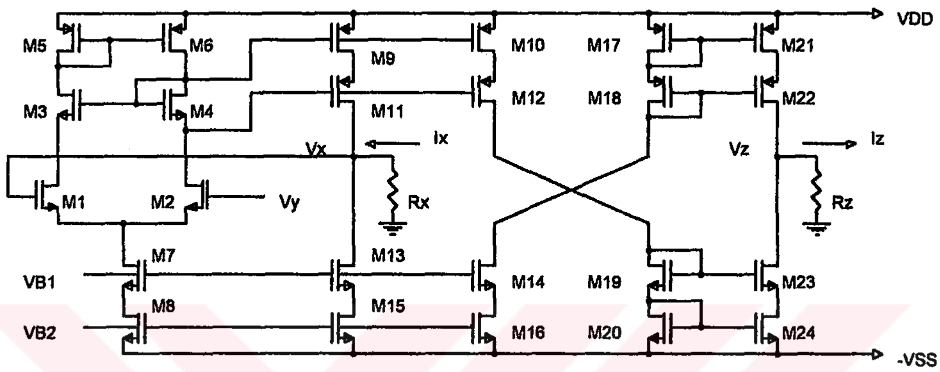

b)

Figure 2.2 Circuit examples for CMOS realization of current conveyors
a) Non-inverting type current conveyor b) Inverting type current conveyor

Table 2.1 Macromodel parameters (* for inverting current conveyor k_I = -1)

Parameter	Value	Parameter	Value
V_{C1}	3.5 V	r_{X1}	327 Ω
V_{E1}	0.5 V	r_{X2}	400 Ω
R_{C1}	833 Ω	R_P	26 kΩ
R_{E1}	1 Ω	C_P	0.1 pF
V_{C2}	2.45 V	L_P	31.2 mH
V_{E2}	0.9 V	r_Y	1E12 Ω
R_{C2}	640 Ω	C_Y	0.0489 pF
R_{E2}	1750 Ω	r_Z	805 kΩ
k_V	1	C_Z	0.16 pF
k_I	1*	I_{S1}	2E-14 A
k_{11}	1	I_{S2}	10E-14 A
k_{12}	1	I_{S3}	2E-14 A
k_2	-9	I_{S4}	10E-14 A
k_3	-0.45	I_{S5}	2E-14 A
V_{OFF}	-63 mV	I_{S6}	2E-14 A

To demonstrate the accurate representation of the non-linear behavior of the current conveyor, the voltage and current dc transfer characteristics obtained from SPICE simulations with device-level models and newly introduced macromodel are illustrated in Fig. 2.3. The voltage transfer characteristics $V_X = V_X(V_Y)$ for open-circuited terminal x are given in Fig. 2.3a. The voltage clipping limits at terminal x were obtained as V_{Xmax} =7.64 V and V_{Xmin} = -10 V. Fig. 2.3b shows the dc voltage transfer characteristics $V_Z = V_Z(V_Y)$ for open-circuited terminal z and short-circuited terminal x. The voltage clipping limits were determined as V_{Zmax} =8.88 V and V_{Zmin} = -9.97 V. Fig. 2.3c illustrates $I_X = I_X(V_Y)$ characteristics for short-circuited terminal x. The lower and upper boundaries of the current I_X were determined as I_{Xmin} =204 mA and I_{Xmax} = -1.45 mA.

The frequency responses of the currents i_z and i_x, voltage gains v_x/v_y and v_z/v_y are shown in Fig. 2.4.

The frequency dependencies of the impedances Z_X, Z_Y ($1/Y_Y$) and Z_Z ($1/Y_Z$) are given in Fig. 2.5. It can be easily observed from Fig. 2.5a that the impedance Z_X has a value of 727 Ω at low frequencies, increases with increasing frequency and shows a maximum of 26 kΩ at a resonant frequency of 89.5 MHz. Simulated variations of the impedance Z_Y with frequency are given in Fig. 2.5b. Since the input resistance of a MOS transistor is very large and of the order of 10^{12} Ω, the resistive component r_Y of the impedance Z_Y can be assumed to be practically infinite. Therefore, the input impedance Z_Y is capacitive which results in an input capacitance of C_Y = 0.0489 pF. Fig. 2.5c shows that the output impedance Z_Z at the terminal z has a value of 805 kΩ at low frequencies and decreases with increasing frequency. The cut-off frequency of the frequency response is determined as f_{Z3dB} =1.22 MHz which results in r_Z=805 kΩ and C_Z=0.16 pF.

It can be observed from Figs. 2.3 through 2.5 that the non-linear dc transfer characteristics and the frequency responses obtained from SPICE simulations by using device models and the newly introduced current conveyor macromodel are in well agreement with each other.

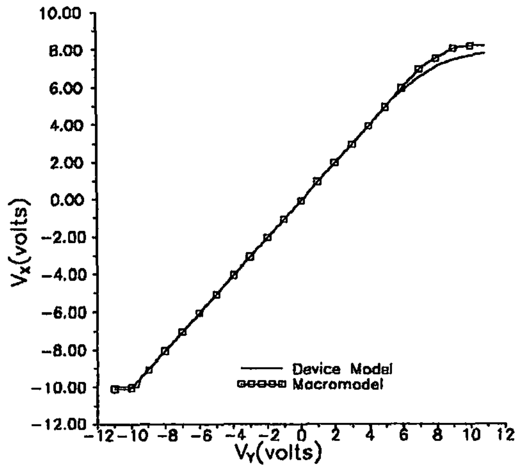

a)

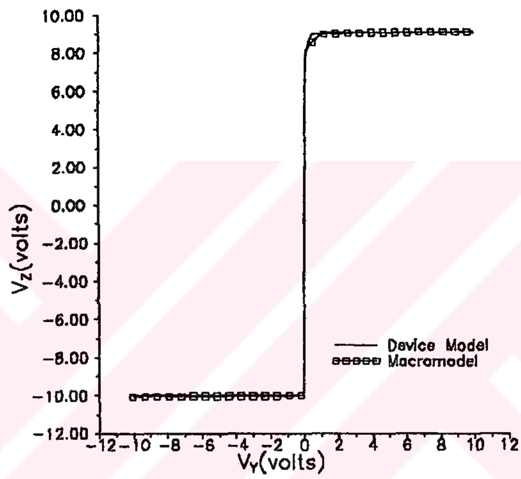

b)

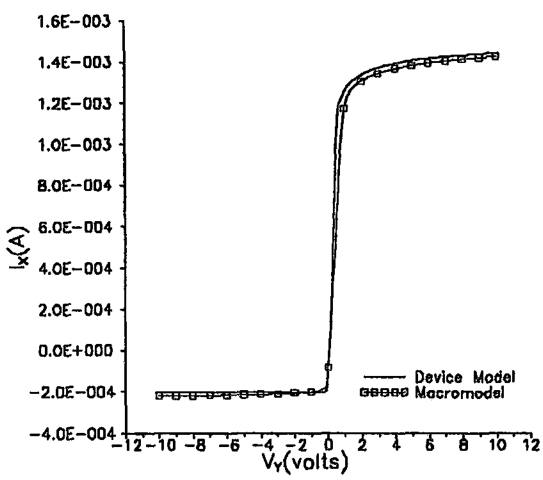

c)

Figure 2.3 Dc transfer characteristics obtained from SPICE simulations:
a) Plots of V_X against V_Y for $R_X = \infty$ b) Plots of V_Z against V_Y for $R_Z = \infty$
c) Plots of I_X against V_Y for $R_X = 0$

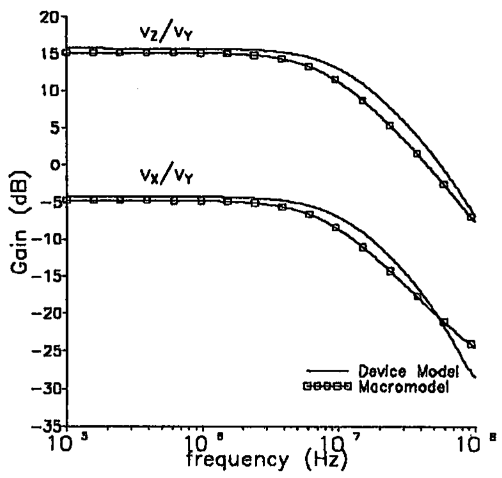

a)

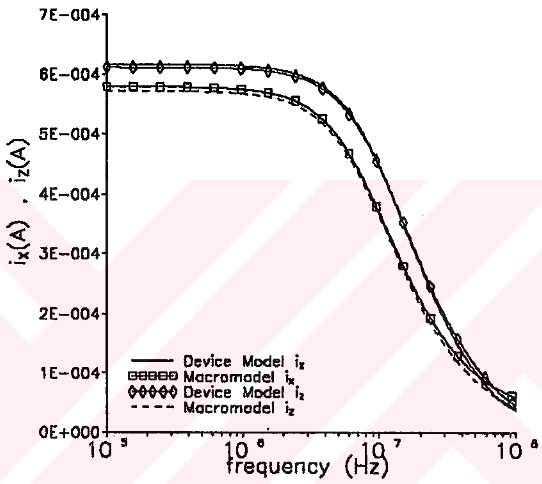

b)

Figure 2.4 Frequency responses of a) Voltage gains v_x/v_y and v_z/v_y b) Currents i_z and i_x

To compare the accuracy of the SPICE simulations with the macromodel and with the device models, an example of a second order lowpass active filter topology was chosen [17]. The complete filter circuit containing three current conveyors is shown in Fig. 2.6. The cut-off frequency of the filter was 159 kHz.

The filter was constructed with the inverting and non-inverting CMOS current conveyor topologies shown in Fig. 2.2. SPICE simulations for ac and transient analyses were performed using device models and macromodels. The frequency

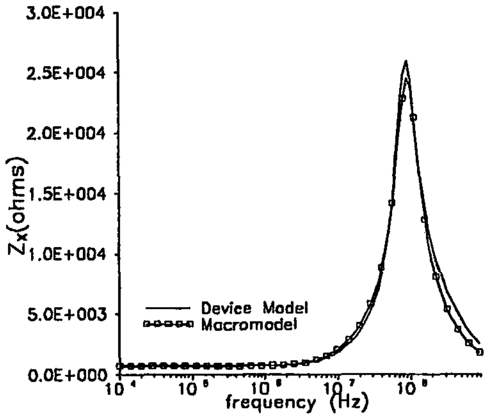

a)

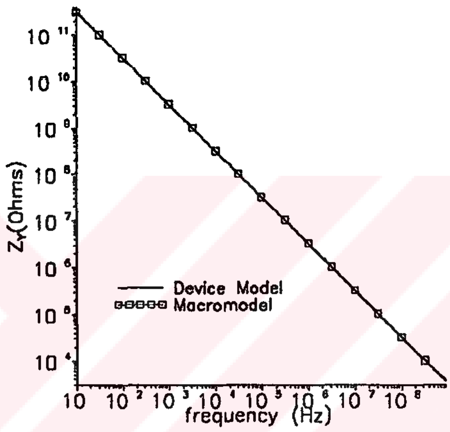

b)

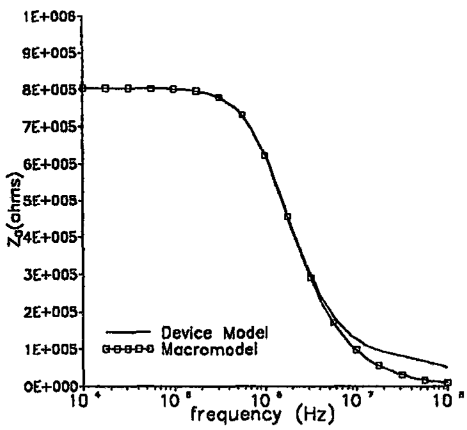

c)

Figure 2.5 Frequency responses of a) the impedance of terminal x, Z_X b) the impedance of terminal y, Z_Y, c) the impedance of terminal z, Z_Z.

response of the filter obtained from SPICE simulation with two models is shown in Fig. 2.7a. The transient analysis results of the same filter for a 100 kHz sinusoidal input voltage with an amplitude of $V_P = 1V$ are illustrated in Fig. 2.7b. As can be observed from Fig. 2.7b, the slew-rate limiting of the current conveyors causes a distorted waveform at the output for high frequency operation. The total harmonic distortion (THD) of the output signal was found to be 3.4% from the SPICE simulation with the device-level model, and 2.8% from the macromodel representation, respectively.

Simulations to obtain the frequency and transient responses of the lowpass filter were performed for two different CMOS current conveyor topologies [7,22] by using two models on a 486-based 50 MHz computer, and the resulting computer times are given in Table 2.2. It is obvious that the computer time needed for SPICE simulations was considerably reduced by the use of the proposed macromodel.

2.5 PARAMETER DETERMINATION

The model parameters of the derived current conveyor macromodel can be determined from measurements on an actual current conveyor or from SPICE simulation results obtained by using semiconductor device models.

Equations to calculate the model parameters for representation of the current conveyor are given in Table 2.3.

Basic static model parameters representing the non-linear current conveyor behavior can be easily determined from dc transfer characteristics $V_X = V_X(V_Y)$, $V_Z = V_Z(V_Y)$, $I_X = I_X(V_Y)$ shown in Fig. 2.3a, b and c, respectively.

The model parameters I_{S1}, I_{S2}, k_{11}, k_{12}, k_2, k_3 represent the current limiting behavior at terminal x of the current conveyor and can be determined from the measured or simulated $I_X = I_X(V_Y)$ characteristic. The maximum and minimum

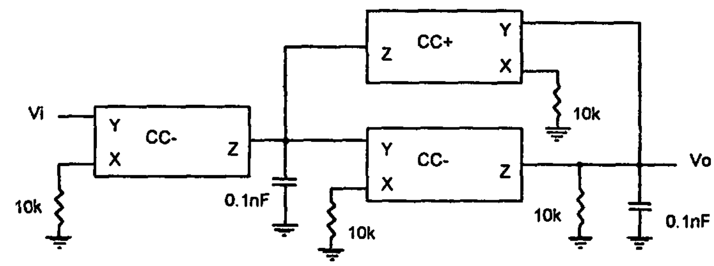

Figure 2.6 An example of a second order lowpass active filter

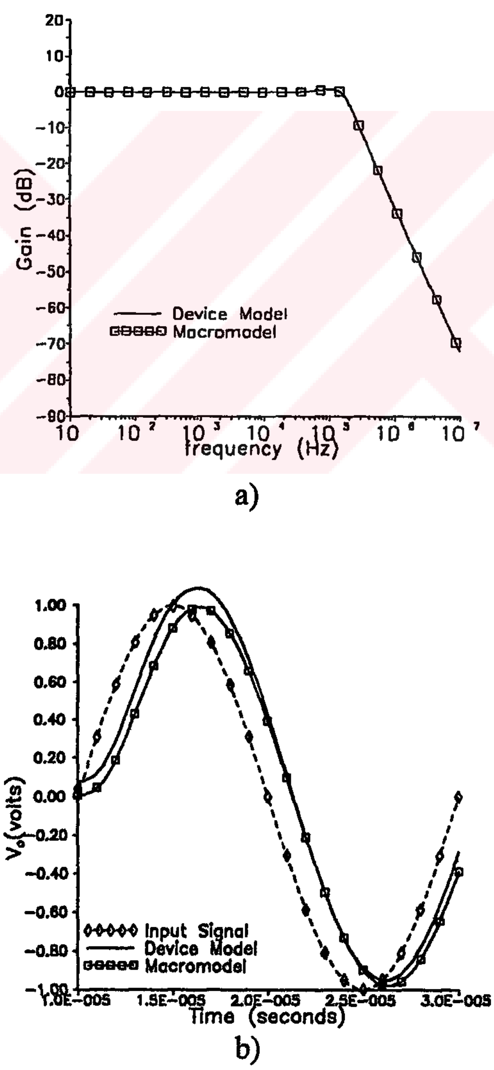

Figure 2.7 a) Simulated frequency response of the filter b) Transient analysis results of the filter

values of the current I_X are specifed as I_{Xmax} and I_{Xmin}. The forward-biasing voltage of the diodes is fixed at a value of V_D =0.62 V, the diode currents are assumed to be equal to I_{Xmax} and I_{Xmin}, respectively.

Model parameters V_{C1}, R_{C1}, V_{E1} and R_{E1} are introduced to represent the boundaries of the voltage swing region at terminal x and can be obtained from the $V_X = V_X(V_Y)$ characteristic. The two boundaries of linear operation are denoted as V_{XM1} and V_{XM2} ,while the maximum and minimum values of the voltage V_X are specifed as V_{Xmax} and V_{Xmin}.

Similarly, model parameters V_{C2}, R_{C2}, V_{E2} and R_{E2} are introduced to represent the boundaries of the voltage swing region at terminal z and can be obtained from the $V_Z = V_Z(V_Y)$ characteristic. The boundaries of linear operating region are denoted as V_{ZM1} and V_{ZM2}, while the maximum and minimum values are specifed as V_{Zmax} and V_{Zmin}.

The model parameters r_Y, C_Y, r_Z and C_Z represent the input and output impedances of the current conveyor and can be specified from measured or simulated plots of input and output impedances against frequency. f_{Y3dB} and f_{Z3dB} are cut-off frequencies.

The model parameters r_{X1}, r_{X2}, R_P, L_P and the capacitor C_P can be extracted from measured and simulated plots of the input impedance at terminal x against frequency. The resonant frequency is denoted with f_P and B represents the 3dB bandwidth of the frequency response. As shown in Fig. 2.5a, at low frequencies the impedance is resistive and has a value of $R_P // r_X$ where $r_X = r_{X1} + r_{X2}$. At the resonant frequency, the impedance becomes $Z_X = r_X + R_P = \omega_P Q_P L_P$. The fraction ratio of r_{X1} / r_{X2} has no physical meaning and can be taken as r_{X1} / r_{X2} =1 for simplicity, though it is a well known technique in the modeling of current limiting [24-26].

Table 2.2 Computer times in seconds needed for SPICE simulations

Type of analysis	ac	transient
Current conveyor 1 (Device model)	20.70	34.99
Current conveyor 1 (Macromodel)	1.92	6.59
Current conveyor 2 (Device model)	60.25	72.18
Current conveyor 2 (Macromodel)	2.03	6.32

Table 2.3 Equations to calculate the macromodel parameters

$V_{C1} = V_{DD} - V_{XM1} + V_Y$	$I_{S1} = -I_{X\max} e^{-V_D/V_T}$
$V_{E1} = V_{SS} - \lvert V_{XM2} \rvert + V_Y$	$I_{S2} = I_{X\min} e^{-V_D/V_T}$
$V_{C2} = V_{DD} - V_{ZM1} + V_Y$	$k_2 = 1 - \dfrac{V_D}{r_{X1} \lvert I_{X\max} \rvert}$
$V_{E2} = V_{SS} - \lvert V_{ZM2} \rvert + V_Y$	$k_3 = 1 - \dfrac{V_D}{r_{X1} I_{X\min}}$
$R_{C1} = \dfrac{V_{X\max} - V_{XM1}}{\lvert I_{X\max} \rvert}$	$Q_P = \dfrac{f_P}{B}$
$R_{E1} = \dfrac{\lvert V_{X\min} \rvert - \lvert V_{XM2} \rvert}{I_{X\min}}$	$C_P = \dfrac{Q_P}{2\pi f_P R_P}$
$R_{C2} = \dfrac{V_{Z\max} - V_{ZM1}}{\lvert I_{Z\max} \rvert}$	$L_P = \dfrac{R_P}{2\pi f_P Q_P}$
$R_{E2} = \dfrac{\lvert V_{Z\min} \rvert - \lvert V_{ZM2} \rvert}{I_{Z\min}}$	$C_Y = \dfrac{1}{2\pi f_{Y3dB} r_Y}$
	$C_Z = \dfrac{1}{2\pi f_{Z3dB} r_Z}$

CHAPTER 3

STUDIES ON THE PERFORMANCE CHARACTERISTICS OF VARIOUS CURRENT CONVEYOR TOPOLOGIES

As mentioned earlier, the trend towards current-mode design techniques requires an improved understanding of its related building blocks, of which here the current conveyor is of our concern. So, as a part of this strategy, we find it necessary to investigate some basic current conveyor structures. This chapter includes the studies made on various current conveyor configurations found in literature [8-16]. Both bipolar and MOS structures, as well as one of the commercially available current conveyors, namely the AD844 circuit will be covered. Compared results of the current conveyor performance characteristics and non-ideality terms mentioned in Chapter 2 will be given for each current conveyor. These results will be used in Chapter 4 and 5 , in order to compare the voltage and current-mode filter performances. Also, a perspective will be established for the basic design considerations of the current conveyors proposed in Chapter 6.

For the SPICE simulation of bipolar implementations, XR B101 and XR B102 device model parameters have been used for the npn and pnp transistors, respectively; whereas Alcatel Mietec 2 μm HBiMOS process parameters have been used for MOS implementations, except for current conveyor CC6. A more suitable parameter set for low voltage applications of the AMS 0.8 μm CMOS process has been used for this circuit. A list of the device model parameters, as well as the MOS transistor dimensions of the current conveyors, are given in Appendix A. The above mentioned npn and pnp transistors have been used for the measurements on bipolar current conveyors as well.

3.1 PERFORMANCE CHARACTERISTICS OF CURRENT CONVEYOR 1

In this section, the current conveyor circuit given in Fig. 3.1a will be studied [8]. The circuit basically consists of complementary emitter followers. Transistors Q1 and Q3 are used to bias the emitter followers Q2 and Q4. The circuit requires a very precise matching of the bias current sources for Q1 and Q3. Otherwise an input error current will result at terminal y. However, an advantage of the circuit is that it does not require a very close matching between npn and pnp transistors. Q5-Q8 form the current mirrors needed to generate output z. Measurements have been made in order to check the performance of the current conveyor. Supply voltages were chosen to be ±10 V and I_O as 600 μA. Simple current mirrors have been used to implement the current sources.

The voltage transfer characteristics $V_X= V_X(V_Y)$ for open-circuited terminal x and $V_Z= V_Z(V_Y)$ for open-circuited terminal z, are given in Figs. 3.2a and b, respectively. The voltage clipping limits at terminal x and terminal z were obtained as V_{Xmax}=9.53 V, V_{Xmin}= -9.50 V, V_{Zmax}=9.28 V and V_{Zmin}= -9.92 V. Fig. 3.2c illustrates $I_X= I_X(V_Y)$ characteristic for short-circuited terminal x. The lower and upper boundaries of current I_X were determined as I_{Xmin}= -6.41 mA and I_{Xmax}=62.6 mA. The $I_X= I_X(V_Y)$ and $I_Z= I_Z(V_Y)$ characteristics for terminal loads of R_X=1 kΩ and R_Z=1 kΩ are given in Fig. 3.2d. The frequency responses of the voltage gain v_x/v_y and current gain i_z/i_x are shown in Fig. 3.2e. We obtain the values of the voltage and current transfer functions at low frequencies as k_V=0.9966 and k_I=0.873, respectively, for terminal loads of R_X=10 kΩ and R_Z=10 kΩ. The 3 dB bandwidth value for the voltage transfer function is above 100 MHz, while f_I=3.5 MHz. Fig. 3.2f shows that the impedance Z_X has a value of 29 Ω at low frequencies and shows a maximum of 32 Ω at a resonant frequency of 25 MHz. Variations of the impedance Z_Y with frequency is given in Fig. 3.2g. Values of r_Y=64 kΩ and C_Y=6.3 pF are obtained. Fig. 3.2h showing the output impedance Z_Z at terminal z, gives the values of r_Z=55 kΩ and C_Z=5.5 pF.

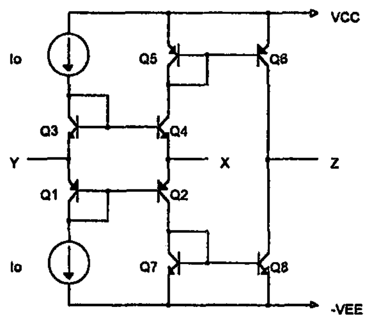

a)

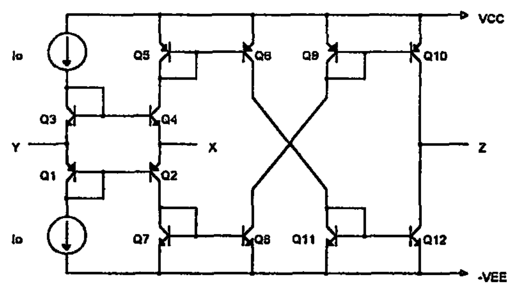

b)

Figure 3.1 a) Circuit diagram of current conveyor 1 b) Inverting type current conveyor derived from a)

The characteristic values of the current conveyor are given in Table 3.1. An inverting type current conveyor has been derived from the circuit above, to be used for later purposes. This circuit is given in Fig. 3.1b.

3.2 PERFORMANCE CHARACTERISTICS OF CURRENT CONVEYOR 2

The current conveyor circuit in Fig. 3.3a has been studied in this section [9,10]. The circuit is fully symmetrical, with Q1-Q4 comprising the input stage. The base terminals of Q1 and Q2, connected together, form node y, while the emitters connected together, form node x, which exhibit high and low impedances, respectively. A voltage applied to input y, is followed by input x. The collector currents of Q3 and Q4 are reflected through Q5 and Q6 to the high output impedance z node. Thus, any current into node x is conveyed with unity gain through to node z.

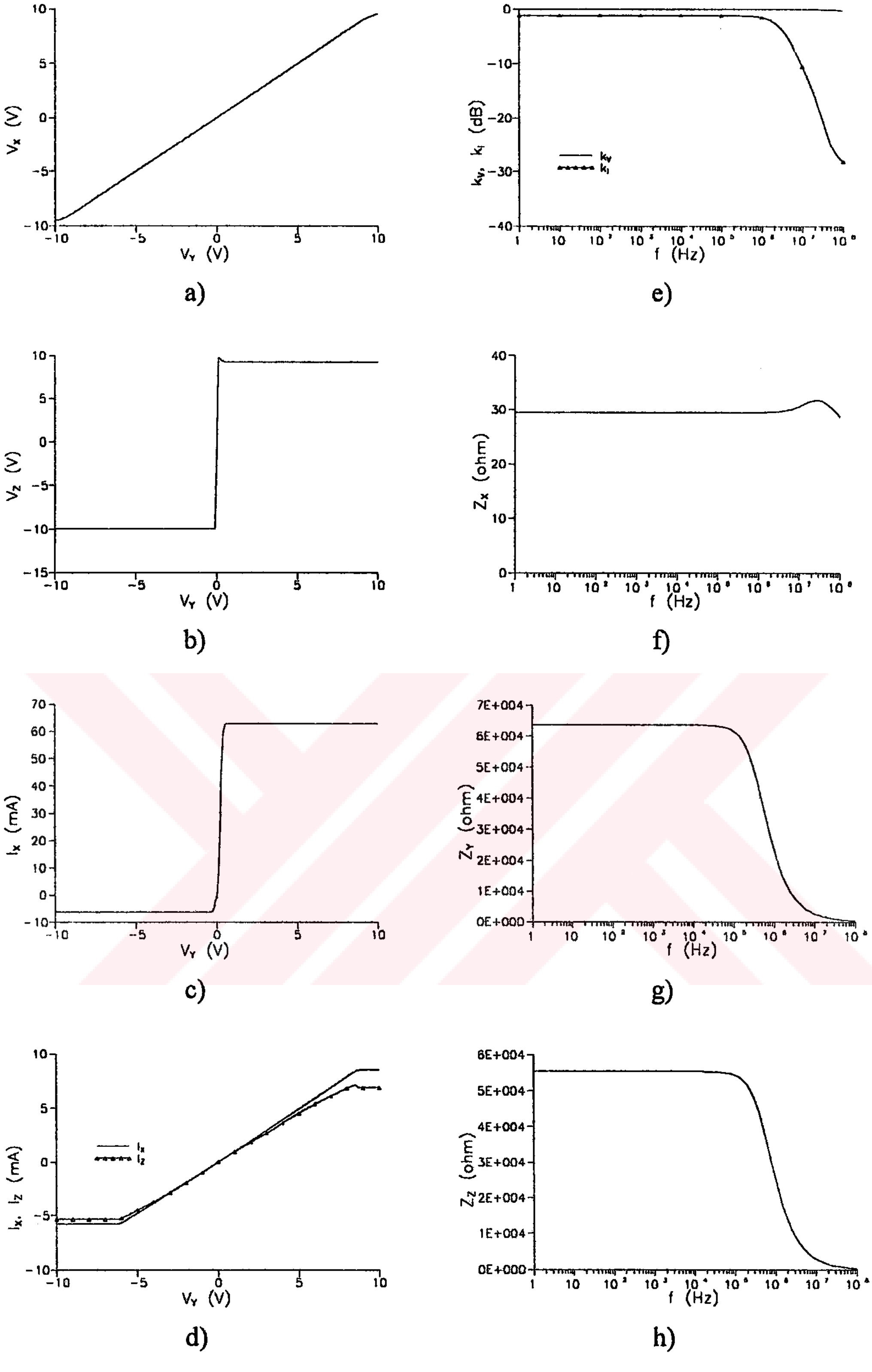

Figure 3.2 Measured device characteristics of current conveyor 1
a) $V_X = V_X(V_Y)$ for $R_X = \infty$ b) $V_Z = V_Z(V_Y)$ for $R_Z = \infty$ c) $I_X = I_X(V_Y)$ for $R_X = 0$ d) $I_X = I_X(V_Y)$, $I_Z = I_Z(V_Y)$ for $R_X = R_Z = 1\ k\Omega$ e) The frequency responses of v_x/v_y and i_z/i_x for $R_X = R_Z = 10\ k\Omega$ f) The frequency response of Z_X g) The frequency response of Z_Y h) The frequency response of Z_Z

Table 3.1 Characteristic values of various current conveyors

	CC1	CC2	CC3	CC4	CC5	CC6	CC7	CC8
V_{Xmax}	9.53 V	14.5 V	13.45 V	5 V	15 V	3.93 V	4.18 V	0.963 V
V_{Xmin}	-9.50 V	-14.5 V	-13.38 V	-5 V	-15 V	-4.56 V	-3.09 V	-1 V
V_{Zmax}	9.28 V	9.8 V	13.8 V	3.37 V	11.5 V	4.72 V	5 V	1.8 V
V_{Zmin}	-9.92 V	-11 V	-14.2 V	-4.28 V	-11.5 V	-5 V	-4.91 V	-1.8 V
I_{Xmax}	62.6 mA	16.5 mA	54.1 mA	11.32 mA	60 mA	4.41 mA	300 μA	360.7 μA
I_{Xmin}	-6.41 mA	-13.9 mA	-8.43 mA	-1.14 mA	-60 mA	-308 μA	-1.68 mA	-162.2 μA
k_V	.9966	0.991	1	0.97	0.996	1.002	0.908	0.974
f_V	> 100 MHz	> 100 MHz	3.5 MHz	29.3 MHz	1.6 GHz	72 MHz	64.1 MHz	80 MHz
k_I	0.873	0.822	0.979	0.89	0.995	1.052	0.911	1
f_I	3.5 MHz	3 MHz	1MHz	18 MHz	3.4 MHz	70 MHz	360 MHz	17.5 MHz
r_X	29 Ω	74 Ω	0.36 Ω	304 Ω	50 Ω	45.1 Ω	637 Ω	174 Ω
r_{X1}	15 Ω	35 Ω	0.18 Ω	150 Ω	25 Ω	22 Ω	320 Ω	90
r_{X2}	14 Ω	39 Ω	0.18 Ω	154 Ω	25 Ω	23.1 Ω	317 Ω	84
R_P	32 Ω	499 Ω	351 Ω	499 Ω	121 Ω	1668 Ω	2120 Ω	1330 Ω
f_P	25 MHz	31.6 MHz	5 MHz	31.6 MHz	1 GHz	79.4 MHz	50.1 MHz	39.8 MHz
r_Y	64 kΩ	55 kΩ	1 TΩ	629 kΩ	11.1 MΩ	1.96 TΩ	2.41 TΩ	118.4 GΩ
C_Y	6.3 pF	1.6 pF	10^{-19} F	7.9 pF	≈0	57.2 fF	46.7 fF	879 fF
r_Z	55 kΩ	273 kΩ	7.9 MΩ	20.2 MΩ	3 MΩ	50.4 kΩ	1.5 MΩ	1 MΩ
C_Z	5.5 pF	5.7 pF	20.15 pF	5.63 pF	5.5 pF	494 fF	220.6 fF	168.1 fF

Supply voltages were chosen to be ±15 V during measurements in order to check the performance of the current conveyor. The performance characteristics are given in Fig. 3.4, whereas the characteristic values of the current conveyor are given in Table 3.1. The inverting type current conveyor given in Fig. 3.3b, will be used for later purposes [9,10].

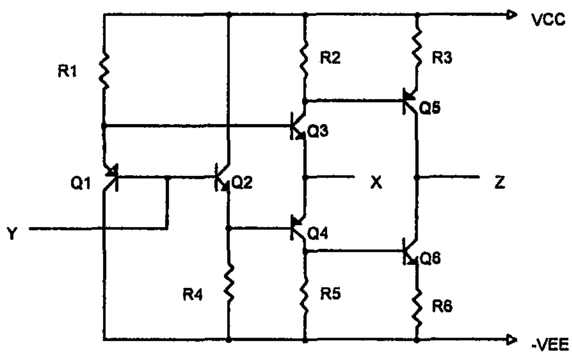

a)

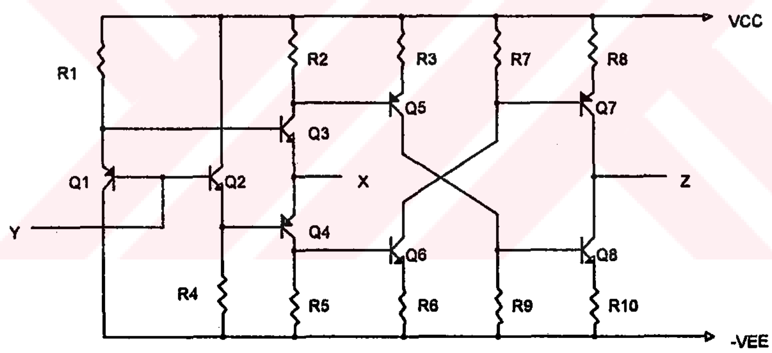

b)

Figure 3.3 a) Circuit diagram of current conveyor 2 b) Inverting type current conveyor derived from a)

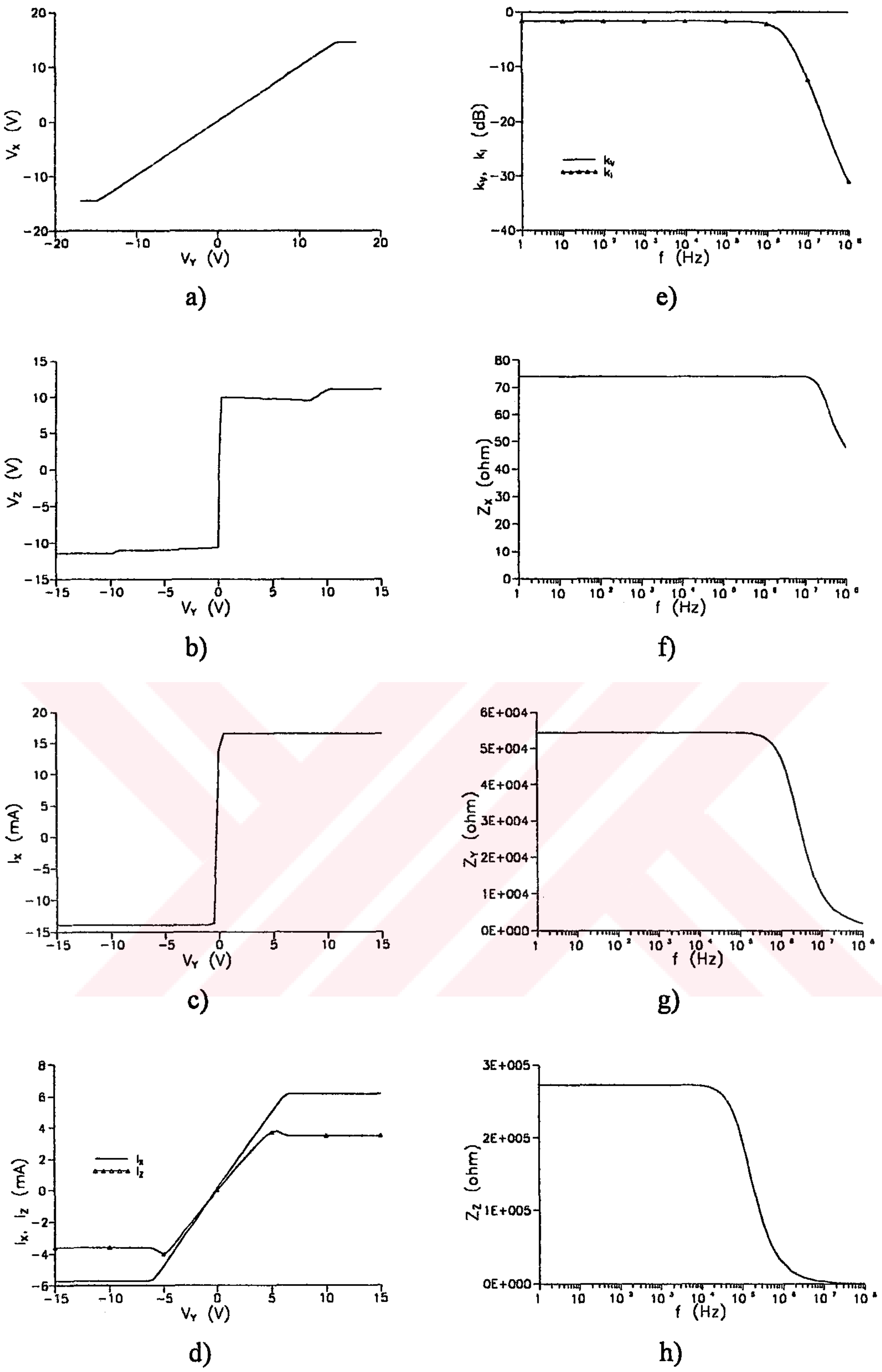

Figure 3.4 Measured device characteristics of current conveyor 2
a) $V_X = V_X(V_Y)$ for $R_X = \infty$ b) $V_Z = V_Z(V_Y)$ for $R_Z = \infty$ c) $I_X = I_X(V_Y)$ for $R_X = 0$ d) $I_X = I_X(V_Y)$, $I_Z = I_Z(V_Y)$ for $R_X = R_Z = 1\ k\Omega$ e) The frequency responses of v_x/v_y and i_z/i_x for $R_X = R_Z = 10\ k\Omega$ f) The frequency response of Z_X g) The frequency response of Z_Y h) The frequency response of Z_Z

3.3 PERFORMANCE CHARACTERISTICS OF CURRENT CONVEYOR 3

The current conveyor circuit given in Fig. 3.5a, consists of an operational amplifier, and a pair of current mirrors which form a voltage/current convertor [11,12]. The transistors Q4 and Q5, together with the diodes, may be thought of as a class AB output stage for the operational amplifier. The positive signal swing of terminal x, is determined by Q4, while the negative swing is determined by Q5. The two current mirrors convert the output voltage of the operational amplifier to current and provide the high impedance output node of the current conveyor. Care should be taken in the choice of current mirrors, since they determine the allowable signal swing at terminal x.

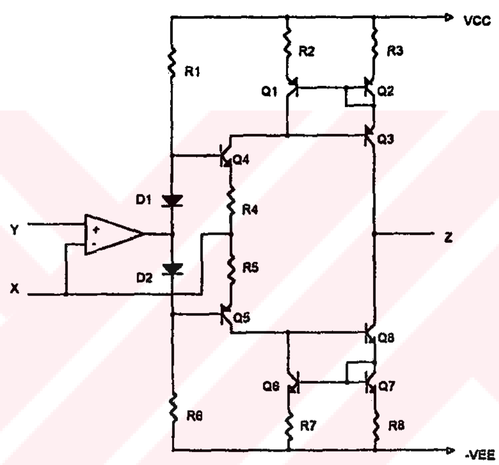

a)

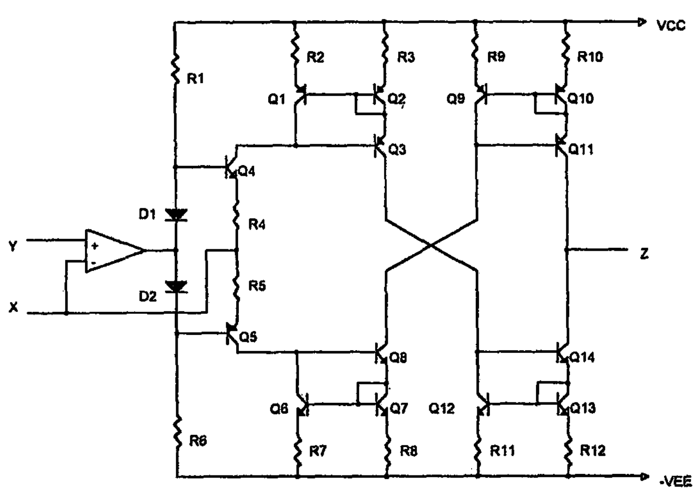

b)

Figure 3.5 a) Circuit diagram of current conveyor 3 b) Inverting type current conveyor derived from a)

The LF351 operational amplifier has been used during the measurements. Supply voltages were chosen to be ±15 V. The performance characteristics are given in Fig. 3.6, whereas the characteristic values of the current conveyor are given in Table 3.1. An inverting type current conveyor has been derived from the circuit above, to be used for later purposes. This circuit is given in Fig. 3.5b.

3.4 PERFORMANCE CHARACTERISTICS OF CURRENT CONVEYOR 4

The current controlled current conveyor described in this section [13] uses a mixed translinear loop at the input and two complementary current mirrors with adjustable gains to form output z. The circuit configuration is given in Fig. 3.7a. The currents I_a and I_b allow control of the gain, which can be varied by modifying the value of I_a. However, the value of I_b cannot be chosen arbitrarily whereas the following two equations need to be satisfied;

$$I_b \gg \frac{I_o}{G\beta_{18}}, \qquad I_b \gg \frac{GI_o}{\beta_{24}} \tag{3.1}$$

where $G = I_a / I_b$ is the gain of the current mirror, β_{18} and β_{24} are the current gains of transistors Q_{18} and Q_{24}, respectively. The circuit contains the mixed translinear loop in its voltage follower configuration. This loop is dc biased by two identical currents in such a way that input y is a high impedance port. The current flowing through port x is reproduced on output z by the two complementary current mirrors with controlled gain, in such a way that I_Z=G.I_X. The input transistors of these two current mirrors are biased by I_o. I_a is applied to the controlled mirrors by means of two supplementary current mirrors arranged in such a way as to reduce the current differences as much as possible. The circuit which controls the gain of the conveyor only acts on the output currents of the mixed loop.

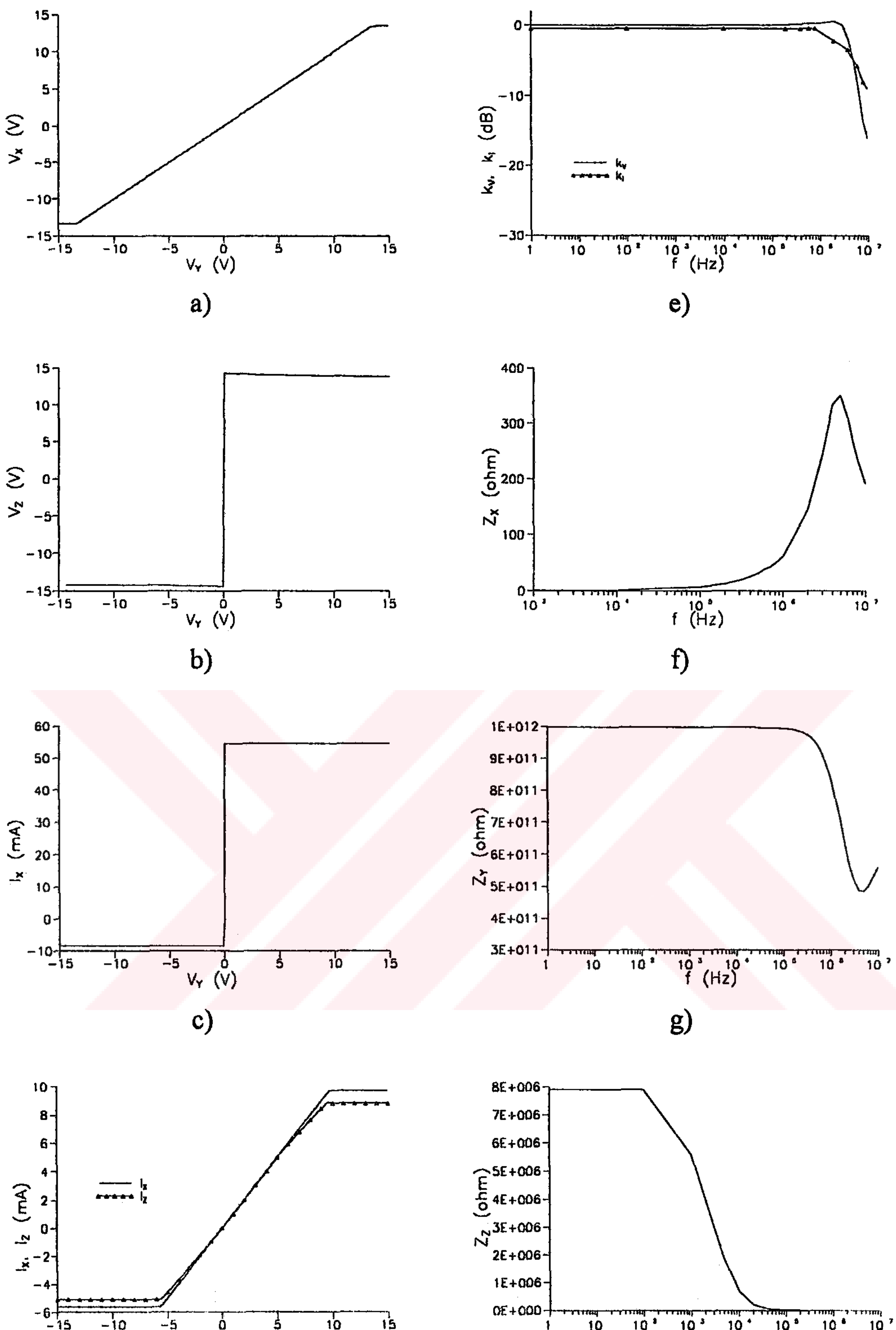

Figure 3.6 Measured device characteristics of current conveyor 3
a) $V_X = V_X(V_Y)$ for $R_X = \infty$ b) $V_Z = V_Z(V_Y)$ for $R_Z = \infty$ c) $I_X = I_X(V_Y)$ for $R_X = 0$ d) $I_X = I_X(V_Y)$, $I_Z = I_Z(V_Y)$ for $R_X = R_Z = 1$ kΩ e) The frequency responses of v_x/v_y and i_z/i_x for $R_X = R_Z = 10$ kΩ f) The frequency response of Z_X g) The frequency response of Z_Y h) The frequency response of Z_Z

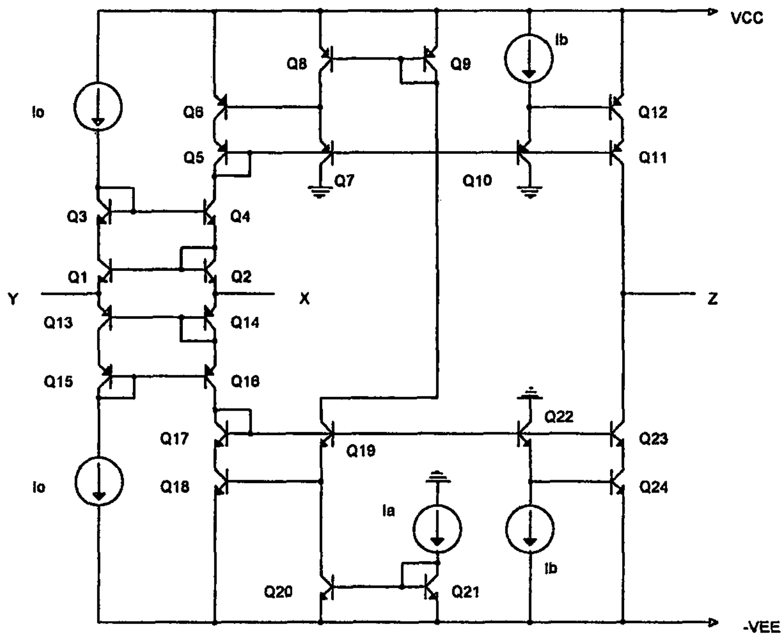

a)

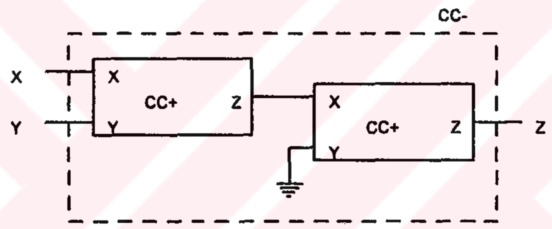

b)

Figure 3.7 a) Circuit diagram of current conveyor 4 b) Inverting type current conveyor derived from a)

SPICE simulations have been carried out to check the performance of the current conveyor. Supply voltages were chosen to be ±5 V. Currents I_o, I_a and I_b have chosen to be equal with a value of 50 μA. The performance characteristics are given in Fig. 3.8, and the characteristic values of the current conveyor are given in Table 3.1. The inverting type current conveyor to be used for later purposes, has been implemented by using two non-inverting type conveyors as shown in Fig. 3.7b.

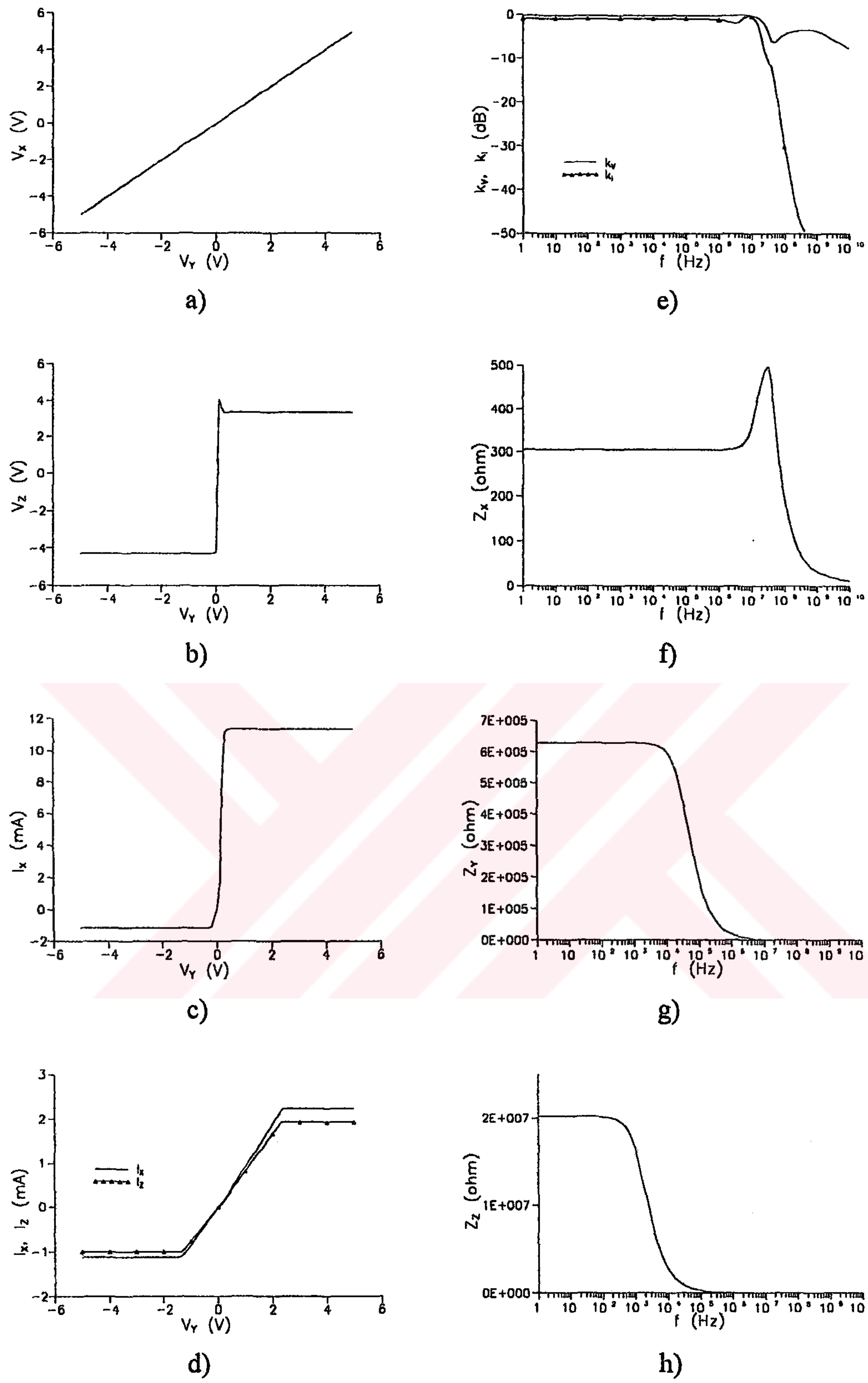

Figure 3.8 SPICE simulated device characteristics of current conveyor 4
a) $V_X = V_X(V_Y)$ for $R_X = \infty$ b) $V_Z = V_Z(V_Y)$ for $R_Z = \infty$ c) $I_X = I_X(V_Y)$ for $R_X = 0$
d) $I_X = I_X(V_Y)$, $I_Z = I_Z(V_Y)$ for $R_X = R_Z = 1\ k\Omega$ e) The frequency responses of v_x/v_y
and i_z/i_x for $R_X = R_Z = 10\ k\Omega$ f) The frequency response of Z_X g) The frequency
response of Z_Y h) The frequency response of Z_Z

3.5 PERFORMANCE CHARACTERISTICS OF CURRENT CONVEYOR 5

In this section, we will deal with one of the commercially available current conveyors, namely the AD844 circuit [4]. This circuit which belongs to a category of amplifiers known as transimpedance amplifiers or current feedback operational amplifiers (CFOA), may be regarded as a current conveyor buffered by a voltage follower, and enables the use of an internal node as an output to form a current conveyor. It overcomes the gain-bandwidth trade-off problem of a conventional operational amplifier and provides a constant bandwidth independent of the closed-loop gain. A simplified schematic of the circuit is shown in Fig. 3.9. In contrary to a conventional operational amplifier, the signal inputs have extremely different impedance levels. The non-inverting input presents the usual high impedance. The voltage at this input is transferred to the inverting input, which is the common emitter node of a complementary pair of grounded base stages and behaves like a current summing node. Ideally, the impedance of this node would be zero. It is important to understand that this low impedance is locally generated, and does not depend on feedback. This is very different from the "virtual ground" concept in a conventional operational amplifier used in the current summing mode which is essentially an open-circuit until the loop settles.

A current applied to the inverting input is transferred to a complementary pair of unity gain current mirrors which deliver the same current to an internal node of which forms the output of the current conveyor.

Basic characteristics of the current conveyor have been obtained by using the device macromodel of AD844 in SPICE simulations. A list of the macromodel is given in Appendix A. Power supply voltages have been chosen as ±10 V. The performance characteristics are given in Fig. 3.10, and the characteristic values of the current conveyor are given in Table 3.1. The inverting type current conveyor to be used for later purposes, has been implemented by using two non-inverting type conveyors as shown previously in Fig. 3.7b.

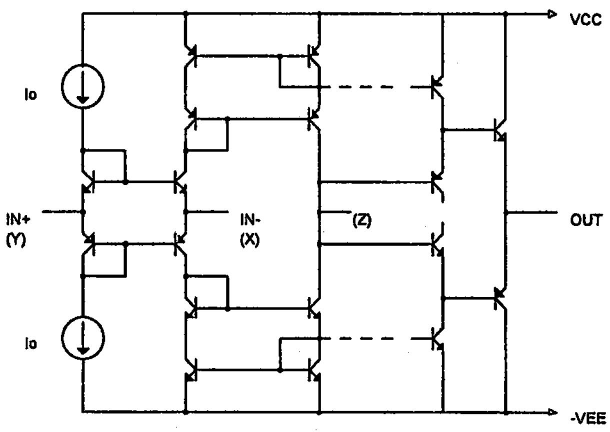

Figure 3.9 Circuit diagram of current conveyor 5

3.6 PERFORMANCE CHARACTERISTICS OF CURRENT CONVEYOR 6

In this section, a class A current conveyor will be investigated [14]. The circuit is given in Fig. 3.11a. M1 is a source follower, M2 is a level shifter, M4 and M6 are common source transistors and M3, M5, M7 are current sources. If the drain current of M3 is set to be equal to half of the drain current of M5 and M1 and M2 have the same dimensions, then the gate-source voltages of M1 and M2 will be equal and fixed to their quiescent value, which yields the voltages of terminals x and y to be equal. The current of terminal x is supplied by M4, since the drain currents of M1-M3 are fixed at their quiescent value.

SPICE simulations have been carried out to check the performance of the current conveyor. Supply voltages were chosen to be ±5 V and I_B as 100 μA. The value of the compensation capacitor is 0.5 pF. The performance characteristics are given in Fig. 3.12, whereas the characteristic values are given in Table 3.1. The inverting type current conveyor derived from the circuit above, to be used for later purposes is given in Fig. 3.11b.

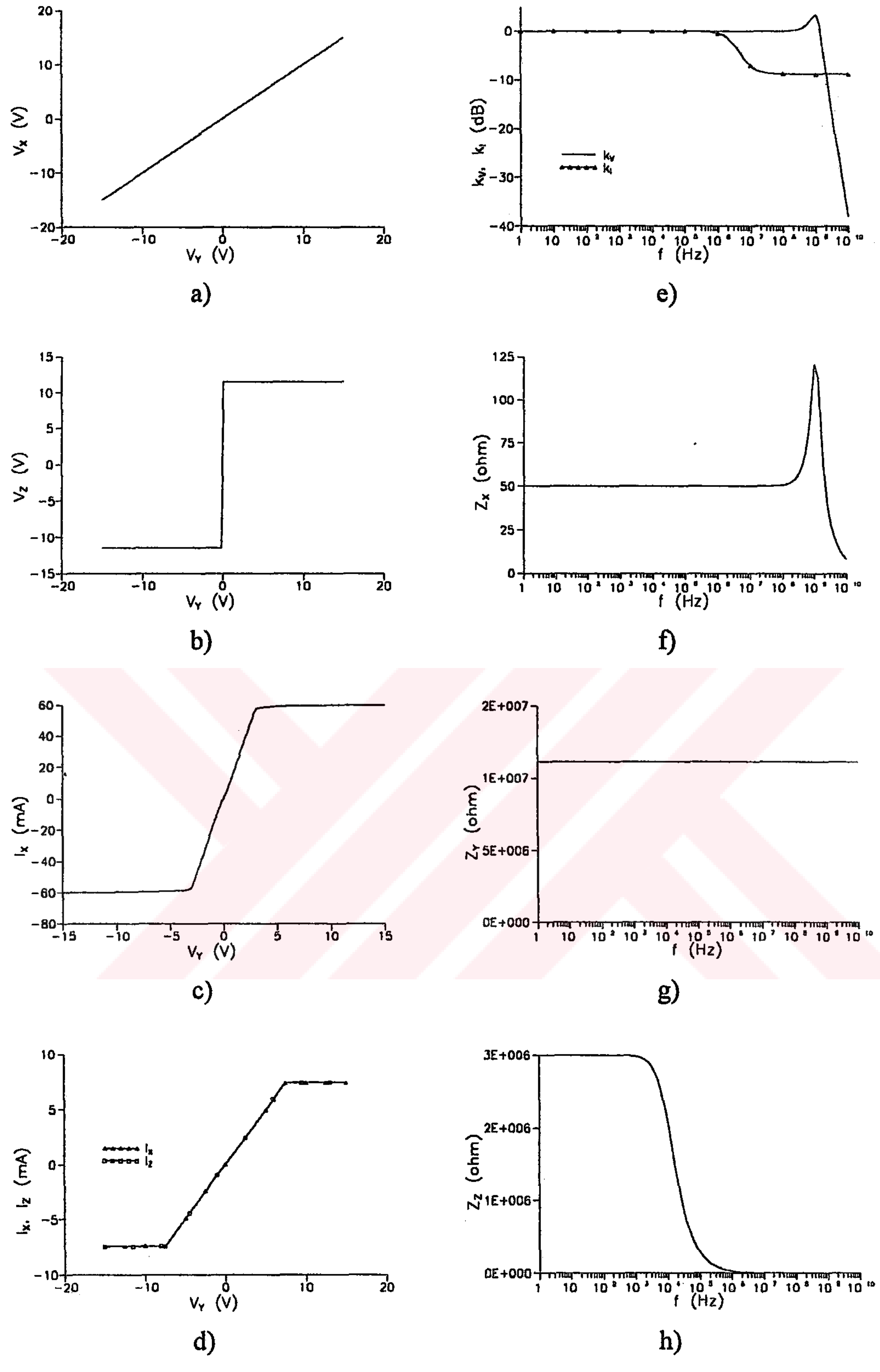

Figure 3.10 SPICE simulated device characteristics of current conveyor 5
a) $V_X = V_X(V_Y)$ for $R_X = \infty$ b) $V_Z = V_Z(V_Y)$ for $R_Z = \infty$ c) $I_X = I_X(V_Y)$ for $R_X = 0$ d) $I_X = I_X(V_Y)$, $I_Z = I_Z(V_Y)$ for $R_X = R_Z = 1k$ e) The frequency responses of v_x/v_y and i_z/i_x for $R_X = R_Z = 10\ k\Omega$ f) The frequency response of Z_X g) The frequency response of Z_Y h) The frequency response of Z_Z

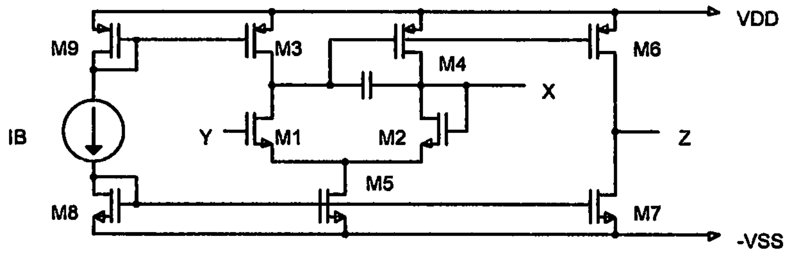

a)

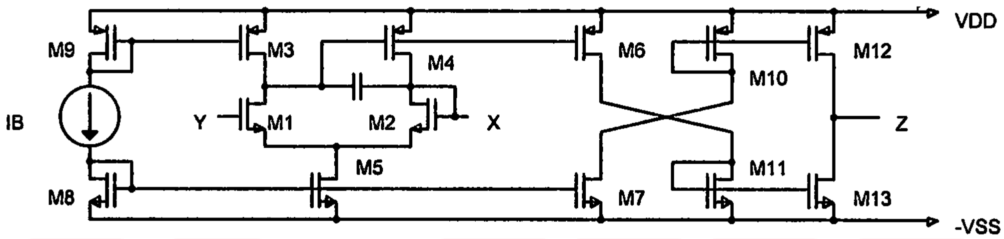

b)

Figure 3.11 a) Circuit diagram of current conveyor 6 b) Inverting type current conveyor derived from a)

3.7 PERFORMANCE CHARACTERISTICS OF CURRENT CONVEYOR 7

The circuit diagram of the wideband CMOS current conveyor investigated in this section is given in Fig. 3.13 [15]. Transistors M2-M4 and M6 form the regulated current cell for the current input and M1 forms the source follower for the voltage input. M3, M5 and M7 form the cascode current mirror which reflects the current of node x to node z. $i_Z=i_X$ is obtained, provided that transistors M3-M5 are well matched. The input impedance at node x can be made small by designing the aspect ratios of M1 and M2 accordingly. The offset voltage due to the mismatch in the threshold voltage between M1 and M2, can be nulled by adjusting the bias voltage of M1.

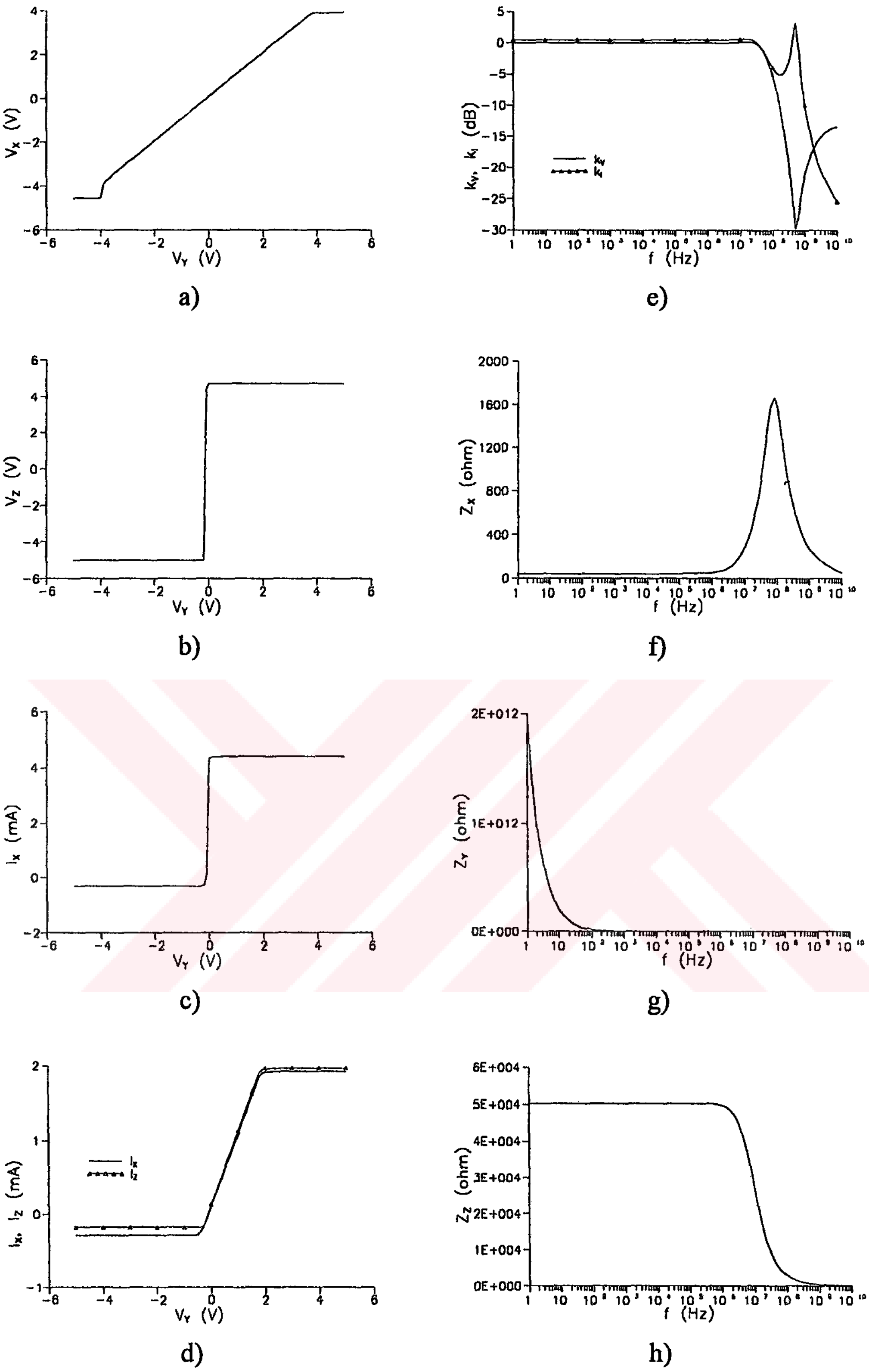

Figure 3.12 SPICE simulated device characteristics of current conveyor 6
a) $V_X = V_X(V_Y)$ for $R_X = \infty$ b) $V_Z = V_Z(V_Y)$ for $R_Z = \infty$ c) $I_X = I_X(V_Y)$ for $R_X = 0$
d) $I_X = I_X(V_Y)$, $I_Z = I_Z(V_Y)$ for $R_X = R_Z = 1$ kΩ e) The frequency responses of v_x/v_y and i_z/i_x for $R_X = R_Z = 10$ kΩ f) The frequency response of Z_X g) The frequency response of Z_Y h) The frequency response of Z_Z

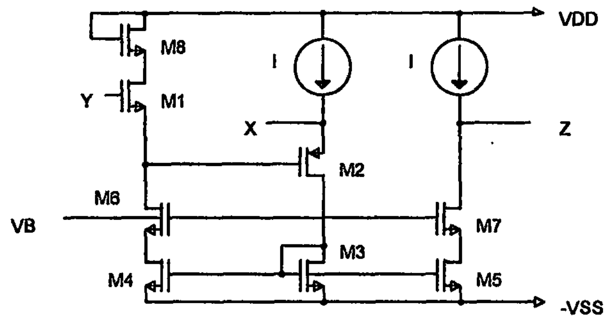

Figure 3.13 Circuit diagram of current conveyor 7

SPICE simulations have been carried out to check the performance of the current conveyor. Supply voltages were ±5 V and V_B= -2.5 V, while I=300 μA. The performance characteristics are given in Fig. 3.14, whereas the characteristic values are given in Table 3.1. The inverting type current conveyor to be used for later purposes, has been implemented by using two non-inverting type conveyors as shown previously in Fig. 3.7b.

3.8 PERFORMANCE CHARACTERISTICS OF CURRENT CONVEYOR 8

In this section, a class AB current conveyor using a floating voltage source is investigated [16]. The circuit is given in Fig. 3.15. The transistors M3 and M4 form two grounded-gate amplifiers, and isolate the gates of M5 and M6. This introduces a negative feedback at the input which reduces the input resistance and also makes it possible to connect a floating voltage source between the gates of M5 and M6. The transistors M1-M4 form a translinear loop, thus they have equal currents, which means the current $I_{B2} - I_{B1}$ flows in M9. The input offset current is determined by the current difference between the current sources I_{B2}. It is suggested that M9 be isolated in its own well, in order to avoid any threshold voltage variation problems.

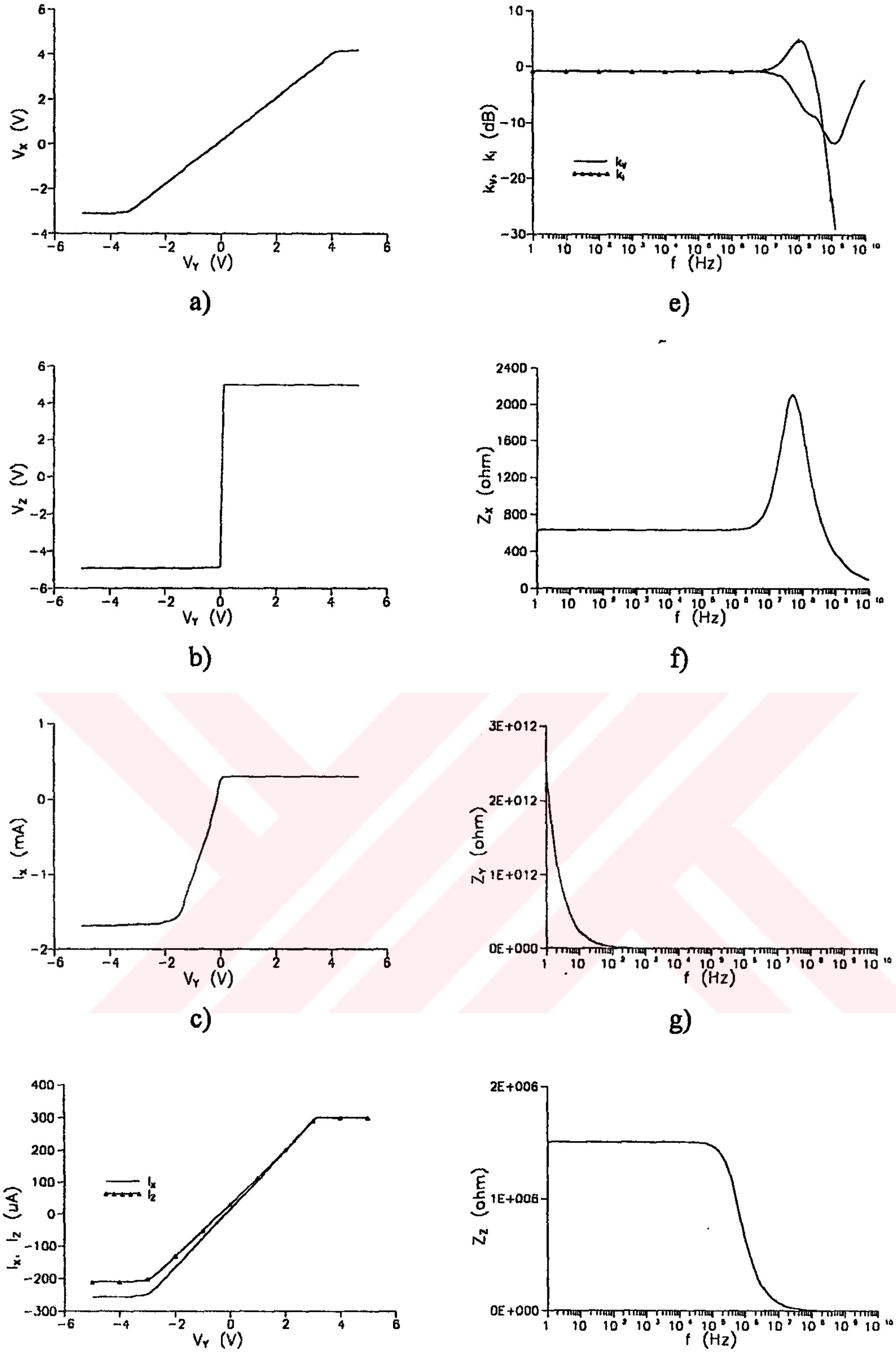

Figure 3.14 SPICE simulated device characteristics of current conveyor 7
a) $V_X = V_X(V_Y)$ for $R_X = \infty$ b) $V_Z = V_Z(V_Y)$ for $R_Z = \infty$ c) $I_X = I_X(V_Y)$ for $R_X = 0$ d) $I_X = I_X(V_Y)$, $I_Z = I_Z(V_Y)$ for $R_X = R_Z = 10\ k\Omega$ e) The frequency responses of v_x / v_y and i_z / i_x for $R_X = R_Z = 10\ k\Omega$ f) The frequency response of Z_X g) The frequency response of Z_Y h) The frequency response of Z_Z

SPICE simulations have been carried out to obtain the device characteristics. Supply voltages were chosen to be ±1.8 V and I_{B1}=50 μA, I_{B2}=100 μA. The performance characteristics are given in Fig. 3.16, whereas the characteristic values are given in Table 3.1. The inverting type current conveyor derived from the circuit above, to be used for later purposes is given in Fig. 3.15b.

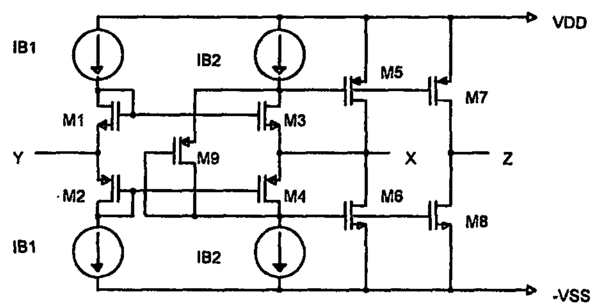

a)

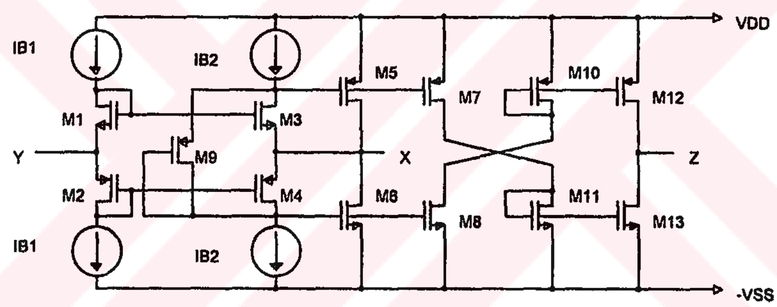

b)

Figure 3.15 a) Circuit diagram of current conveyor 8 b) Inverting type current conveyor derived from a)

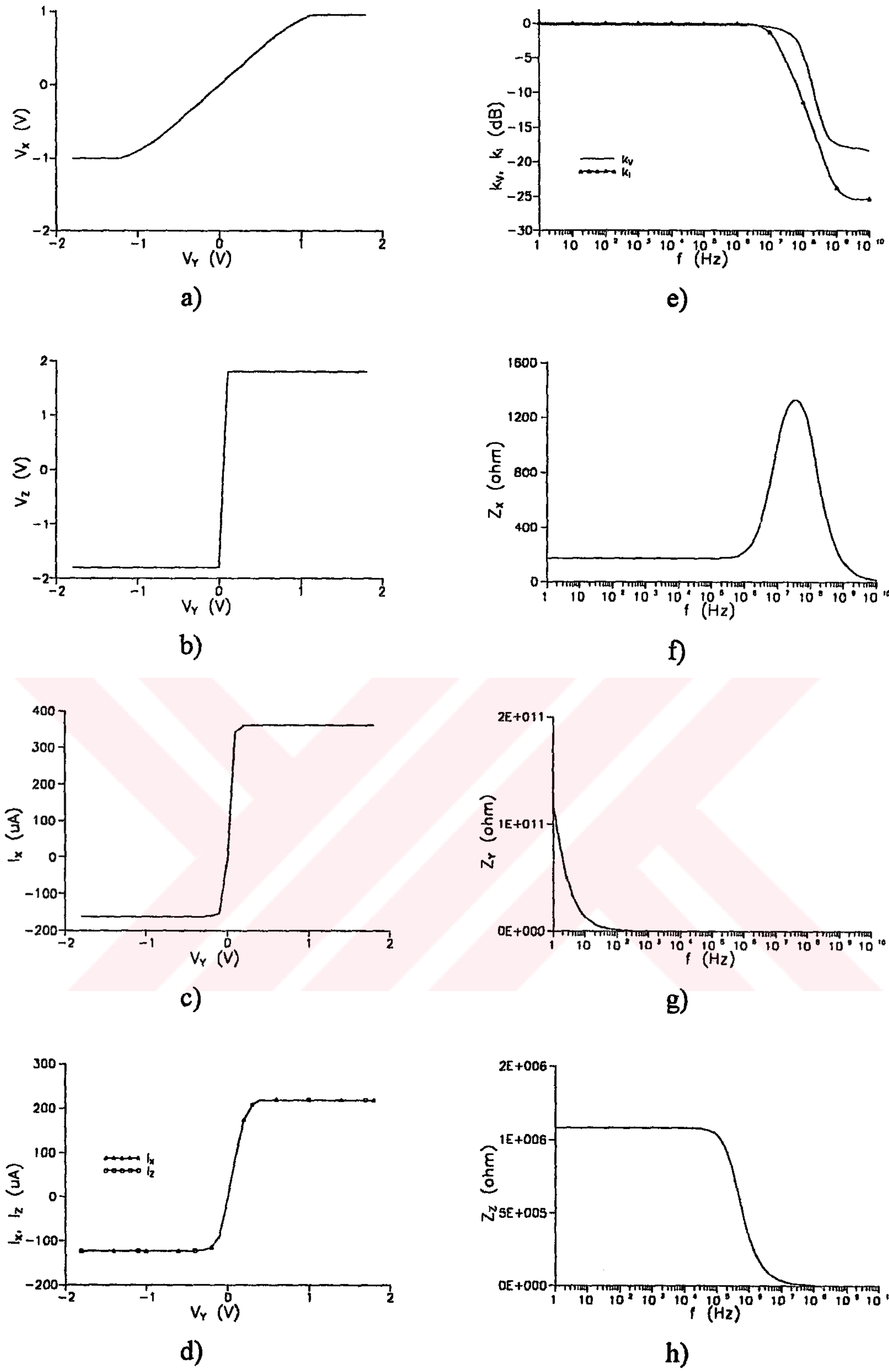

Figure 3.16 SPICE simulated device characteristics of current conveyor 8
a) $V_X = V_X(V_Y)$ for $R_X = \infty$ b) $V_Z = V_Z(V_Y)$ for $R_Z = \infty$ c) $I_X = I_X(V_Y)$ for $R_X = 0$ d) $I_X = I_X(V_Y)$, $I_Z = I_Z(V_Y)$ for $R_X = R_Z = 1\ k\Omega$ e) The frequency responses of v_x/v_y and i_z/i_x for $R_X = R_Z = 10\ k\Omega$ f) The frequency response of Z_X g) The frequency response of Z_Y h) The frequency response of Z_Z

CHAPTER 4

THE EFFECTS OF CURRENT CONVEYOR NON-IDEALITIES ON A VOLTAGE-MODE ACTIVE FILTER

The function of a filter is to provide a frequency-weighted transmission of analog signals. Signals falling within selected regions of the frequency spectrum are attenuated or amplified selectively, relative to those in other parts of the spectrum. The term active filter refers to a filter that incorporates active devices in its schematic. Typically, in such a filter, active circuits replace the function of inductors in what would otherwise be a RLC circuit. In the design of frequency selective integrated circuits, the lack of inductors is a serious disadvantage. In many applications, this drawback can be overcome by using conventional active RC filter techniques. In designing active RC filters, one uses a combination of resistors, capacitors and gain blocks in linear feedback loops to obtain the desired frequency selectivity without the need for inductors.

In this study, active filters using the current conveyor as the active component, will be covered. Effects of current conveyor non-idealities on both voltage and current-mode active filters will be investigated. Limit values of non-ideality terms will be determined. This chapter will be devoted to the effects on voltage-mode filters. The first section will discover the effect of each non-ideality term on the filter characteristics. A comparable demonstration of the filter performances for each current conveyor circuit studied in Chapter 3, will be given in the second section. Chapter 5 will include the same analysis for current-mode filters.

4.1 THE EFFECTS OF CURRENT CONVEYOR NON-IDEALITIES ON FILTER CHARACTERISTICS

In this section, the effects of current conveyor non-idealities on voltage-mode filter characteristics will be investigated. The biquadratic filter configuration chosen for this purpose has been given in Fig. 4.1 [17]. The ideal transfer function of the filter given in terms of circuit components is as follows:

$$\frac{V_O}{V_I} = \frac{C_1C_2s^2 + C_1G_4s + G_1G_3}{C_1C_3s^2 + C_1G_5s + G_2G_3} \tag{4.1}$$

It is apparent that the bandpass, lowpass and highpass configurations of the filter are obtained for $G_1 = 0$, $C_2 = 0$; $G_1 = 0$, $G_4 = 0$ and $C_2 = 0$, $G_4 = 0$, respectively. The filter parameters are given by the following expressions;

$$w_O = \sqrt{\frac{G_2G_3}{C_1C_3}} \tag{4.2}$$

$$Q_O = \frac{1}{G_5}\sqrt{\frac{G_2G_3C_3}{C_1}} \tag{4.3}$$

$$H_{BP} = \frac{G_4}{G_5} \qquad H_{LP} = \frac{G_1}{G_2} \qquad H_{HP} = \frac{C_2}{C_3} \tag{4.4}$$

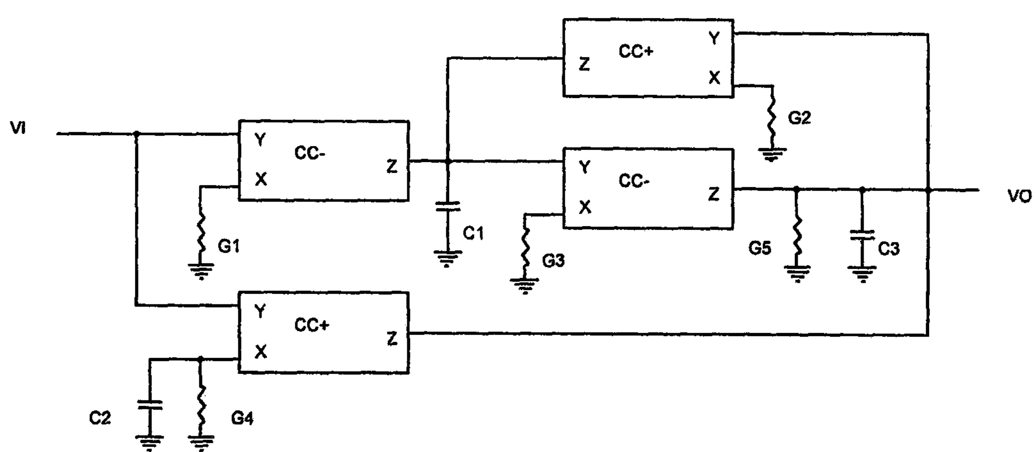

Figure 4.1 A voltage-mode biquadratic filter configuration

where ω_O denotes the angular cutoff frequency (in case of bandpass filter the resonant frequency), Q_O the quality factor, and H the gain of the related type of filter.

The component values for all three filters have been considered for a maximally flat Butterworth filter, with unity gain; thus $Q_O = 1/\sqrt{2}$ and H=1. For f_O =10 kHz; the component values are $R_2 = R_3 = R_4 = R_5 = 10$ kΩ, $C_1 = 2.25$ nF, $C_3 = 1.125$ nF for the bandpass filter, $R_1 = R_2 = R_3 = R_5 = 10$ kΩ, $C_1 = 2.25$ nF, $C_3 = 1.125$ nF for the lowpass filter and $R_2 = R_3 = R_5 = 10$ kΩ, $C_1 = 2.25$ nF, $C_2 = C_3 = 1.125$ nF for the highpass filter.

By using the results obtained in Chapter 2, one can express the non-ideality terms of a current conveyor as follows;

$$Z_X = Z_{XO} \frac{a_1 s + a_0}{s^2 + b_1 s + b_0} \tag{4.5}$$

$$k_V = k_{VO} \frac{1}{1 + s\tau_V} \tag{4.6}$$

$$k_I = k_{IO} \frac{1}{1 + s\tau_I} \tag{4.7}$$

$$Y_Z = sC_Z + g_Z \tag{4.8}$$

where

$$a_1 = \frac{\omega_{PX}^{\ 2}}{\omega_{ZX}} \tag{4.9a}$$

$$a_0 = b_0 = \omega_{PX}^{\ 2} \tag{4.9b}$$

$$b_1 = \frac{\omega_{PX}}{Q_{PX}} \tag{4.9c}$$

$$\tau_V = \frac{1}{2\pi f_V} \tag{4.9d}$$

$$\tau_I = \frac{1}{2\pi f_I} \tag{4.9e}$$

In the above equations; Z_{XO}, k_{VO} and k_{IO} denote their corresponding low frequency values, ω_{PX} and ω_{ZX} the angular pole and zero frequencies, respectively, and Q_{PX} the quality factor of the frequency dependent impedance of terminal x, whereas f_V and f_I denote the 3 dB bandwidths of the voltage and current transfer functions, respectively.

Although Eq. 2.6 indicates a second order characteristic for the voltage transfer function of a current conveyor, in the analysis below, it will be reduced to a first order approximation for simplicity reasons. Also, various investigations have shown that the high impedance of terminal y is one of the easiest requirements to be met in the design of a current conveyor, which has led the way to this term to be neglected.

If we introduce the above four non-ideality terms into Eq. 4.1, the first step gives us the non-ideal voltage transfer function of the filter as follows;

$$\frac{V_O}{V_I} = \frac{m_2 s^2 + m_1 s + m_0}{n_3 s^3 + n_2 s^2 + n_1 s + n_0} \tag{4.10}$$

where

$$m_2 = C_1 C_2 G_3 k_I k_V ABD \tag{4.11a}$$

$$m_1 = G_3 k_I k_V B(AD(G_4 C_1 + C_2 Y_Z) + C_2 Z_X G_1 G_3 k_I k_V) \tag{4.11b}$$

$$m_0 = G_3 k_I k_V B(ADG_4 Y_Z + G_1 G_3 k_I k_V E) \tag{4.11c}$$

$$n_3 = C_1 C_2 C_3 G_3 Z_X ABD \tag{4.11d}$$

$$n_2 = C_1 C_3 G_3 ABDE + C_2 G_3 Z_X ABD(C_1 F + C_3 Y_Z) \tag{4.11e}$$

$$n_1 = C_2 G_3 Z_X A(BDFY_Z + G_2 G_3 (k_I k_V)^2) + G_3 ABDE(C_1 F + C_3 Y_Z) \tag{4.11f}$$

$$n_0 = G_3 AE(BDFY_Z + G_2 G_3 (k_I k_V)^2) \tag{4.11g}$$

and

$$A = Z_X G_1 + 1 \tag{4.12a}$$

$$B = Z_X G_2 + 1 \tag{4.12b}$$

$$C = Z_X G_3 + 1 \tag{4.12c}$$

$$D = Z_X G_4 + 1 \tag{4.12d}$$

$$F = G_5 + Y_Z \tag{4.12e}$$

Substituting Eqs. (4.5) and (4.8) into expressions A, B, D, E, F, and then together with Eqs. (4.6) and (4.7) into Eq. (4.10) yields the final transfer function in the form of

$$\frac{V_O}{V_I} = \frac{p_{12}s^{12} + p_{11}s^{11} + \ldots + p_4 s^4 + p_3 s^3 + p_2 s^2 + p_1 s + p_0}{q_{14}s^{14} + q_{13}s^{13} + \ldots + q_4 s^4 + q_3 s^3 + q_2 s^2 + q_1 s + q_0} \tag{4.13}$$

It is clear that the transfer function above will give us no information about how the filter characteristics and parameters will be affected. Therefore, each non-ideality term will be analyzed independently. Now, let us investigate the contribution of each non-ideality term to the transfer function above.

4.1.1 The Effect of r_X

The effect of the resistive component of the impedance of terminal x has been studied in this section. First, our analysis will focus on the bandpass type filter. Arrangements on Eq. 4.10 gives us the effect of r_X on the transfer function as

$$\left(\frac{V_O}{V_I}\right)_{BP} = \frac{\dfrac{G_4}{C_3}\dfrac{1}{r_X G_4 + 1}s}{s^2 + \dfrac{G_5}{C_3}s + \dfrac{G_2 G_3}{C_1 C_3}\dfrac{1}{(r_X G_2 + 1)(r_X G_3 + 1)}} \tag{4.14}$$

The relative deviation in each filter parameter can be derived from Eq. 4.14 as

$$\left|\frac{\Delta\omega_{OBP}}{\omega_{OBP}}\right| = \sqrt{\frac{1}{(r_X G_2 + 1)(r_X G_3 + 1)}} - 1 = \frac{r_X G}{r_X G + 1} \tag{4.15}$$

$$\left|\frac{\Delta Q_{OBP}}{Q_{OBP}}\right| = \sqrt{\frac{1}{(r_X G_2 + 1)(r_X G_3 + 1)}} - 1 = \frac{r_X G}{r_X G + 1} \tag{4.16}$$

$$\left|\frac{\Delta H_{BP}}{H_{BP}}\right| = \frac{r_X G_4}{r_X G_4 + 1} = \frac{r_X G}{r_X G + 1} \tag{4.17}$$

for $G = G_2 = G_3 = G_4$. It is apparent from Eqs. 4.15 through 4.17 that the condition of $r_X G \ll 1$ should be satisfied for small deviations in the resonant frequency, quality factor and filter gain.

The repetition of the above analysis for the lowpass filter yields the following transfer function and filter parameter deviations

$$\left(\frac{V_O}{V_I}\right)_{LP} = \frac{\dfrac{G_1}{C_1}\dfrac{1}{(r_X G_1 + 1)(r_X G_3 + 1)}}{s^2 + \dfrac{G_5}{C_3}s + \dfrac{G_2 G_3}{C_1 C_3}\dfrac{1}{(r_X G_2 + 1)(r_X G_3 + 1)}} \tag{4.18}$$

$$\left|\frac{\Delta \omega_{OLP}}{\omega_{OLP}}\right| = \sqrt{\frac{1}{(r_X G_2 + 1)(r_X G_3 + 1)}} - 1 = \frac{r_X G}{r_X G + 1} \tag{4.19}$$

$$\left|\frac{\Delta Q_{OLP}}{Q_{OLP}}\right| = \sqrt{\frac{1}{(r_X G_2 + 1)(r_X G_3 + 1)}} - 1 = \frac{r_X G}{r_X G + 1} \tag{4.20}$$

$$\left|\frac{\Delta H_{LP}}{H_{LP}}\right| = \frac{r_X G_2 + 1}{r_X G_1 + 1} - 1 = 0 \tag{4.21}$$

for $G = G_1 = G_2 = G_3$. As in the case of a bandpass filter, the condition of $r_X G \ll 1$ should be satisfied for small deviations in the cutoff frequency and quality factor. Eq. 4.21 yields that the filter gain is not affected by the resistance of terminal x.

However, the results obtained for the highpass filter are somewhat different than that of the previous type of filters. In this case, the analysis yields a third order transfer function as follows:

$$\left(\frac{V_O}{V_I}\right)_{HP} = \frac{\dfrac{1}{C_3 r_X} s^2}{\left(s + \dfrac{1}{C_2 r_X}\right)\left[s^2 + \dfrac{G_5}{C_3} s + \dfrac{G_2 G_3}{C_1 C_3} \dfrac{1}{(r_X G_2 + 1)(r_X G_3 + 1)}\right]} \tag{4.22}$$

It is obvious that an extra pole has emerged in the transfer function. However, provided that the corresponding frequency is high enough with respect to the filter cutoff frequency, the relative deviations in the filter parameters will be determined by the following expressions

$$\left|\frac{\Delta\omega_{OHP}}{\omega_{OHP}}\right| = \sqrt{\frac{1}{(r_X G_2 + 1)(r_X G_3 + 1)}} - 1 = \frac{r_X G}{r_X G + 1} \tag{4.23}$$

$$\left|\frac{\Delta Q_{OHP}}{Q_{OHP}}\right| = \sqrt{\frac{1}{(r_X G_2 + 1)(r_X G_3 + 1)}} - 1 = \frac{r_X G}{r_X G + 1} \tag{4.24}$$

for $G = G_2 = G_3$. Again, the condition of $r_X G \ll 1$ should be satisfied for small deviations in the cutoff frequency and quality factor.

SPICE simulations have been carried out in order to prove the results obtained above. Results for four different values of r_X, namely, $r_X = 10\ \Omega$, $100\ \Omega$, $1\ k\Omega$, $10\ k\Omega$ and two different cutoff frequencies of $f_O = 10$ kHz, 10 MHz have been demonstrated in Fig. 4.2.

4.1.2 The Effect of Y_Z

The effect of the admittance of terminal z has been studied in this section. We will start our analysis with the bandpass type filter. Arrangements on Eq. 4.10 gives us the effect of Y_Z on the transfer function as

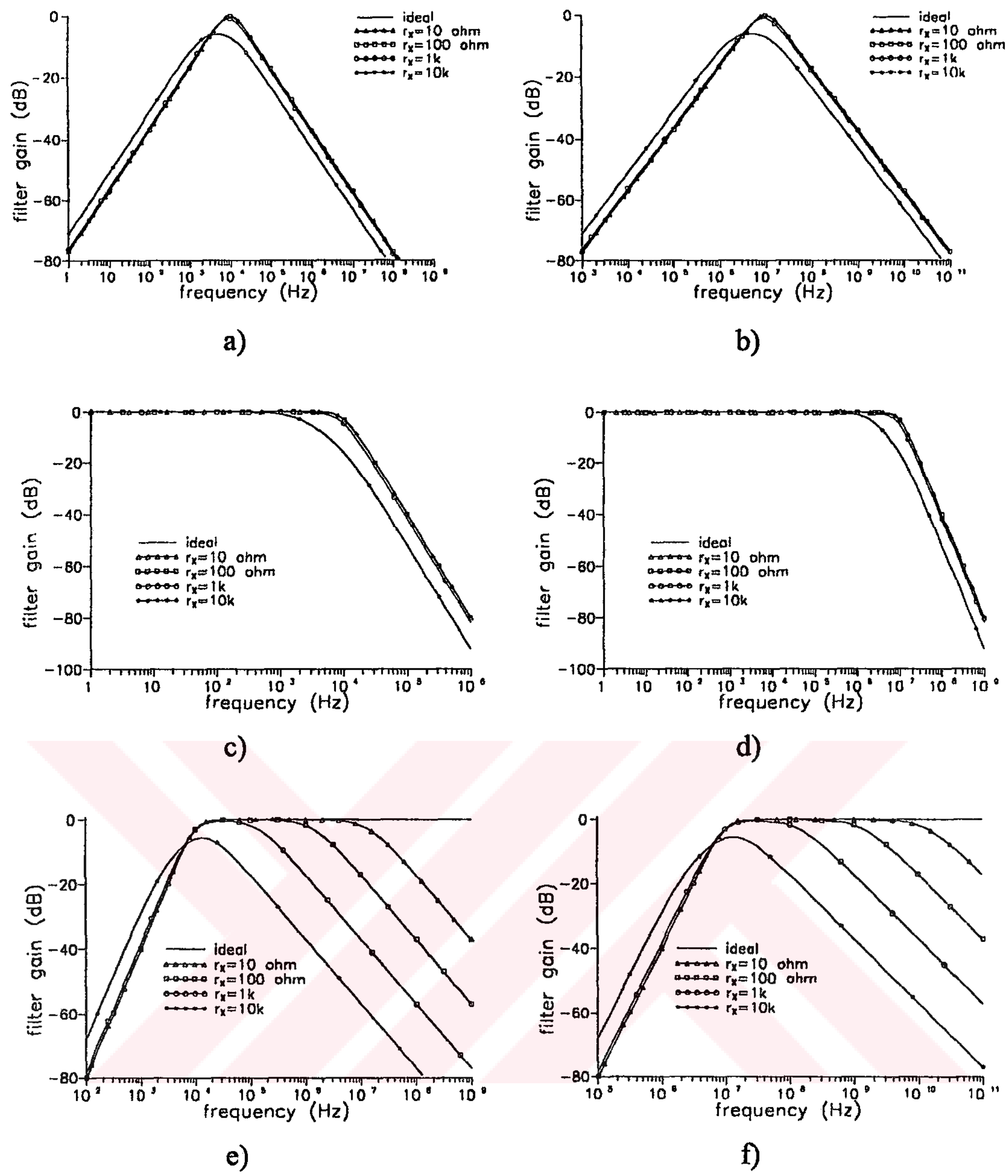

Figure 4.2 The effect of r_X on filter characteristics a) Bandpass filter of f_O =10 kHz b) Bandpass filter of f_O =10 MHz c) Lowpass filter of f_O =10 kHz d) Lowpass filter of f_O =10 MHz e) Highpass filter of f_O =10 kHz f) Highpass filter of f_O =10 MHz

$$\left(\frac{V_O}{V_I}\right)_{BP} = \frac{(C_1 + C_Z)G_4 s + g_Z G_4}{d_2 s^2 + d_1 s + d_0} \tag{4.25}$$

where

$$d_2 = C_1C_3 + C_Z(C_1 + C_3 + C_Z) \tag{4.26a}$$

$$d_1 = C_1G_5 + g_Z(C_1 + C_3) + C_Z(G_5 + 2g_Z) \tag{4.26b}$$

$$d_0 = G_2G_3 + g_Z(g_Z + G_5) \tag{4.26c}$$

The relative deviation in each filter parameter can be derived from Eq. 4.25 as

$$\left|\frac{\Delta\omega_{OBP}}{\omega_{OBP}}\right| = \sqrt{\frac{1+\frac{g_Z(g_Z+G_5)}{G_2G_3}}{1+\frac{C_Z(C_1+C_3+C_Z)}{C_1C_3}}} - 1 \tag{4.27}$$

$$\left|\frac{\Delta Q_{OBP}}{Q_{OBP}}\right| = \frac{1}{1+\frac{g_Z(C_1+C_3)+C_Z(G_5+2g_Z)}{C_1G_5}}\sqrt{\left(1+\frac{g_Z(g_Z+G_5)}{G_2G_3}\right)\left(1+\frac{C_Z(C_1+C_3+C_Z)}{C_1C_3}\right)} - 1 \tag{4.28}$$

$$\left|\frac{\Delta H_{BP}}{H_{BP}}\right| = \frac{1+\frac{C_Z}{C_1}}{1+\frac{g_Z(C_1+C_3)+C_Z(G_5+2g_Z)}{C_1G_5}} - 1 \tag{4.29}$$

Eqs. 4.27 through 4.29 yields that, an adjustment in the values of G_5, C_1 and C_3 can help reducing the filter parameter deviations.

The repetition of the above analysis for the lowpass filter gives us the following transfer function:

$$\left(\frac{V_O}{V_I}\right)_{LP} = \frac{G_1G_3}{d_2s^2 + d_1s + d_0} \tag{4.30}$$

where the denominator coefficients are as given in Eq. 4.26. Since the denominator of the transfer functions in Eqs. 4.25 and 4.30 are the same, the relative deviations in the cutoff frequency and quality factor for the lowpass filter can be given as in Eqs. 4.27 and 4.28, respectively. The relative deviation in the filter gain is obtained as follows:

$$\left|\frac{\Delta H_{LP}}{H_{LP}}\right| = \frac{1}{1+\dfrac{g_Z(G_s+g_Z)}{G_2G_3}} - 1 \tag{4.31}$$

Eq. 4.31 yields that the filter gain is only affected by the resistive part of the impedance of terminal z.

The transfer function of the highpass filter is obtained as follows:

$$\left(\frac{V_O}{V_I}\right)_{HP} = \frac{C_2(C_1+C_Z)s^2 + g_Z C_2 s}{d_2 s^2 + d_1 s + d_0} \tag{4.32}$$

The denominator coefficients are as given in Eq. 4.26. Since the above equation has the same denominator as the previous filter types, the relative deviations in the cutoff frequency and quality factor will be as given in Eqs. 4.27 and 4.28, respectively. The relative deviation in the filter gain can be expressed as follows:

$$\left|\frac{\Delta H_{HP}}{H_{HP}}\right| = \frac{1+\dfrac{C_Z}{C_3}}{1+\dfrac{C_Z(C_1+C_3+C_Z)}{C_1C_3}} - 1 \tag{4.33}$$

It is apparent that only the capacitive part of the output impedance has an affect on the filter gain.

SPICE simulations have been carried out in order to check the results obtained above. Results for four different values of r_Z, namely, r_Z=100 kΩ, 1 MΩ, 10 MΩ, 100 MΩ; four different values of C_Z, namely C_Z= 1 pF, 10 pF, 100 pF, 1 nF and four different cutoff frequencies of f_O =10 kHz, 100 kHz, 1 MHz, 10 MHz have been demonstrated in Figs. 4.3, 4.4 and 4.5.

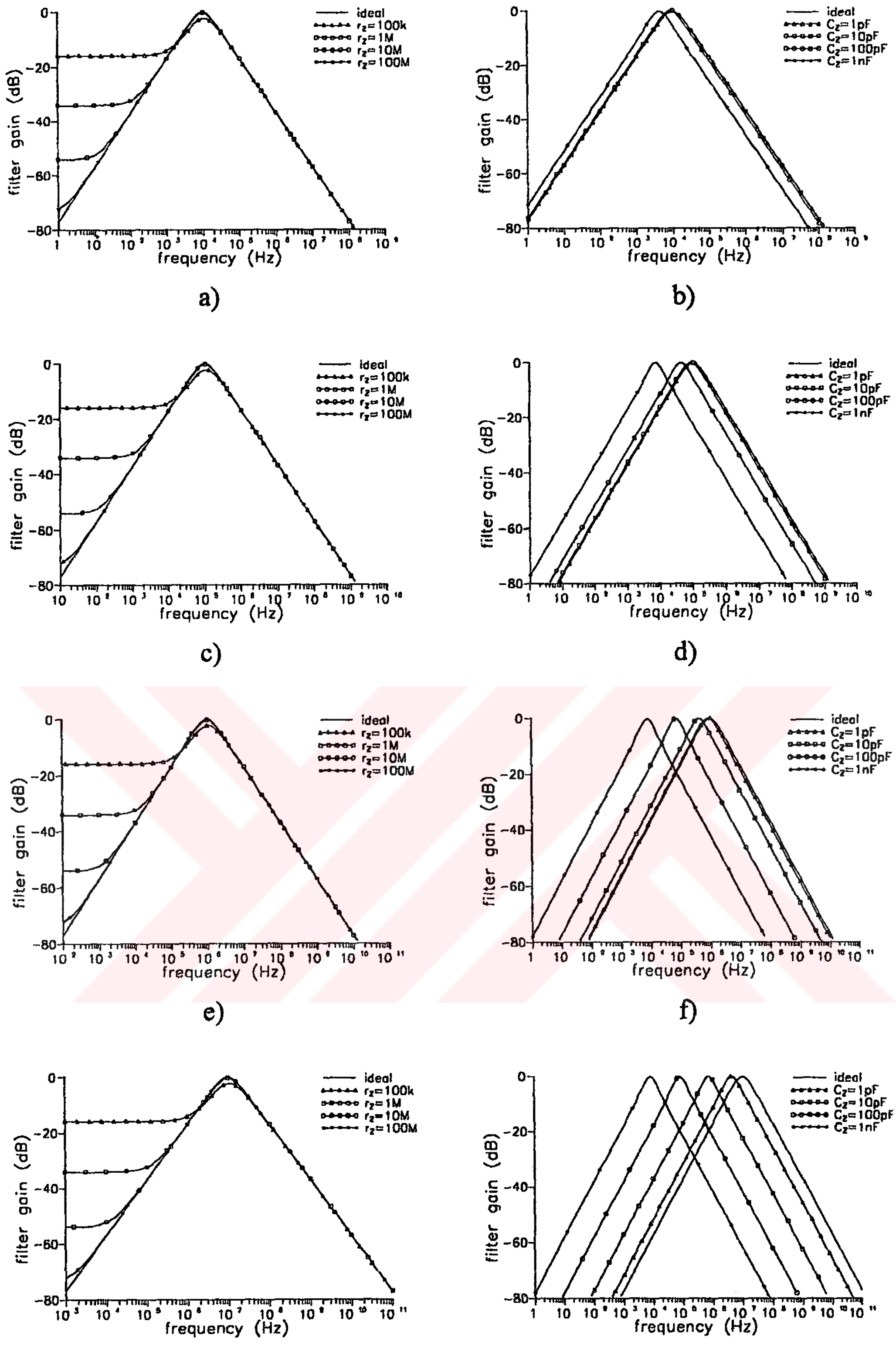

Figure 4.3 The effect of r_Z and C_Z on the bandpass filter characteristics
a) and b) f_O =10 kHz c) and d) f_O =100 kHz e) and f) f_O =1 MHz g) and h) f_O =10 MHz

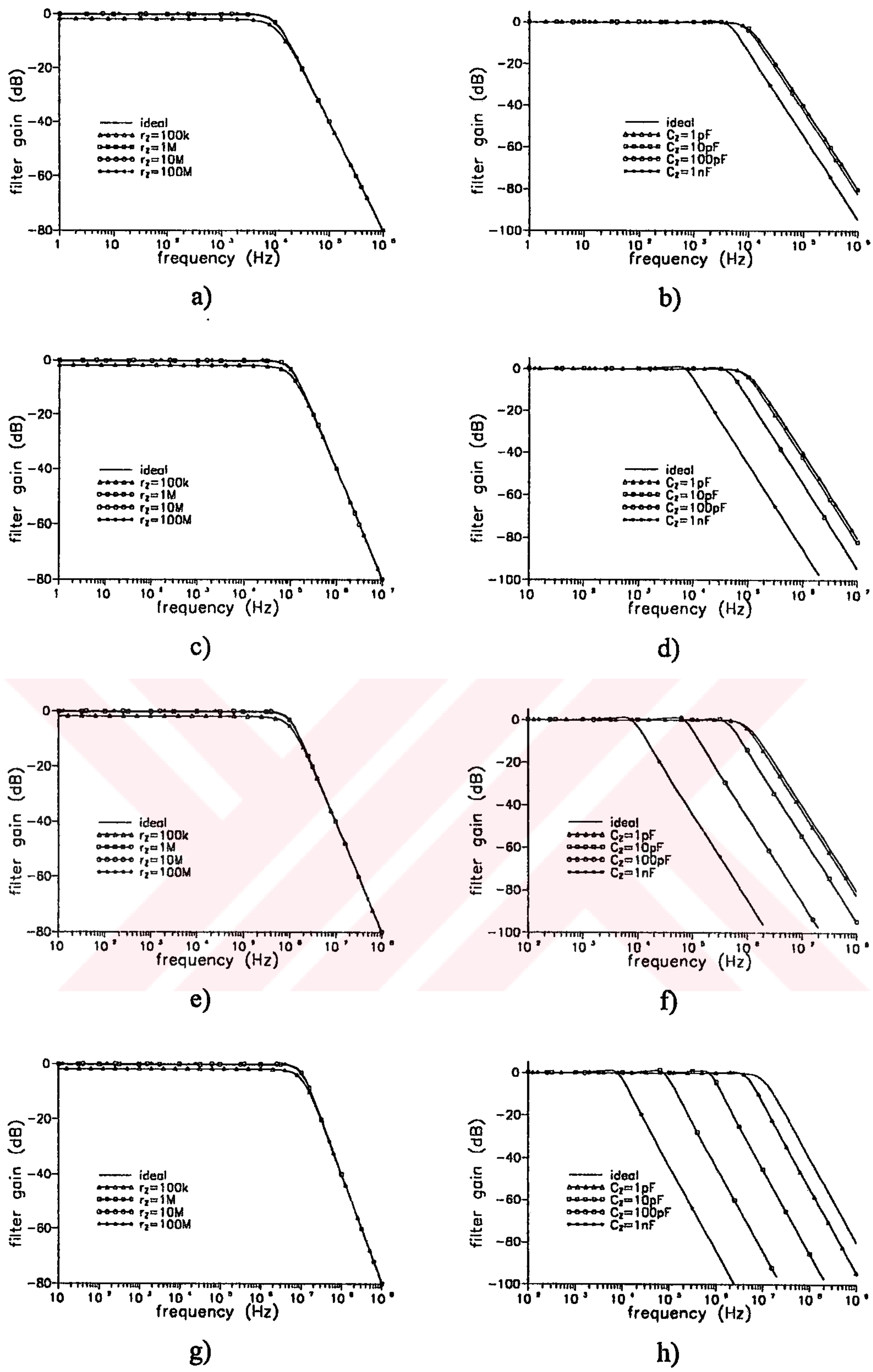

Figure 4.4 The effect of r_Z and C_Z on the lowpass filter characteristics
a) and b) f_O =10 kHz c) and d) f_O =100 kHz e) and f) f_O =1 MHz g) and h) f_O =10 MHz

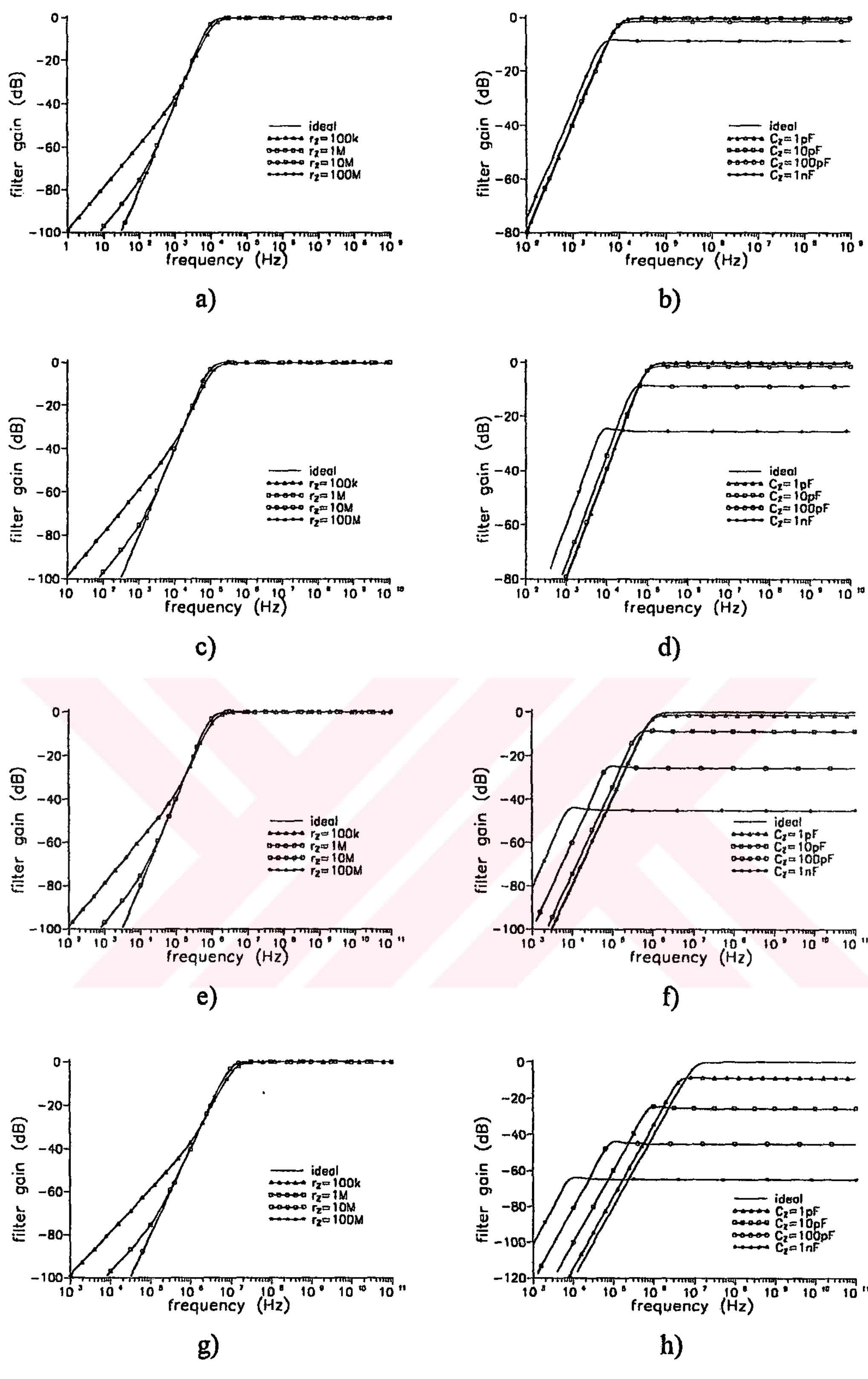

Figure 4.5 The effect of r_Z and C_Z on the highpass filter characteristics
a) and b) f_O =10 kHz c) and d) f_O =100 kHz e) and f) f_O =1 MHz g) and h) f_O =10 MHz

4.1.3 The Effect of k_I (k_V)

Since the effects of the voltage and current transfer functions of a current conveyor on the filter characteristics are identical, only the current transfer function has been studied in this section. Once again, we will start our analysis with the bandpass type filter. Arrangements on Eq. 4.10 gives us the effect of k_I on the transfer function as

$$\left(\frac{V_O}{V_I}\right)_{BP} = \frac{C_1 G_4 k_{IO} s(1+s\tau_I)}{2\tau_I C_1 C_3 s^3 + (C_1 C_3 + 2\tau_I C_1 G_5)s^2 + C_1 G_5 s + G_2 G_3 k_{IO}{}^2} \tag{4.34}$$

provided that the condition of $s\tau_I << 1$ is satisfied. It is obvious that an extra pole determined by τ_I appears in the filter characteristic and a shift occurs in the location of the complex pole pair. Now, let us consider the effect of τ_I on the filter parameters. The third order polynomial of the denominator given in Eq. 4.34 can be written in terms of the ideal resonant frequency and quality factor as below:

$$\hat{D}(s) = 2\tau_I s^3 + (1 + 2\tau_I \frac{\omega_O}{Q_O})s^2 + \frac{\omega_O}{Q_O}s + \omega_O{}^2 k_{IO}{}^2 \tag{4.35}$$

Application of the Routh-Hurwitz test to Eq. 4.35 shows that there is no stability problem caused by the poles. The deviation in the pole can be estimated by the following expression [33,34]:

$$\frac{\Delta p}{p} = -\left.\frac{\dfrac{\partial \hat{D}(s)}{\partial \tau_I}}{s\dfrac{\partial \hat{D}(s)}{\partial s}}\right|_{s\to p,\ \tau_I\to 0} .\tau_I \tag{4.36}$$

where the pole can be expressed as

$$p = \omega_O \left(-\frac{1}{2Q_O} + j\sqrt{1 - \frac{1}{4{Q_O}^2}} \right) \tag{4.37}$$

Substituting the related polynomials into Eq. 4.36 yields the deviation in the pole as below, provided that k_{IO}=1:

$$\frac{\Delta p}{p} = -j2\tau_I \omega_O \frac{Q_O}{\sqrt{4{Q_O}^2 - 1}} \tag{4.38}$$

The deviations in the cutoff frequency and quality factor can be estimated by [33,34];

$$\frac{\Delta \omega_O}{\omega_O} = \mathrm{Re}\left\{ \frac{\Delta p}{p} \right\} = 0 \tag{4.39}$$

$$\frac{\Delta Q_O}{Q_O} = -\sqrt{4{Q_O}^2 - 1}\,\mathrm{Im}\left\{ \frac{\Delta p}{p} \right\} = 2\tau_I \omega_O Q_O \tag{4.40}$$

The above analysis shows that the deviation in the resonant frequency is zero, whereas the deviation in the quality factor is dependent on the resonant frequency as well as itself. This yields that this filter is not so attractive for high Q designs.

The effect of k_I on the lowpass and highpass transfer functions is given by

$$\left(\frac{V_O}{V_I} \right)_{LP} = \frac{G_1 G_3 {k_{IO}}^2 (1 + s\tau_I)}{2\tau_I C_1 C_3 s^3 + (C_1 C_3 + 2\tau_I C_1 G_5) s^2 + C_1 G_5 s + G_2 G_3 {k_{IO}}^2} \tag{4.41}$$

$$\left(\frac{V_O}{V_I} \right)_{HP} = \frac{C_1 C_2 k_{IO} s^2 (1 + s\tau_I)}{2\tau_I C_1 C_3 s^3 + (C_1 C_3 + 2\tau_I C_1 G_5) s^2 + C_1 G_5 s + G_2 G_3 {k_{IO}}^2} \tag{4.42}$$

provided that the condition of $s\tau_I << 1$ is satisfied. Since the denominator of all three types of filters are identical, the above analysis remains valid for the lowpass and highpass filters as well.

MATLAB simulations have been carried out in order to check the effect of the pole of the current conveyor current transfer function. Results are demonstrated in Fig. 4.6, for f_O =100 kHz and the ratio of f_I/f_O =1, 10, 100, 1000.

4.1.4 The Effect of Y_Y

Although not analyzed above in detail for simplicity reasons, the effect of the admittance at terminal y has been given in Figs. 4.7, 4.8 and 4.9 for demonstration purposes. Not surprisingly, this admittance has a similar affect as the output admittance on the filter characteristics.

Section 4.1 has covered the effects of current conveyor non-idealities on a voltage-mode active filter. The filter parameters in terms of non-ideality terms have been derived. Table 4.1 summarizes the minimum/maximum values for the non-ideality terms, provided that 10% deviations in the filter cutoff frequency (resonant frequency) and quality factor is acceptable. Please note that the results obtained are valid for the three types of filters.

Table 4.1 Limits of non-ideality terms for a deviation of 10% in filter parameters

	ω_O	Q_O
r_X	< R/9	< R/9
r_Z	> 5.61 R	> 11.83 R
C_Z	< 0.12 C	< 0.53 C
τ_I (τ_V)	0	$< \dfrac{1}{20\omega_O Q_O}$

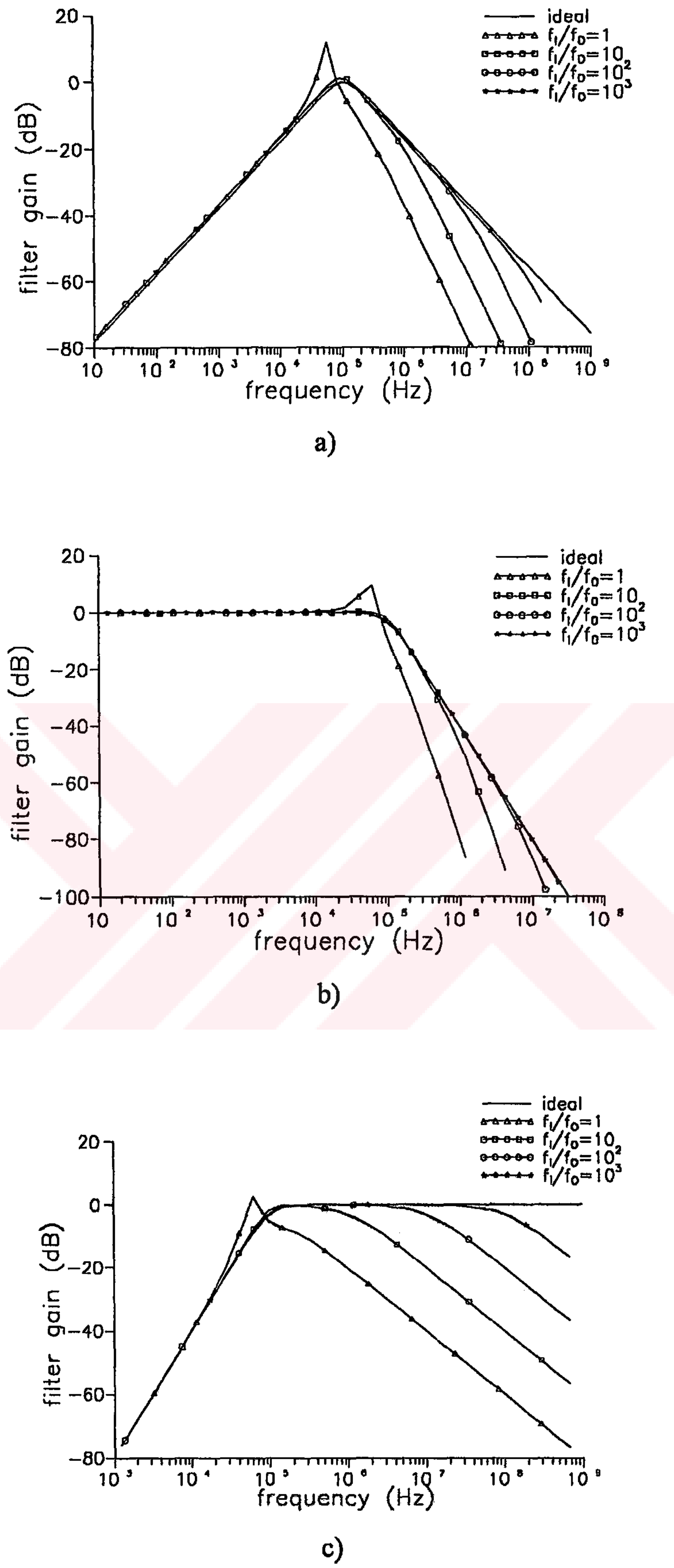

Figure 4.6 The effect of k_I (k_V) on the filter characteristics

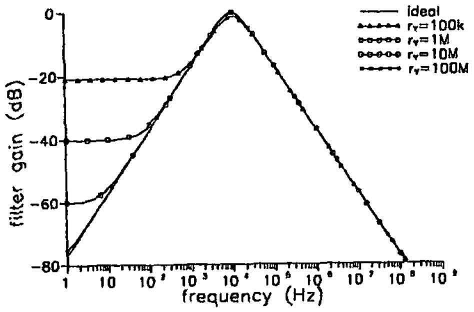

a)

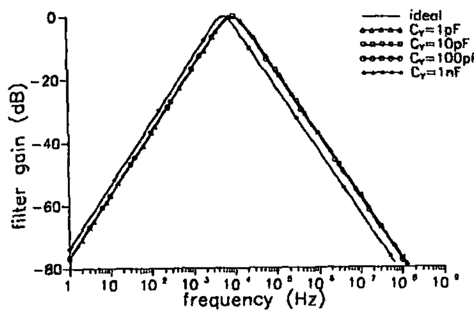

b)

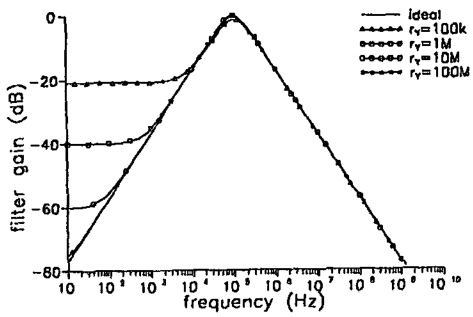

c)

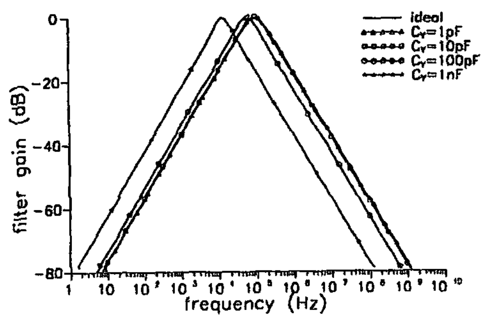

d)

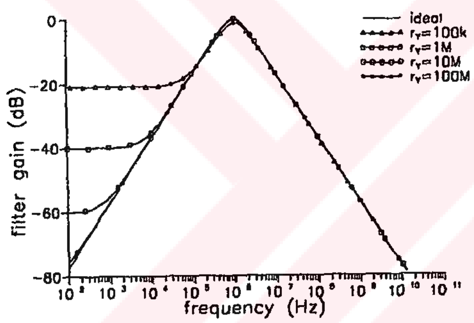

e)

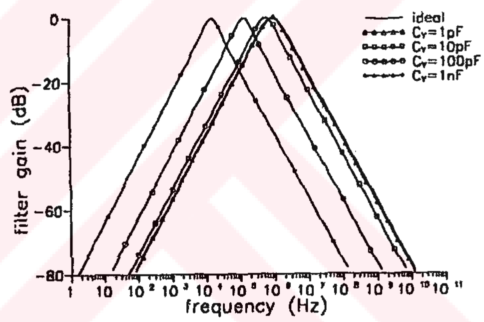

f)

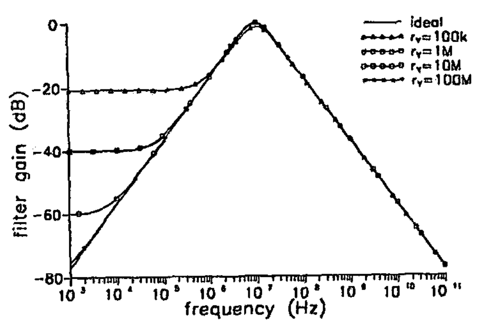

g)

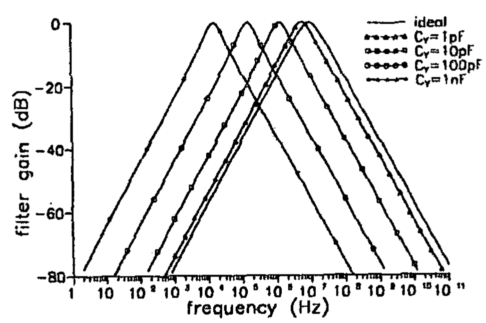

h)

Figure 4.7 The effect of r_Y and C_Y on the bandpass filter characteristics
a) and b) f_O =10 kHz c) and d) f_O =100 kHz e) and f) f_O =1 MHz g) and h) f_O =10 MHz

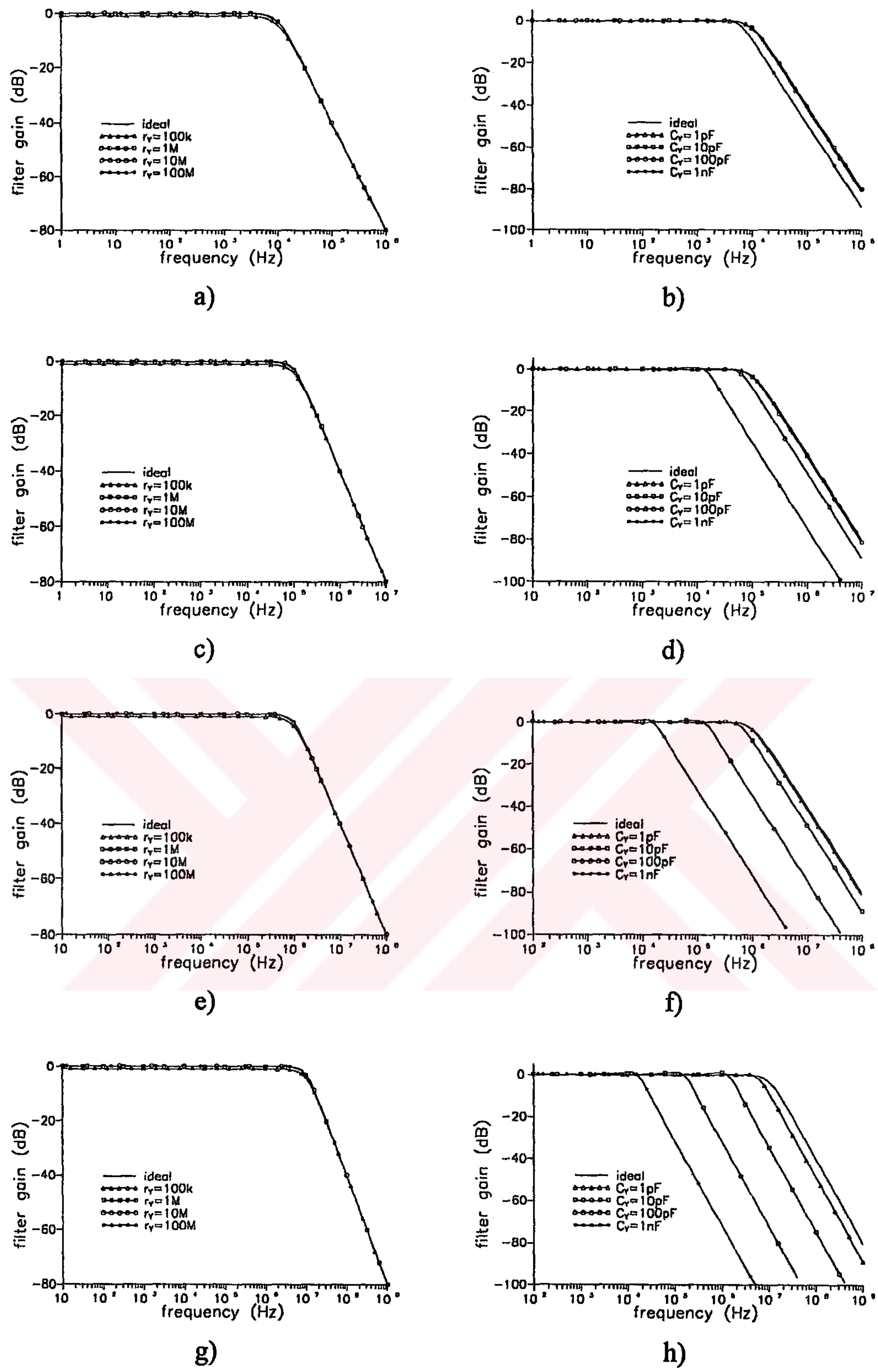

Figure 4.8 The effect of r_Y and C_Y on the lowpass filter characteristics
a) and b) f_O =10 kHz c) and d) f_O =100 kHz e) and f) f_O =1 MHz g) and h) f_O =10 MHz

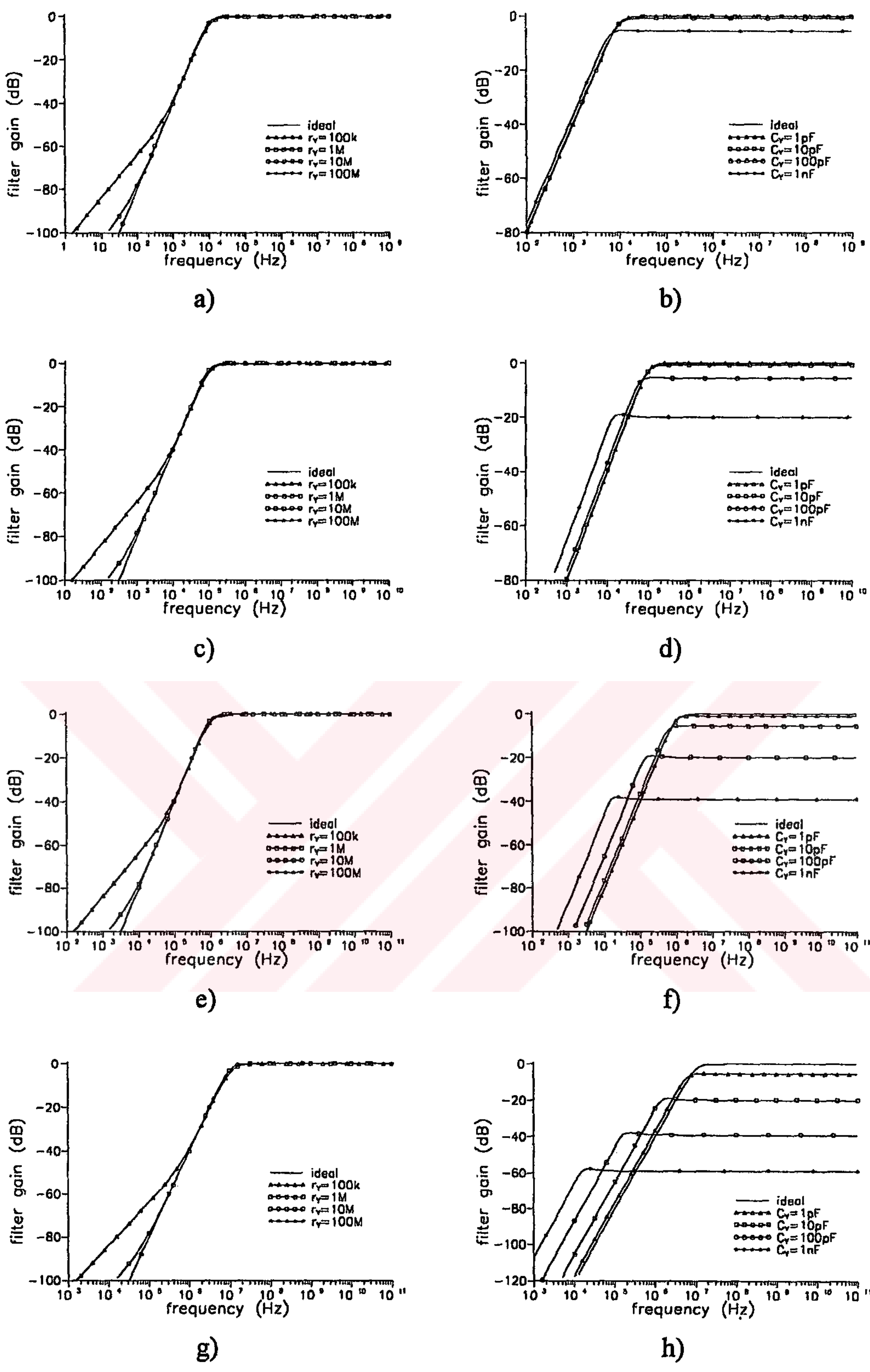

Figure 4.9 The effect of r_Y and C_Y on the highpass filter characteristics
a) and b) f_O =10 kHz c) and d) f_O =100 kHz e) and f) f_O =1 MHz g) and h) f_O =10 MHz

4.2 THE FILTER PERFORMANCE FOR VARIOUS CURRENT CONVEYOR CIRCUITS

This section will include a comparable demonstration of the filter performance for each current conveyor circuit studied in Chapter 3. Discussions will be made on how the non-ideality terms of the current conveyors affect the filter characteristics, based on the previous section. Figs. 4.10 through 4.15 depict the performance of the three types of filters when current conveyors CC1-CC8 are employed in the filter, for four different filter frequencies of f_O =10 kHz, 100 kHz, 1 MHz and 10 MHz.

In the previous section, the effect of each non-ideality term on the ideal voltage-mode filter transfer functions has been analyzed independently. Eqs. 4.15 through 4.17, 4.19 through 4.21, 4.23 and 4.24 demonstrate the results obtained for the relative deviations in the filter parameters when the effect of the resistive component of the impedance of terminal x is introduced into the ideal filter transfer functions. Eqs. 4.14 and 4.18 show that the rearranged bandpass and lowpass filter transfer functions preserve their second order characteristic forms, whereas an extra pole given by $f_{HPpole} = \dfrac{1}{2\pi C_2 r_X}$ emerges in the highpass filter transfer function. However, provided that the corresponding pole is high enough with respect to the filter cutoff frequency, Eqs. 4.23 and 4.24 remain valid. The results show that the effect of the resistive component of the impedance of terminal x on the relative deviations of the filter cutoff (resonant) frequency and quality factor for all three types of filters can be given as $\dfrac{r_X G}{r_X G+1}$, provided that $G= G_1 = G_2 = G_3 = G_4$. It is apparent from this expression that the condition of $r_X G \ll 1$ should be satisfied for small deviations in the filter cutoff (resonant) frequency and quality factor. The deviation in the bandpass filter gain can also be given as above, whereas Eq. 4.21 yields that the lowpass filter gain is not affected by the resistance of terminal x. Table 3.1 shows that even the highest value of r_X = 637 Ω for current conveyor CC7 satisfies the condition above. As a result, no significant effect can be observed on the filter characteristics given in Figs. 4.10

through 4.15, caused by this non-ideality term. Although the voltage and current transfer functions for CC7 show wideband characteristics, the highpass filter characteristics given in 4.15e through h, suffer from the low values of f_{HPpole}.

Eqs. 4.27 through 4.29, 4.31 and 4.33 exhibit the results obtained for the relative deviations in the filter parameters when the effect of the admittance of terminal z is introduced into the ideal filter transfer functions. Although Eq. 4.30 shows that the rearranged lowpass filter transfer funtion preserves its second order characteristic form, non-ideality terms dominant in the low frequency range appear in the bandpass and highpass filter functions as observed in Eqs. 4.25 and 4.32. However, the effect is more notable on the bandpass filter characteristics, due to the ineffectiveness of C_2 in the low frequency range. Therefore, low values of terminal z resistances remain less critical for highpass filter applications. This can be proved by comparing Figs. 4.10 and 4.11 with 4.14 and 4.15, respectively. The poor performances in the low frequency range observed in Figs. 4.10a through d and 4.11a through d, can be devoted to the fairly low terminal z resistance values of current conveyors CC1, CC2 and CC6. Since the values of C_1, C_3 and G_5 can be adjusted to make the corresponding sum terms given in Eqs. 4.27 through 4.29, 4.31 and 4.33 constant, the values of g_Z and C_Z remain less critical and the deviations in the filter cutoff (resonant) frequency, quality factor and filter gains can easily be minimized. The conditions of $g_Z << G^2$ and $C_Z << C^2$ should be satisfied for small deviations in the filter parameters, provided that $G=G_1=G_2=G_3=G_4$ and $C_1=2C_2=2C_3=2C$. All values of terminal z impedances given in Table 3.1 satisfy the conditions above. Eq. 4.31 yields that the lowpass filter gain is only affected by the resistive part of the impedance of terminal z, whereas Eq. 4.33 yields that only the capacitive part of the output impedance has an effect on the highpass filter gain. No significant effect on the highpass filter gains can be observed on the filter characteristics given in Figs. 4.14 and 4.15, caused by this non-ideality term, whereas the lowpass filter gains of the characteristics given in Figs. 4.12a through d suffer from the low terminal z resistance values of current conveyors CC1 and CC2.

The results obtained for the relative deviations in the filter parameters, when the voltage and current transfer functions of a current conveyor are introduced, are given in Eqs. 4.39 and 4.40. Analyses show that the effects of the voltage and current transfer functions of a current conveyor on the filter characteristics are identical. Since the denominators of Eqs. 4.34, 4.41 and 4.42 are identical, we obtain the same expressions for the relative deviations in the filter cutoff (resonant) frequency and quality factor for all three types of filters, provided that the condition of $s\tau_I << 1$ is satisfied. It is obvious that an extra pole determined by τ_I appears in the filter characteristics and a shift occurs in the location of the complex pole pair. The deviation in the resonant frequency is zero, whereas the deviation in the quality factor is dependent on the resonant frequency as well as itself. This yields that this filter configuration is not so attractive for high Q designs. The high frequency behavior of the filter characteristics is greatly determined by the voltage and current transfer characteristics of the current conveyors. The relatively low values of f_I and f_V of current conveyors CC1-CC5, yield acceptable filter performances upto 100 kHz, whereas for CC6 and CC8 the range extends to 1 MHz, and for CC7 even to 10 MHz.

Since various investigations have shown that the high impedance of terminal y is one of the easiest requirements to be met in the design of a current conveyor, the effect of this term has not been analyzed in detail. However, it can be shown that, this admittance has a similar effect as the output admittance on the filter characteristics. Fairly low terminal y resistance values of CC1 and CC2, contribute to poor bandpass filter performance observed in Figs. 4.10a through d.

The results obtained in the previous section have been used to determine the minimum/maximum values for the non-ideality terms, provided that 10% deviations in the filter frequency and quality factor is acceptable. These values are given in Table 4.1. Analyses show that the deviation in filter parameters remain within the specified limit of 10% for current conveyors CC3, CC5, CC7 and CC8, whereas the others extend beyond this limit, dominantly due to poor values of terminal y and z resistances. Figs. 4.10 through 4.15 yield that CC7 exhibits the best filter performances in all aspects. The relatively bad performance of CC1 and

CC2, can be attributed to the insufficient terminal y and z impedances, which play an important role especially in the bandpass filter performance. As a result, the above mentioned impedances remain as the most critical non-ideality terms which determine the performance of the voltage-mode filter. The related figures prove that the lowpass filter is the most tolerable filter type to active component non-idealities.

The large-signal behavior of the three types of filters for a cutoff (resonant) frequency of 10 kHz have been demonstrated in Figs. 4.16 through 4.18. The frequency of the input signal for the highpass filter is 100 kHz, whereas a frequency of 100 Hz has been chosen for the lowpass filter input signal. The maximum input signal amplitude for each current conveyor has been listed in Table 4.2, provided that a distortion of 1% for the output signal is acceptable. Please note that these values are not necessarily the optimum values which requires a thorough analysis, and remain valid for the set of filter component values chosen.

Table 4.2 The maximum input signal amplitude for various current conveyors

	v_{IBP}	v_{ILP}	v_{IHP}
CC1	8 V	8 V	9 V
CC2	8 V	8 V	8 V
CC4	2.5 V	2.1 V	1.8 V
CC5	11 V	11 V	5 V
CC6	2 V	1.8 V	0.2 V
CC7	4.2 V	3.7 V	3.7 V
CC8	0.6 V	0.5 V	0.3 V

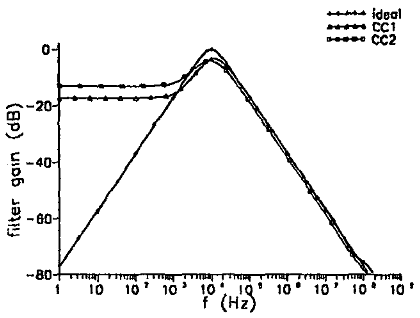

a)

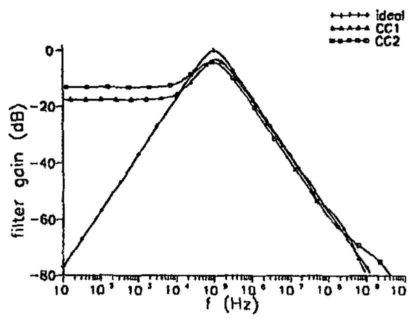

b)

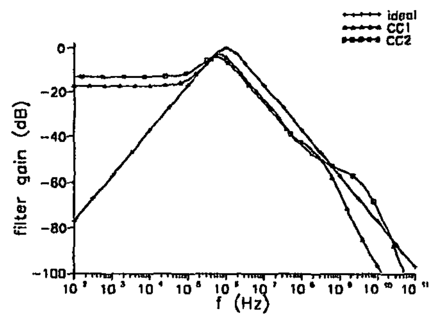

c)

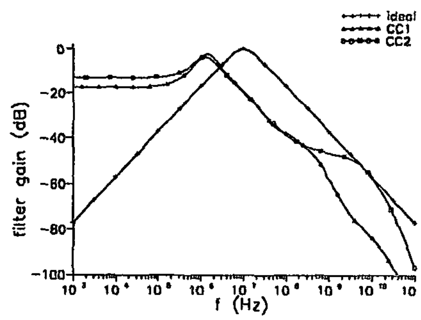

d)

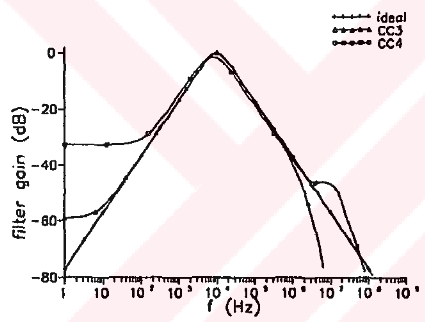

e)

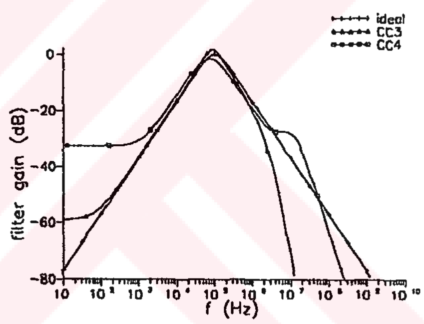

f)

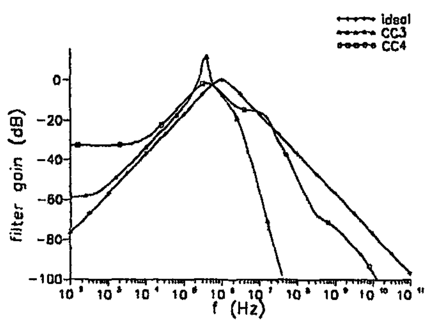

g)

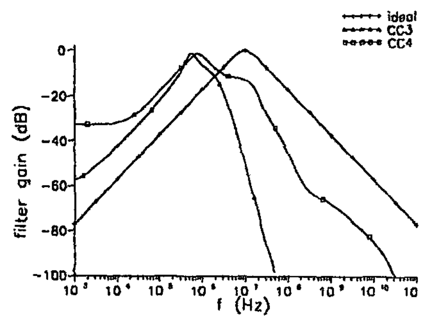

h)

Figure 4.10 The bandpass filter performance for CC1-CC4 at four different resonant frequencies of a) and e) $f_O = 10$ kHz b) and f) $f_O = 100$ kHz c) and g) $f_O = 1$ MHz d) and h) $f_O = 10$ MHz

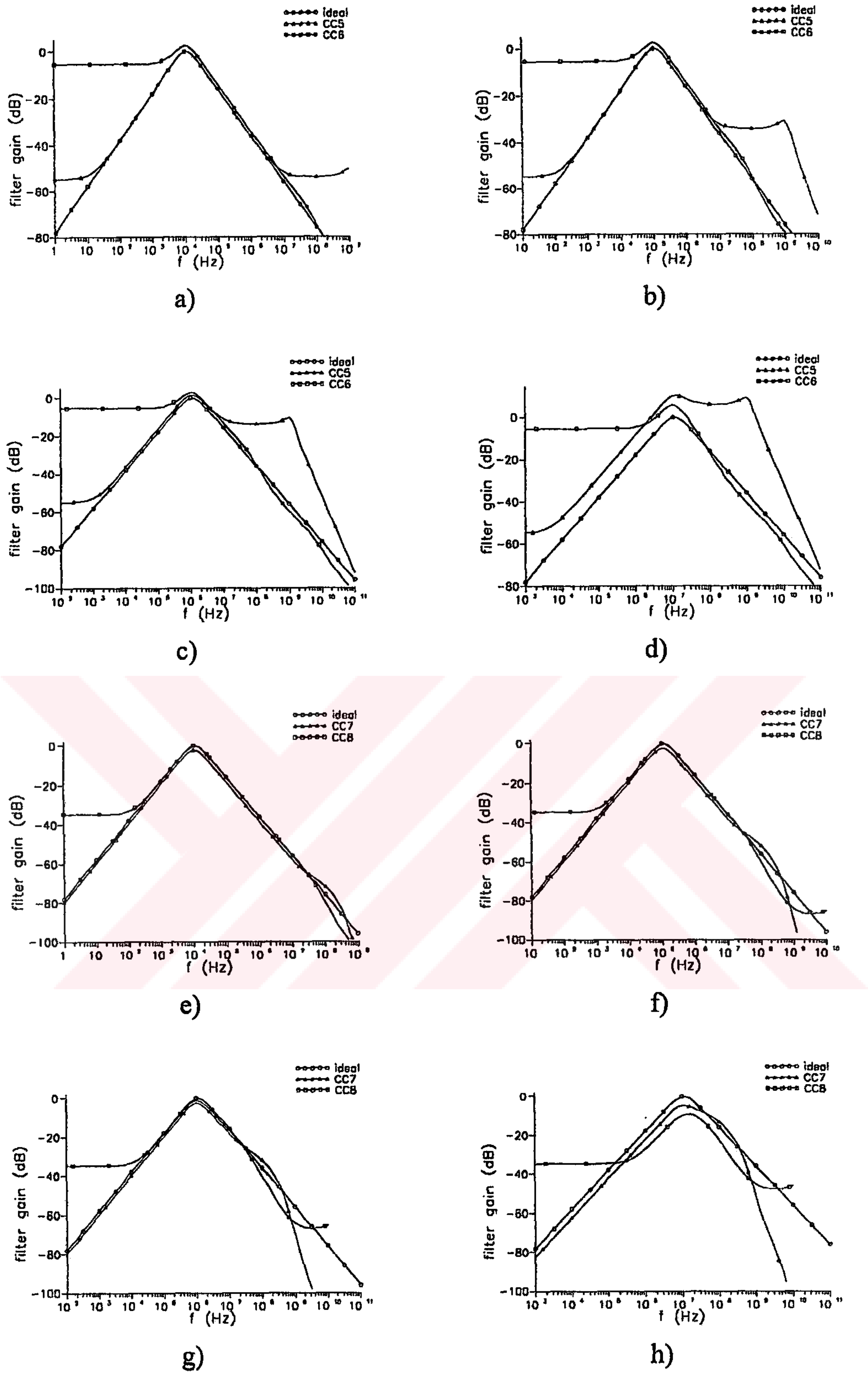

Figure 4.11 The bandpass filter performance for CC5-CC8 at four different resonant frequencies of a) and e) $f_o = 10$ kHz b) and f) $f_o = 100$ kHz c) and g) $f_o = 1$ MHz d) and h) $f_o = 10$ MHz

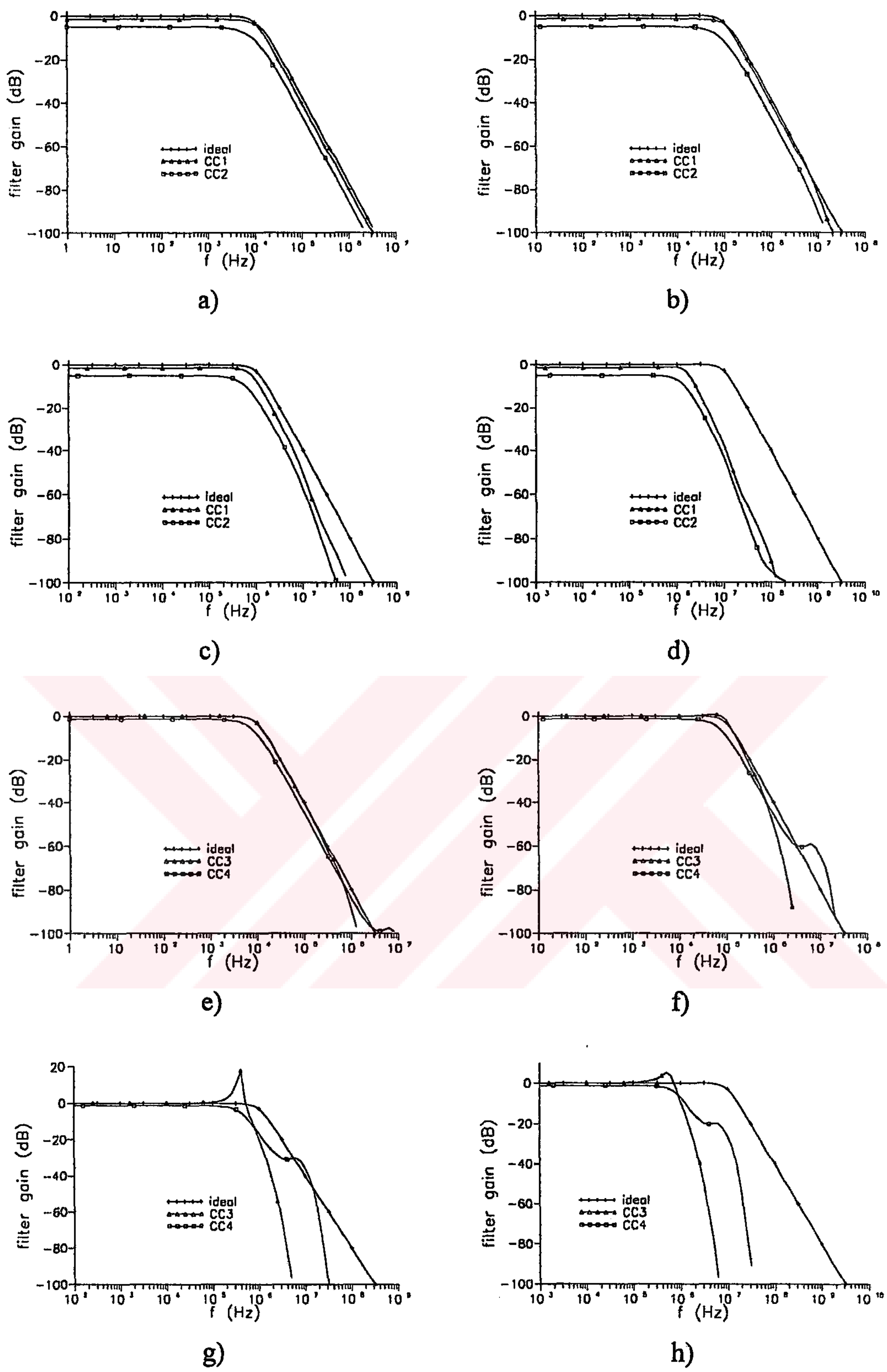

Figure 4.12 The lowpass filter performance for CC1-CC4 at four different cutoff frequencies of a) and e) $f_o = 10$ kHz b) and f) $f_o = 100$ kHz c) and g) $f_o = 1$ MHz d) and h) $f_o = 10$ MHz

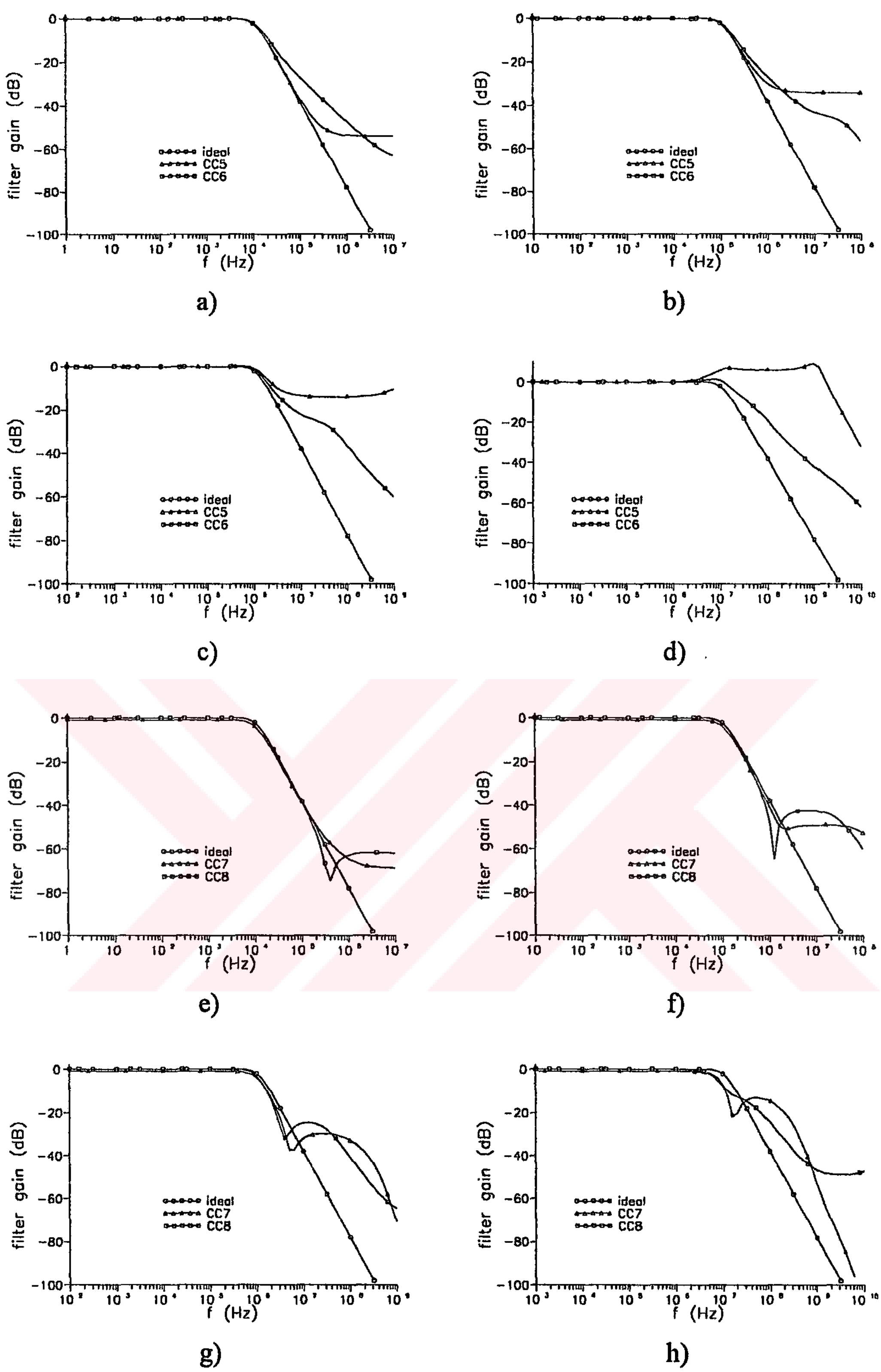

Figure 4.13 The lowpass filter performance for CC5-CC8 at four different cutoff frequencies of a) and e) $f_O = 10$ kHz b) and f) $f_O = 100$ kHz c) and g) $f_O = 1$ MHz d) and h) $f_O = 10$ MHz

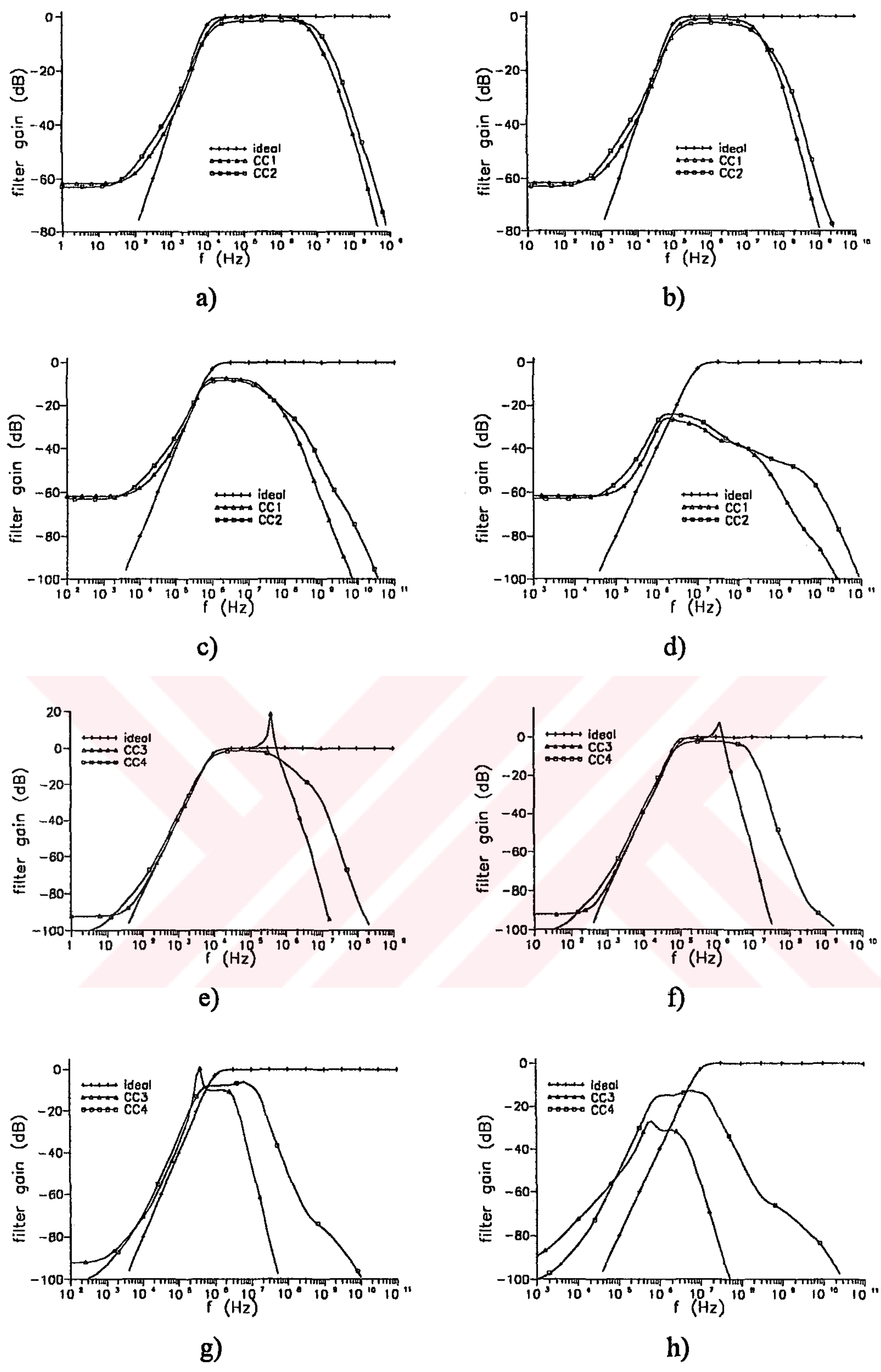

Figure 4.14 The highpass filter performance for CC1-CC4 at four different cutoff frequencies of a) and e) $f_O = 10$ kHz b) and f) $f_O = 100$ kHz c) and g) $f_O = 1$ MHz d) and h) $f_O = 10$ MHz

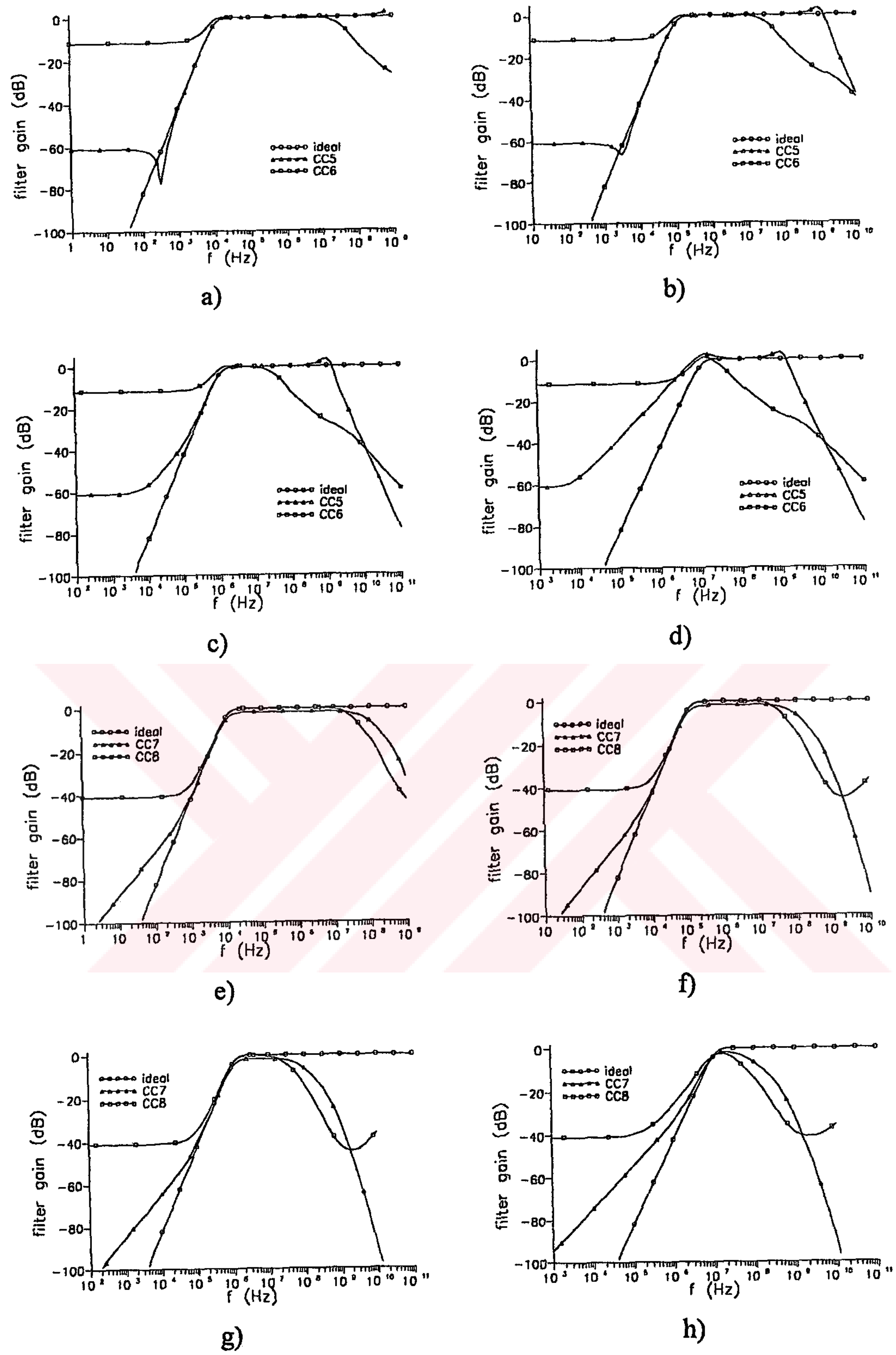

Figure 4.15 The highpass filter performance for CC5-CC8 at four different cutoff frequencies of a) and e) $f_o = 10$ kHz b) and f) $f_o = 100$ kHz c) and g) $f_o = 1$ MHz d) and h) $f_o = 10$ MHz

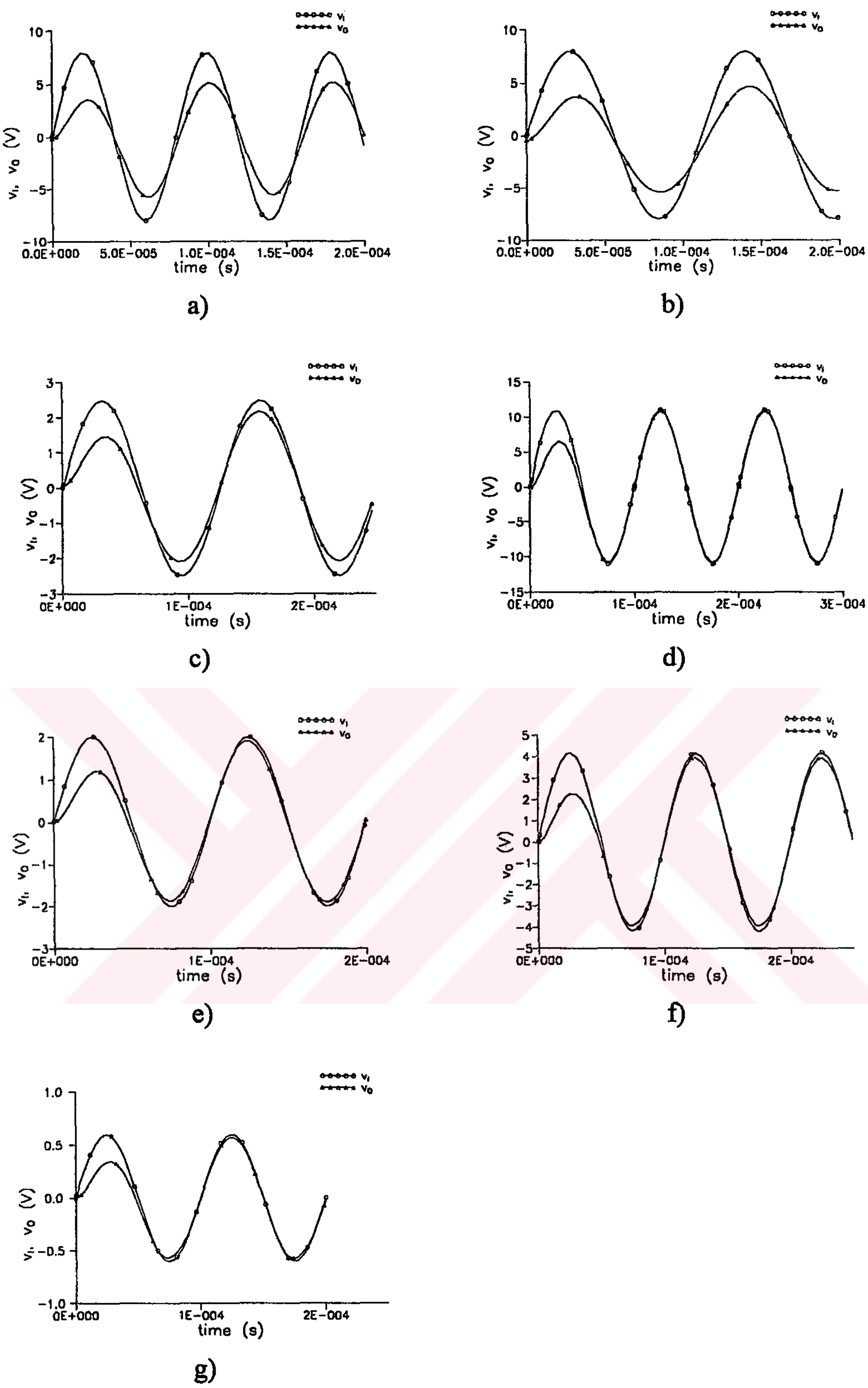

Figure 4.16 The large-signal behavior of the bandpass filter for various current conveyors a) CC1 b) CC2 c) CC4 d) CC5 e) CC6 f) CC7 g) CC8

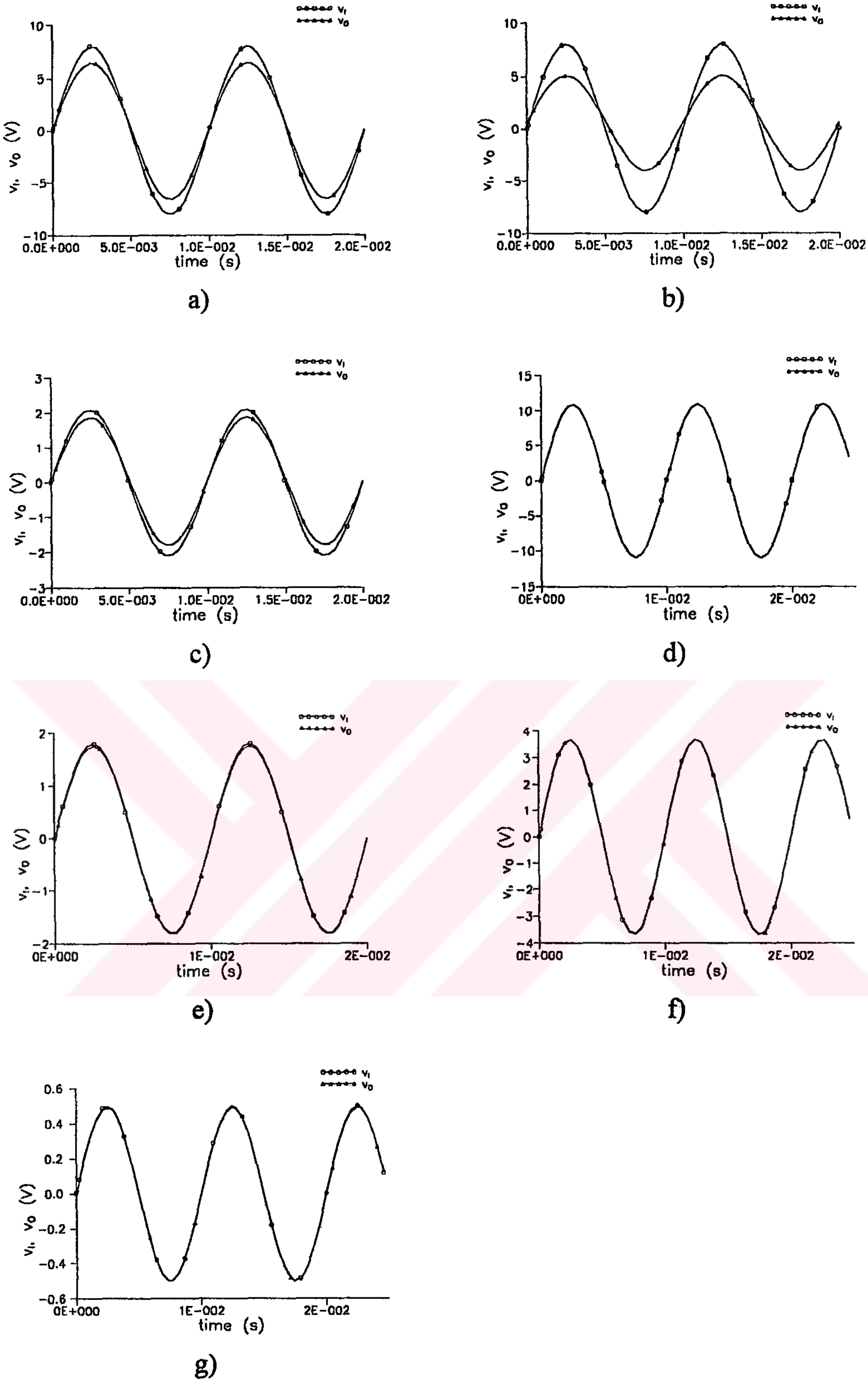

Figure 4.17 The large-signal behavior of the lowpass filter for various current conveyors a) CC1 b) CC2 c) CC4 d) CC5 e) CC6 f) CC7 g) CC8

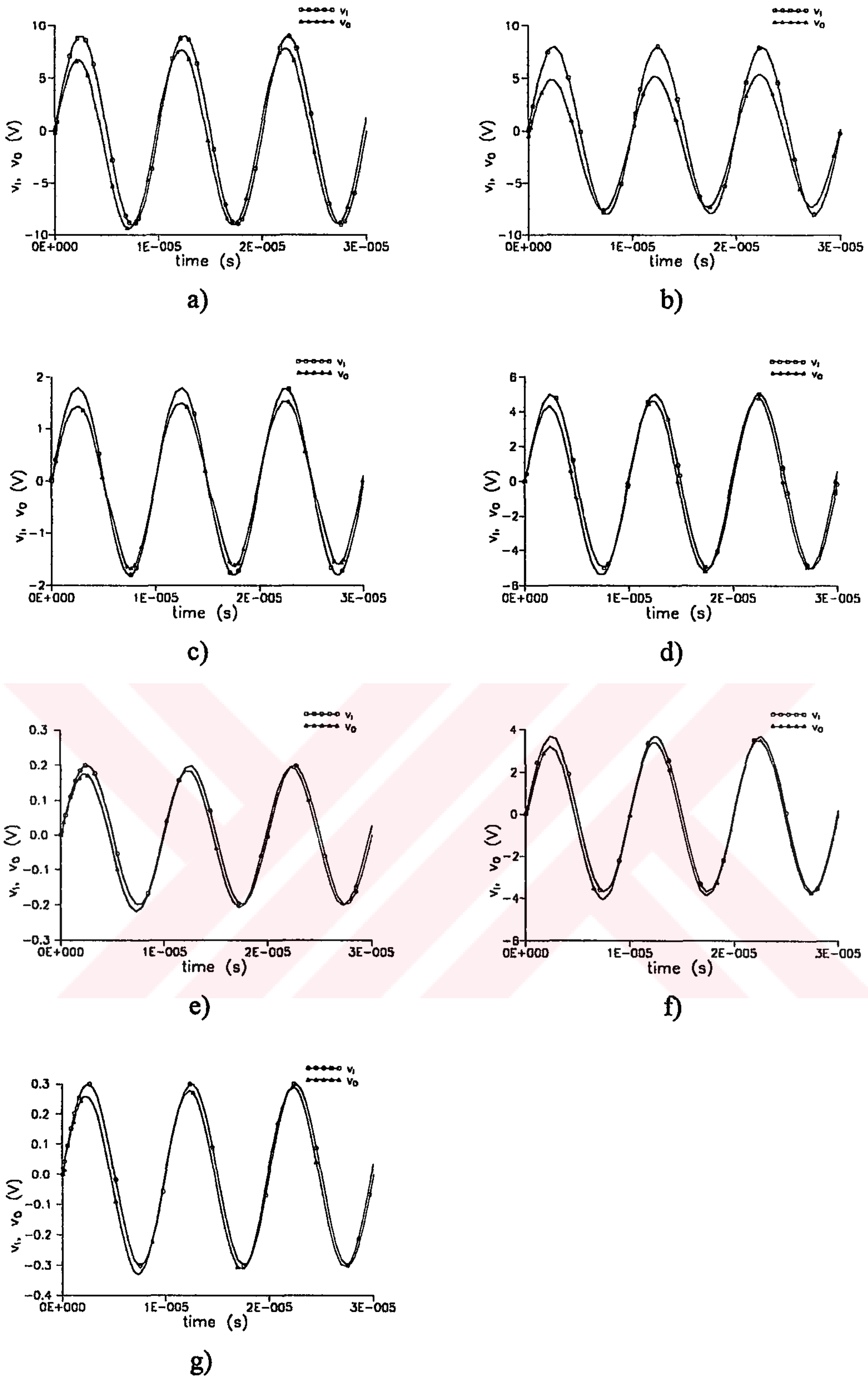

Figure 4.18 The large-signal behavior of the highpass filter for various current conveyors a) CC1 b) CC2 c) CC4 d) CC5 e) CC6 f) CC7 g) CC8

CHAPTER 5

THE EFFECTS OF CURRENT CONVEYOR NON-IDEALITIES ON A CURRENT-MODE ACTIVE FILTER

This chapter will include a thorough study on a current-mode active filter with the same procedure followed as in Chapter 4 [35]. The first section will be devoted to analyzing the effect of each non-idealitiy term on the filter characteristics. A comparable demonstration of the filter performances for each current conveyor circuit studied in Chapter 3, will be given in the second section.

5.1 THE EFFECTS OF CURRENT CONVEYOR NON-IDEALITIES ON FILTER CHARACTERISTICS

In this section, the effects of current conveyor non-idealities on current-mode filter characteristics will be investigated. The circuit configuration for realizing a bandpass filter transfer function is given in Fig. 5.1a, whereas Fig. 5.1b depicts the configuration for the lowpass and highpass filters [18]. A proper choice of the admittances in Fig. 5.1 gives the ideal transfer functions of the three types of filters in terms of circuit components as follows:

$$\left(\frac{I_2}{I_1}\right)_{BP} = \frac{\frac{1}{C_1 R_2} s}{s^2 + \frac{R_2 + R_3}{R_2 R_3 C_4} s + \frac{1}{C_1 R_2 R_3 C_4}} \tag{5.1}$$

$$\left(\frac{I_2}{I_1}\right)_{LP} = -\frac{\dfrac{1}{C_1R_2C_3R_4}}{s^2 + \dfrac{C_1 + C_3}{C_1C_3R_4}s + \dfrac{1}{C_1R_2C_3R_4}} \tag{5.2}$$

$$\left(\frac{I_2}{I_1}\right)_{HP} = -\frac{s^2}{s^2 + \dfrac{R_1 + R_3}{R_1C_2R_3}s + \dfrac{1}{R_1C_2R_3C_4}} \tag{5.3}$$

The filter parameters of the bandpass, lowpass and highpass filters can be derived from Eqs. 5.1, 5.2 and 5.3, respectively, as below:

$$\omega_{OBP} = \sqrt{\frac{1}{C_1R_2R_3C_4}} \tag{5.4}$$

$$Q_{OBP} = \frac{1}{R_2 + R_3}\sqrt{\frac{R_2R_3C_4}{C_1}} \tag{5.5}$$

$$H_{BP} = \frac{C_4}{C_1}\frac{R_3}{R_2 + R_3} \tag{5.6}$$

$$\omega_{OLP} = \sqrt{\frac{1}{C_1R_2C_3R_4}} \tag{5.7}$$

$$Q_{OLP} = \frac{1}{C_1 + C_3}\sqrt{\frac{C_1C_3R_4}{R_2}} \tag{5.8}$$

$$H_{LP} = 1 \tag{5.9}$$

$$\omega_{OHP} = \sqrt{\frac{1}{R_1C_2R_3C_4}} \tag{5.10}$$

The substitution of corresponding admittances into the equations above, yields the non-ideal filter transfer functions in the form of

$$\frac{I_2}{I_1}=\frac{u_4s^4+u_3s^3+u_2s^2+u_1s+u_0}{v_7s^7+v_6s^6+v_5s^5+v_4s^4+v_3s^3+v_2s^2+v_1s+v_0} \tag{5.15}$$

As in the previous chapter, since Eq. 5.15 will give us no clear information about how the filter characteristics and parameters will be affected, each non-ideality term will be analyzed independently.

5.1.1 The Effect of r_X

The effect of the resistive component of the impedance of terminal x has been studied in this section. First, our analysis will focus on the bandpass type filter. Arrangements on Eq. 5.13 gives us the effect of r_X on the transfer function as

$$\left(\frac{I_2}{I_1}\right)_{BP}=\frac{R_3C_4s}{(C_1R_2R_3C_4+C_1C_4(R_2+R_3)r_X)s^2+(C_1(R_2+R_3)+C_4r_X)s+1} \tag{5.16}$$

The relative deviation in each filter parameter can be derived from Eq. 5.16 as

$$\left|\frac{\Delta\omega_{OBP}}{\omega_{OBP}}\right|=\sqrt{\frac{R_2R_3}{R_2R_3+r_X(R_2+R_3)}}-1=\sqrt{\frac{R}{R+2r_X}}-1 \tag{5.17}$$

$$\left|\frac{\Delta Q_{OBP}}{Q_{OBP}}\right|=\frac{1}{1+\dfrac{C_4r_X}{C_1(R_2+R_3)}}\sqrt{1+\frac{r_X(R_2+R_3)}{R_2R_3}}-1=\frac{R}{R+r_X}\sqrt{\frac{R}{R+2r_X}}-1 \tag{5.18}$$

$$\left|\frac{\Delta H_{BP}}{H_{BP}}\right|=\frac{1}{1+\dfrac{C_4r_X}{C_1(R_2+R_3)}}-1=\frac{r_X}{R+r_X} \tag{5.19}$$

for $R=R_2=R_3$ and $2C=2C_1=C_4$. It is apparent from Eqs. 5.17 through 5.19 that the condition of $2r_X \ll R$ should be satisfied for small deviations in the resonant frequency, quality factor and filter gain.

The repetition of the above analysis for the lowpass filter yields the following transfer function and filter parameter deviations:

$$\left(\frac{I_2}{I_1}\right)_{LP} = -\frac{1}{(C_1R_2C_3R_4 + C_1C_3R_4r_X)s^2 + (C_1 + C_3)(R_2 + r_X)s + 1} \tag{5.20}$$

$$\left|\frac{\Delta\omega_{OLP}}{\omega_{OLP}}\right| = \sqrt{\frac{R_2}{R_2 + r_X}} - 1 \tag{5.21}$$

$$\left|\frac{\Delta Q_{OLP}}{Q_{OLP}}\right| = \sqrt{\frac{R_2}{R_2 + r_X}} - 1 \tag{5.22}$$

$$\left|\frac{\Delta H_{LP}}{H_{LP}}\right| = 0 \tag{5.23}$$

It can be observed that the condition of $r_X \ll R_2$ should be satisfied for small deviations in the cutoff frequency and quality factor. Eq. 5.23 yields that the filter gain is not affected by the resistance of terminal x.

The transfer function obtained for the highpass filter can be given as follows:

$$\left(\frac{I_2}{I_1}\right)_{HP} = -\frac{R_1C_2R_3C_4s^2}{(R_1C_2R_3C_4 + C_2C_4(R_1 + R_3)r_X)s^2 + (C_4(R_1 + R_3) + C_2r_X)s + 1} \tag{5.24}$$

The relative deviation in each filter parameter can be derived from Eq. 5.24 as

$$\left|\frac{\Delta\omega_{OHP}}{\omega_{OHP}}\right| = \sqrt{\frac{R_1R_3}{R_1R_3 + r_X(R_1 + R_3)}} - 1 = \sqrt{\frac{R}{R + 2r_X}} - 1 \tag{5.25}$$

$$\left|\frac{\Delta Q_{OHP}}{Q_{OHP}}\right| = \frac{1}{1+\dfrac{C_2 r_X}{C_4(R_1+R_3)}}\sqrt{1+\frac{r_X(R_1+R_3)}{R_1 R_3}}-1 = \frac{R}{R+r_X}\sqrt{\frac{R}{R+2r_X}}-1 \tag{5.26}$$

$$\left|\frac{\Delta H_{HP}}{H_{HP}}\right| = \frac{1}{1+\dfrac{r_X(R_1+R_3)}{R_1 R_3}}-1 = \frac{2r_X}{R+2r_X} \tag{5.27}$$

for $R=R_1=R_3$ and $C_2=2C_4=2C$. It is apparent from Eqs. 5.25 through 5.27 that the condition of $2r_X \ll R$ should be satisfied for small deviations in the cutoff frequency, quality factor and filter gain.

SPICE simulations have been carried out in order to prove the results obtained above. Results for four different values of r_X, namely, r_X =10 Ω, 100 Ω, 1 kΩ, 10 kΩ and two different cutoff frequencies of f_O =10 kHz, 10 MHz have been demonstrated in Fig. 5.2. The load resistance was chosen to be 100 Ω.

5.1.2 The Effect of Y_Z

The effect of the admittance of terminal z has been studied in this section. We will start our analysis with the bandpass type filter. Arrangements on Eq. 5.13 gives us the effect of Y_Z on the transfer function as

$$\left(\frac{I_2}{I_1}\right)_{BP} = \frac{\dfrac{1}{C_1 R_2}s}{s^2+\dfrac{R_2+R_3}{R_2 R_3 C_4}s+\dfrac{1}{C_1 R_2 R_3 C_4}}\frac{1}{(sC_Z+g_Z)R_L+1} \tag{5.28}$$

where R_L denotes the resistive load. It is apparent that g_Z has no effect on the resonant frequency and quality factor, whereas the deviation in filter gain can be given as follows:

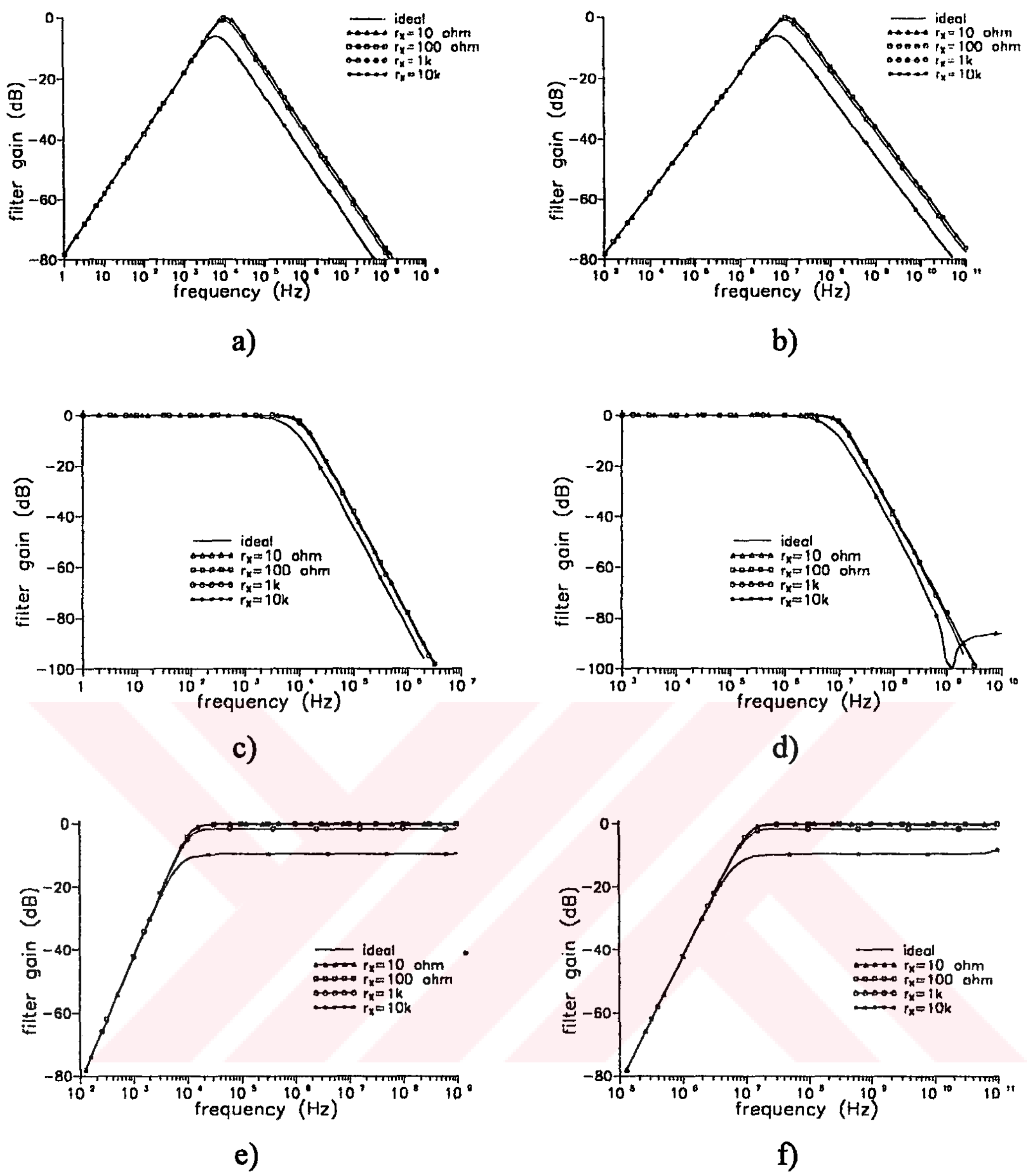

Figure 5.2 The effect of r_X on filter characteristics a) Bandpass filter of f_O =10 kHz b) Bandpass filter of f_O =10 MHz c) Lowpass filter of f_O =10 kHz d) Lowpass filter of f_O =10 MHz e) Highpass filter of f_O =10 kHz f) Highpass filter of f_O =10 MHz

$$\left|\frac{\Delta H_{BP}}{H_{BP}}\right| = \frac{g_Z R_L}{1+g_Z R_L} \tag{5.29}$$

However, the effect of C_Z yields a third order transfer function and an extra pole determined by C_Z, as well as g_Z and R_L appears in the filter characteristic. A thorough analysis shows that the relative deviations in the cutoff frequency and quality factor are zero. The Routh-Hurwitz test yields that, the poles of Eq. 5.28 causes no stability problem.

The repetition of the above analysis for the lowpass and highpass filters yields that Eq. 5.29 remains valid and the output capacitance has the same effect on the filter transfer functions.

SPICE simulations have been carried out in order to check the results obtained above. Results for four different values of r_Z, namely, r_Z=100 kΩ, 1 MΩ, 10 MΩ, 100 MΩ; four different values of C_Z, namely C_Z= 1 pF, 10 pF, 100 pF, 1 nF and four different cutoff frequencies of f_O =10 kHz, 100 kHz, 1 MHz, 10 MHz have been demonstrated in Figs. 5.3, 5.4 and 5.5, for a load resistance of R_L=100 Ω.

5.1.3 The Effect of k_I

The effect of the current transfer function of a current conveyor on the filter characteristics has been studied in this section. Arrangements on Eqs. 5.13 and 5.14 gives us the effect of k_I on the ideal bandpass, lowpass and highpass transfer functions, respectively, as

$$\left(\frac{I_2}{I_1}\right)_{BP} = \frac{\frac{1}{C_1 R_2} s}{s^2 + \frac{R_2 + R_3}{R_2 R_3 C_4} s + \frac{1}{C_1 R_2 R_3 C_4}} \frac{k_{IO}}{1+s\tau_I} \tag{5.30}$$

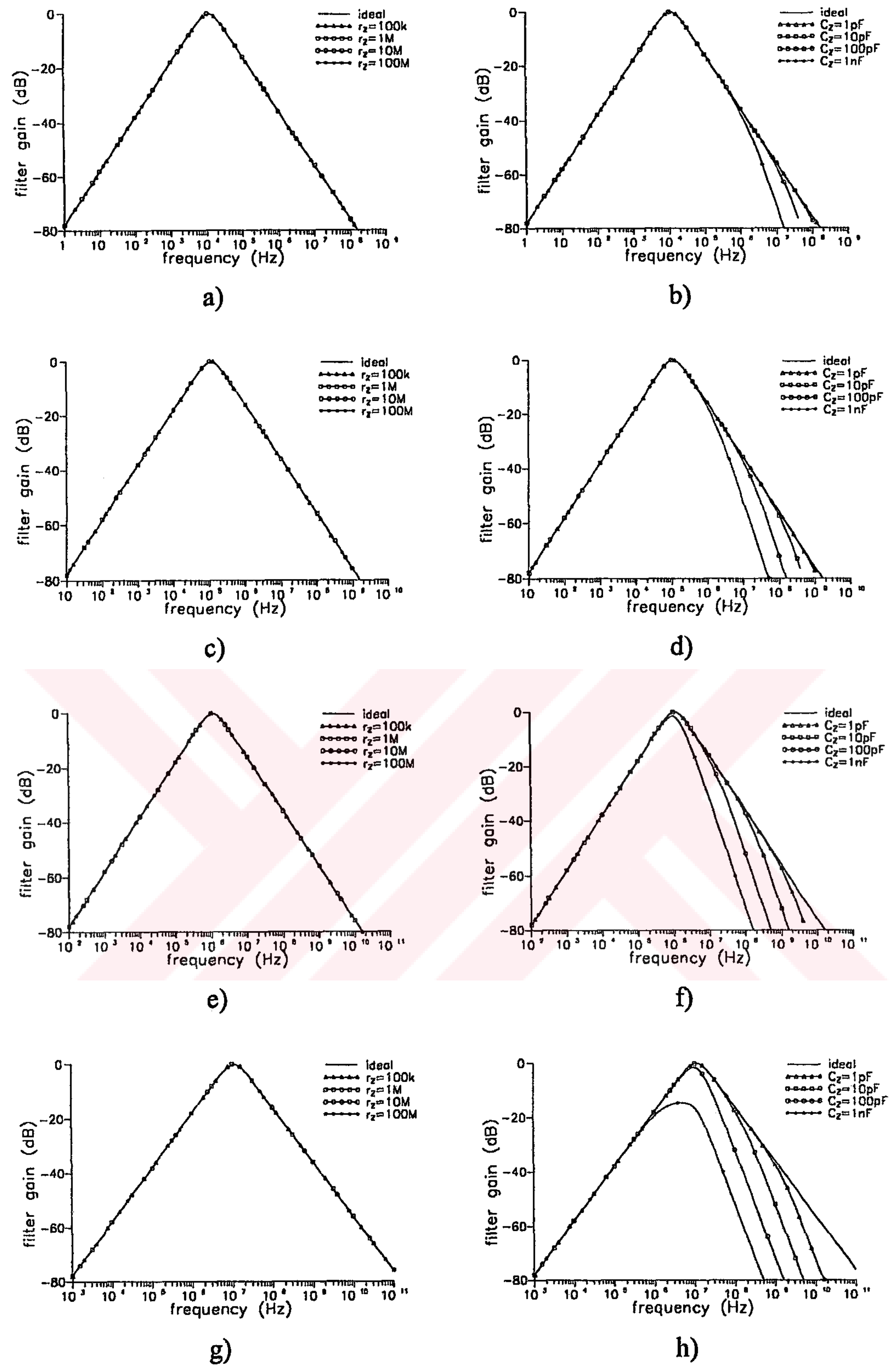

Figure 5.3 The effect of r_Z and C_Z on the bandpass filter characteristics
a) and b) f_O =10 kHz c) and d) f_O =100 kHz e) and f) f_O =1 MHz g) and h) f_O =10 MHz

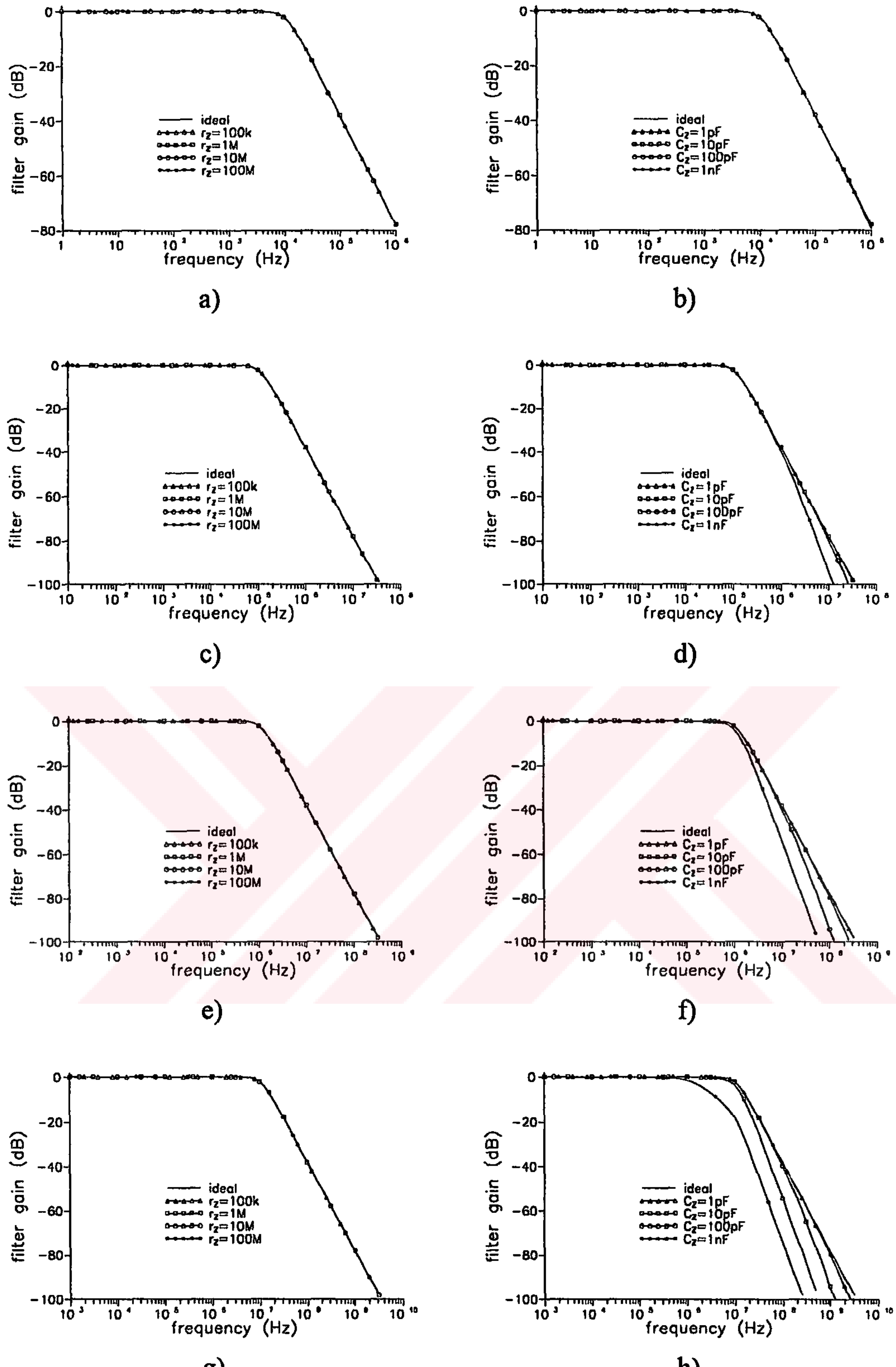

Figure 5.4 The effect of r_Z and C_Z on the lowpass filter characteristics
a) and b) f_O =10 kHz c) and d) f_O =100 kHz e) and f) f_O =1 MHz g) and h) f_O =10 MHz

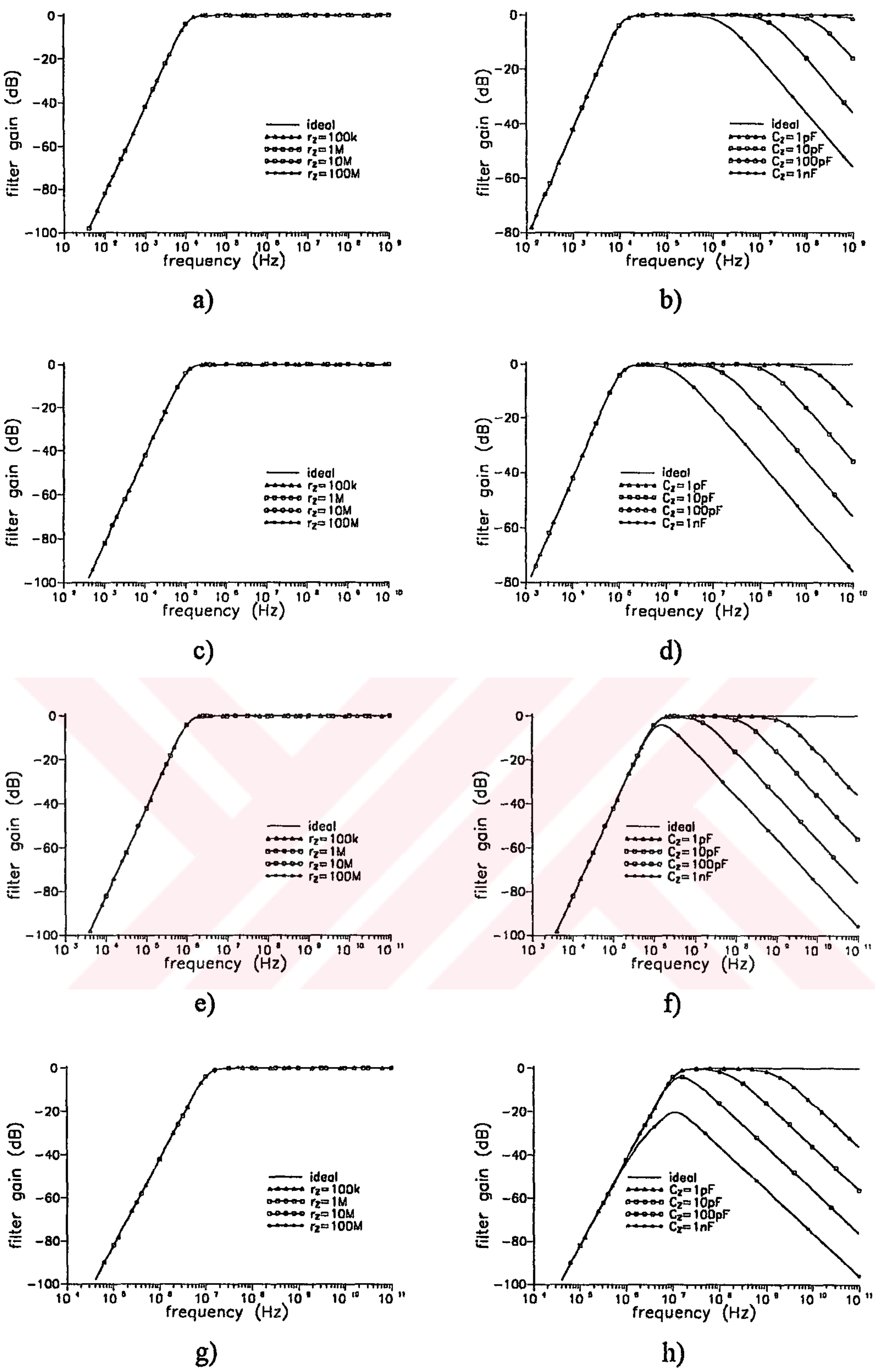

Figure 5.5 The effect of r_Z and C_Z on the highpass filter characteristics
a) and b) f_O =10 kHz c) and d) f_O =100 kHz e) and f) f_O =1 MHz g) and h) f_O =10 MHz

$$\left(\frac{I_2}{I_1}\right)_{LP} = -\frac{\dfrac{1}{C_1R_2C_3R_4}}{s^2+\dfrac{C_1+C_3}{C_1C_3R_4}s+\dfrac{1}{C_1R_2C_3R_4}}\frac{k_{IO}}{1+s\tau_I} \tag{5.31}$$

$$\left(\frac{I_2}{I_1}\right)_{HP} = -\frac{s^2}{s^2+\dfrac{R_1+R_3}{R_1C_2R_3}s+\dfrac{1}{R_1C_2R_3C_4}}\frac{k_{IO}}{1+s\tau_I} \tag{5.32}$$

It is obvious that an extra pole determined by τ_I appears in the filter characteristics and the cutoff frequency and quality factor remains unchanged, provided that the condition of $s\tau_I << 1$ is satisfied.

MATLAB simulations have been carried out in order to check the effect of the pole of the current conveyor current transfer function. Results are demonstrated in Fig. 5.6, for f_O =100 kHz and the ratio of f_I / f_O =1, 10, 100, 1000. The load resistance was chosen to be 100 Ω.

5.1.4 The Effect of k_V

This section will include the effect of the voltage transfer function of a current conveyor on the filter characteristics. Arrangements on Eq. 5.13 gives us the effect of k_V on the ideal bandpass transfer function as

$$\left(\frac{I_2}{I_1}\right)_{BP} = \frac{\left(\dfrac{k_{VO}}{C_1R_2}-\dfrac{\tau_V}{C_1R_3C_4}\right)s}{\tau_V s^3+\left(1+\left(\dfrac{R_2+R_3}{R_2R_3C_4}+\dfrac{1}{C_1R_3}\right)\tau_V\right)s^2+\left(\dfrac{R_2+R_3}{R_2R_3C_4}+\dfrac{\tau_V}{C_1R_2R_3C_4}+\dfrac{1-k_{VO}}{C_1R_3}\right)s+\dfrac{1}{C_1R_2R_3C_4}} \tag{5.33}$$

It is obvious that an extra pole determined by τ_V appears in the filter characteristic and a shift occurs in the location of the complex pole pair. Now, let us consider the effect of τ_V on the filter parameters. The third order polynomial of the denominator in Eq. 5.33 can be written in terms of the ideal resonant frequency and quality factor as below;

$$\hat{D}_{BP}(s) = \tau_V s^3 + (1 + \tau_V(\frac{\omega_O}{Q_O} + \frac{1}{C_1 R_3}))s^2 + (\frac{\omega_O}{Q_O} + \tau_V \omega_O{}^2)s + \omega_O{}^2 \qquad (5.34)$$

provided that $k_{VO}=1$.

Application of the Routh-Hurwitz test to Eq. 5.34 shows that there is no stability problem caused by the poles. Substituting the related polynomials into Eq. 4.36 yields the deviations in the pole, resonant frequency and quality factor as

$$\left(\frac{\Delta p}{p}\right)_{BP} = -j\tau_V \frac{Q_O}{\sqrt{4Q_O{}^2 - 1}}(\omega_O + \frac{1}{2Q_O C_1 R_3}) - \frac{\tau_V}{2C_1 R_3} \qquad (5.35)$$

$$\left(\frac{\Delta\omega_O}{\omega_O}\right)_{BP} = \mathrm{Re}\left\{\frac{\Delta p}{p}\right\}_{BP} = -\frac{\tau_V}{2C_1 R_3} \qquad (5.36)$$

$$\left(\frac{\Delta Q_O}{Q_O}\right)_{BP} = -\sqrt{4Q_O{}^2 - 1}\ \mathrm{Im}\left\{\frac{\Delta p}{p}\right\}_{BP} = \tau_V Q_O(\omega_O + \frac{1}{2Q_O C_1 R_3}) \qquad (5.37)$$

The results obtained yields that the deviation in the quality factor caused by τ_V is more notable than that of the resonant frequency.

The effect of k_V on the lowpass transfer function is given by

$$\left(\frac{I_2}{I_1}\right)_{LP} = \frac{\frac{\tau_V}{C_1 R_2}s^2 + (\frac{\tau_V + (1 - k_{VO})C_3 R_4}{C_1 R_2 C_3 R_4})s + \frac{1}{C_1 R_2 C_3 R_4}}{\tau_V s^3 + (1 + (\frac{C_1 + C_3}{C_1 C_3 R_4} + \frac{1}{C_1 R_2})\tau_V)s^2 + (\frac{C_1 + C_3}{C_1 C_3 R_4} + \frac{\tau_V}{C_1 R_2 C_3 R_4} + \frac{1 - k_{VO}}{C_1 R_2})s + \frac{1}{C_1 R_2 C_3 R_4}}$$

(5.38)

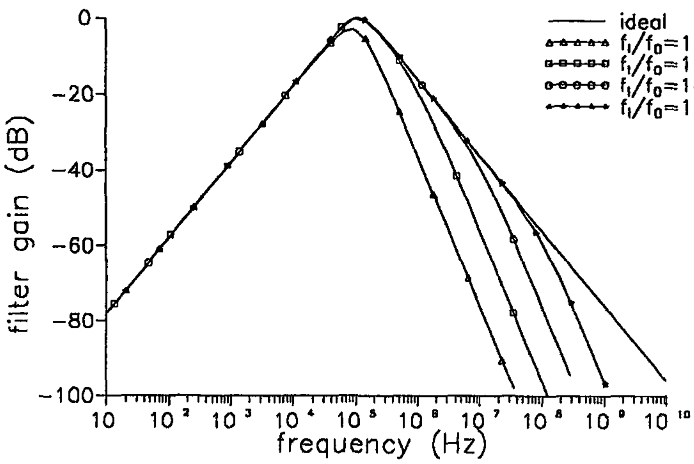

a)

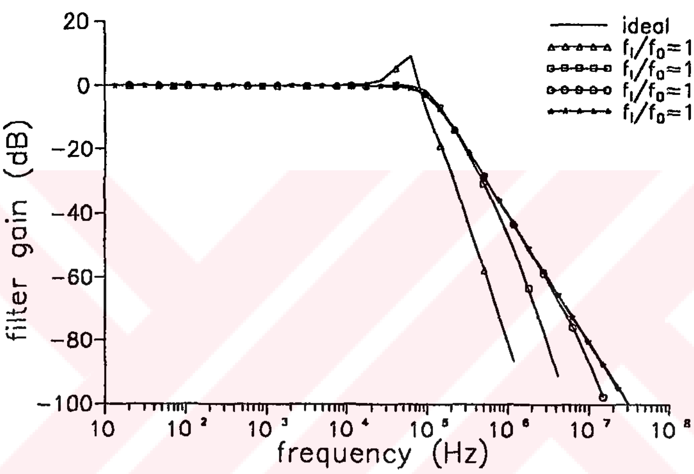

b)

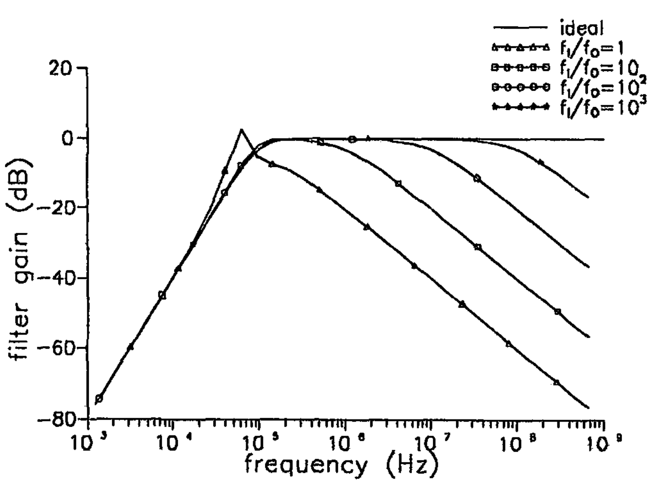

c)

Figure 5.6 The effect of k_l on the filter characteristics

A similar analysis yields the third order denominator of the lowpass filter transfer function and deviations in the cutoff frequency and quality factor as below, provided that k_{VO}=1;

$$\hat{D}_{LP}(s) = \tau_V s^3 + (1 + \tau_V(\frac{\omega_O}{Q_O} + \frac{1}{C_1 R_2}))s^2 + (\frac{\omega_O}{Q_O} + \tau_V \omega_O{}^2)s + \omega_O{}^2 \qquad (5.39)$$

$$\left(\frac{\Delta\omega_O}{\omega_O}\right)_{LP} = -\frac{\tau_V}{2C_1 R_2} \qquad (5.40)$$

$$\left(\frac{\Delta Q_O}{Q_O}\right)_{LP} = \tau_V Q_O(\omega_O + \frac{1}{2Q_O C_1 R_2}) \qquad (5.41)$$

The effect of k_V on the highpass transfer function can be expressed as below:

$$\left(\frac{I_2}{I_1}\right)_{HP} = \frac{\tau_V s^3 + (1 + \frac{\tau_V}{R_1 R_3 C_4})s^2 + \frac{1-k_{VO}}{R_1 R_3 C_4} s}{\tau_V s^3 + (1 + (\frac{R_1 + R_3}{R_1 C_2 R_3} + \frac{1}{R_3 C_4})\tau_V)s^2 + (\frac{R_1 + R_3}{R_1 C_2 R_3} + \frac{\tau_V}{R_1 C_2 R_3 C_4} + \frac{1-k_{VO}}{R_3 C_4})s + \frac{1}{R_1 C_2 R_3 C_4}} \qquad (5.42)$$

The denominator and deviations in the cutoff frequency and quality factor can be expressed as

$$\hat{D}_{HP}(s) = \tau_V s^3 + (1 + \tau_V(\frac{\omega_O}{Q_O} + \frac{1}{R_3 C_4}))s^2 + (\frac{\omega_O}{Q_O} + \tau_V \omega_O{}^2)s + \omega_O{}^2 \qquad (5.43)$$

$$\left(\frac{\Delta\omega_O}{\omega_O}\right)_{HP} = -\frac{\tau_V}{2R_3 C_4} \qquad (5.44)$$

$$\left(\frac{\Delta Q_O}{Q_O}\right)_{HP} = \tau_V Q_O(\omega_O + \frac{1}{2Q_O R_3 C_4}) \qquad (5.45)$$

provided that $k_{VO}=1$.

The results obtained for the lowpass and highpass filters show that the effect of τ_V on the filter parameters are somewhat similar to the case observed on the bandpass type.

MATLAB simulations have been carried out in order to check the effect of the pole of the current conveyor voltage transfer function. Results are demonstrated in Fig. 5.7, for f_O =100 kHz and the ratio of f_l/f_O =1, 10, 100, 1000. The load resistance was chosen to be 100 Ω.

5.1.5 The Effect of Y_Y

The effect of the admittance of terminal y has been studied in this section. First, our analysis will focus on the bandpass type filter. Arrangements on Eq. 5.13 gives us the effect of Y_Y on the transfer function as

$$\left(\frac{I_2}{I_1}\right)_{BP} = \frac{R_3C_4s}{R_2R_3C_4(C_1+C_Y)s^2+((C_1+C_Y)(R_2+R_3)+R_2R_3C_4g_Y)s+g_Y(R_2+R_3)+1} \tag{5.46}$$

The relative deviation in each filter parameter can be derived from Eq. 5.46 as

$$\left|\frac{\Delta\omega_{OBP}}{\omega_{OBP}}\right| = \sqrt{\frac{1+2g_YR}{1+\frac{C_Y}{C}}}-1 \tag{5.47}$$

$$\left|\frac{\Delta Q_{OBP}}{Q_{OBP}}\right| = \frac{1}{1+\frac{C_Y}{C}\frac{g_YR}{4}}\sqrt{(1+2g_YR)(1+\frac{C_Y}{C})}-1 \tag{5.48}$$

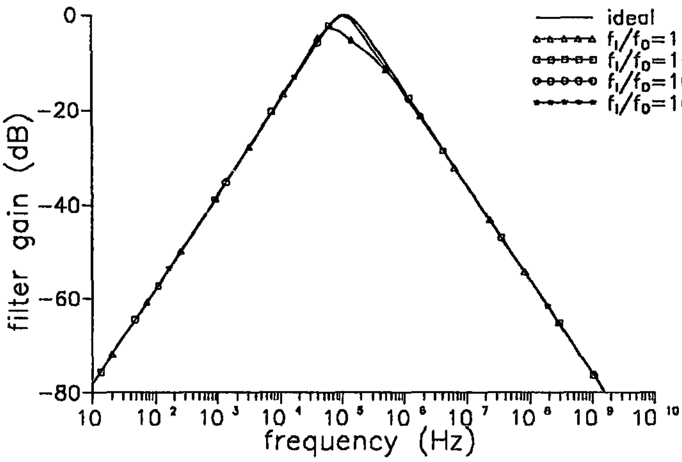

a)

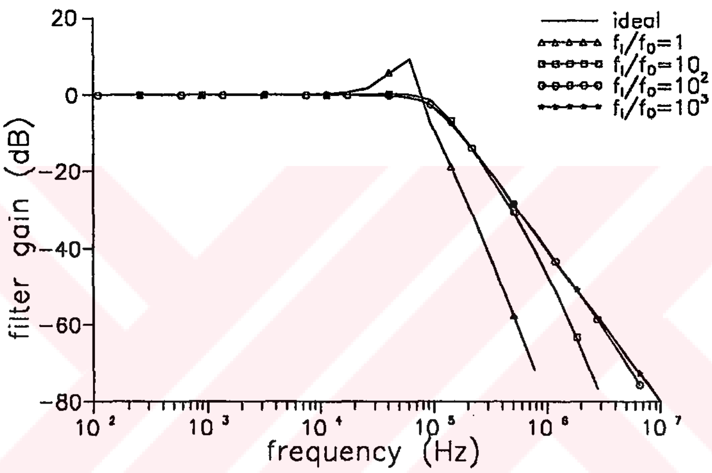

b)

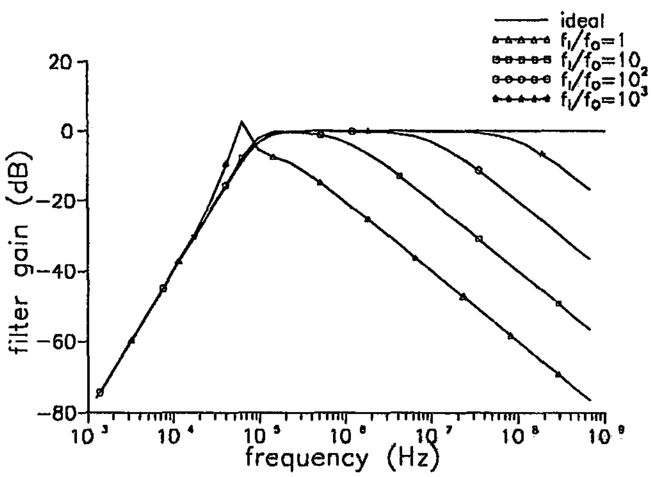

c)

Figure 5.7 The effect of k_V on the filter characteristics

$$\left|\frac{\Delta H_{BP}}{H_{BP}}\right| = \frac{1}{1+\frac{C_Y}{C}+g_Y R} - 1 \tag{5.49}$$

for $R=R_2=R_3$ and $2C=2C_1=C_4$. It is apparent from Eqs. 5.47 through 5.49 that the conditions of $2g_YR \ll 1$ and $C_Y \ll C$ should be satisfied for small deviations in the resonant frequency, quality factor and filter gain.

The repetition of the above analysis for the lowpass filter yields the transfer function and filter parameter deviations as;

$$\left(\frac{I_2}{I_1}\right)_{LP} = -\frac{R_4 C_Y s + R_4 g_Y + 1}{e_2 s^2 + e_1 s + e_0} \tag{5.50}$$

where

$$e_2 = C_1 R_2 C_3 R_4 + R_2 R_4 C_Y (C_1 + C_3) \tag{5.51a}$$

$$e_1 = R_2 (C_1 + C_3) + R_4 C_Y + R_2 R_4 g_Y (C_1 + C_3) \tag{5.51b}$$

$$e_0 = R_4 g_Y + 1 \tag{5.51c}$$

and

$$\left|\frac{\Delta\omega_{OLP}}{\omega_{OLP}}\right| = \sqrt{\frac{1+2g_Y R}{1+2\frac{C_Y}{C}}} - 1 \tag{5.52}$$

$$\left|\frac{\Delta Q_{OLP}}{Q_{OLP}}\right| = \frac{1}{1+\frac{C_Y}{C}+2g_Y R}\sqrt{(1+2g_Y R)(1+2\frac{C_Y}{C})} - 1 \tag{5.53}$$

$$\left|\frac{\Delta H_{LP}}{H_{LP}}\right| = 0 \tag{5.54}$$

for $2R=2R_2=R_4$ and $C=C_1=C_3$. The conditions of $2g_YR \ll 1$ and $2C_Y \ll C$ should be satisfied for small deviations in the cutoff frequency and quality factor. Eq. 5.54 yields that the filter gain is not affected by the admittance of terminal y.

The transfer function obtained for the highpass filter can be given as follows:

$$\left(\frac{I_2}{I_1}\right)_{HP} = -\frac{R_1C_2R_3(C_4+C_Y)s^2 + R_1C_2R_3g_Ys}{h_2s^2+h_1s+h_0} \tag{5.55}$$

where

$$h_2 = R_1C_2R_3(C_4+C_Y) \tag{5.56a}$$

$$h_1 = (R_1+R_3)(C_4+C_Y)+R_1C_2R_3g_Y \tag{5.56b}$$

$$h_0 = (R_1+R_3)g_Y+1 \tag{5.56c}$$

Eq. 5.55 yields the filter parameters for the highpass filter as;

$$\left|\frac{\Delta\omega_{OHP}}{\omega_{OHP}}\right| = \sqrt{\frac{1+2g_YR}{1+\frac{C_Y}{C}}}-1 \tag{5.57}$$

$$\left|\frac{\Delta Q_{OHP}}{Q_{OHP}}\right| = \frac{1}{1+\frac{C_Y}{C}+\frac{g_YR}{2}}\sqrt{(1+2g_YR)(1+\frac{C_Y}{C})}-1 \tag{5.58}$$

$$\left|\frac{\Delta H_{HP}}{H_{HP}}\right| = 0 \tag{5.59}$$

for $R=R_1=R_3$ and $2C=C_2=2C_4$. The conditions of $g_YR \ll 1$ and $C_Y \ll C$ should be satisfied for small deviations in the cutoff frequency and quality factor. Eq. 5.59 yields that the filter gain is not affected by the admittance of terminal y.

The effect of the admittance at terminal y has been given in Figs. 5.8, 5.9 and 5.10 for demonstration purposes. Results for four different values of r_Y, namely,

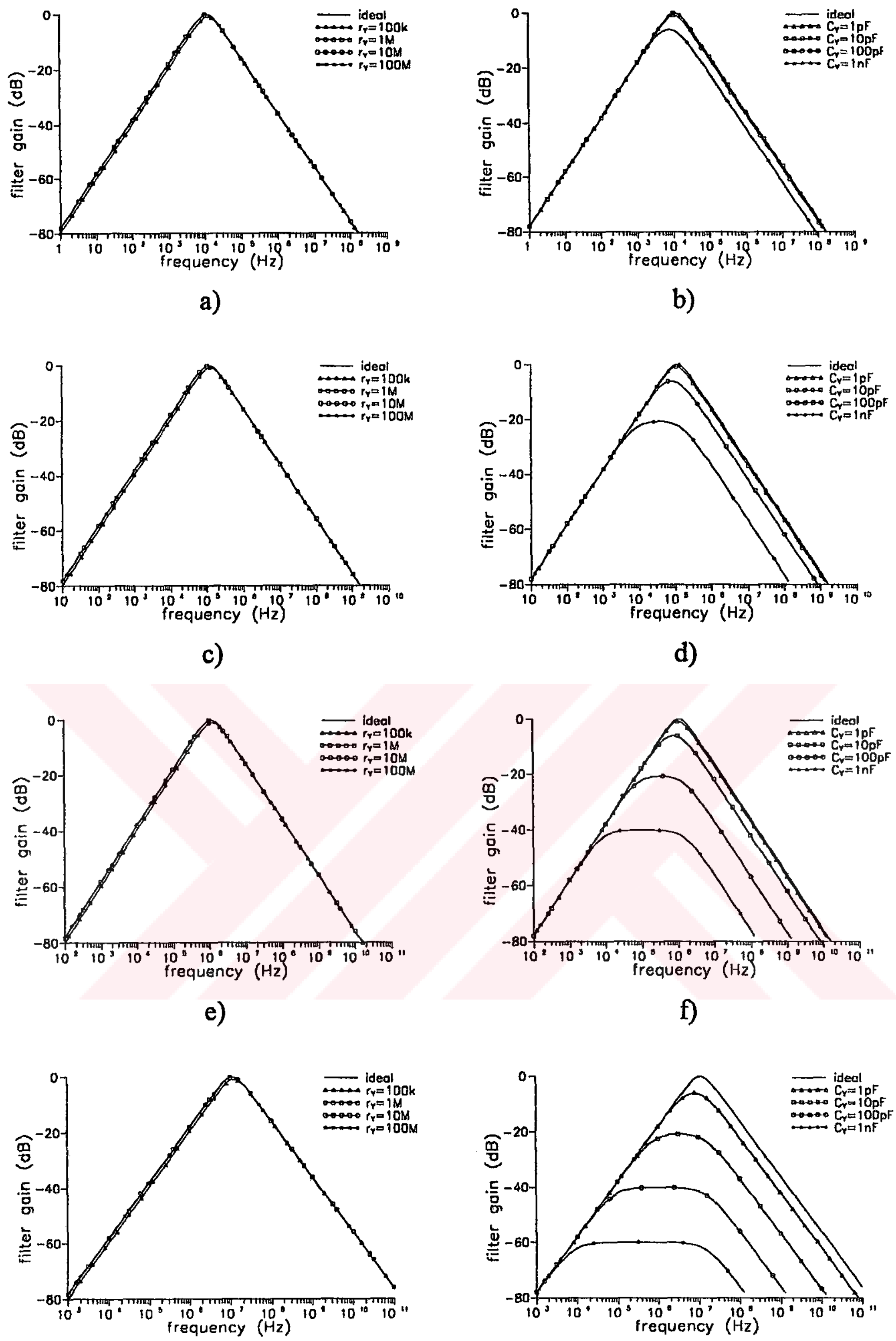

Figure 5.8 The effect of r_Y and C_Y on the bandpass filter characteristics
a) and b) f_O =10 kHz c) and d) f_O =100 kHz e) and f) f_O =1 MHz g) and h) f_O =10 MHz

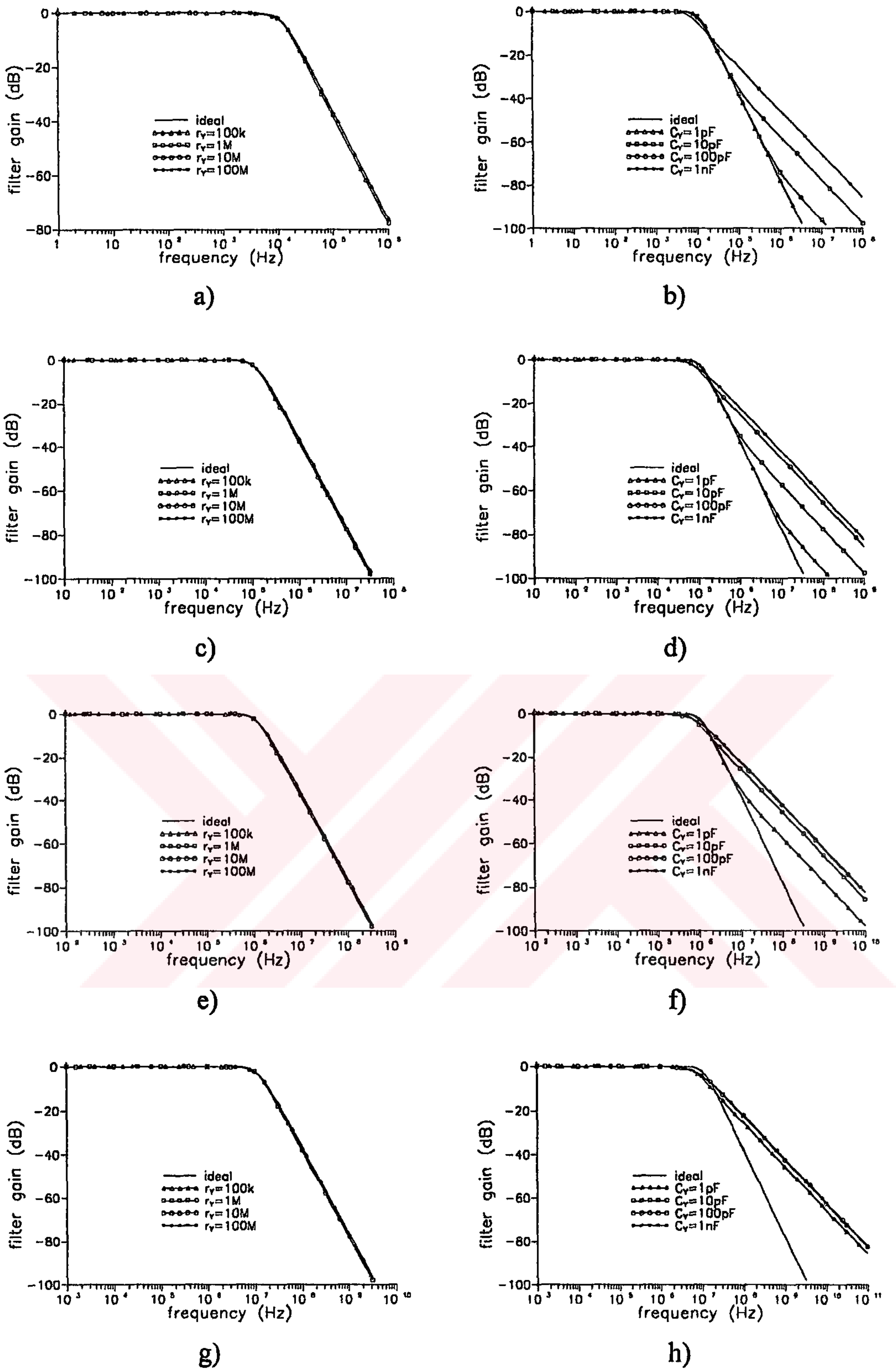

Figure 5.9 The effect of r_Y and C_Y on the lowpass filter characteristics
a) and b) f_O =10 kHz c) and d) f_O =100 kHz e) and f) f_O =1 MHz g) and h) f_O =10 MHz

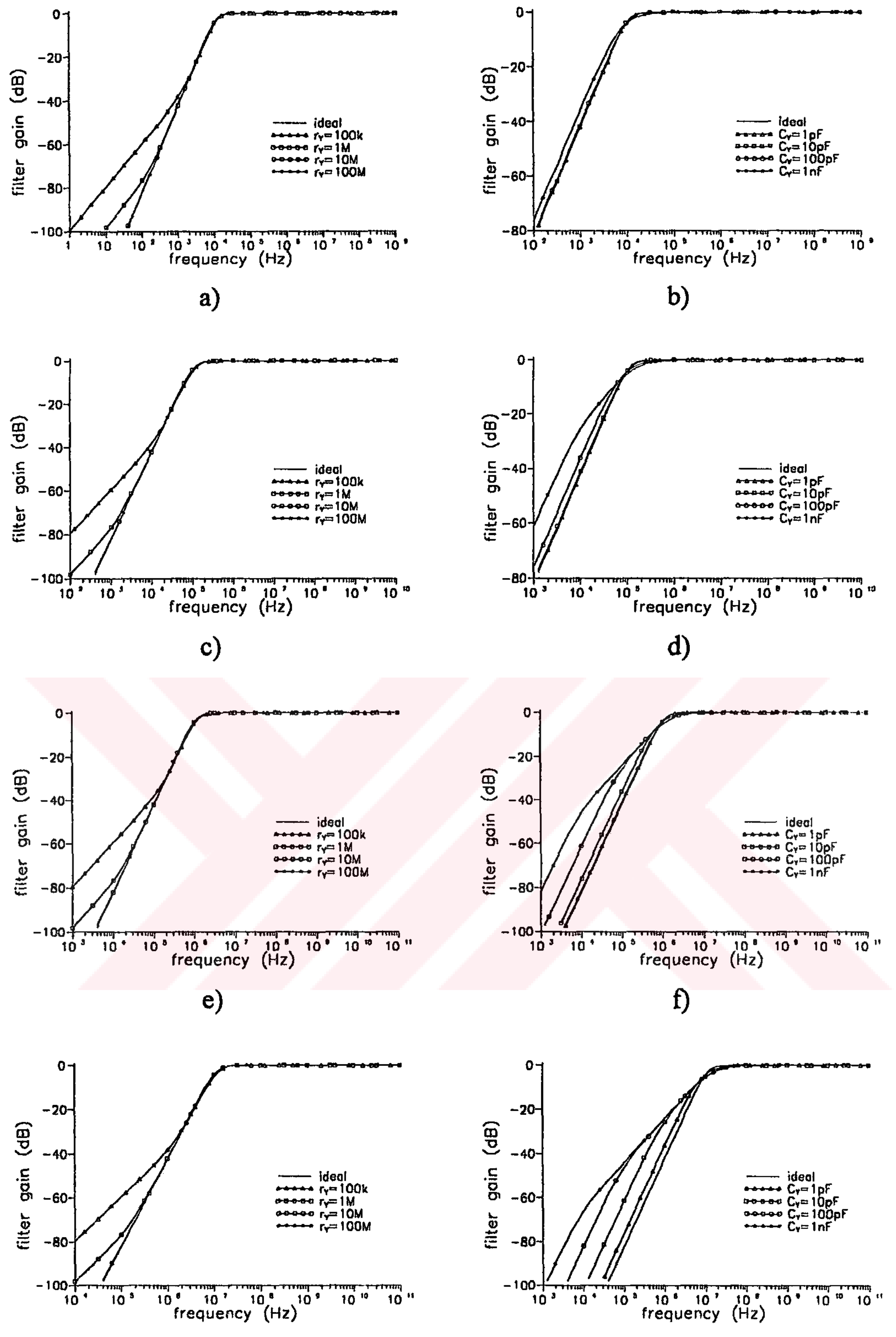

Figure 5.10 The effect of r_Y and C_Y on the highpass filter characteristics
a) and b) f_O =10 kHz c) and d) f_O =100 kHz e) and f) f_O =1 MHz g) and h) f_O =10 MHz

r_Y =100 kΩ, 1 MΩ, 10 MΩ, 100 MΩ; four different values of C_Y, namely C_Y=1 pF, 10 pF, 100 pF, 1 nF and four different cutoff frequencies of f_O =10 kHz, 100 kHz, 1 MHz, 10 MHz have been demonstrated.

Section 5.1 has covered the effects of current conveyor non-idealities on a current-mode active filter. The filter parameters in terms of non-ideality terms have been derived. Table 5.1 summarizes the minimum/maximum values for the non-ideality terms, provided that a 10% deviation in the filter cutoff frequency (resonant frequency) and quality factor is acceptable. Please note that the results obtained are valid for the three types of filters unless specified otherwise.

Table 5.1 Limits of non-ideality terms for a deviation of 10% in filter parameters

	ω_O	Q_O
r_X	< 0.12 R for BP and HP < 0.23 R for LP	< 0.12 R for BP < 0.23 R for LP < 0.05 R for HP
r_Y	> 9.52 R	> 6.59 R for BP > 8.53 R for LP > 3.33 R for HP
C_Y	< 0.23 C for BP and HP < 0.12 C for LP	< 0.23 C for BP and HP < 0.77 C for LP
r_Z	0	0
C_Z	0	0
τ_I	0	0
τ_V	< 0.2 RC	$< \dfrac{1}{10Q_O(\omega_O + \dfrac{1}{2Q_O RC})}$

5.2 THE FILTER PERFORMANCE FOR VARIOUS CURRENT CONVEYOR CIRCUITS

In this section, a comparable demonstration of the filter performance for each current conveyor circuit studied in Chapter 3 has been given. Figs. 5.11 through

5.16 depict the performance of the three types of filters when current conveyors CC1-CC8 are employed in the filter, for four different filter frequencies of f_O=10 kHz, 100 kHz, 1 MHz and 10 MHz.

The current-mode filter studied in the previous section appears to be the current conveyor based counterpart of filters classified as "multi-feedback filters using a single infinite gain operational amplifier". Therefore the results obtained in this chapter apply to all filters under this class which form a great deal of amount.

Eqs. 5.17 through 5.19, 5.21 through 5.23, 5.25 through 5.27, demonstrate the results obtained for the relative deviations in the filter parameters when the effect of the resistive component of the impedance of terminal x is introduced into the ideal current-mode filter transfer functions. Eqs. 5.16, 5.20 and 5.24 show that the rearranged bandpass, lowpass and highpass filter transfer functions preserve their second order characteristic forms. The related equations show that small relative deviations of the filter cutoff (resonant) frequency and quality factor for all three types of filters require the condition of $2r_X \ll R$ to be satisfied, where R= 10 kΩ. Eq. 5.23 yields that the lowpass filter gain is not affected by the resistance of terminal x. Table 3.1 shows that only the value of r_X = 637 Ω for current conveyor CC7 slightly exceeds the condition above. However, no significant effect can be observed on the filter characteristics given in Figs. 5.11 through 5.16, caused by this non-ideality term.

Section 5.1.2 summarizes the results obtained for the relative deviations in the filter parameters when the effect of the admittance of terminal z is introduced into the ideal filter transfer functions. Eq. 5.28 yields a third order transfer function and an extra pole of $f_{pole} = \frac{1}{2\pi}\frac{g_Z R_L + 1}{C_Z R_L}$ appears in all three filter characteristics. Introduction of the corresponding values in Table 3.1 into this expression gives pole frequencies above 1 GHz even for the worst values of CC1. Analysis of Eq. 5.28 shows that the relative deviations in the cutoff (resonant) frequency and quality factor are zero. Therefore, no significant effect of this non-ideality term can be observed on the filter characteristics given in Figs. 5.11 through 5.16.

Eqs. 5.30 through 5.32 demonstrate the filter transfer functions obtained, when the current transfer function of a current conveyor is introduced into their ideal counterparts. It is obvious that an extra pole determined by τ_I appears in the filter characteristics, and the cutoff (resonant) frequency and quality factor remains unchanged, provided that the condition of $s\tau_I << 1$ is satisfied. Table 3.1 shows that this condition is well satisfied for CC1-CC3 and CC5 upto filter frequencies of 100 kHz, whereas for CC4 and CC6-CC8 upto 10 MHz.

The results obtained for the relative deviations in the filter parameters, when the voltage transfer function of a current conveyor is introduced, are expressed in Eqs. 5.36, 5.37, 5.40, 5.41, 5.44, 5.45. Eqs. 5.33, 5.38 and 5.42 yield that additional zeros caused by this non-ideality term are introduced to the transfer functions, which results with the poor performances in the low frequency range observed in Figs. 5.11 through 5.16. Table 3.1 shows that CC3 demonstrates the worst performance in terms of voltage transfer function bandwidth, enabling use for filters upto 300-400 kHz, whereas the others allow filter cutoff (resonant) frequencies upto 1 MHz and even 10 MHz.

Eqs. 5.47 through 5.49, 5.52 through 5.54, 5.57 through 5.59 demonstrate the results obtained for the relative deviations in the filter parameters when the effect of the admittance of terminal y is introduced into the ideal filter transfer functions. Eq. 5.46 yields that while the rearranged bandpass filter transfer function preserves its second order form, additional zeros are introduced into the lowpass and highpass filter transfer functions, which are clearly demonstrated in Figs. 5.9 and 5.10. It is apparent that care should be taken that these zeros given by the expressions of $f_{LPzero} = \frac{1}{2\pi}\frac{g_Y R_4 + 1}{C_Y R_4}$ and $f_{HPzero} = \frac{1}{2\pi}\frac{g_Y}{C_4 + C_Y}$, lie well beyond the filter cutoff frequencies. The related equations dictate that the conditions of $2g_Y R << 1$ and $2C_Y << C$ should be satisfied for small deviations in the filter cutoff (resonant) frequency and quality factor. All eight current conveyors prove to satisfy these equations.

The results obtained in the previous section have been used to determine the minimum/maximum values for the non-ideality terms, provided that 10% deviations in the filter cutoff (resonant) frequency and quality factor is acceptable. These values are given in Table 5.1. Analyses show that the deviation in filter parameters remain within the specified limit of 10% for all current conveyors listed. Once again, Figs. 5.11 through 5.16 yield that CC7 exhibits the best filter performances in all aspects. The relatively bad performance of CC1-CC2, CC6 and CC8, in the bandpass and of CC6 and CC8 in the highpass configurations can be attributed to the terminal z impedance and voltage transfer function of the current conveyors, which introduce additional zeros. As a result, the above mentioned impedance and transfer ratio, remain as the most critical non-ideality terms which determine the performance of the current-mode filter. The related figures once more prove that the lowpass filter is the most tolerable filter type to active component non-idealities.

The large-signal behavior of the three types of filters for a cutoff (resonant) frequency of 10 kHz have been demonstrated in Figs. 5.17 through 5.19. The frequency of the input signal for the highpass filter is 500 kHz, whereas a frequency of 100 Hz has been chosen for the lowpass filter input signal. The maximum input signal amplitude for each current conveyor has been listed in Table 5.2, provided that a distortion of 1% for the output signal is acceptable. Once again, please note that these values are not necessarily the optimum values.

Table 5.2 The maximum input signal amplitude for various current conveyors

	i_{1BP}	i_{1LP}	i_{1HP}
CC1	550 μA	550 μA	15 mA
CC2	700 μA	8 mA	8 mA
CC3	800 μA	10 mA	10 mA
CC4	170 μA	2 mA	1.2 mA
CC5	900 μA	11 mA	12 mA
CC6	180 μA	200 μA	180 μA
CC7	240 μA	300 μA	300 μA
CC8	35 μA	2 mA	50 μA

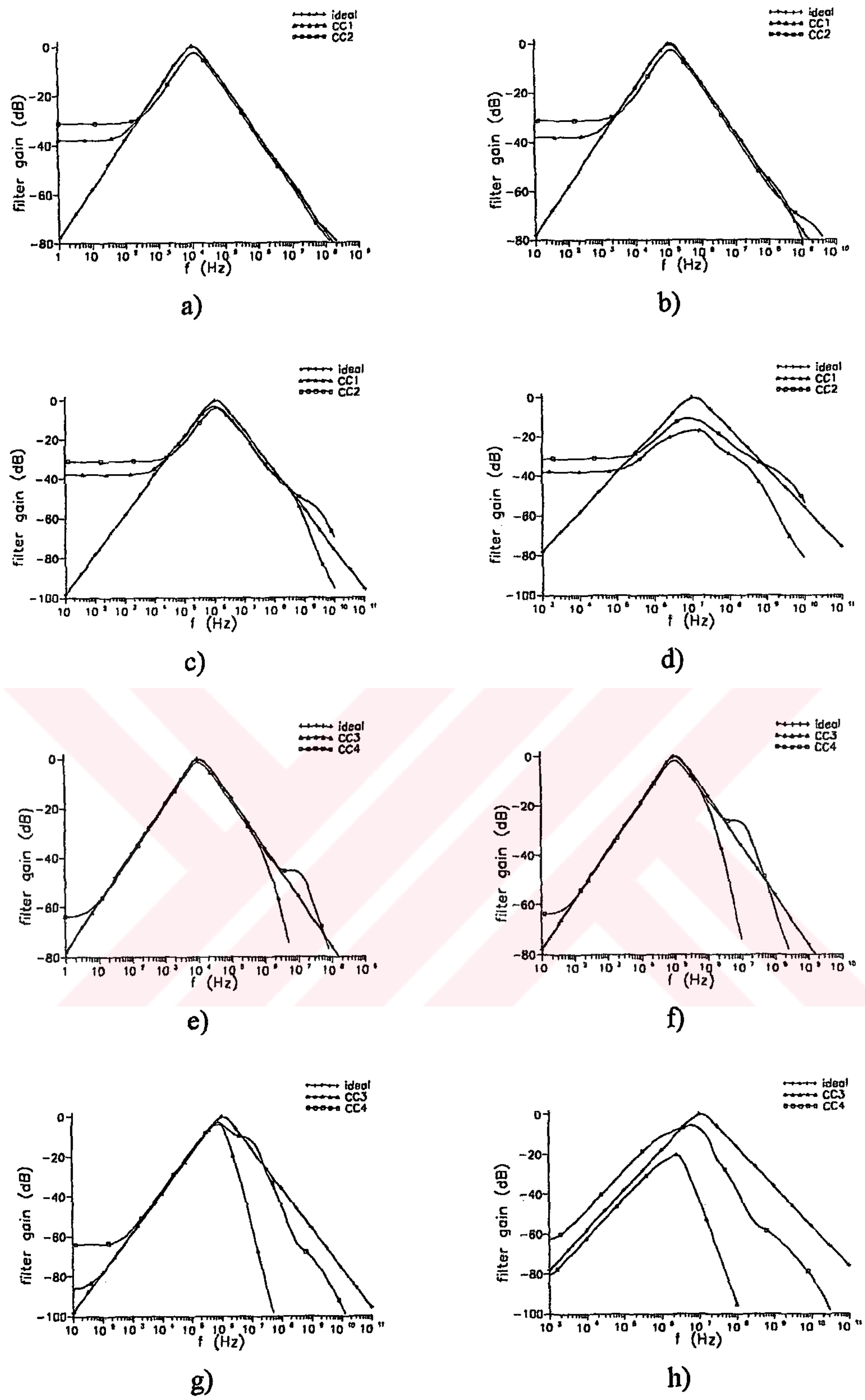

Figure 5.11 The bandpass filter performance for CC1-CC4 at four different resonant frequencies of a) and e) $f_o = 10$ kHz b) and f) $f_o = 100$ kHz c) and g) $f_o = 1$ MHz d) and h) $f_o = 10$ MHz

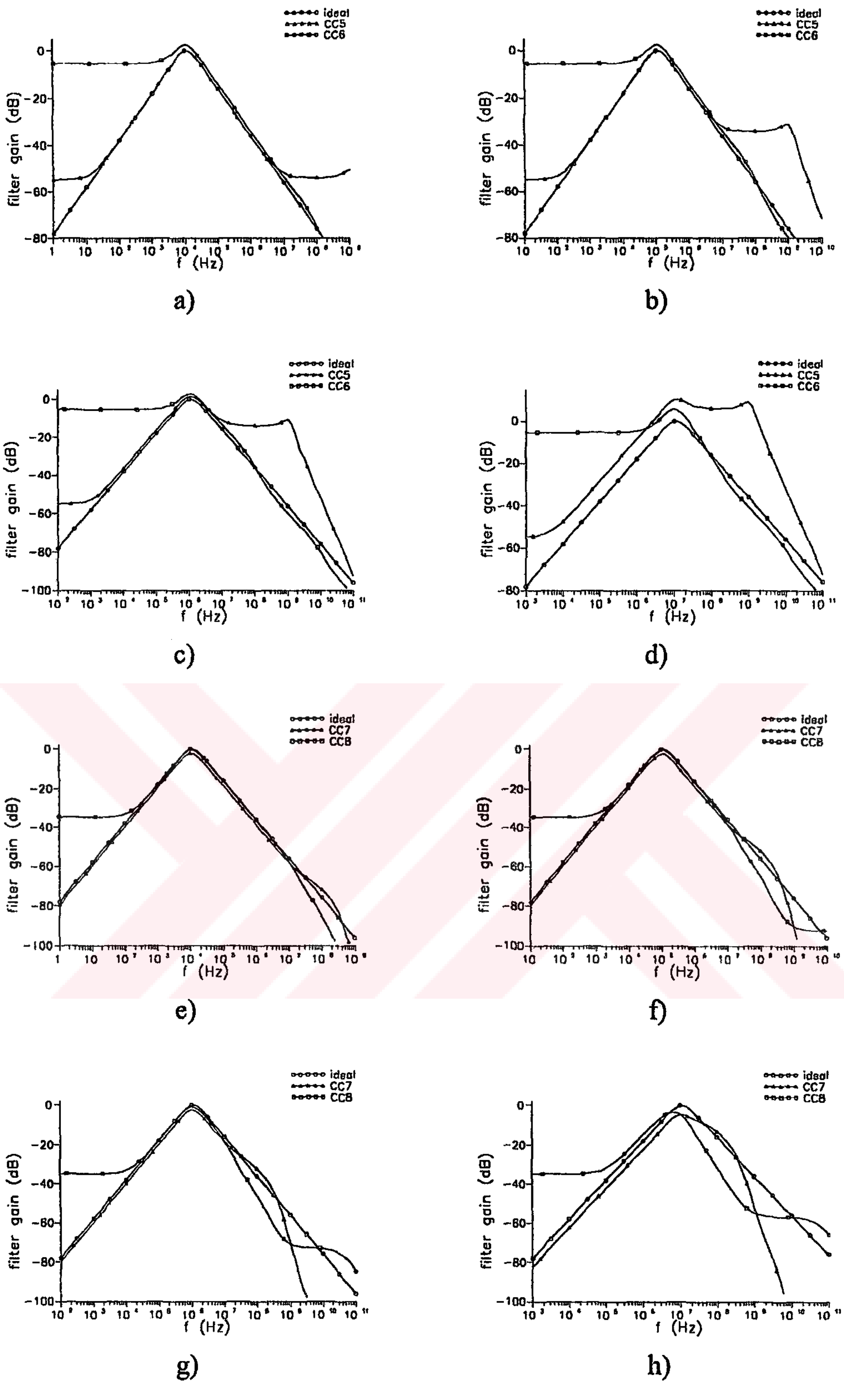

Figure 5.12 The bandpass filter performance for CC5-CC8 at four different resonant frequencies of a) and e) $f_0 = 10$ kHz b) and f) $f_0 = 100$ kHz c) and g) $f_0 = 1$ MHz d) and h) $f_0 = 10$ MHz

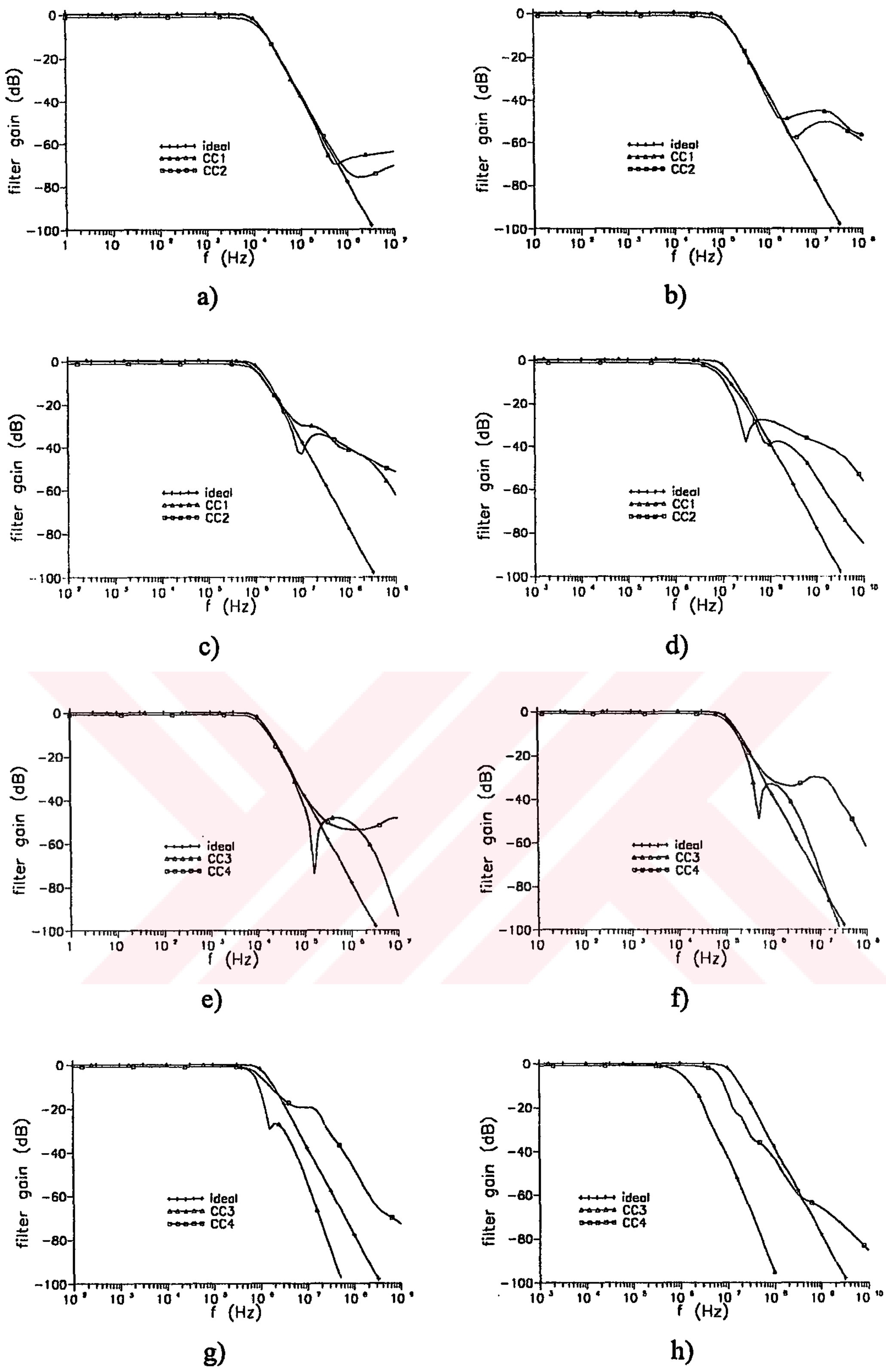

Figure 5.13 The lowpass filter performance for CC1-CC4 at four different cutoff frequencies of a) and e) $f_o = 10$ kHz b) and f) $f_o = 100$ kHz c) and g) $f_o = 1$ MHz d) and h) $f_o = 10$ MHz

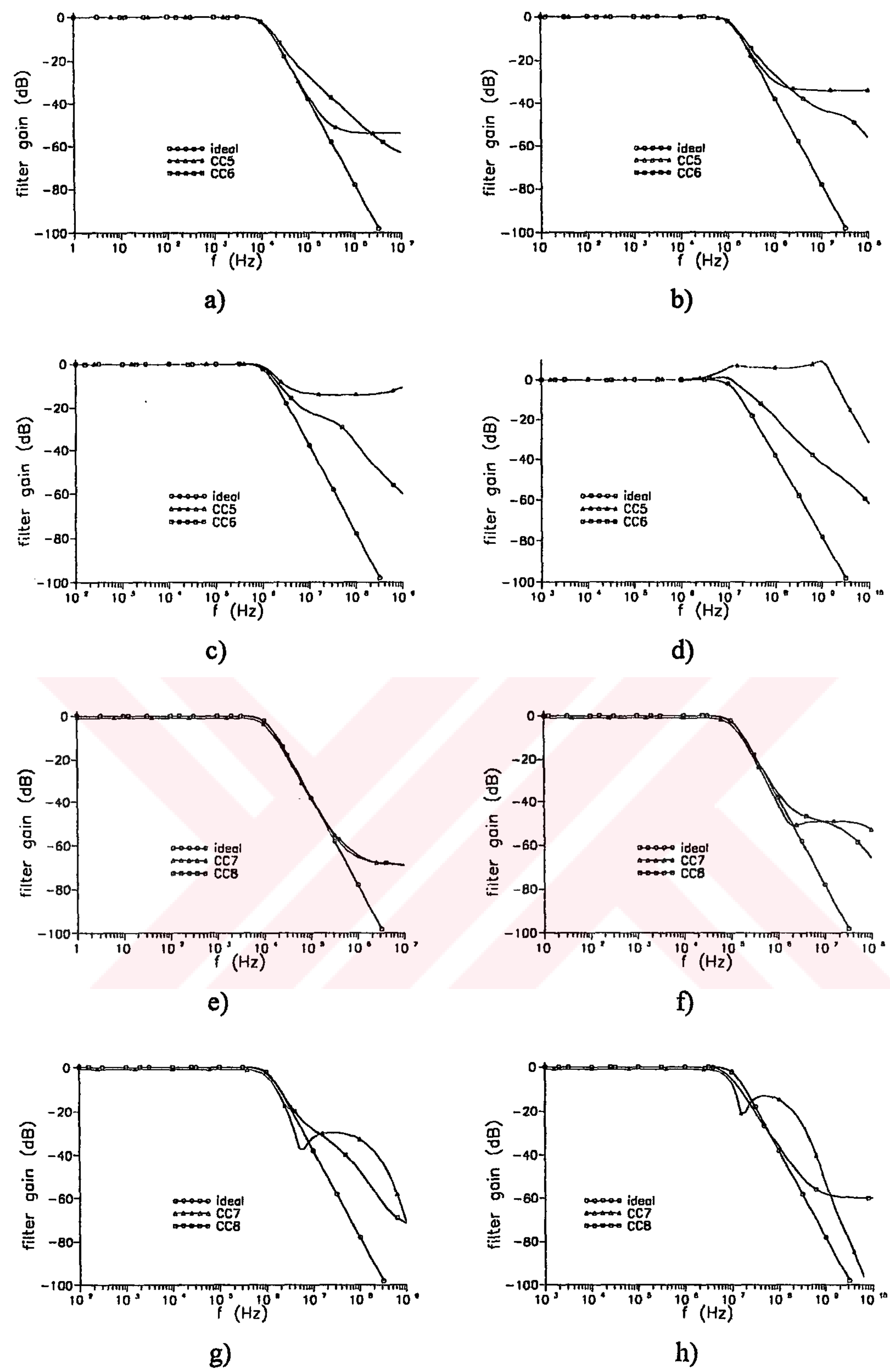

Figure 5.14 The lowpass filter performance for CC5-CC8 at four different cutoff frequencies of a) and e) f_o = 10 kHz b) and f) f_o = 100 kHz c) and g) f_o = 1 MHz d) and h) f_o = 10 MHz

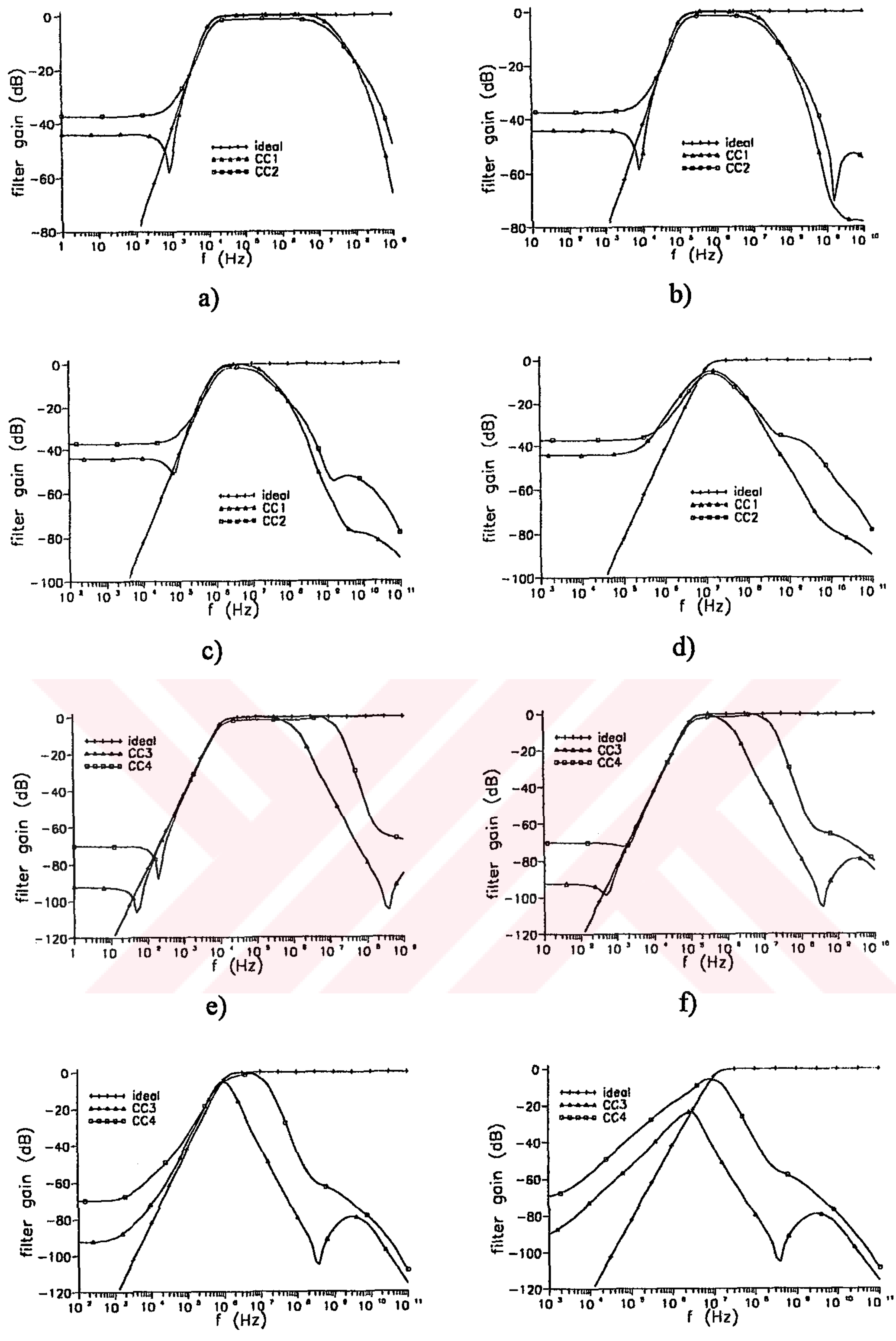

Figure 5.15 The highpass filter performance for CC1-CC4 at four different cutoff frequencies of a) and e) $f_o = 10$ kHz b) and f) $f_o = 100$ kHz c) and g) $f_o = 1$ MHz d) and h) $f_o = 10$ MHz

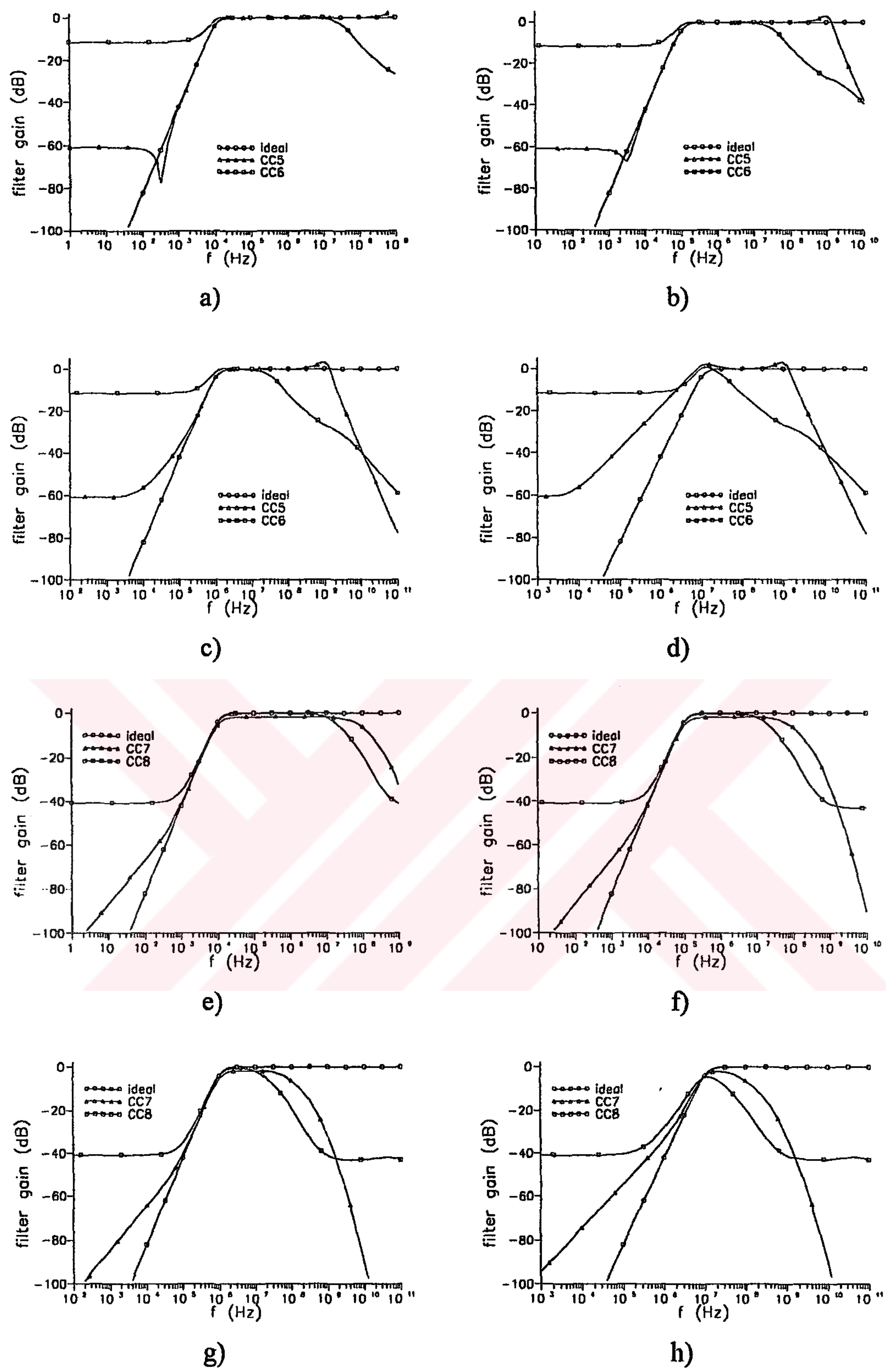

Figure 5.16 The highpass filter performance for CC5-CC8 at four different cutoff frequencies of a) and e) $f_O = 10$ kHz b) and f) $f_O = 100$ kHz c) and g) $f_O = 1$ MHz d) and h) $f_O = 10$ MHz

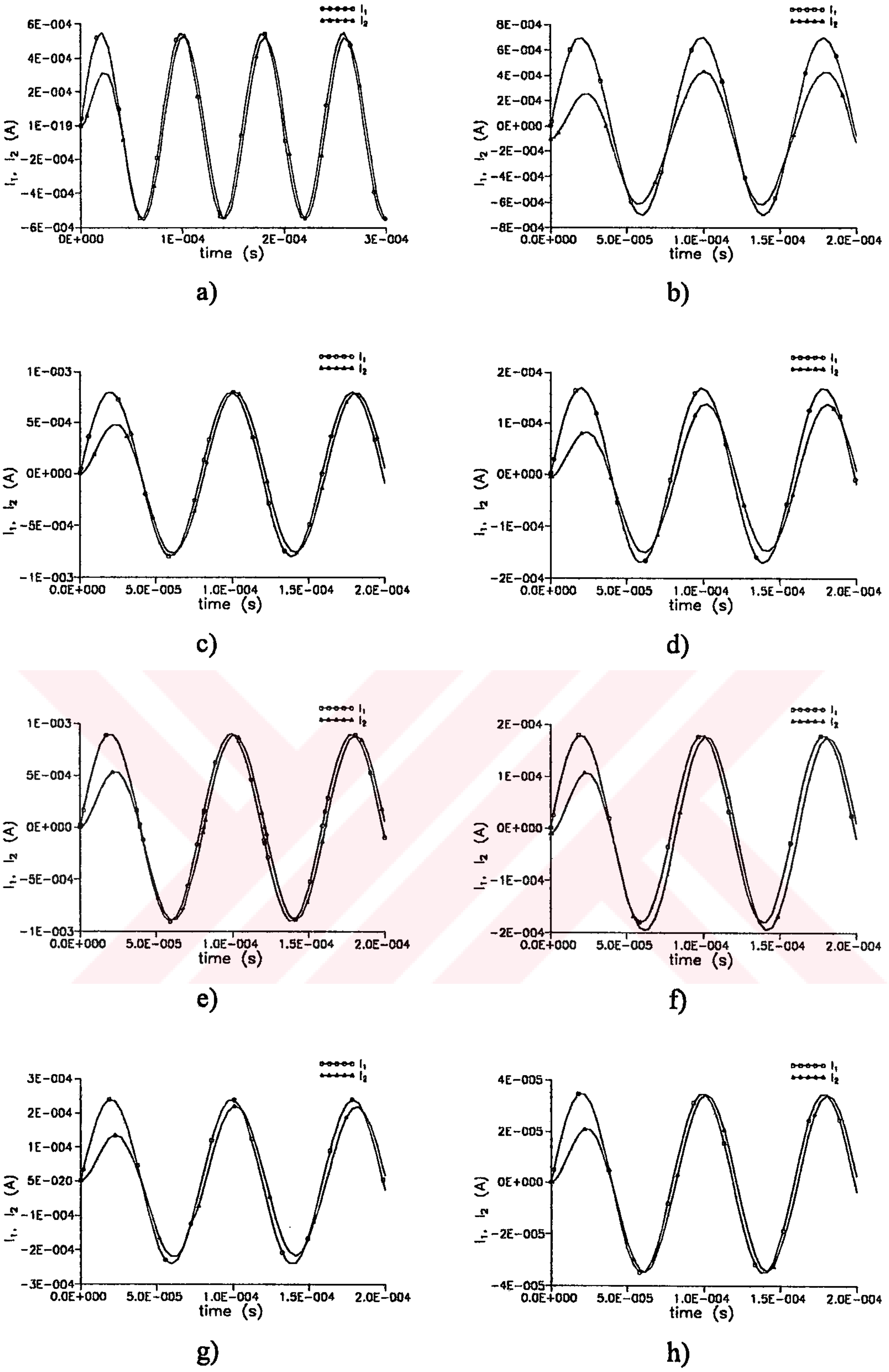

Figure 5.17 The large-signal behavior of the bandpass filter for various current conveyors a) CC1 b) CC2 c) CC3 d) CC4 e) CC5 f) CC6 g) CC7 h) CC8

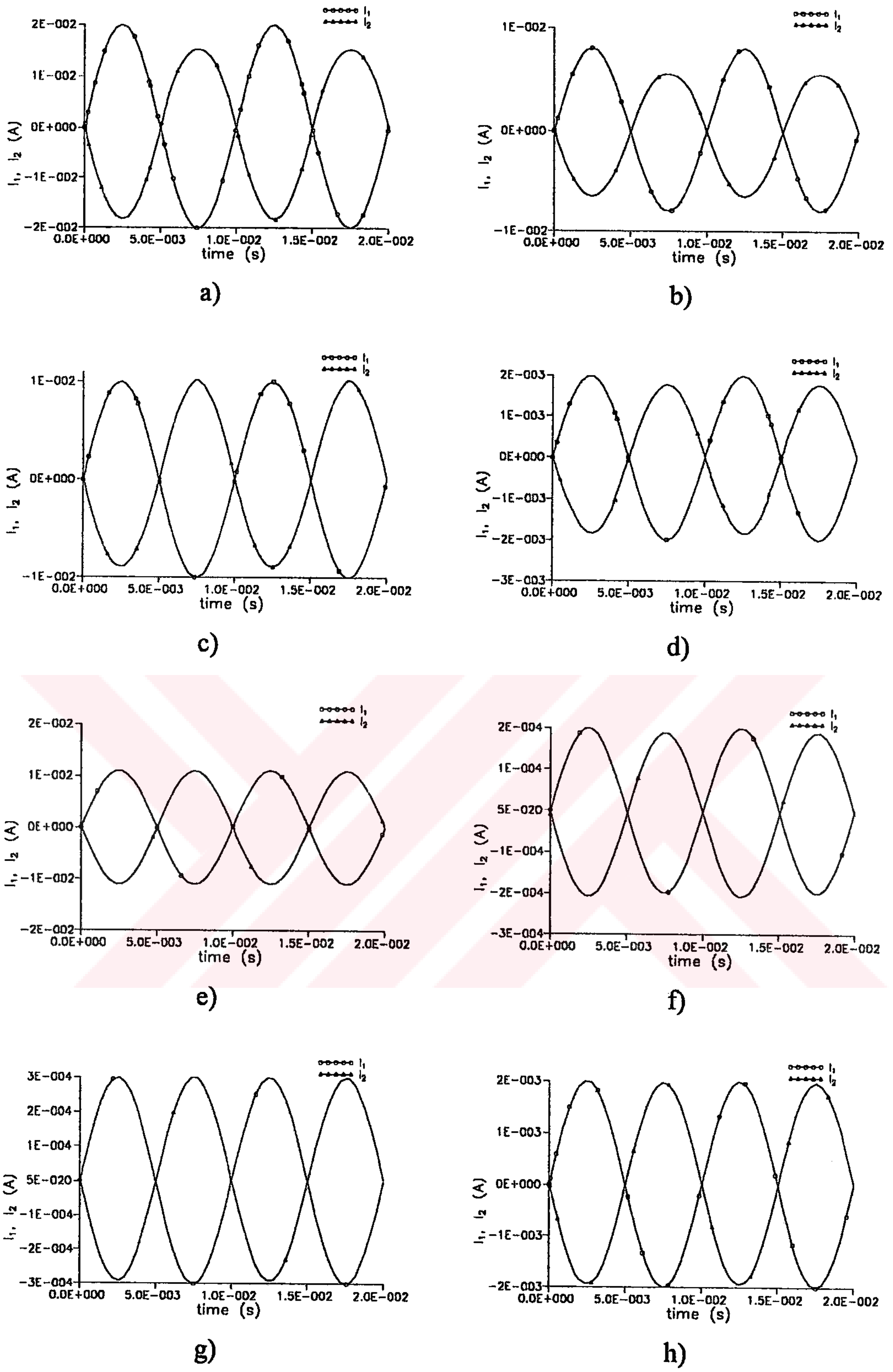

Figure 5.18 The large-signal behavior of the lowpass filter for various current conveyors a) CC1 b) CC2 c) CC3 d) CC4 e) CC5 f) CC6 g) CC7 h) CC8

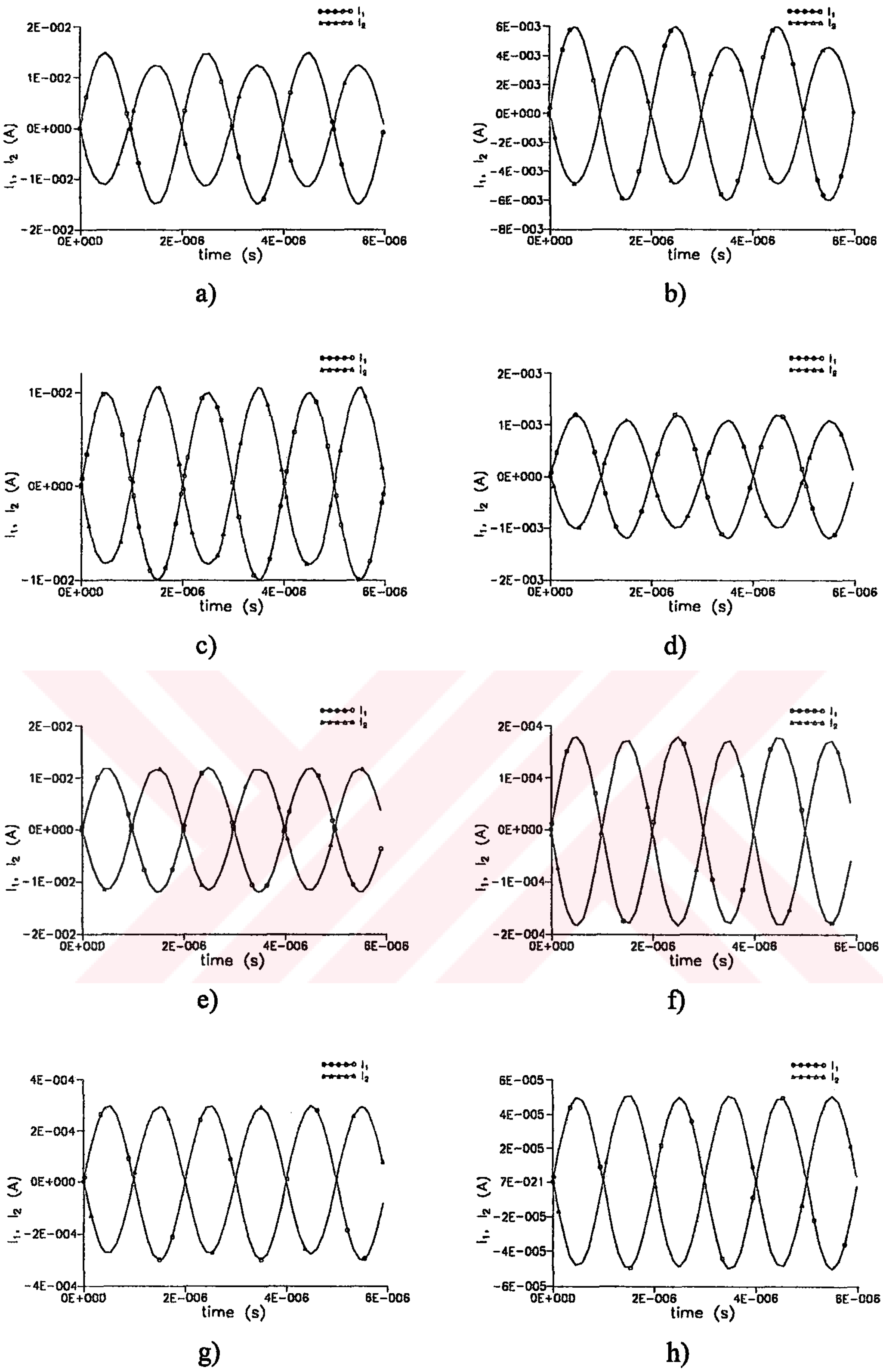

Figure 5.19 The large-signal behavior of the highpass filter for various current conveyors a) CC1 b) CC2 c) CC3 d) CC4 e) CC5 f) CC6 g) CC7 h) CC8

CHAPTER 6

NOVEL CURRENT CONVEYOR STRUCTURES SUITABLE FOR CONTINUOUS-TIME ACTIVE FILTERS

An extensive study on the effects of current conveyor non-idealities on active filters has been given in the previous chapters. Tables 4.1 and 5.1 summarize the results obtained and demonstrate the limitations for the non-ideality terms. It is apparent that careful consideration should be given if a specified filter performance is to be obtained. This chapter includes some current conveyor proposals which satisfy the conditions obtained previously and offers new opportunities to be used in analog circuit design.

As in Chapter 3, XR B101 and XR B102 device model parameters have been used for the npn and pnp transistors, respectively, during the SPICE simulation of the bipolar current conveyor, whereas Alcatel Mietec 2 μm HBiMOS process parameters have been used for the MOS implementations. MOS transistor dimensions of the current conveyors are given in Appendix A.

6.1 PERFORMANCE CHARACTERISTICS OF CURRENT CONVEYOR 1N

In this section, the current conveyor circuit given in Fig. 6.1a will be studied. Two simple current mirrors, two modified Wilson current mirrors and four current mirrors based on the modified Wilson current mirror [36] have been combined to form a translinear current conveyor [37]. In Fig. 6.1b, Q1-Q9 form the circuit based on the modified Wilson current mirror, where Q1-Q2 and Q4-Q5 act as the modified Wilson circuit and the remaining transistors form a negative feedback

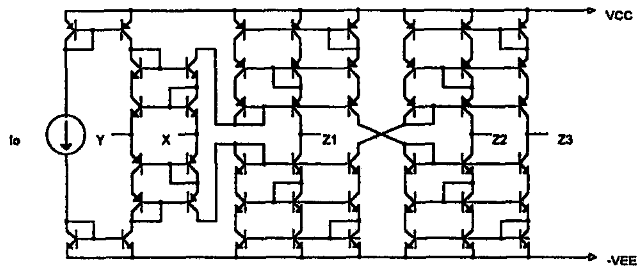

a)

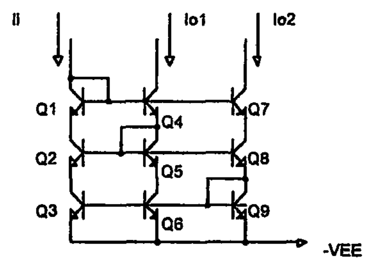

b)

Figure 6.1 a) Circuit diagram of current conveyor 1n b) Two-output mirror based on the modified Wilson current mirror

loop which returns the base currents of Q7 and Q8 to the modified Wilson current mirror to provide $I_i + I_{o1} \approx I_{e3} + I_{e6}$. The equal base-emitter voltages of Q3 and Q6 which forces their emitter currents to be equal, together with the modified Wilson current mirror, yields $I_{o1} = I_i$. Since $I_i + I_{o1} + I_{o2} = I_{e3} + I_{e6} + I_{e9}$, then $I_{o2} = I_i$. The translinear current equation and mirror arrangements force the currents of terminal z1 and x to be in the same direction, whereas the currents of terminals z2 and z3 will be identically in opposite directions. It is clear that the voltage of terminal x will track terminal y. Thus, a combined structure of an inverting and non-inverting current conveyor will be obtained, which offers an advantage for certain filter structures.

Supply voltages were chosen to be ±10 V and I_O as 100 μA. The voltage transfer characteristics $V_X = V_X(V_Y)$ for open-circuited terminal x and $V_Z = V_Z(V_Y)$ for open-circuited terminal z1 (z2), are given in Figs. 6.2a and b, respectively. The voltage clipping limits at terminal x and terminal z1 (z2) were obtained as V_{Xmax}= 8.96 V, V_{Xmin}= -8.96 V, V_{Zmax}= 7.07 V (8.21 V) and V_{Zmin}= -8.36 V (-8.32 V).

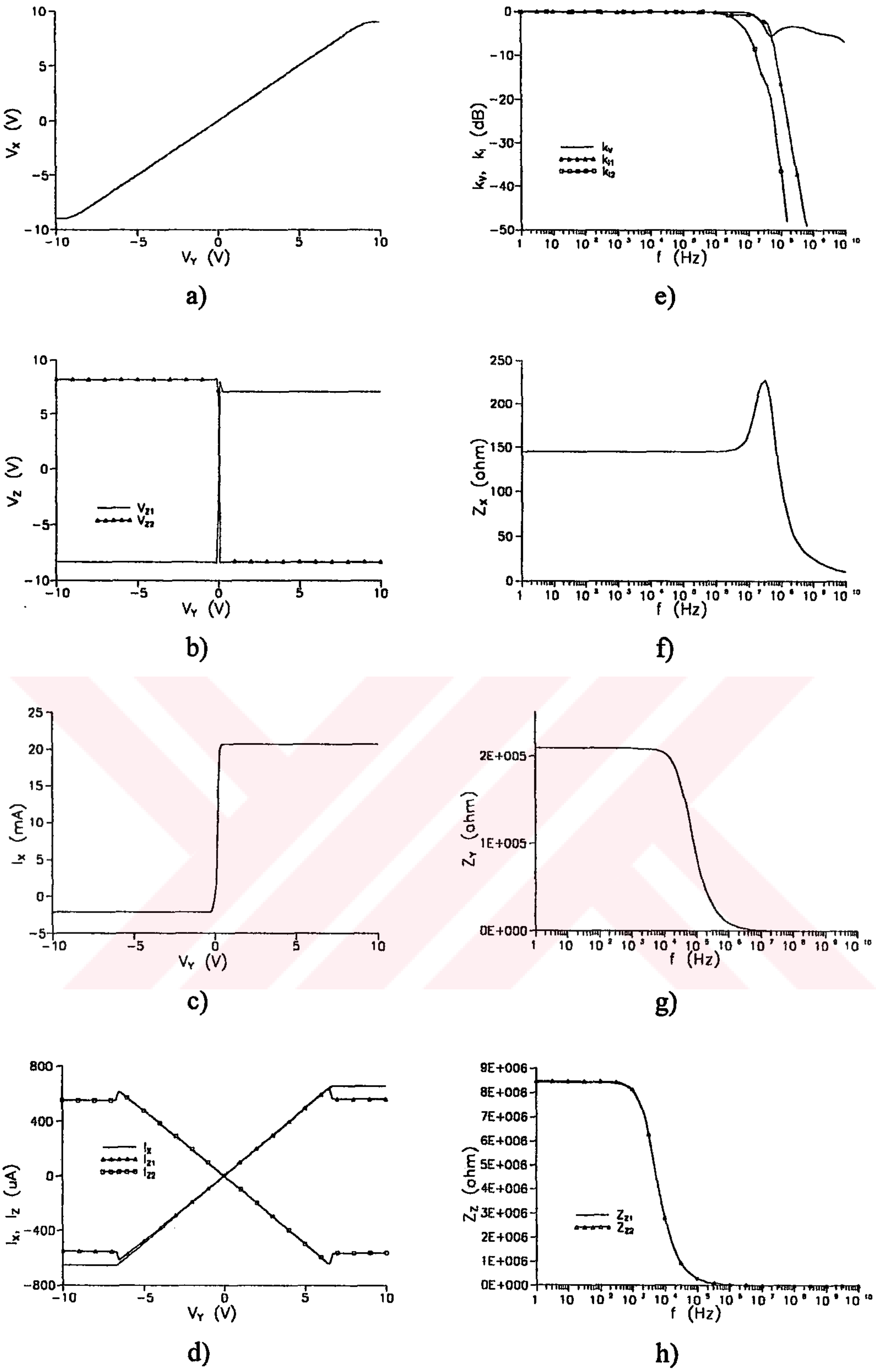

Figure 6.2 SPICE simulated device characteristics of current conveyor 1n
a) $V_X = V_X(V_Y)$ for $R_X = \infty$ b) $V_Z = V_Z(V_Y)$ for $R_Z = \infty$ c) $I_X = I_X(V_Y)$ for $R_X = 0$ d) $I_X = I_X(V_Y)$, $I_Z = I_Z(V_Y)$ for $R_X = R_Z = 10\ k\Omega$ e) The frequency responses of v_x / v_y and i_z / i_x for $R_X = R_Z = 10\ k\Omega$ f) The frequency response of Z_X g) The frequency response of Z_Y h) The frequency response of Z_Z

Fig. 6.2c illustrates $I_X = I_X(V_Y)$ characteristic for short-circuited terminal x. The lower and upper boundaries of the current I_X were determined as I_{Xmin}= -2.10 mA and I_{Xmax}=20.67 mA. The $I_X = I_X(V_Y)$ and $I_Z = I_Z(V_Y)$ characteristics for terminal loads of R_X=10 kΩ and R_Z=10 kΩ are given in Fig. 6.2d.

The frequency responses of the voltage gain v_x/v_y and current gain i_z/i_x are shown in Fig. 6.2e. We obtain the values of the voltage and current transfer functions at low frequencies as k_V=0.985 and k_I=0.992 (0.996), respectively, for terminal loads of R_X=10 kΩ and R_Z=10 kΩ. The 3 dB bandwidth values are f_V=30 MHz and f_I=41 MHz (6.2 MHz), respectively.

Fig. 6.2f shows that the impedance Z_X has a value of 145 Ω at low frequencies and shows a maximum of 227 Ω at a resonant frequency of 31.6 MHz. Simulated variations of the impedance Z_Y with frequency are given in Fig. 6.2g. Values of r_Y=209 kΩ and C_Y=16.9 pF are obtained. Fig. 6.2h showing the output impedance Z_Z at terminal z, gives the values of r_Z=8.4 MΩ (8.45 MΩ) and C_Z=5.4 pF (5.38 pF). The results obtained are summarized in Table 6.1.

6.2 PERFORMANCE CHARACTERISTICS OF CURRENT CONVEYOR 2N

Figs. 4.11, 4.13, 4.15 and 5.12, 5.14, 5.16 show that the current conveyor circuit of CC6 investigated in Chapter 3 exhibits poor performance for frequencies below the cutoff (resonant) frequency. Efforts have been made towards an improved current conveyor circuit which overcomes this problem mainly caused by the unsatisfactory output characteristic. The circuit is given in Fig. 6.3. M44 and M66 have been added in order to increase the output impedances of M4 and M6, whereas M55, M77 and M88 together with the related transistors, form cascode current mirrors which also contribute to an improved output impedance. Results show that the goal of satisfying the conditions in Table 4.1, and an improved performance in the filter characteristics have been achieved.

Table 6.1 Characteristic values of the proposed current conveyors

	CC1N	CC2N	CC3N	CC4N	CC5N	CC6N
V_{Xmax}	8.96 V	1.3 V	4.06 V	4.76 V	6.91 V	8.41 V
V_{Xmin}	-8.96 V	-4.46 V	-4.59 V	-7.52 V	-8.74 V	-8.94 V
V_{Zmax}	7.07 V	2.71 V	4.39 V	9.52 V	9.93 V	6.31 V
V_{Zmin}	-8.36 V	-5 V	-5 V	-9.42 V	-9.56 V	-7.18 V
I_{Xmax}	20.67 mA	103.4 μA	50.1 μA	1.87 mA	5.78 mA	0.82 mA
I_{Xmin}	-2.10 mA	-195.8 μA	-166.9 μA	-69.7 μA	-100.6 μA	-0.91 mA
k_V	0.985	0.909	0.977	0.996	≈1	0.9897
f_V	30 MHz	26.4 MHz	68.3 MHz	123 MHz	272 MHz	216 MHz
k_I	0.992	0.958	0.987	1.019	0.997	1.052
f_I	41 MHz	66 MHz	20 MHz	32.6 MHz	188 MHz	19 MHz
r_X	145 Ω	766.5 Ω	2015 Ω	3.4 Ω	1.9 Ω	350.7 Ω
r_{X1}	70 Ω	366.5 Ω	1015 Ω	1.4 Ω	0.9 Ω	150.7 Ω
r_{X2}	75 Ω	400 Ω	1000 Ω	2 Ω	1 Ω	200 Ω
R_P	227 Ω	10.9 kΩ	3141 Ω	3281 Ω	5797 Ω	17.5 kΩ
f_P	31.6 MHz	50.1 MHz	39.8 MHz	125.9 MHz	158.5 MHz	125.9 MHz
r_Y	209 kΩ	11.1 TΩ	1.6 TΩ	18.9 TΩ	22.4 TΩ	20.9 TΩ
C_Y	16.9 pF	10.1 fF	70 fF	6 fF	5 fF	5.4 fF
r_Z	8.4 MΩ	438 kΩ	2.81 MΩ	788.4 MΩ	23.7 kΩ	62.6 MΩ
C_Z	5.4 pF	43.3 fF	182.7 fF	151.9 fF	161.8 fF	33.2 fF

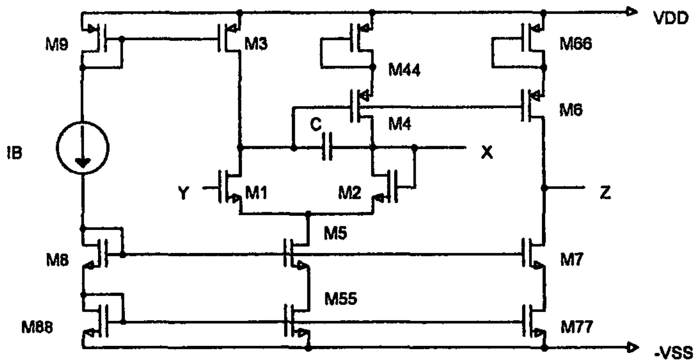

Figure 6.3 Circuit diagram of current conveyor 2n

SPICE simulations have been carried out to check the performance of the improved current conveyor. Supply voltages were chosen to be ±5 V and I_B as 100 μA. The value of the compensation capacitor is 0.5 pF. The performance characteristics are given in Fig. 6.4, whereas the characteristic values are given in Table 6.1.

6.3 PERFORMANCE CHARACTERISTICS OF CURRENT CONVEYOR 3N

Fig. 6.5 depicts another improved circuit configuration derived from the current conveyor circuit of CC6 investigated in Chapter 3. Cascode current mirrors were introduced to the circuit to provide low capacitance nodes. Low impedance nodes appear except the output stage which helps improve the frequency behavior.

SPICE simulations have been carried out to check the performance of the improved current conveyor. Supply voltages were chosen to be ±5 V and I_B as 100 μA. Capacitor values were chosen to be 0.5 pF. The performance characteristics are given in Fig. 6.6 and the characteristic values are given in Table 6.1.

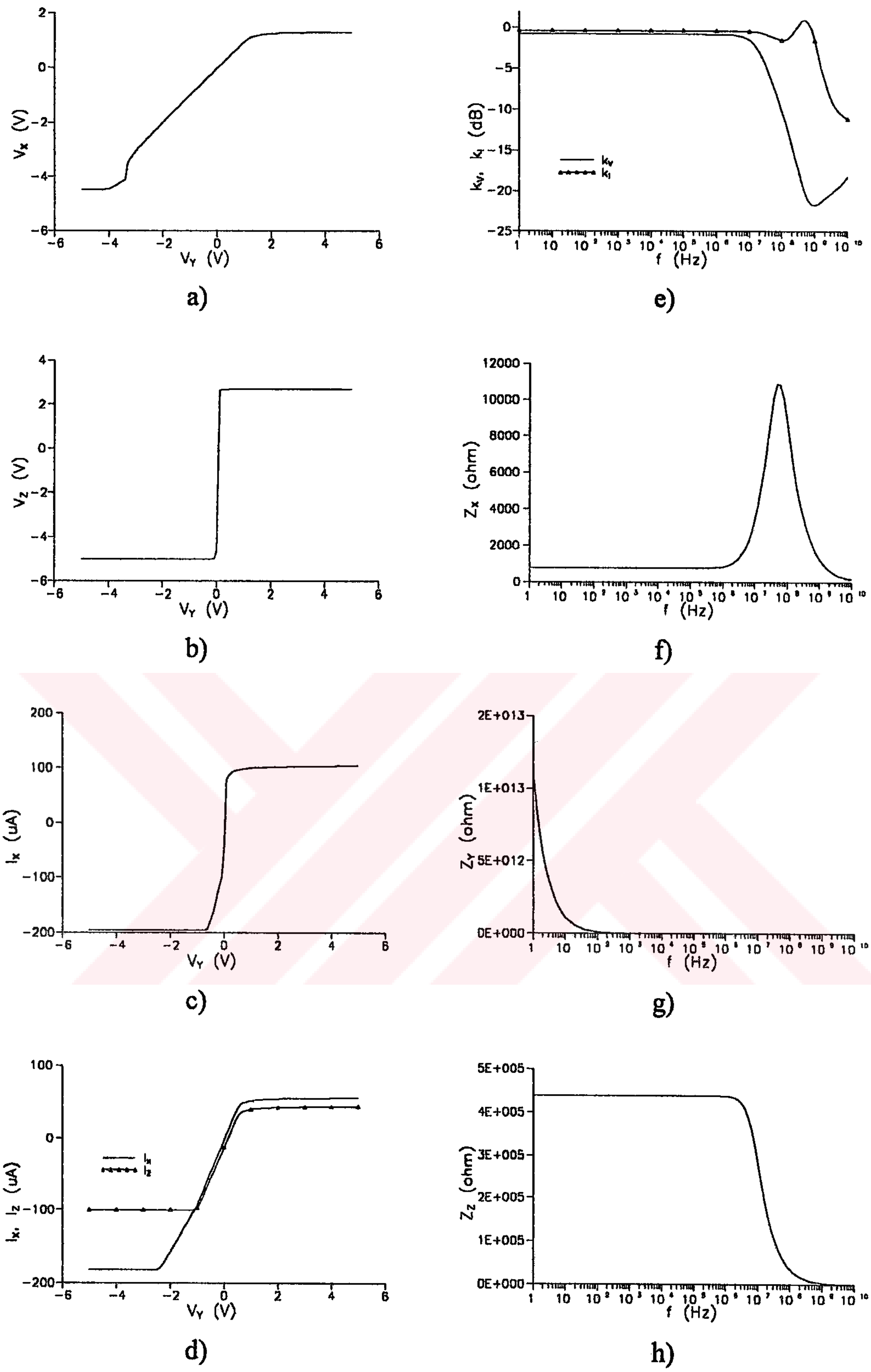

Figure 6.4 SPICE simulated device characteristics of current conveyor 2n
a) $V_X = V_X(V_Y)$ for $R_X = \infty$ b) $V_Z = V_Z(V_Y)$ for $R_Z = \infty$ c) $I_X = I_X(V_Y)$ for $R_X = 0$ d) $I_X = I_X(V_Y)$, $I_Z = I_Z(V_Y)$ for $R_X = R_Z = 10$ kΩ e) The frequency responses of v_x / v_y and i_z / i_x for $R_X = R_Z = 10$ kΩ f) The frequency response of Z_X g) The frequency response of Z_Y h) The frequency response of Z_Z

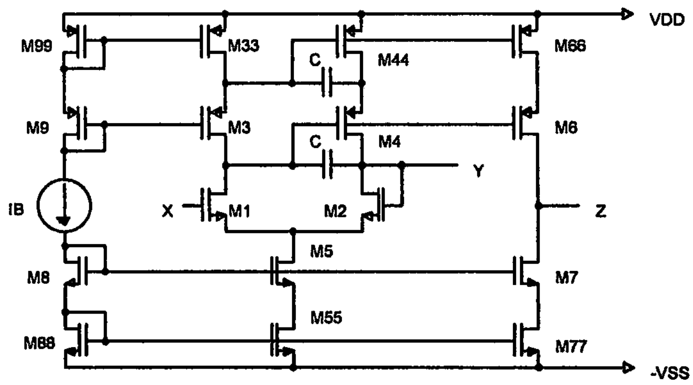

Figure 6.5 Circuit diagram of current conveyor 3n

6.4 PERFORMANCE CHARACTERISTICS OF CURRENT CONVEYOR 4N

Circuits employing operational amplifiers have been used to realize current conveyors. One of the most successful configurations, relies on the operational amplifier supply current sensing technique, in which current mirrors are used to sense the output current of the operational amplifier via its power supply rails [23,38]. This provides a voltage transfer function close to unity and small values of input error currents and offset voltages. A current conveyor based on this technique has been developed. The current conveyor circuit is given in Fig. 6.7a. Complementary cascode current mirrors which have been used in order to sense the output current of the operational amplifier enable a high output impedance. The high performance operational amplifier (OA1) depicted in Fig. 6.8 has been used in unity gain configuration to obtain the voltage transfer function between terminals y and x. M10-M13 and Q1-Q2 form the output stage to obtain a low output impedance. Fig 6.9a and b demonstrate the dc voltage transfer characteristic and the unity gain frequency response of the output voltage, respectively. Supply voltages were chosen as ±5 V and R=1 kΩ. Simulation results yield the output voltage clipping limits as V_{Omax}=3.51 V and V_{Omin}= -5 V, whereas the maximum output current is I_{Omax}= 3.38 mA. The 3 dB bandwidth of the operational amplifier was obtained as f_{BW}=130 MHz, while the open-loop gain is K = 56.5 dB. The input and output resistances are 872 GΩ and 8 Ω,

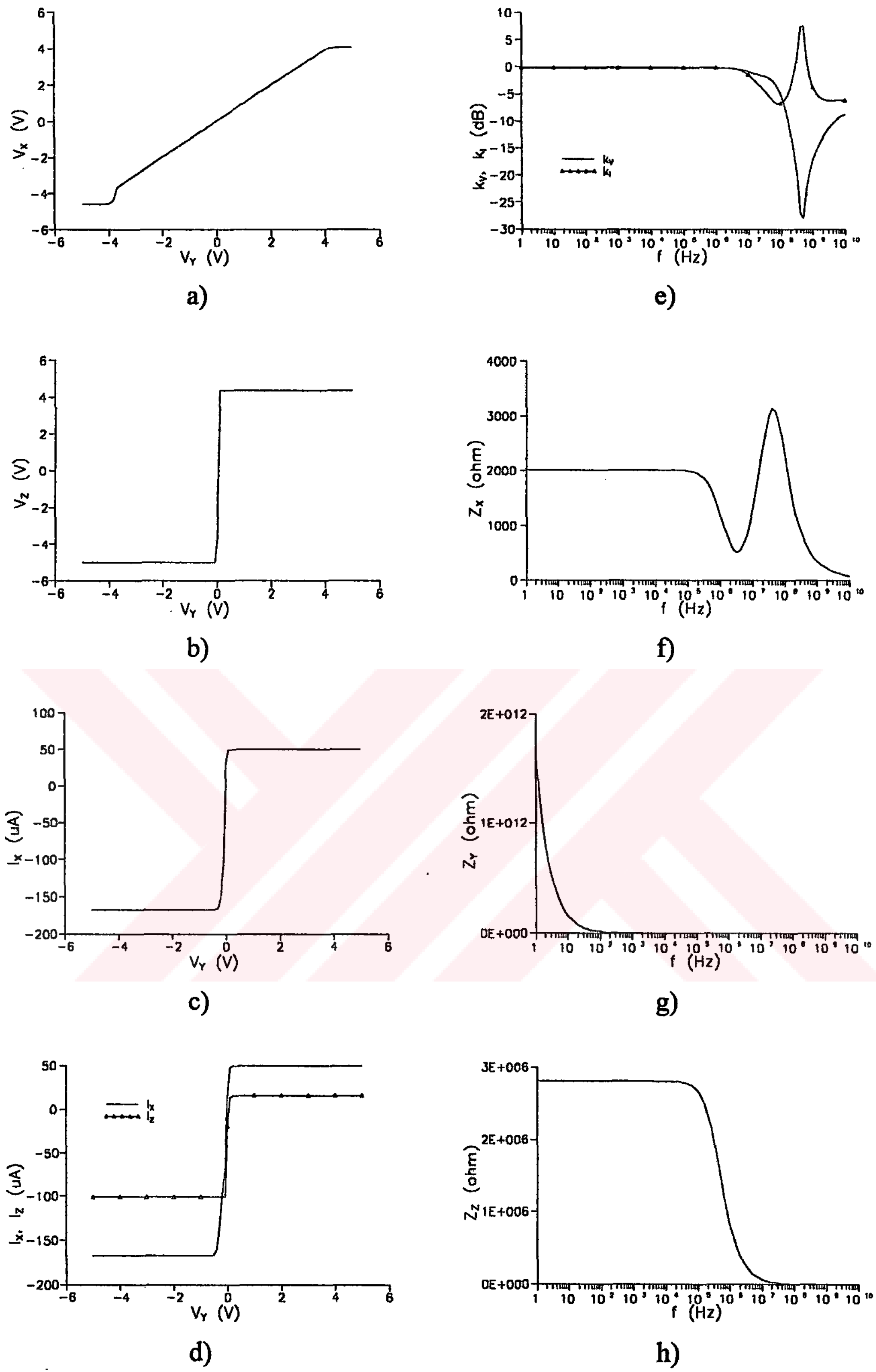

Figure 6.6 SPICE simulated device characteristics of current conveyor 3n
a) $V_X = V_X(V_Y)$ for $R_X = \infty$ b) $V_Z = V_Z(V_Y)$ for $R_Z = \infty$ c) $I_X = I_X(V_Y)$ for $R_X = 0$ d) $I_X = I_X(V_Y)$, $I_Z = I_Z(V_Y)$ for $R_X = R_Z = 1$ kΩ e) The frequency responses of v_x/v_y and i_z/i_x for $R_X = R_Z = 10$ kΩ f) The frequency response of Z_X g) The frequency response of Z_Y h) The frequency response of Z_Z

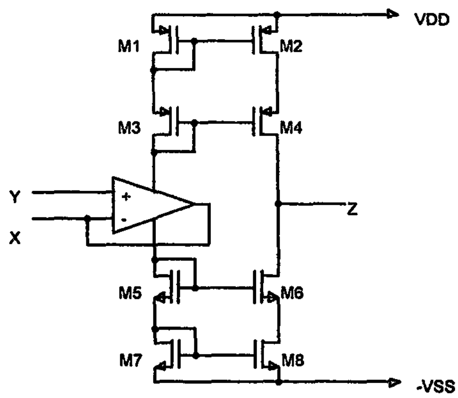

a)

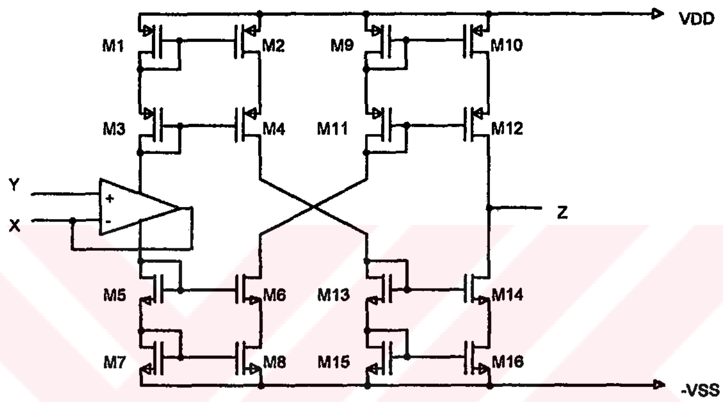

b)

Figure 6.7 a) Circuit diagram of current conveyor 4n b) Inverting type current conveyor derived from a)

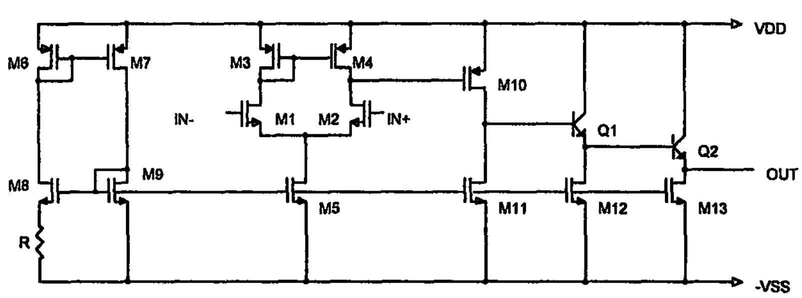

Figure 6.8 Circuit diagram of operational amplifier 1

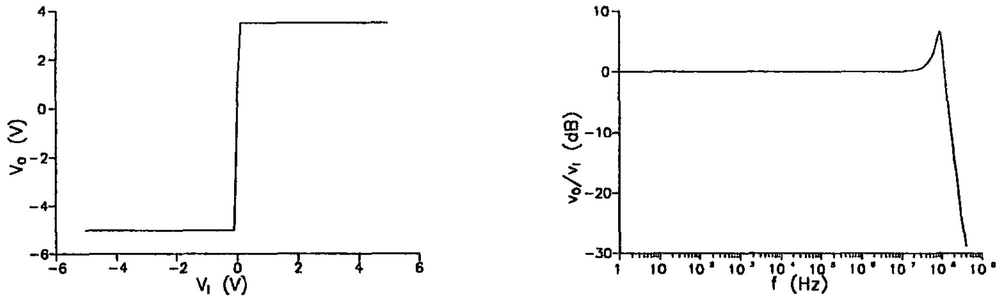

a) b)

Figure 6.9 Device characteristics of operational amplifier 1
a) Dc voltage transfer characteristic b) The unity gain frequency response of the output voltage

respectively, whereas the related capacitances can be neglected. The characteristic values of the operational amplifier are summarized in Table 6.2.

SPICE simulations have been carried out in order to check the performance of the current conveyor. Supply voltages were chosen to be ±10 V, which provides biasing the operational amplifier section of the circuit as previously mentioned. The performance characteristics are given in Fig. 6.10, whereas Table 6.1 summarizes the characteristic values. The inverting type current conveyor given in Fig. 6.7b, will be used for later purposes.

Table 6.2 Characteristic values of operational amplifiers OA1 and OA2

	OA1	OA2
V_{Omax}	3.51	4.21
V_{Omin}	-5 V	-5 V
I_{Omax}	3.38 mA	3 mA
f_{BW}	130 MHz	134 MHz
K	56.5 dB	56.6 dB
r_I	872 GΩ	874 GΩ
r_O	8 Ω	261.5 Ω

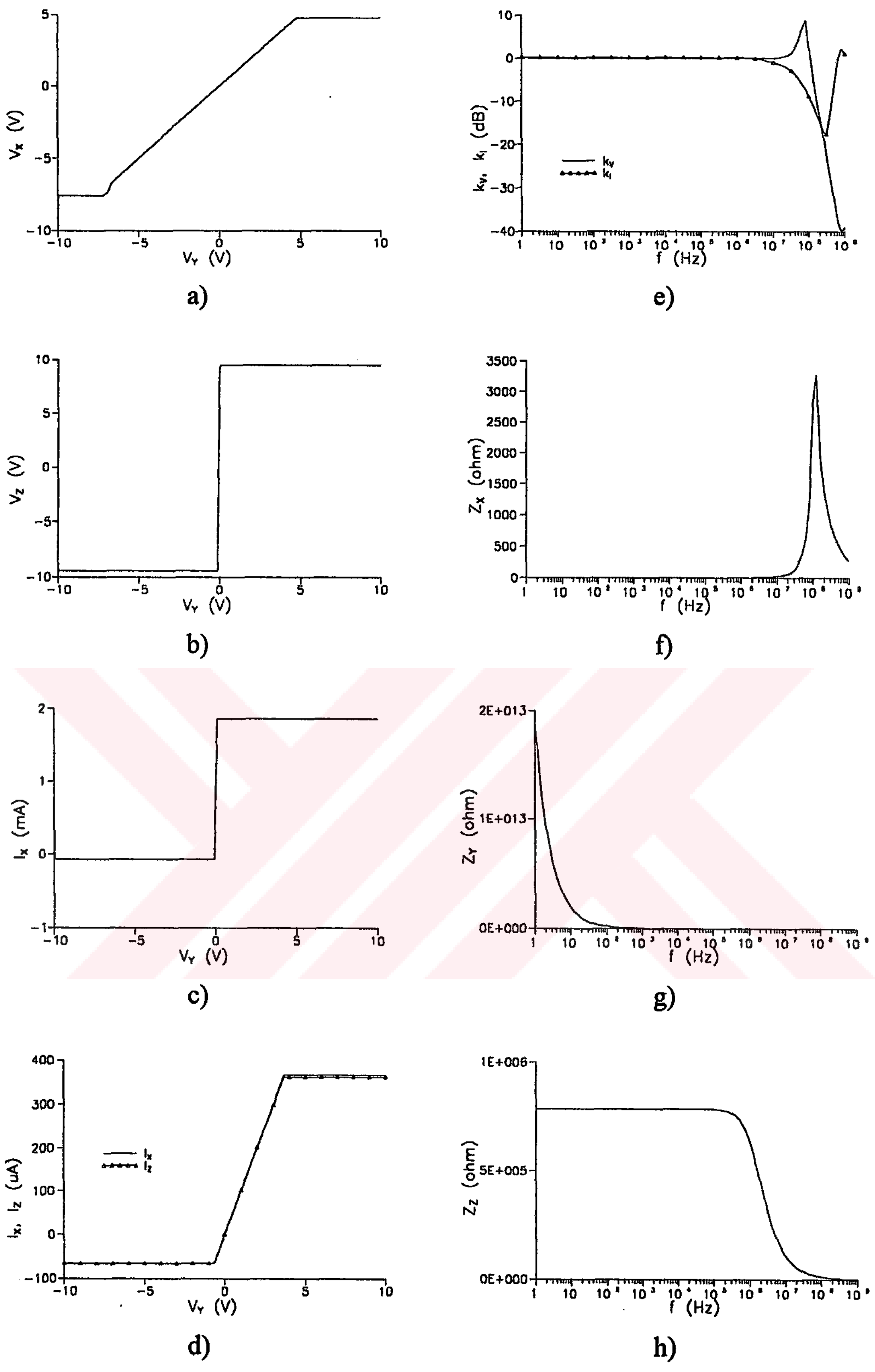

Figure 6.10 SPICE simulated device characteristics of current conveyor 4n
a) $V_X = V_X(V_Y)$ for $R_X = \infty$ b) $V_Z = V_Z(V_Y)$ for $R_Z = \infty$ c) $I_X = I_X(V_Y)$ for $R_X = 0$ d) $I_X = I_X(V_Y)$, $I_Z = I_Z(V_Y)$ for $R_X = R_Z = 1\ k\Omega$ e) The frequency responses of v_x/v_y and i_z/i_x for $R_X = R_Z = 10\ k\Omega$ f) The frequency response of Z_X g) The frequency response of Z_Y h) The frequency response of Z_Z

6.5 PERFORMANCE CHARACTERISTICS OF CURRENT CONVEYOR 5N

It can be observed from Table 6.1 that the current conveyor circuit given in Fig 6.7a will appreciate an improvement in the maximum attainable voltage from the output. The output stage of the operational amplifier as well as the complementary cascode current mirrors contribute to the result obtained from the previous configuration. The structure given in Fig. 6.11a uses simple current mirrors to sense the output current of the operational amplifier and enables higher voltage clipping limits at the output to a price of low output impedance. M13 and Q2 were left out of the operational amplifier (OA2) for higher output voltages to be obtained. Simulation results for this case yield the output voltage clipping limits as V_{Omax}=4.21 V and V_{Omin}= -5 V, whereas the maximum output current is I_{Omax}=3 mA. The 3 dB bandwidth of the operational amplifier was obtained as f_{BW}=134 MHz, while the output resistance is 261.5 Ω. The open-loop gain and input resistance of the operational amplifier remain unchanged. The characteristic values of the operational amplifier are summarized in Table 6.2.

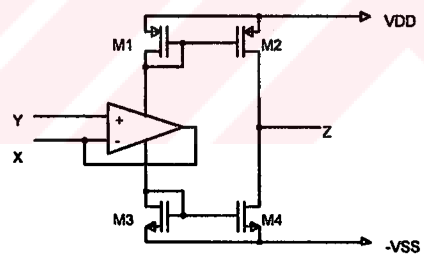

a)

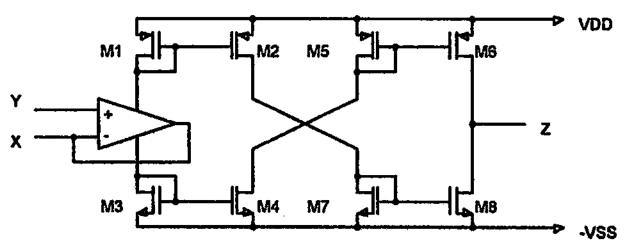

b)

Figure 6.11 a) Circuit diagram of current conveyor 5n b) Inverting type current conveyor derived from a)

SPICE simulations have been carried out in order to check the performance of the current conveyor. Supply voltages were chosen to be ±10 V. The performance characteristics are given in Fig. 6.12, and the characteristic values are given in Table 6.1. Fig. 6.11b depicts the inverting type current conveyor which will be used for later purposes.

6.6 PERFORMANCE CHARACTERISTICS OF CURRENT CONVEYOR 6N

An alternative current conveyor configuration realized from operational amplifiers is based on the output current sensing technique [23,39]. An operational amplifier exists as the main gain block and is provided with two equal but opposite output currents via complementary current mirrors. The circuit configuration is given in Fig. 6.13a. Transistors M1-M4 and M5-M8 serve as the complementary modified Wilson current mirrors which enable high output impedance and accurate current transfer performance, whereas M9-M10 form a class B connection. The operational amplifier OA2 has been used in unity gain configuration which contributes to a high performance voltage transfer characteristic.

Supply voltages were chosen to be ±5 V for the SPICE simulations. The performance characteristics are given in Fig. 6.14, whereas the characteristic values are given in Table 6.1. The inverting type current conveyor given in Fig. 6.13b, will be used for later purposes.

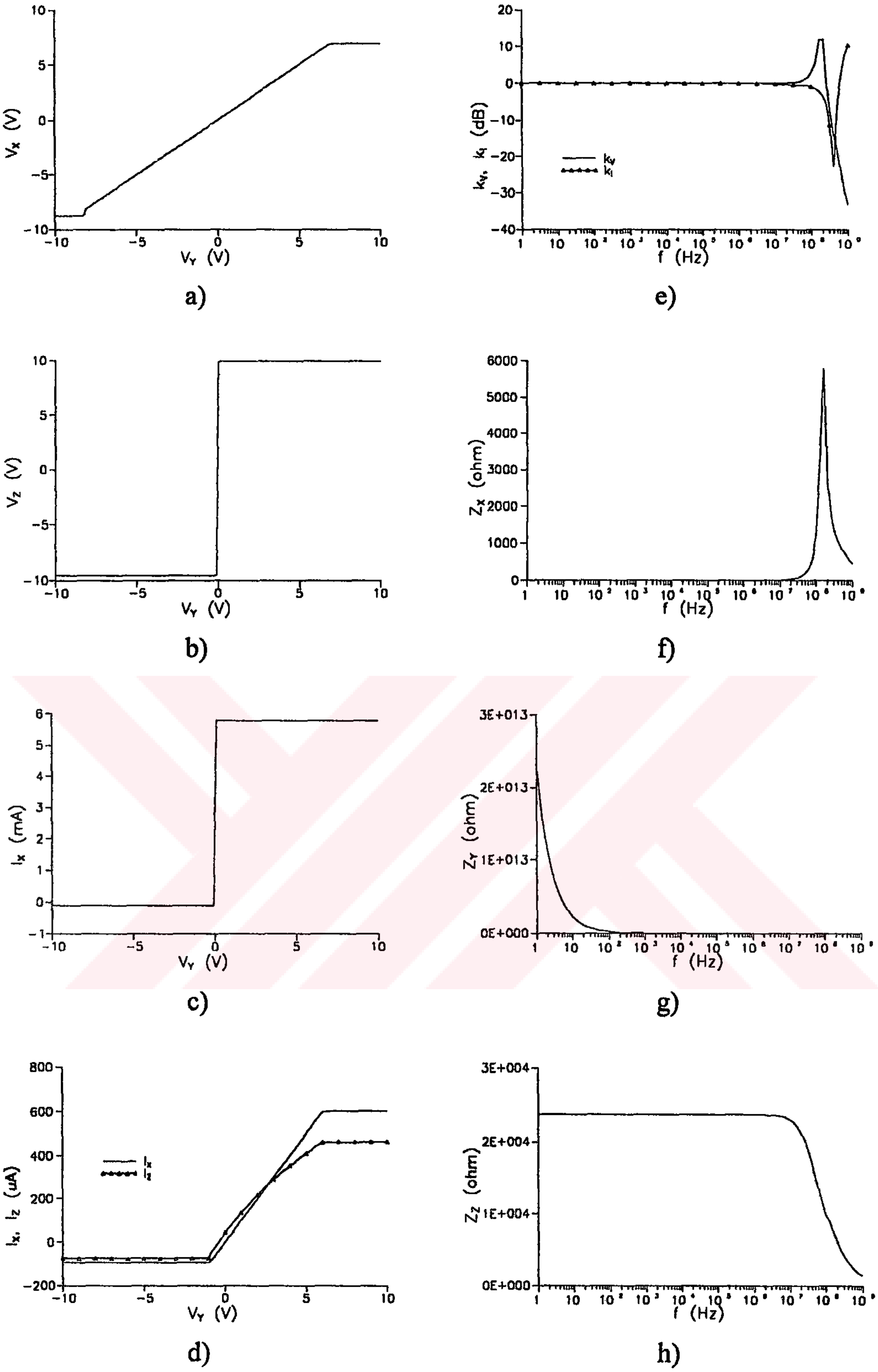

Figure 6.12 SPICE simulated device characteristics of current conveyor 5n
a) $V_X = V_X(V_Y)$ for $R_X = \infty$ b) $V_Z = V_Z(V_Y)$ for $R_Z = \infty$ c) $I_X = I_X(V_Y)$ for $R_X = 0$ d) $I_X = I_X(V_Y)$, $I_Z = I_Z(V_Y)$ for $R_X = R_Z = 10$ kΩ e) The frequency responses of v_x/v_y and i_z/i_x for $R_X = R_Z = 10$ kΩ f) The frequency response of Z_X g) The frequency response of Z_Y h) The frequency response of Z_Z

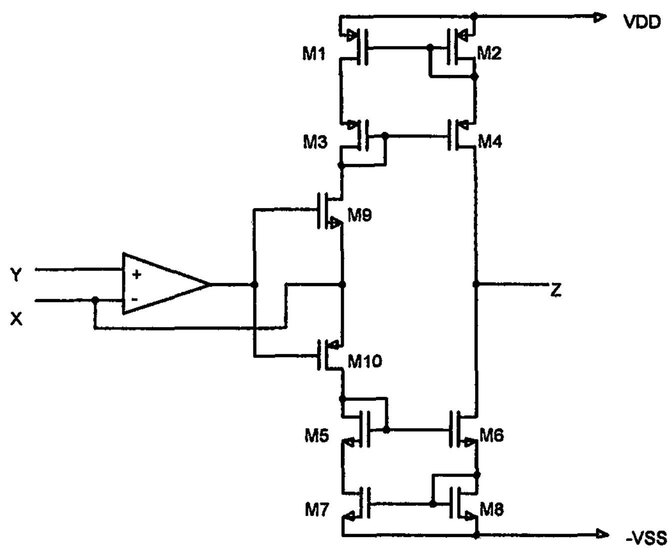

a)

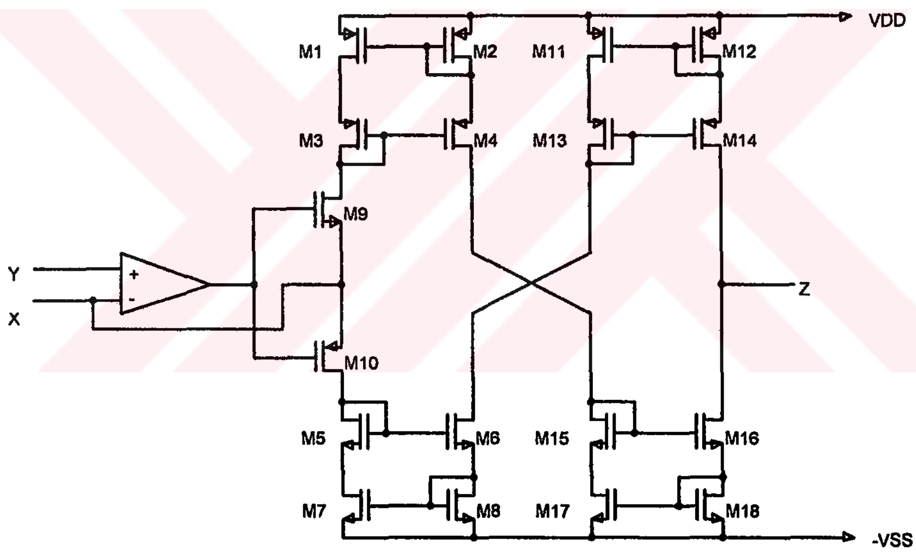

b)

Figure 6.13 a) Circuit diagram of current conveyor 6n b) Inverting type current conveyor derived from a)

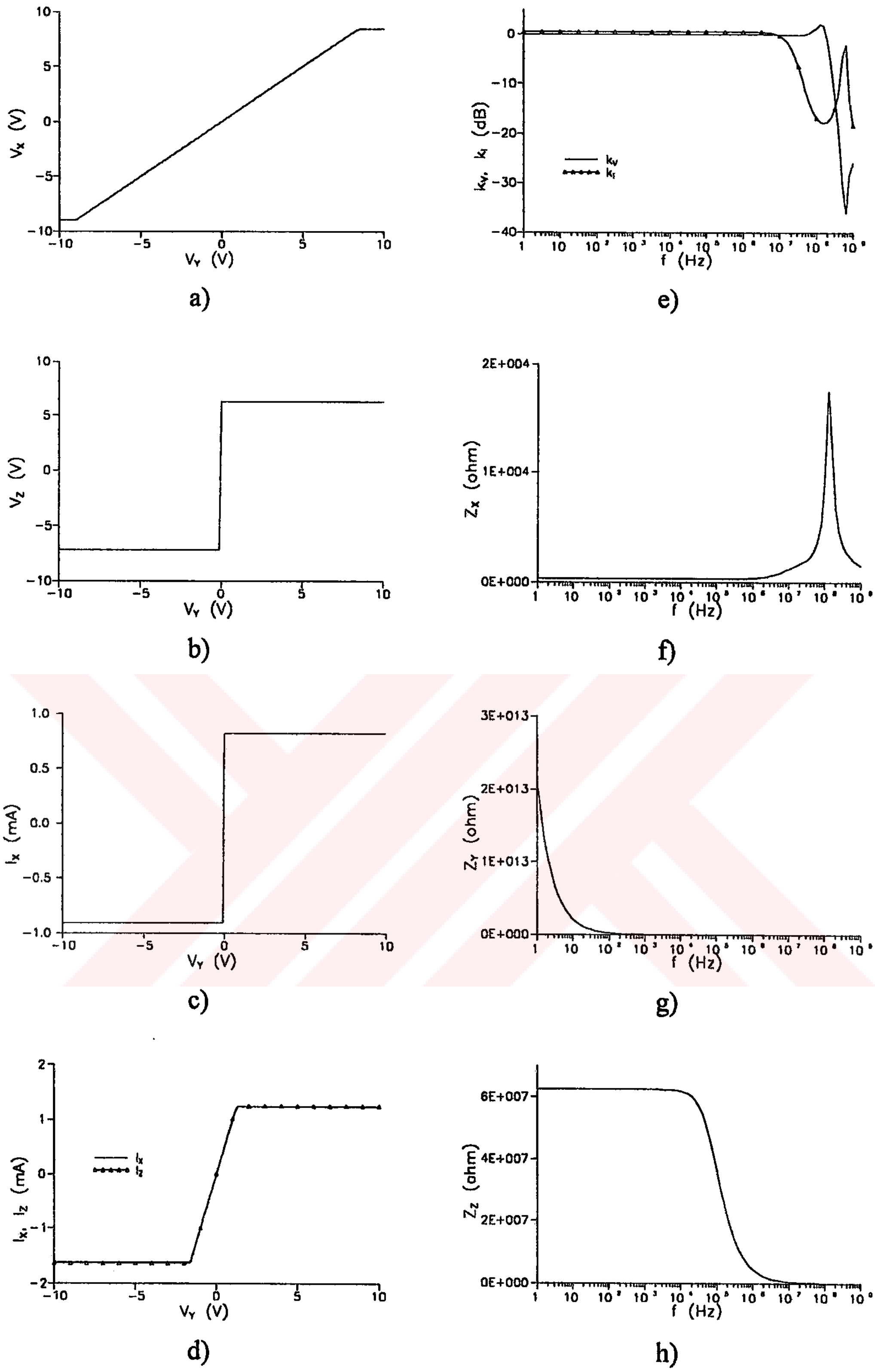

Figure 6.14 SPICE simulated device characteristics of current conveyor 6n
a) $V_X = V_X(V_Y)$ for $R_X = \infty$ b) $V_Z = V_Z(V_Y)$ for $R_Z = \infty$ c) $I_X = I_X(V_Y)$ for $R_X = 0$ d) $I_X = I_X(V_Y)$, $I_Z = I_Z(V_Y)$ for $R_X = R_Z = 1\ k\Omega$ e) The frequency responses of v_x / v_y and i_z / i_x for $R_X = R_Z = 10\ k\Omega$ f) The frequency response of Z_X g) The frequency response of Z_Y h) The frequency response of Z_Z

6.7 THE VOLTAGE-MODE FILTER PERFORMANCE FOR THE PROPOSED CURRENT CONVEYORS

In this section, a comparable demonstration of the voltage-mode filter performance for example current conveyor circuits proposed in the previous section has been given. Figs. 6.15 through 6.20 depict the performance of the three types of filters when current conveyors CC1N-CC6N are employed in the filter, for four different filter frequencies of f_O =10 kHz, 100 kHz, 1 MHz and 10 MHz. The figures show that these circuits offer an opportunity to be used in filter designs which exhibit well performance.

The large-signal behavior of the three types of filters for a cutoff (resonant) frequency of 10 kHz have been demonstrated in Figs. 6.21 and 6.22. The frequency of the input signal for the highpass filter is 100 kHz, whereas a frequency of 100 Hz has been chosen for the lowpass filter input signal. The maximum input signal amplitude for the current conveyors has been listed in Table 6.3, provided that a distortion of 1% for the output signal is acceptable.

Table 6.3 The maximum input signal amplitude for example current conveyors

	v_{IBP}	v_{ILP}	v_{IHP}
CC2N	3 V	2.5 V	2.5 V
CC3N	4 V	3 V	4.1 V
CC4N	5 V	4 V	4 V
CC5N	1 V		0.1 V

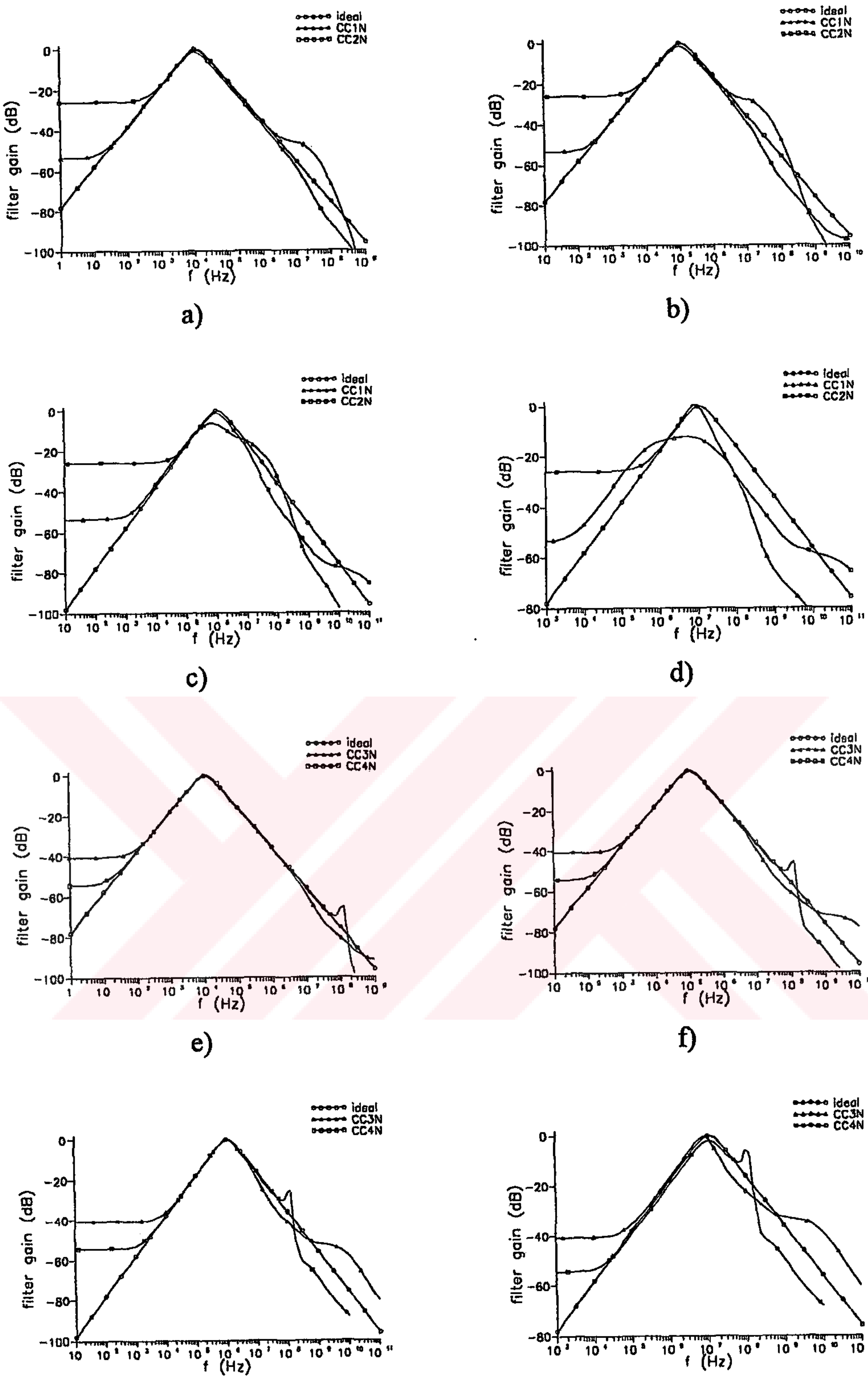

Figure 6.15 The voltage-mode bandpass filter performance for CC1N-CC4N at four different resonant frequencies of a) and e) $f_o = 10$ kHz b) and f) $f_o = 100$ kHz c) and g) $f_o = 1$ MHz d) and h) $f_o = 10$ MHz

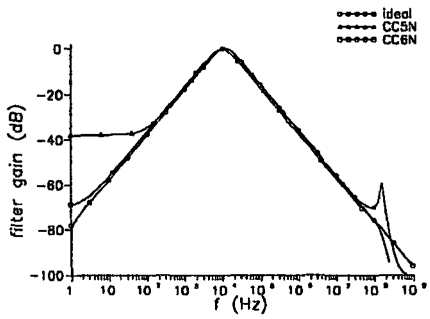

a)

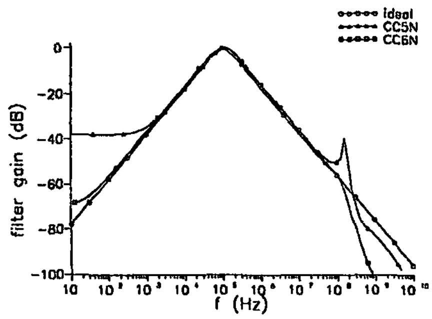

b)

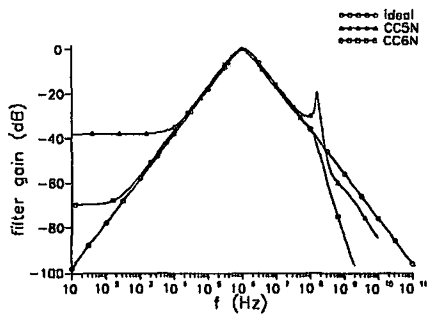

c)

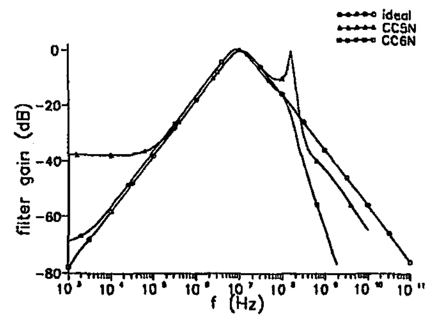

d)

Figure 6.16 The voltage-mode bandpass filter performance for CC5N-CC6N at four different resonant frequencies of a) and e) f_O = 10 kHz b) and f) f_O = 100 kHz c) and g) f_O = 1 MHz d) and h) f_O = 10 MHz

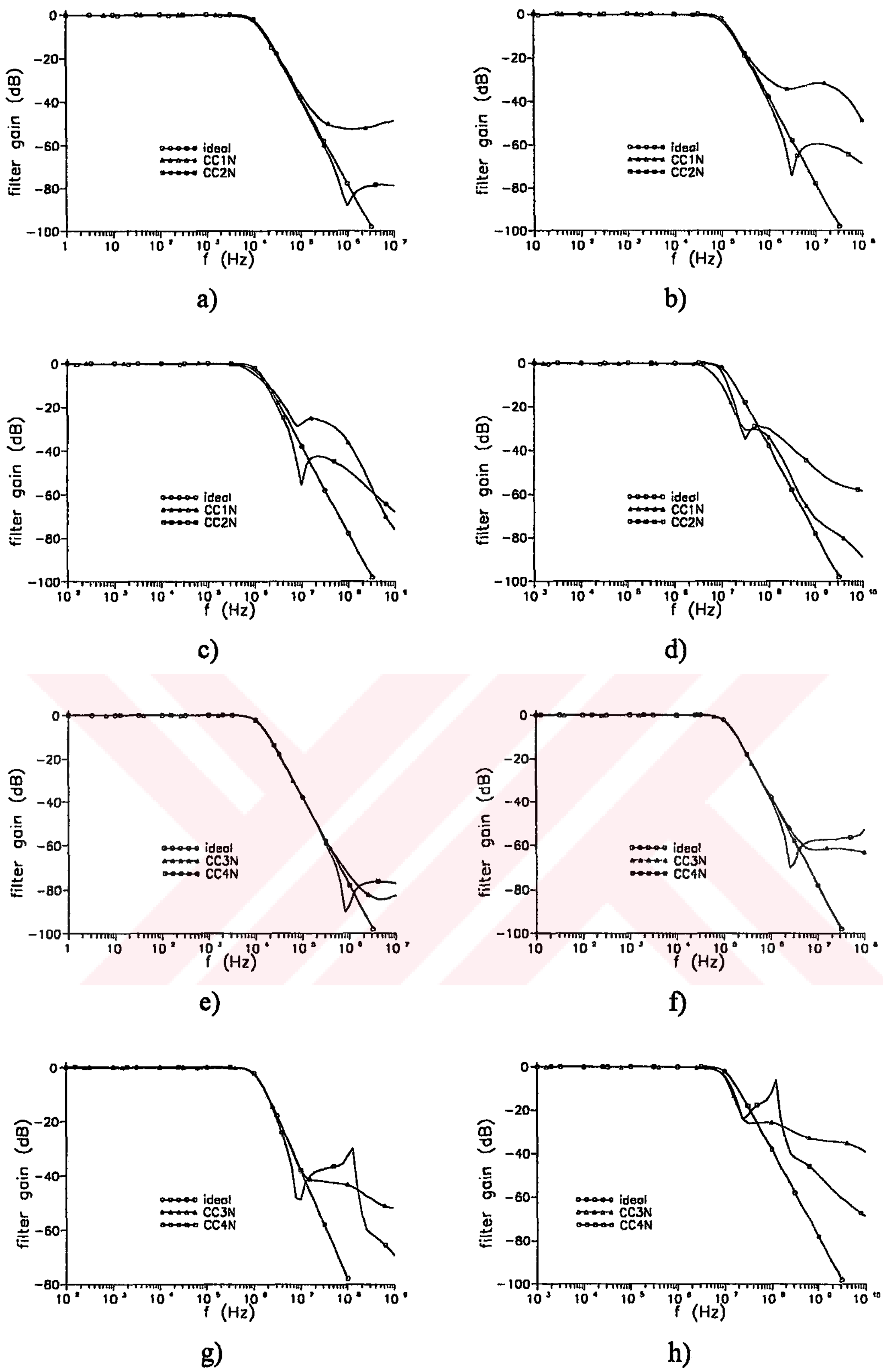

Figure 6.17 The voltage-mode lowpass filter performance for CC1N-CC4N at four different resonant frequencies of a) and e) $f_o = 10$ kHz b) and f) $f_o = 100$ kHz c) and g) $f_o = 1$ MHz d) and h) $f_o = 10$ MHz

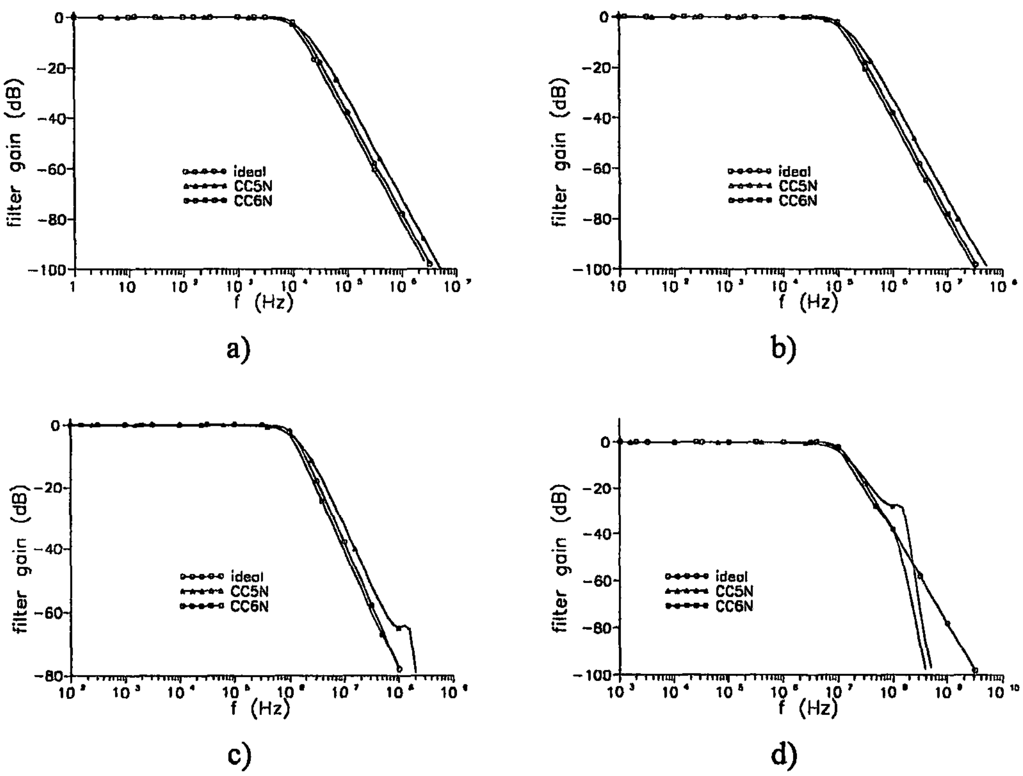

Figure 6.18 The voltage-mode lowpass filter performance for CC5N-CC6N at four different resonant frequencies of a) and e) f_O = 10 kHz b) and f) f_O = 100 kHz c) and g) f_O = 1 MHz d) and h) f_O = 10 MHz

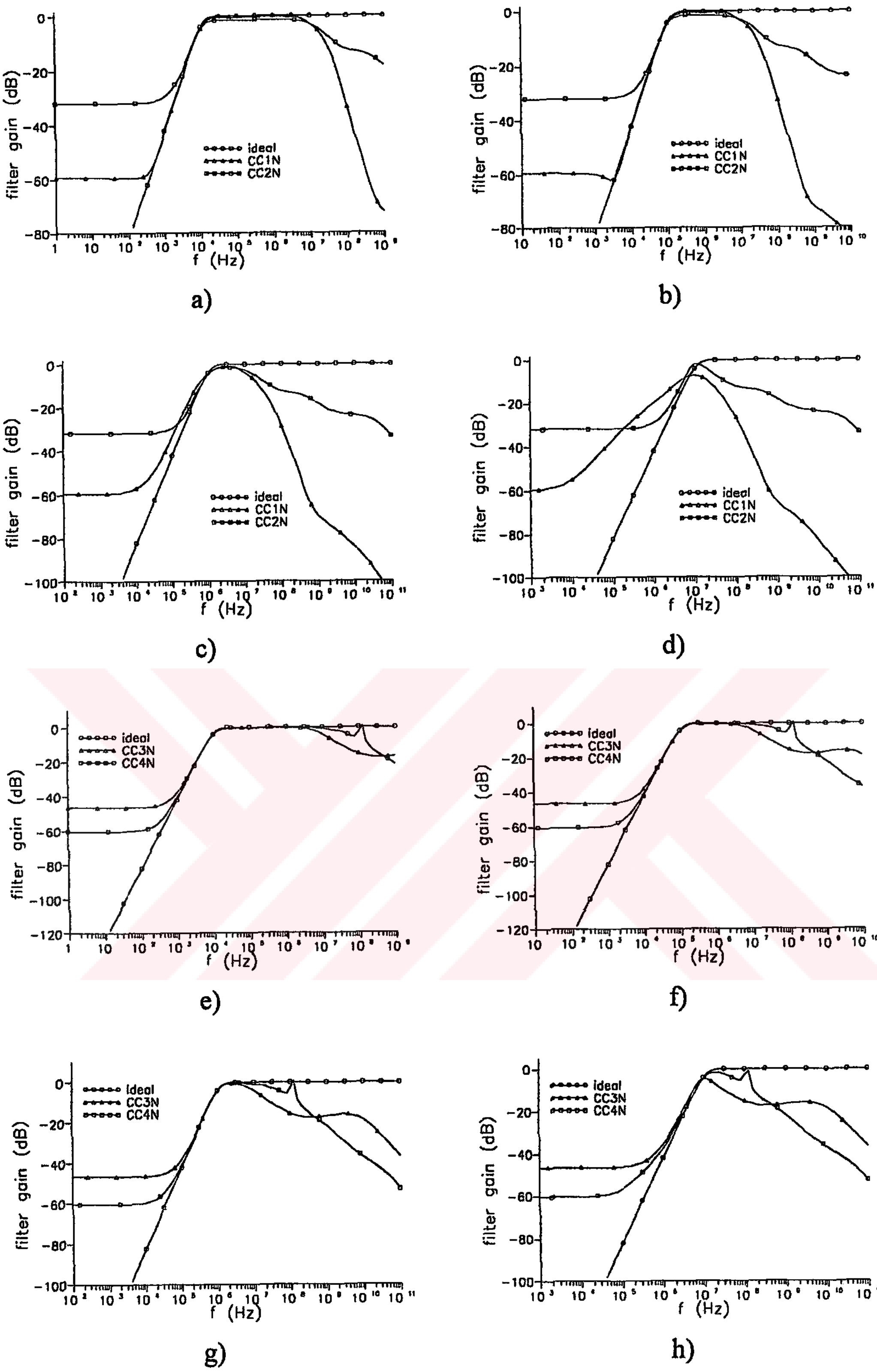

Figure 6.19 The voltage-mode highpass filter performance for CC1N-CC4N at four different resonant frequencies of a) and e) f_O = 10 kHz b) and f) f_O = 100 kHz c) and g) f_O = 1 MHz d) and h) f_O = 10 MHz

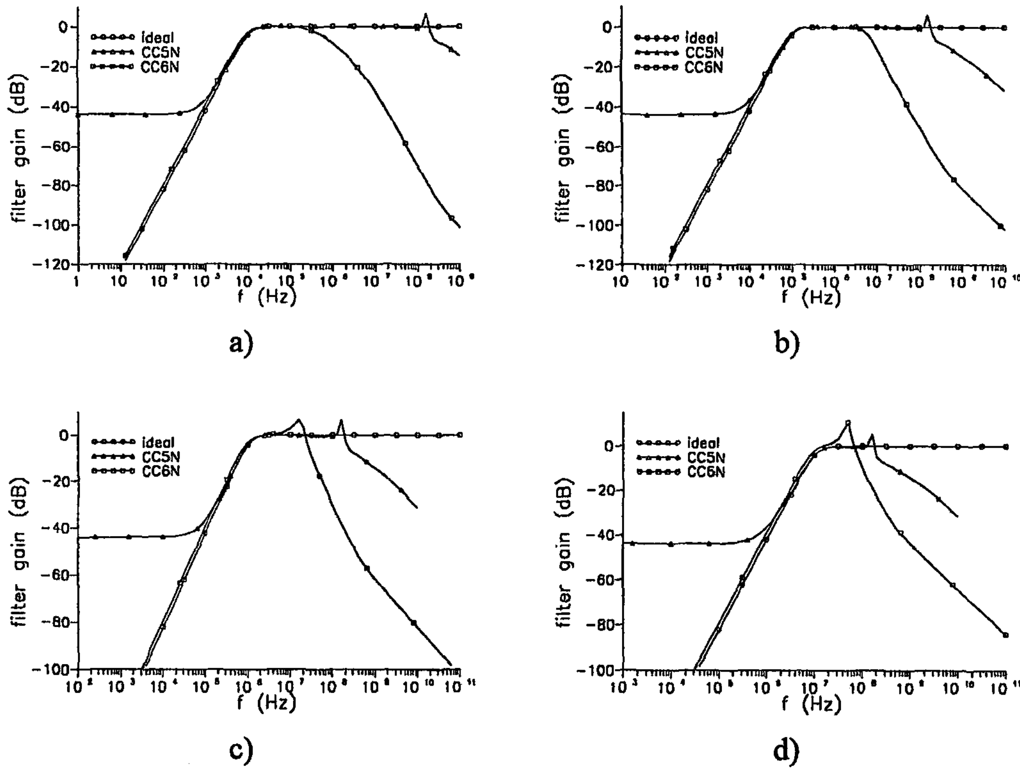

Figure 6.20 The voltage-mode highpass filter performance for CC5N-CC6N at four different resonant frequencies of a) and e) $f_O = 10$ kHz b) and f) $f_O = 100$ kHz c) and g) $f_O = 1$ MHz d) and h) $f_O = 10$ MHz

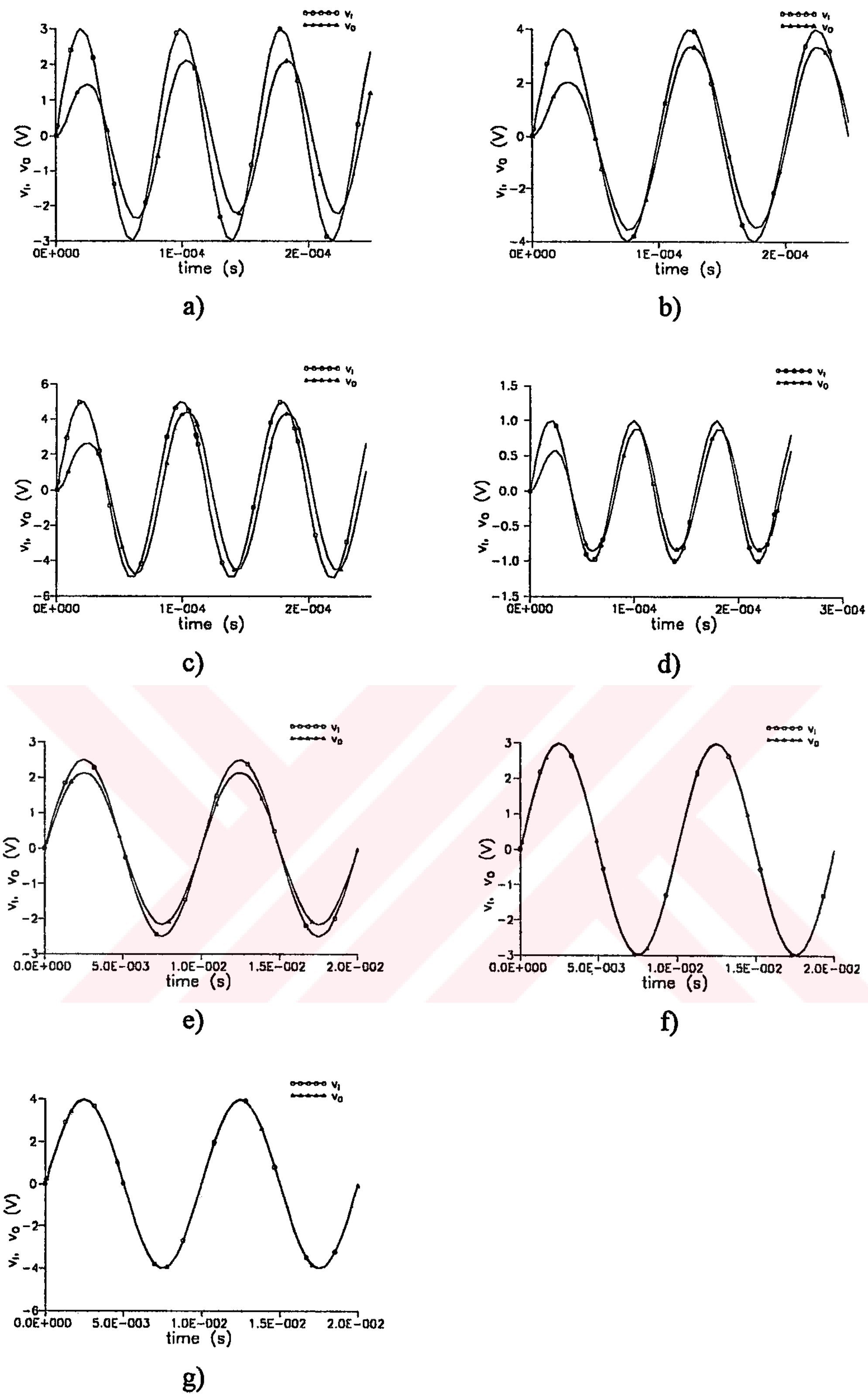

Figure 6.21 The large-signal behavior of the bandpass and lowpass filters for various current conveyors a) BP-CC2N b) BP-CC3N c) BP-CC4N d) BP-CC5N e) LP-CC2N f) LP-CC3N g) LP-CC4N

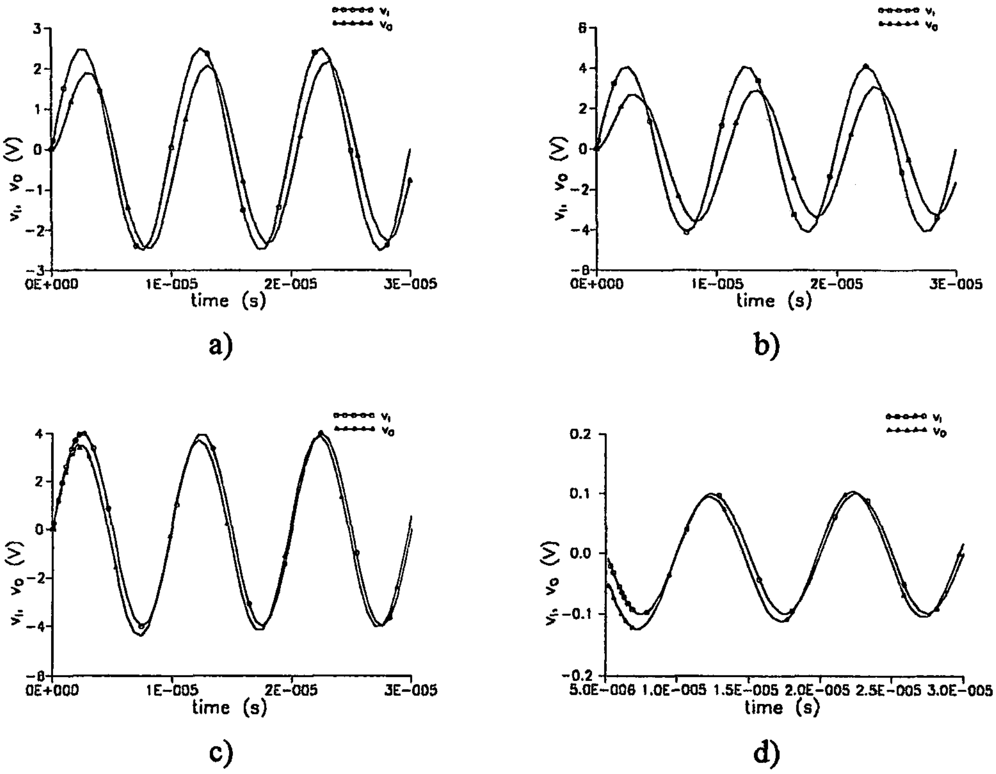

Figure 6.22 The large-signal behavior of the highpass filter for various current conveyors a) CC2N b) CC3N c) CC4N d) CC5N

6.8 THE CURRENT-MODE FILTER PERFORMANCE FOR THE PROPOSED CURRENT CONVEYORS

In this section, a comparable demonstration of the current-mode filter performance for example current conveyor circuits proposed in the previous section has been given. Figs. 6.23 through 6.28 depict the performance of the three types of filters when current conveyors CC1N-CC6N are employed in the filter, for four different filter frequencies of f_O=10 kHz, 100 kHz, 1 MHz and 10 MHz. The figures show that acceptable performance has been obtained for the filters.

The large-signal behavior of the three types of filters for a cutoff (resonant) frequency of 10 kHz have been demonstrated in Figs. 6.29 through 6.31. The frequency of the input signal for the highpass filter is 500 kHz, whereas a frequency of 100 Hz has been chosen for the lowpass filter input signal. The maximum input signal amplitude for the current conveyors has been listed in Table 6.4, provided that a distortion of 1% for the output signal is acceptable.

Table 6.4 The maximum input signal amplitude for example current conveyors

	i_{1BP}	i_{1LP}	i_{1HP}
CC1N	450 μA	3 mA	2 mA
CC2N	90 μA	100 μA	110 μA
CC3N	20 μA	20 μA	25 μA
CC4N	130 μA	130 μA	150 μA
CC5N	80 μA	130 μA	100 μA
CC6N	360 μA	5 mA	7 mA

6.9 DISCUSSIONS ON THE CURRENT CONVEYOR PERFORMANCES

All factors mentioned in Chapter 4 and 5, were taken under consideration in the design of the current conveyors proposed in the previous sections. Comparison of Table 3.1 and 6.1, proves that the proposed current conveyors have wider voltage and current transfer function bandwidths, much higher terminal y and terminal z output resistances and lower capacitance values. The input resistance values of terminal x are sufficiently low and remain to be within the limits required. Comparison of Figs 6.15 through 6.20 and 6.23 through 6.28 with their counterparts in Chapter 4 and 5, respectively, yields that much better performances are obtained especially for the low frequency ranges of the bandpass and highpass filter characteristics. This owes to the comparably higher terminal y and terminal z output resistance values obtained by operational amplifiers used at the input stages and high performance current mirrors used at the output stages. Care was taken for the additional zero and pole values not to conflict with the cutoff frequency of the filter, providing a wider operating frequency range. As a result, the current conveyor circuits designed, fulfill the requirements obtained in Chapter 4 and 5, and the corresponding figures show that acceptable and better filter performances have been obtained.

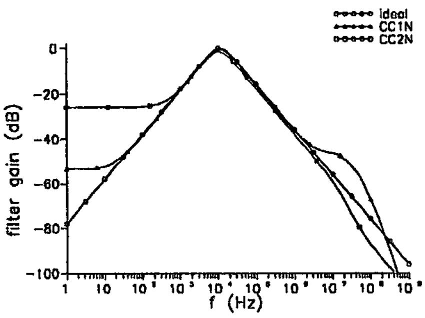

a)

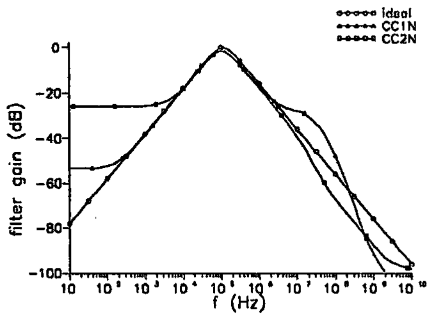

b)

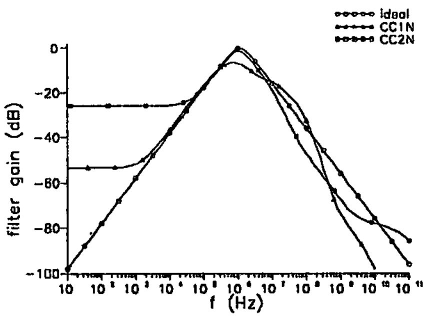

c)

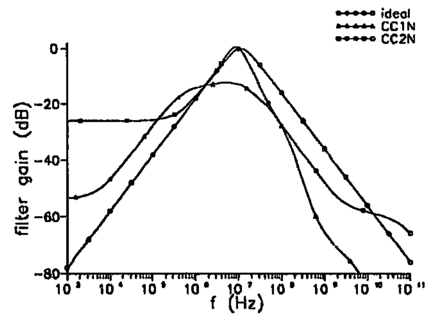

d)

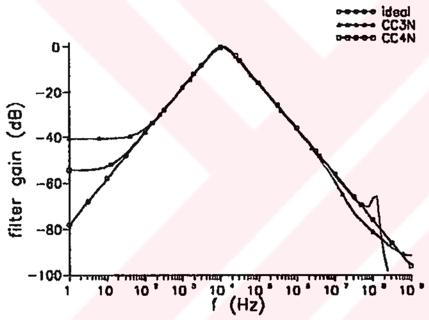

e)

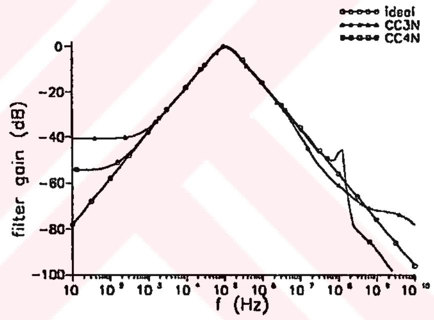

f)

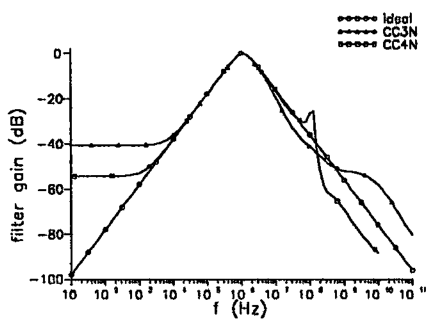

g)

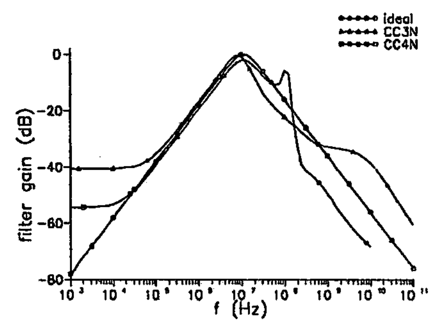

h)

Figure 6.23 The current-mode bandpass filter performance for CC1N-CC4N at four different resonant frequencies of a) and e) $f_O = 10$ kHz b) and f) $f_O = 100$ kHz c) and g) $f_O = 1$ MHz d) and h) $f_O = 10$ MHz

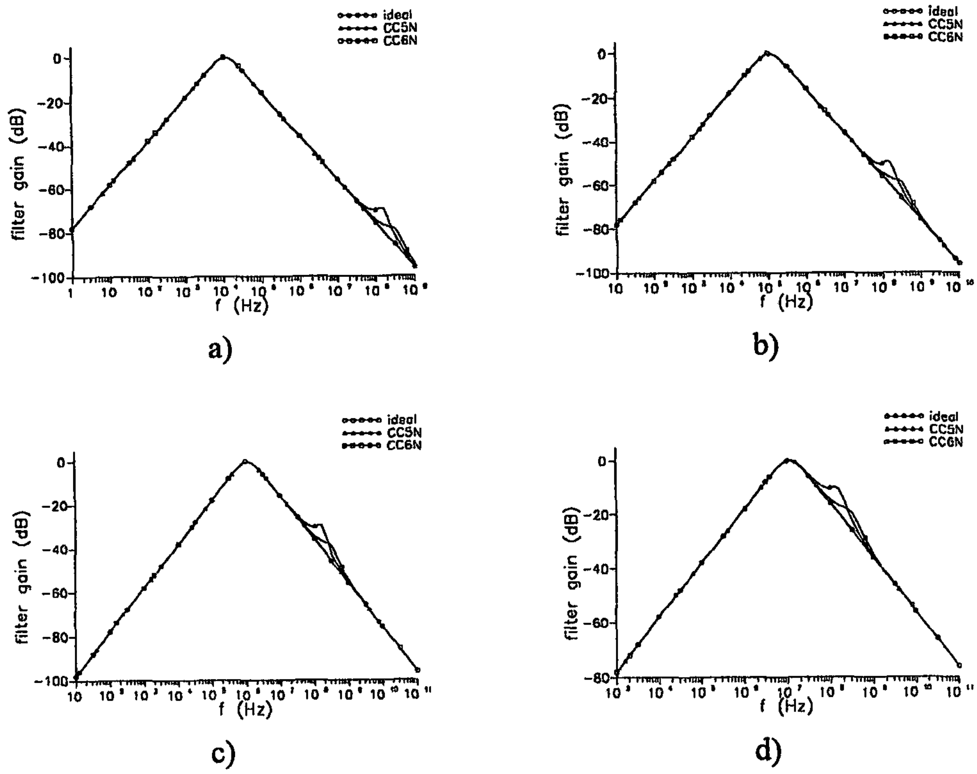

Figure 6.24 The current-mode bandpass filter performance for CC5N-CC6N at four different resonant frequencies of a) and e) f_O = 10 kHz b) and f) f_O = 100 kHz c) and g) f_O = 1 MHz d) and h) f_O = 10 MHz

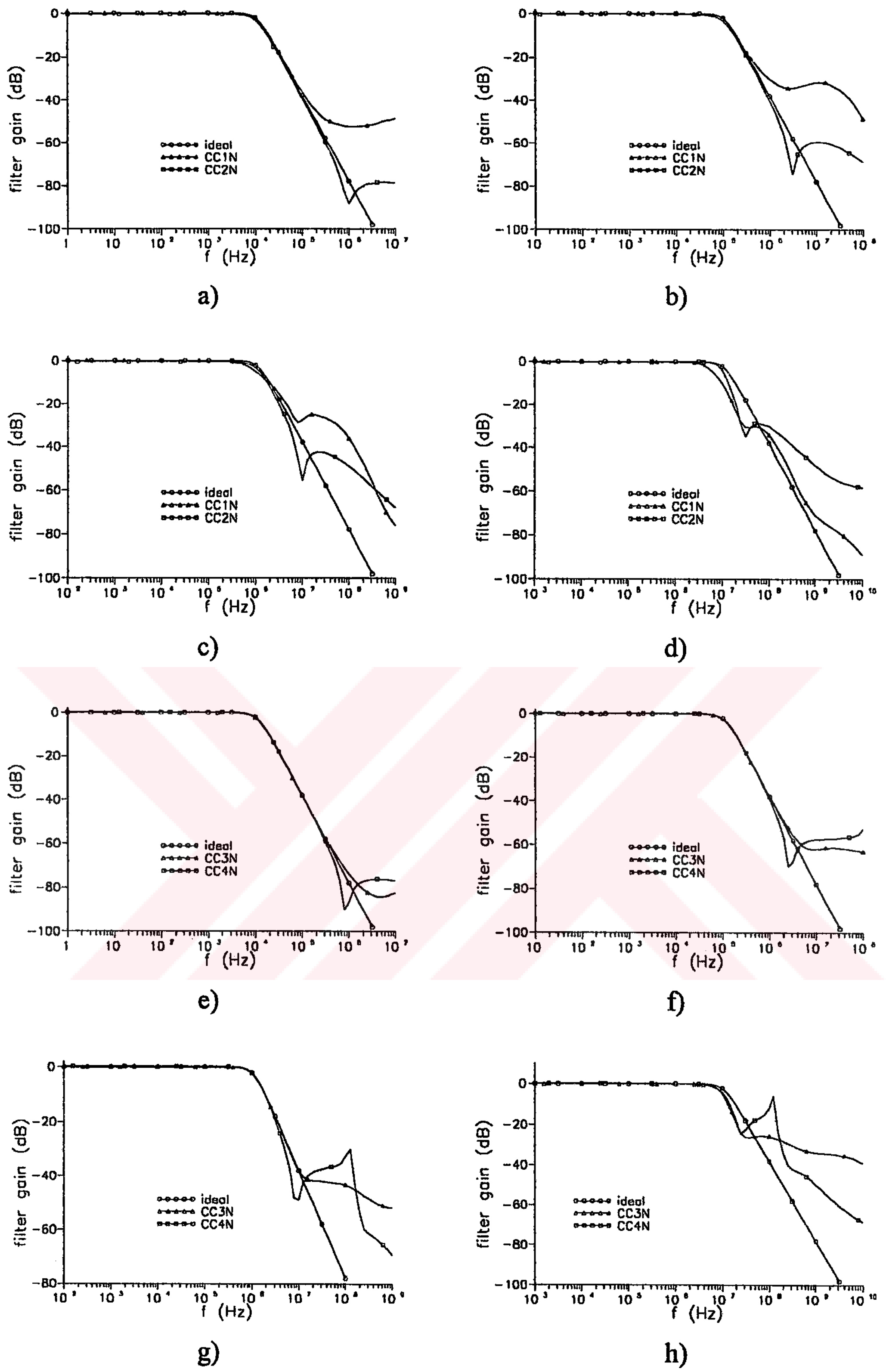

Figure 6.25 The current-mode lowpass filter performance for CC1N-CC4N at four different cutoff frequencies of a) and e) f_O = 10 kHz b) and f) f_O = 100 kHz c) and g) f_O = 1 MHz d) and h) f_O = 10 MHz

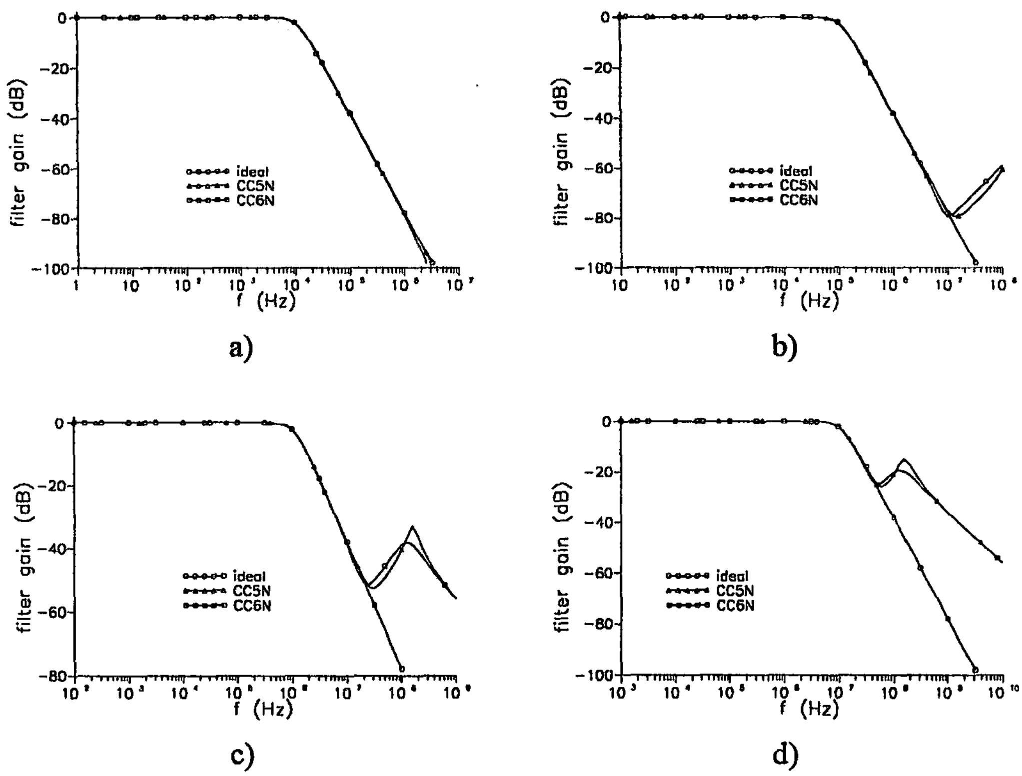

Figure 6.26 The current-mode lowpass filter performance for CC5N-CC6N at four different resonant frequencies of a) and e) $f_O = 10$ kHz b) and f) $f_O = 100$ kHz c) and g) $f_O = 1$ MHz d) and h) $f_O = 10$ MHz

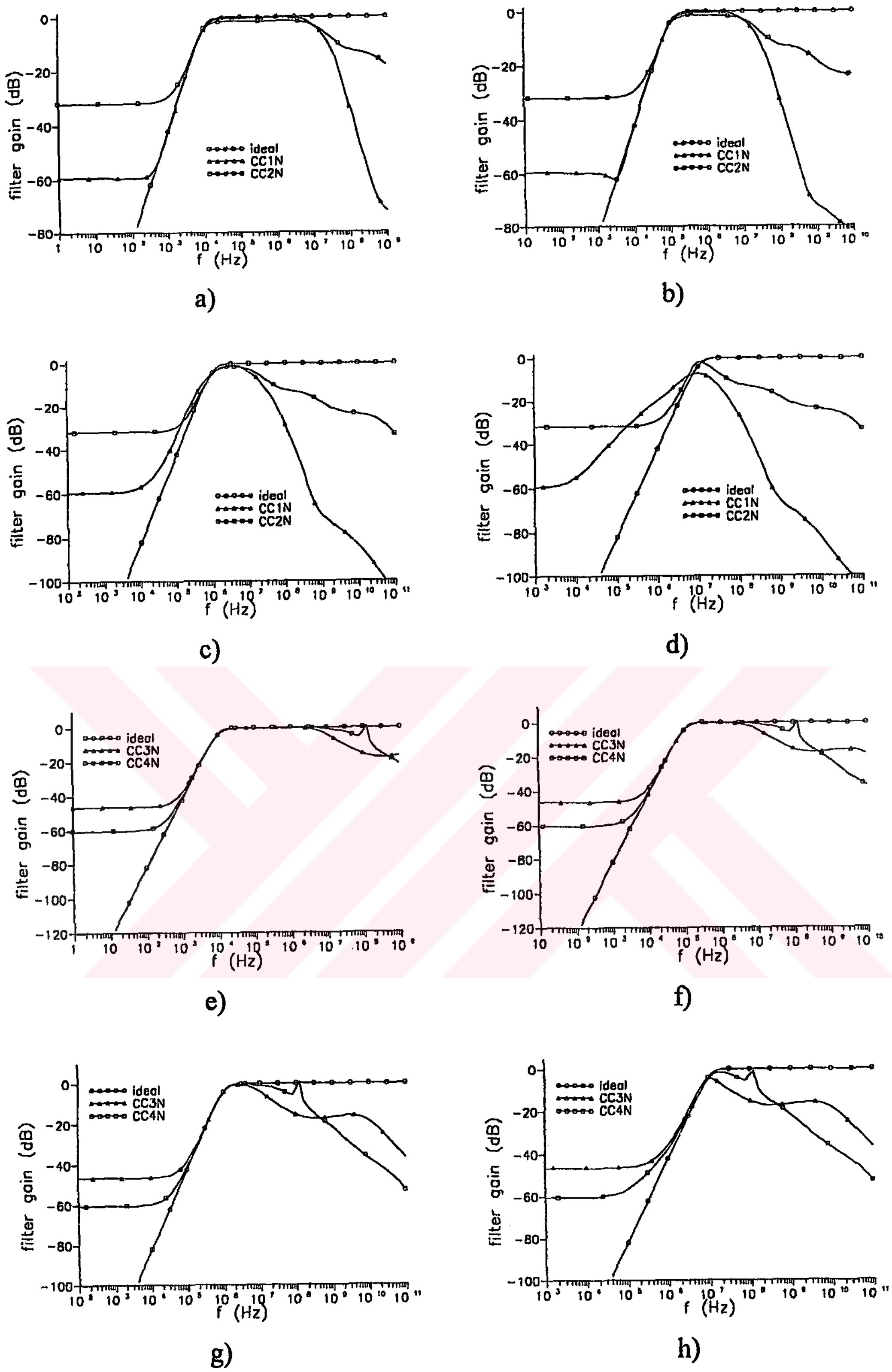

Figure 6.27 The current-mode highpass filter performance for CC1N-CC4N at four different cutoff frequencies of a) and e) $f_O = 10$ kHz b) and f) $f_O = 100$ kHz c) and g) $f_O = 1$ MHz d) and h) $f_O = 10$ MHz

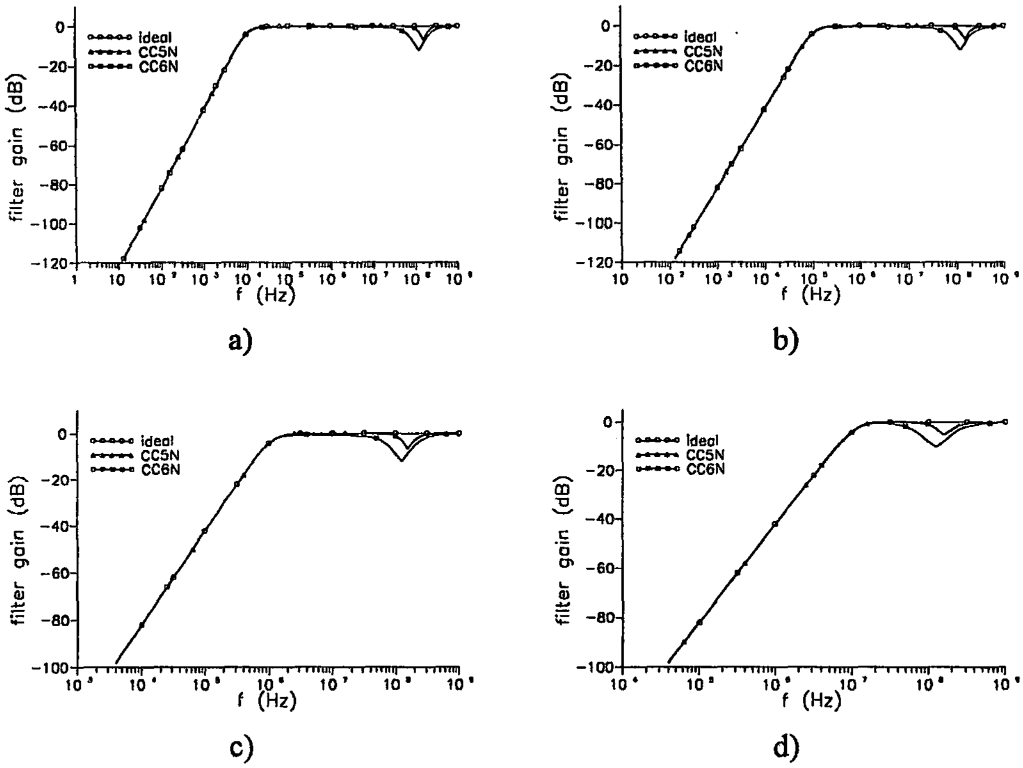

Figure 6.28 The current-mode lowpass filter performance for CC5N-CC6N at four different resonant frequencies of a) and e) $f_O = 10$ kHz b) and f) $f_O = 100$ kHz c) and g) $f_O = 1$ MHz d) and h) $f_O = 10$ MHz

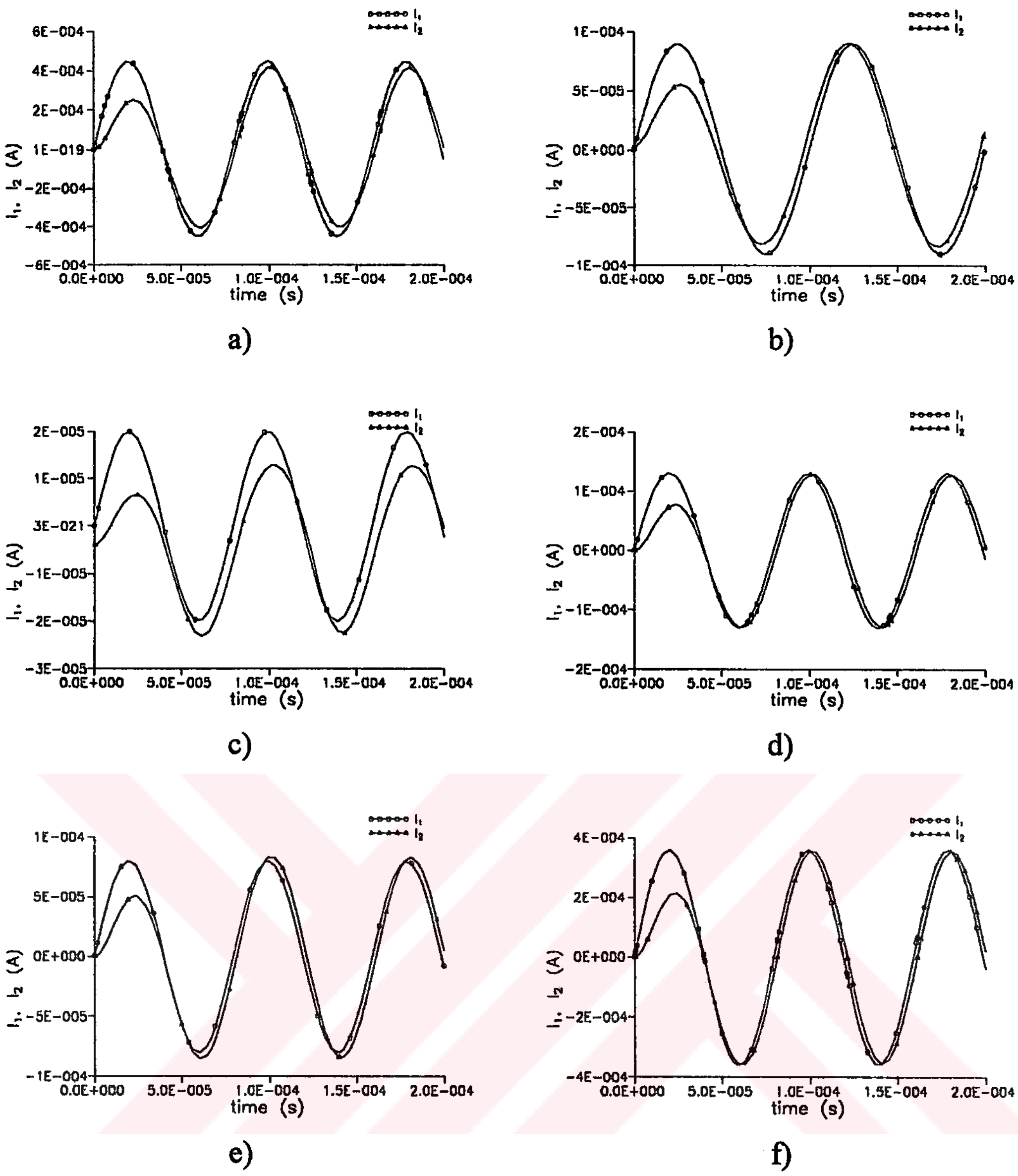

Figure 6.29 The large-signal behavior of the bandpass filter for various current conveyors a) CC1N b) CC2N c) CC3N d) CC4N e) CC5N f) CC6N

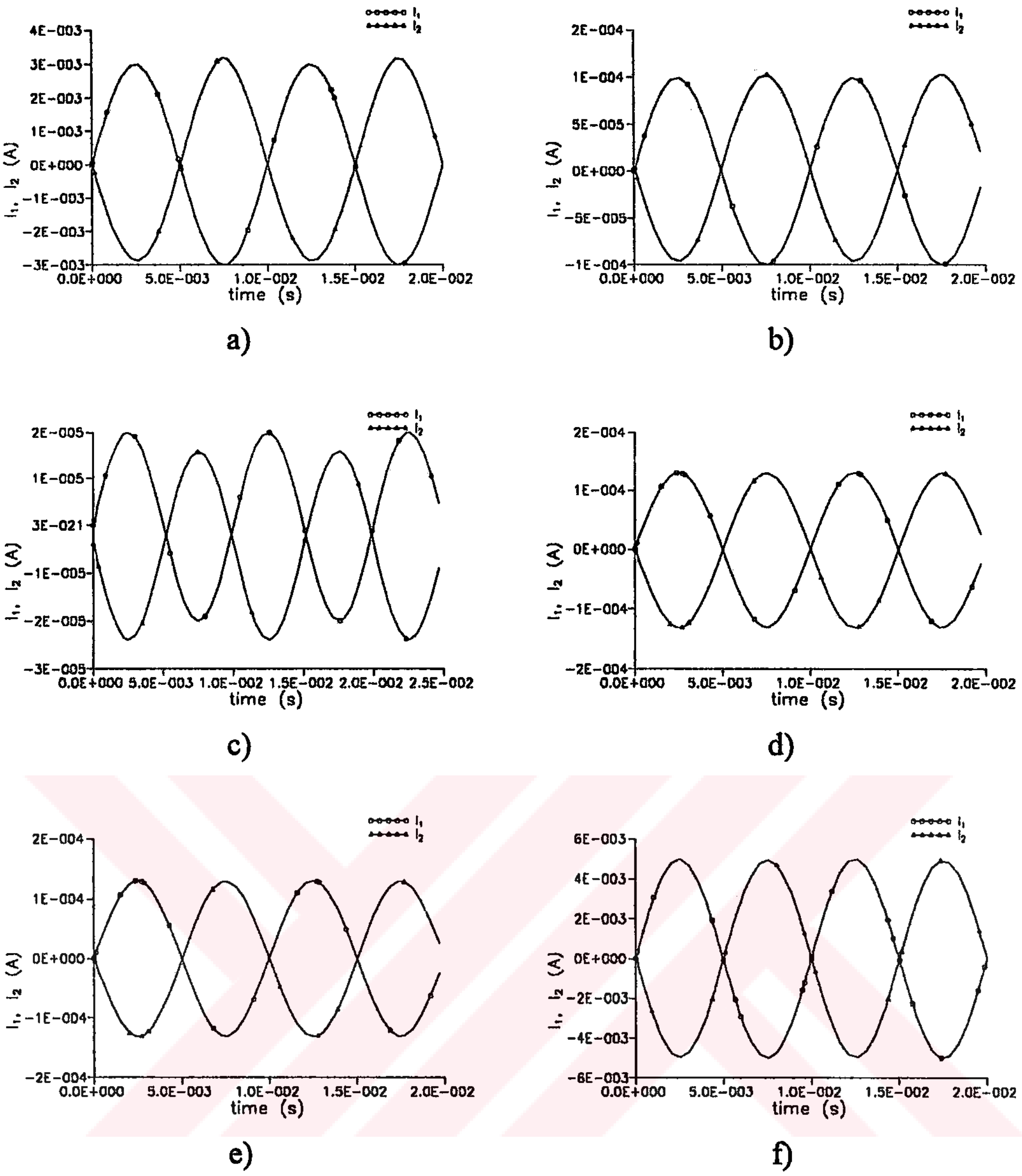

Figure 6.30 The large-signal behavior of the lowpass filter for various current conveyors a) CC1N b) CC2N c) CC3N d) CC4N e) CC5N f) CC6N

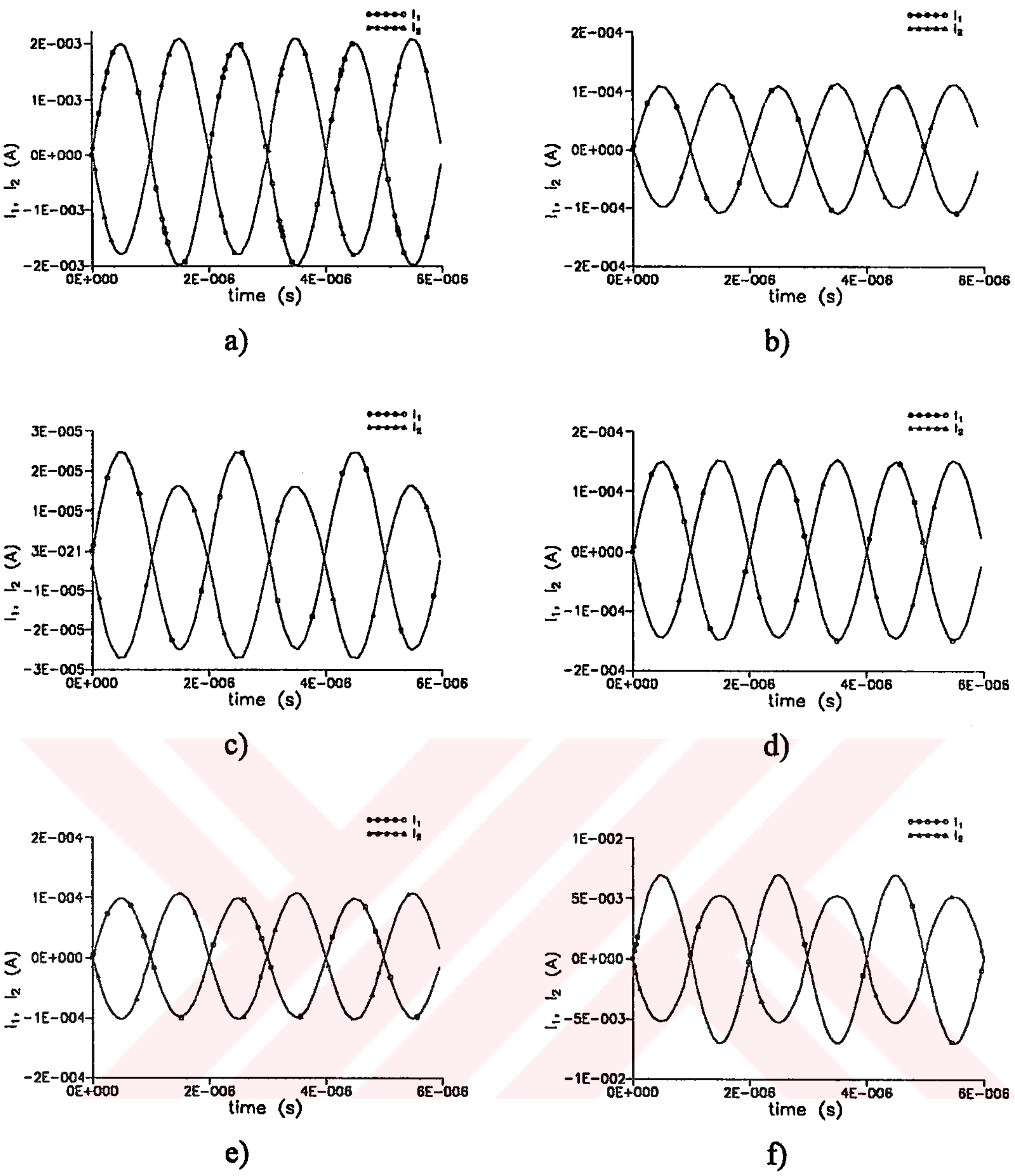

Figure 6.31 The large-signal behavior of the highpass filter for various current conveyors a) CC1N b) CC2N c) CC3N d) CC4N e) CC5N f) CC6N

CHAPTER 7

CONCLUSION

The current conveyor can potentially provide the high accuracy, wide bandwidth, low input impedance and high output impedance characteristics needed for many current domain signal processing applications. Since its first proposal in 1968 and its reformulation named as the second generation current conveyor in 1970, this circuit element continues to receive a great deal of attention and find numerous applications. However, high performance implementations have emerged only in the last decade, and has enabled current conveyors to challenge traditional voltage operational amplifier applications such as active filters, amplifiers, oscillators and immitance simulators.

In this study, active filters using the current conveyor as the active component, has been covered. In active filters, the performance of the active element, of which here the current conveyor is of our concern, plays an important role in the overall performance of the filter, besides the filter configuration itself. Device characteristics close to ideal case, help provide the best performance for a certain filter configuration. It is obvious that the non-idealities of the current conveyor will result in deviations in filter parameters such as the cutoff frequency, quality factor and filter gain, and affect the filter characteristics. Therefore the derivation of analytical expressions for the deviations in the filter parameters in terms of current conveyor non-idealities may be of vital importance. This enables one to realize the effect of each non-ideality term on the filter parameters and help design or choose a suitable current conveyor configuration for a specified filter performance.

Early stages of this study, include a complete macromodel, which fully represents both the small and large-signal behavior of the current conveyor, which is especially suitable for the simulation of active filter applications. Results show that the simple and yet accurate model provides a relative amount of simulation speedup.

Studies on eight current conveyor configurations found in literature in order to obtain the device characteristics have been made. Both bipolar and MOS structures, as well as one of the commercially available current conveyors, namely the AD844 circuit has been covered and compared results of the current conveyor performance characteristics have been given.

Provided that a certain filter configuration is given, the effects of current conveyor non-idealities on both voltage and current-mode active filter examples have been investigated. Analytical expressions for the filter parameter deviations in terms of non-ideality terms were derived, which enables one to determine the requirements for the current conveyor non-ideality terms in order to obtain a specified filter performance. The filter configurations chosen, actually represent certain classes of active filters and makes it possible to generalize the results obtained. A comparable demonstration of the filter transfer function and large-signal behavior for the current conveyor circuits has been given. Simulations including three types of filters, namely, the bandpass, lowpass and highpass filters, confirm the analytical expressions obtained.

The final stage of the study includes a number of current conveyor circuit proposals suitable for continuous-time active filter applications, under the guidance of the results obtained previously. Comparison of Table 3.1 and 6.1, proves that the proposed current conveyors have wider voltage and current transfer function bandwidths, much higher terminal y and terminal z output resistances and lower capacitance values. The input resistance values of terminal x are sufficiently low and remain to be within the limits required. Comparison of Figs 6.15 through 6.17 and 6.20 through 6.22 with their counterparts in Chapter 4 and

5, respectively, yields that much better performances are obtained especially for the low frequency ranges of the bandpass and highpass filter characteristics. This owes to the comparably higher terminal y and terminal z output resistance values obtained by operational amplifiers used at the input stages and high performance current mirrors used at the output stages. Care was taken for the additional zero and pole values not to conflict with the cutoff frequency of the filter, providing a wider operating frequency range. As a result, the current conveyor circuits designed, fulfill the requirements obtained in Chapter 4 and 5, and the corresponding figures show that acceptable and better filter performances have been obtained.

Device characteristics of the current conveyors and the comparable demonstration of the voltage and current-mode filter performances show that these circuits offer a good opportunity to be used in filter designs which exhibit well performance, as well as in other analog circuit design applications.

REFERENCES

[1] **WIDLAR, R.J.,** A Unique Circuit Design for a High Performance Operational Amplifier Especially Suited to Monolithic Construction, Proceedings NEC, pp.85-89, (1965).

[2] **WIDLAR, R.J.,** Monolithic Op Amp with Simplified Frequency Compensation, EEE, 15, pp.58-63, (1967).

[3] **NELSON, D. and EVANS, S.,** A New Approach to Op Amp Design, Comlinear Corporation Application Note 300-1, (1985).

[4] Analog Devices, AD844 Datasheet, (1990).

[5] **SMITH, K.C. and SEDRA, A.S.,** The Current Conveyor, A New Circuit Building Block, IEEE Proceedings, 56, pp.1368-1369, (1968).

[6] **SEDRA, A.S. and SMITH, K.C.,** A Second Generation Current Conveyor and Its Applications, IEEE Transactions on Circuit Theory, CT-17, pp.132-134, (1970).

[7] **LIU, S.-I. , TSAO, H.-W, WU, J. and LIN, T.-K,** MOSFET Capacitor Filters Using Unity Gain CMOS Current Conveyors, Electronics Letters, 26, pp.1430-1431, (1990).

[8] **ALAMI, M. and FABRE, A.,** Insensitive Current-Mode Bandpass Filter Implemented From Two Current Conveyors, Electronics Letters, 27, pp.897-898, (1991).

[9] **HIGASHIMURA; M. and FUKUI, Y.,** Type 1 Mutator Using Current Conveyor and Its Application to Immitance Simulation, International Journal of Electronics, pp.377-383, (1988).

[10] **MATSUURA, K., HORITA, M. and YAMAMOTO, G.,** Analysis of a Gyrator and a RC Oscillator Using Current Conveyor, Trans. IECE Japan, C, 12, pp.891-892, (1981).

[11] **HIGASHIMURA; M. and FUKUI, Y.,** Realization of Impedance Function Using Current Conveyors, International Journal of Electronics, pp.223-231, (1988).

[12] **FUKASAWA, H. and FUJII, N.,** Realization of Current Conveyor and Its Application to Filter Simulation, Research Report of IECE Japan on Circuits and Systems, 81-6, pp.39-45, (1981).

[13] **FABRE, A. and MIMECHE, N.,** Class A/AB Second Generation Current Conveyor with Controlled Current Gain, Electronics Letters, 30, pp.1267-1269, (1994).

[14] **PALMISANO, G., and PALUMBO, G.,** A Simple CMOS CCII+, International Journal of Circuit Theory and Applications, 23, pp.599-603, (1995).

[15] **CHA, H.-W. and WATANABE, K.,** Wideband CMOS Current Conveyor, Electronics Letters, 32, pp.1245-1246, (1996).

[16] **OLIAEI, O. and LOUMEAU, P.,** Current-Mode Class AB Design Using Floating Voltage-Source, Electronics Letters, 32, pp.1526-1528, (1996).

[17] **TEK, H. and ANDAY, F.,** Voltage Transfer Function Synthesis Using Current Conveyors, Electronics Letters, 25, pp.1552-1553, (1989).

[18] **HIGASHIMURA, M., FUKUI, Y. and MASARU, I.,** Synthesis of Current-Mode Transfer Functions Using a Single Current Conveyor, Microelectronics Journal, 22, pp.35-46, (1991).

[19] **KUMAR, U.,** Current Conveyors: A Review of the State of the Art, IEEE Circuits and Systems Magazine, 3, pp.10-14, (1981).

[20] **KUMAR, U. and SHUKLA, S.K.,** Recent Developments in Current Conveyors and Their Applications, Microelectronics Journal, 16, pp.47-52, (1985).

[21] **WILSON, B.,** Recent Developments in Current Conveyors and Current-Mode Circuits, IEE Proceedings, 137, pp.63-77, (1990).

[22] **SEDRA, A.S., ROBERTS, G.W. and GOHH, F.,** The Current Conveyor: History, Progress and New Results, IEE Proceedings, 137, pp.78-87, (1990).

[23] **TOUMAZOU, C., LIDGEY, F.J. and MAKRIS, C.A.,** Extending Voltage-Mode Op Amps to Current-Mode Performance, IEE Proceedings, 137, pp.116-130, (1990).

[24] **BOYLE, G.R., COHN, P.M., PEDERSON, D.O. and SOLOMON, J.E.,** Macromodeling of Integrated Circuit Operational Amplifiers, IEEE Journal of Solid-State Circuits, 9, pp.353-363, (1974).

[25] **PEIC, R.V.,** Simple and Accurate Non-Linear Macromodel for Operational Amplifiers, IEEE Journal of Solid-State Circuits, 26, pp.896-899, (1991).

[26] **KUNTMAN, H.**, Simple and Accurate Non-Linear OTA Macromodel for Simulation of CMOS OTA-C Active Filters, International Journal of Electronics, 77, pp.993-1006, (1994).

[27] **WILSON, B.**, Performance Analysis of Current Conveyors, Electronics Letters, 25, pp.1596-1597, (1989).

[28] **YENEN, B.**, CMOS Akım Taşıyıcıların Makromodellerinin Oluşturulması ve Akım Taşıyıcılı Süzgeçlerin Analizi, M.Sc. Thesis, Istanbul Technical University, Institute of Science and Technology, (1995).

[29] **YENEN, B., TARIM, N. and KUNTMAN, H.**, Aktif Süzgeç Simülasyonuna Yönelik Bir Akım Taşıyıcı Makromodeli, Proceedings of the 6th National Congress on Electrical Engineering, Uludağ University, Bursa-Turkey, 3, pp.1023-1026, (1995).

[30] **FABRE, A. and ALAMI, M.**, A Precise Macromodel for Second Generation Current Conveyors, IEEE Transactions on Circuits and Systems, 44, pp. 639-642, (1997).

[31] **TARIM, N. and KUNTMAN H.**, Simple and Accurate Non-Linear Current Conveyor Macromodel Suitable for Simulation of Active Filters Using CCII+s, International Journal of Circuit Theory and Applications, 26, pp.27-38, (1998).

[32] **TARIM, N., YENEN, B. and KUNTMAN, H.**, Simple and Accurate Non-Linear Current Conveyor Macromodel, Proceedings of 8th Mediterranean Electrotechnical Conference, Melecon'96 - Italy, 1, pp.447-450, (1996).

[33] **ACAR, C. and GHAUSI, M.S.**, Fully Integrated Active RC Filters Using MOS and Non-Balanced Structure, International Journal of Circuit Theory and Applications, 15, pp.105-121, (1987).

[34] **BUDAK, A.**, Passive and Active Network Analysis and Synthesis, Houghton Mifflin Company, Boston, (1974).

[35] **TARIM, N. and KUNTMAN H.**, The Effects of CCII Non-Idealities on Current-Mode Active Filters, Proceedings - International Symposium on Signals, Circuits and Systems, SCS'97 - Romania, 2, pp.397-400, (1997).

[36] **DUNCAN, R.A., CHAN, K.M. and SEDRA, A.S.**, Designs for a Wideband Current Amplifier and a Current Conveyor, IEEE Transactions on Circuits and Systems, 41, pp. 272-280, (1994).

[37] **NORMAND, G.**, Translinear Current Conveyors, International Journal of Electronics, 59, pp.771-777, (1985).

[38] **GRAEME, J.G.**, Applications of Operational Amplifiers, pp.93-94, McGraw-Hill, (1973).

[39] **HART, B.L. and BARKER, R.W.J.,** A Precision Bilateral Voltage-Current Converter, IEEE J., SC-10, pp.501-503, (1975).

APPENDIX A

A.1 MOS device model parameters used for SPICE simulations in Chapter 2

.MODEL N NMOS LEVEL=2 LD=0.414747U TOX=505.0E-10 NSUB=1.35634E16 VTO=0.864893 KP=44.9E-6 GAMMA=0.981 PHI=0.6 UO=656 UEXP=0.211012 UCRIT=107603 DELTA=3.53172 VMAX=100000 XJ=0.4U LAMBDA=0.0107351 NFS=1E11 NEFF=1.001 NSS=1E12 TPG=1 RSH=9.925 CGDO=2.83588E-10 CGSO=2.83588E-10 CGBO=7.968E-10 CJ=0.0003924 MJ=0.456300 CJSW=5.284E-10 MJSW=0.3199 PB=0.7 XQC=1

.MODEL P PMOS LEVEL=2 LD=0.580687U TOX=432.0E-10 NSUB=1E16 VTO=-0.944048 KP=18.5E-6 GAMMA=0.435 PHI=0.6 UO=271 UEXP=0.242315 UCRIT=20581.4 DELTA=4.32096E-5 VMAX=33274.4 XJ=0.4U LAMBDA=0.0620118 NFS=1E11 NEFF=1.001 NSS=1E12 TPG=-1 RSH=10.25 CGDO=4.83117E-10 CGSO=4.83117E-10 CGBO=1.293E-9 CJ=0.0001307 MJ=0.4247 CJSW=4.613E-10 MJSW=0.2185 PB=0.75 XQC=1

A.2 XR B101 and XR B102 device model parameters used for SPICE simulations

.MODEL XRB101 NPN IS=5.24E-16 BF=384.5 BR=2.345 NF=1.06 VAF=79.5
IKF=.025 ISE=8.3E-14 NE=1.935 NR=1.005 VAR=9.64 IKR=1.845E-4
ISC=7.5E-15 NC=1.22 RE=2.85 RC=30.15 RB=7.5 CJC=.6E-12 VJC=.85
MJC=.475 CJE=.94E-12 VJE=.75 MJE=.32 CJS=1.883E-12 VJS=.7 MJS=.333
XTB=.213 XTI=4.71 TF=.64E-9 TR=3E-9

.MODEL XRB102 PNP IS=6.2E-16 BF=98.1 BR=1.005 NF=1.155 VAF=50.3
IKF=9.15E-4 ISE=2.55E-15 NE=1.46 NR=1.03 VAR=12.2 IKR=3.86E-5
ISC=1.35E-14 NC=1.22 RE=16.4 RC=225 RB=5 CJC=.9471E-12 VJC=.5
MJC=.471 CJE=.21E-12 VJE=.5 MJE=.439 CJS=2.51E-12 VJS=.5 MJS=.315
XTB=.0737 XTI=5.39 TF=6.4E-9 TR=30E-9

A.3 AMS 0.8 μm CMOS process parameters

.MODEL N NMOS LEVEL=2 UO=462 VTO=.844 NFS=.835E12 TOX=15.5E-9 NSUB=63.8E15 UCRIT=37.7E4 UEXP=0.324 VMAX=61.9E3 RSH=25 XJ=0.08E-6 LD=0.000E-6 DELTA=0.237 PB=.860 JS=0.01E-3 NEFF=10 CJ=0.290E-3 MJ=460E-3 CJSW=0.230E-9 MJSW=.33 CGSO=.035E-9 CGDO=.35E-9 CGBO=0.15E-9 UTRA=0 WD=0.580E-6 KF=0.276E-25 AF=1.53

.MODEL P PMOS LEVEL=2 UO=160 VTO=-.734 NFS=.483E12 TOX=15.5E-9 NSUB=32.8E16 UCRIT=30.8E4 UEXP=0.336 VMAX=61.3E3 RSH=47 XJ=0.087E-6 LD=-0.076E-6 DELTA=0.949 PB=.8 JS=0.04E-3 NEFF=2.57 CJ=.49E-3 MJ=0.47 CJSW=0.21E-9 MJSW=.29 CGSO=0.350E-9 CGDO=0.350E-9 CGBO=0.15E-9 UTRA=0 WD=0.331E-6 KF=0.466E-26 AF=1.61

A.4 Alcatel Mietec 2 μm HBiMOS process parameters

.MODEL N NMOS LEVEL=2 TOX=750E-10 XJ=.3U VTO=1.1 NSUB=7.5E14 DELTA=2.2 NFS=1.5E11 UO=730 UCRIT=6E4 UEXP=.166 LD=.45U WD=.15U RSH=275 JS=1E-3 DELL=0U CGSO=2.8E-10 CGDO=2.8E-10 PB=.8 FC=.5 CJ=1E-4 MJ=.5 CJSW=4E-10 MJSW=.33 AF=1 KF=5E-28

.MODEL P PMOS LEVEL=2 TOX=750E-10 XJ=.1U VTO=-1.1 NSUB=6.6E15 DELTA=1.5 NFS=.86E11 UO=240 UCRIT=5E4 UEXP=.25 LD=.48U WD=.25U RSH=565 JS=1E-3 DELL=0U CGSO=2.9E-10 CGDO=2.9E-10 PB=.8 FC=.5 CJ=2.5E-4 MJ=.5 CJSW=4.5E-10 MJSW=.33 AF=1 KF=2E-30

A.5 AD844 device macromodel

```
* Node assignments
*          non-inverting input
*           | inverting input
*           | | positive supply
*           | | | negative supply
*           | | | | output
*           | | | | | compensation node
*           | | | | | |
.SUBCKT AD844/AD 1 2 99 50 28 12
```

```
* INPUT STAGE
R1   99 8     1E3
R2   10 50    1E3
V1   99 9     11
D1   9  8     DX
V2   11 50    11
D2   10 11    DX
I1   99 5     258E-6
I2   4  50    258E-6
Q1   50  3  5  QP
Q2   99  3  4  QN
Q3   8   6 30  QN
Q4   10  7 30  QP
R3   5   6    300E3
R4   4   7    300E3
*C1   99 6    8.8E-15
*C2   50 7    8.8E-15

* INPUT ERROR SOURCES
GB1  99  1    POLY(1)  1  22  150E-9  90E-9
GB2  99 30    POLY(1)  1  22  200E-9  90E-9
VOS  3   1    50E-6
LS1  30  2    1E-8
CS1  99  2    1E-12
CS2  50  2    1E-12
EREF 97  0    22  0  1

* GAIN STAGE & DOMINANT POLE
R5   12 97    3E6
C3   12 97    5.5E-12
G1   97 12    99  8  1E-3
G2   12 97    10 50  1E-3
V3   99 13    4.3
V4   14 50    4.3
D3   12 13    DX
D4   14 12    DX

* POLE AT 70 MHZ
R8  17 97    1E6
C4  17 97    3.18E-15
G4  97 17    12 22  1E-6

* POLE AT 300 MHZ
R12 21 97    1E6
C8  21 97    0.318E-15
G8  97 21    17 22  1E-6
```

```
* OUTPUT STAGE
ISY 99 50    5.1E-3
R13 22 99    16.7E3
R14 22 50    16.7E3
R15 27 99    30
R16 27 50    30
L2  27 28    6E-8
G9  25 50    21 27  33.33E-3
G10 26 50    27 21  33.33E-3
G11 27 99    99 21  33.33E-3
G12 50 27    21 50  33.33E-3
V5  23 27    0.5
V6  27 24    0.5
D5  21 23    DX
D6  24 21    DX
D7  99 25    DX
D8  99 26    DX
D9  50 25    DY
D10 50 26    DY

* MODELS USED
.MODEL QN   NPN(BF=1E9 IS=1E-15)
.MODEL QP   PNP(BF=1E9 IS=1E-15)
.MODEL DX   D(IS=1E-15)
.MODEL DY   D(IS=1E-15 BV=50)
.ENDS AD844/AD
```

A.6 Transistor dimensions of the current conveyor given in Fig. 2.2a

```
M1  N  W=17U  L=10U
M2  N  W=17U  L=10U
M3  N  W=17U  L=10U
M4  N  W=17U  L=10U
M5  P  W=24U  L=5U
M6  P  W=24U  L=5U
M7  N  W=40U  L=5U
M8  N  W=40U  L=5U
M9  P  W=24U  L=5U
M10 P  W=24U  L=5U
M11 P  W=24U  L=5U
M12 P  W=24U  L=5U
M13 N  W=40U  L=5U
M14 N  W=40U  L=5U
M15 N  W=40U  L=5U
M16 N  W=40U  L=5U
```

A.7 Transistor dimensions of the current conveyor given in Fig. 2.2b

M1 N W=17U L=10U
M2 N W=17U L=10U
M3 N W=17U L=10U
M4 N W=17U L=10U
M5 P W=24U L=5U
M6 P W=24U L=5U
M7 N W=40U L=5U
M8 N W=40U L=5U
M9 P W=24U L=5U
M10 P W=24U L=5U
M11 P W=24U L=5U
M12 P W=24U L=5U
M13 N W=23U L=5U
M14 N W=23U L=5U
M15 N W=23U L=5U
M16 N W=23U L=5U
M17 P W=24U L=5U
M18 P W=24U L=5U
M19 N W=23U L=5U
M20 N W=23U L=5U
M21 P W=24U L=5U
M22 P W=24U L=5U
M23 N W=23U L=5U
M24 N W=23U L=5U

A.8 Transistor dimensions of CC6

M1 N W=200U L=2U AD=1300P AS=1300P PD=413U PS=413U
M2 N W=200U L=2U AD=1300P AS=1300P PD=413U PS=413U
M3 P W=200U L=4U AD=1300P AS=1300P PD=413U PS=413U
M4 P W=200U L=4U AD=1300P AS=1300P PD=413U PS=413U
M5 N W=400U L=4U AD=2600P AS=2600P PD=813U PS=813U
M6 P W=200U L=4U AD=1300P AS=1300P PD=413U PS=413U
M7 N W=200U L=4U AD=1300P AS=1300P PD=413U PS=413U
M8 N W=200U L=4U AD=1300P AS=1300P PD=413U PS=413U
M9 P W=200U L=4U AD=1300P AS=1300P PD=413U PS=413U

A.9 Transistor dimensions of CC7

M1	N	W=270U	L=2U	AD=1755P	AS=1755P	PD=553U	PS=553U
M2	P	W=840U	L=2U	AD=5460P	AS=5460P	PD=1693U	PS=1693U
M3	N	W=210U	L=4U	AD=1365P	AS=1365P	PD=433U	PS=433U
M4	N	W=210U	L=4U	AD=1365P	AS=1365P	PD=433U	PS=433U
M5	N	W=210U	L=4U	AD=1365P	AS=1365P	PD=433U	PS=433U
M6	N	W=210U	L=4U	AD=1365P	AS=1365P	PD=433U	PS=433U
M7	N	W=210U	L=4U	AD=1365P	AS=1365P	PD=433U	PS=433U
M8	N	W=210U	L=4U	AD=1365P	AS=1365P	PD=433U	PS=433U

A.10 Transistor dimensions of CC8

M1	N	W=60U	L=3U	AD=390P	AS=390P	PD=133U	PS=133U
M2	P	W=240U	L=3U	AD=1560P	AS=1560P	PD=493U	PS=493U
M3	N	W=60U	L=3U	AD=390P	AS=390P	PD=133U	PS=133U
M4	P	W=240U	L=3U	AD=1560P	AS=1560P	PD=493U	PS=493U
M5	P	W=126U	L=3U	AD=819P	AS=819P	PD=265U	PS=265U
M6	N	W=60U	L=6U	AD=390P	AS=390P	PD=133U	PS=133U
M7	P	W=126U	L=3U	AD=819P	AS=819P	PD 265U	PS=265U
M8	N	W=60U	L=6U	AD=390P	AS=390P	PD=133U	PS=133U
M9	P	W=25U	L=3U	AD=162.5P	AS=162.5P	PD=63U	PS=63U

A.11 Transistor dimensions of CC2N

M1	N	W=20U	L=2U	AD=130P	AS=130P	PD=53U	PS=53U
M2	N	W=20U	L=2U	AD=130P	AS=130P	PD=53U	PS=53U
M3	P	W=20U	L=4U	AD=130P	AS=130P	PD=53U	PS=53U
M4	P	W=20U	L=4U	AD=130P	AS=130P	PD=53U	PS=53U
M44	P	W=400U	L=4U	AD=2600P	AS=2600P	PD=813U	PS=813U
M5	N	W=100U	L=4U	AD=650P	AS=650P	PD=213U	PS=213U
M6	P	W=20U	L=4U	AD=130P	AS=130P	PD=53U	PS=53U
M66	P	W=400U	L=4U	AD=2600P	AS=2600P	PD=813U	PS=813U
M7	N	W=20U	L=4U	AD=130P	AS=130P	PD=53U	PS=53U
M8	N	W=20U	L=4U	AD=130P	AS=130P	PD=53U	PS=53U
M9	P	W=20U	L=4U	AD=130P	AS=130P	PD=53U	PS=53U
M88	N	W=20U	L=4U	AD=130P	AS=130P	PD=53U	PS=53U
M55	N	W=40U	L=4U	AD=260P	AS=260P	PD=93U	PS=93U
M77	N	W=20U	L=4U	AD=130P	AS=130P	PD=53U	PS=53U

A.12 Transistor dimensions of CC3N

```
M1  N  W=200u  L=2u  AD=1300P AS=1300P PD=413U PS=413U
M2  N  W=200u  L=2u  AD=1300P AS=1300P PD=413U PS=413U
M3  P  W=200u  L=4u  AD=1300P AS=1300P PD=413U PS=413U
M33 P  W=200u  L=4u  AD=1300P AS=1300P PD=413U PS=413U
M4  P  W=200u  L=4u  AD=1300P AS=1300P PD=413U PS=413U
M44 P  W=200u  L=4u  AD=1300P AS=1300P PD=413U PS=413U
M6  P  W=200u  L=4u  AD=1300P AS=1300P PD=413U PS=413U
M66 P  W=200u  L=4u  AD=1300P AS=1300P PD=413U PS=413U
M5  N  W=400u  L=4u  AD=2600P AS=2600P PD=813U PS=813U
M55 N  W=400u  L=4u  AD=2600P AS=2600P PD=813U PS=813U
M7  N  W=200u  L=4u  AD=1300P AS=1300P PD=413U PS=413U
M77 N  W=200u  L=4u  AD=1300P AS=1300P PD=413U PS=413U
M9  P  W=200u  L=4u  AD=1300P AS=1300P PD=413U PS=413U
M99 P  W=200u  L=4u  AD=1300P AS=1300P PD=413U PS=413U
M8  N  W=200u  L=4u  AD=1300P AS=1300P PD=413U PS=413U
M88 N  W=200u  L=4u  AD=1300P AS=1300P PD=413U PS=413U
```

A.13 Transistor dimensions of CC4N

```
M1   P W=80U L=2U AD=520P AS=520P PD=173U PS=173U
M2   P W=80U L=2U AD=520P AS=520P PD=173U PS=173U
M3   P W=80U L=2U AD=520P AS=520P PD=173U PS=173U
M4   P W=80U L=2U AD=520P AS=520P PD=173U PS=173U
M5   N W=20U L=2U AD=130P AS=130P PD=53U  PS=53U
M6   N W=20U L=2U AD=130P AS=130P PD=53U  PS=53U
M7   N W=20U L=2U AD=130P AS=130P PD=53U  PS=53U
M8   N W=20U L=2U AD=130P AS=130P PD=53U  PS=53U
```

A.14 Transistor dimensions of CC5N

```
M1   P W=80U L=2U  AD=520P AS=520P PD=173U PS=173U
M2   P W=80U L=2U  AD=520P AS=520P PD=173U PS=173U
M3   N W=20U L=2U  AD=130P AS=130P PD=53U  PS=53U
M4   N W=20U L=2U  AD=130P AS=130P PD=53U  PS=53U
```

A.15 Transistor dimensions of CC6N

M1 P W=50U L=2U AD=325P AS=325P PD=113U PS=113U
M2 P W=50U L=2U AD=325P AS=325P PD=113U PS=113U
M3 P W=50U L=2U AD=325P AS=325P PD=113U PS=113U
M4 P W=50U L=2U AD=325P AS=325P PD=113U PS=113U
M5 N W=20U L=2U AD=130P AS=130P PD=53U PS=53U
M6 N W=20U L=2U AD=130P AS=130P PD=53U PS=53U
M7 N W=20U L=2U AD=130P AS=130P PD=53U PS=53U
M8 N W=20U L=2U AD=130P AS=130P PD=53U PS=53U
M9 N W=20U L=2U AD=130P AS=130P PD=53U PS=53U
M10 P W=50U L=2U AD=325P AS=325P PD=113U PS=113U

A.16 Transistor dimensions of OA1

M1 N W=20U L=2U AD=130P AS=130P PD=53U PS=53U
M2 N W=20U L=2U AD=130P AS=130P PD=53U PS=53U
M3 P W=50U L=2U AD=325P AS=325P PD=113U PS=113U
M4 P W=50U L=2U AD=325P AS=325P PD=113U PS=113U
M5 N W=40U L=2U AD=260P AS=260P PD=93U PS=93U
M6 P W=100U L=2U AD=650P AS=650P PD=213U PS=213U
M7 P W=100U L=2U AD=650P AS=650P PD=213U PS=213U
M8 N W=40U L=2U AD=260P AS=260P PD=93U PS=93U
M9 N W=40U L=2U AD=260P AS=260P PD=93U PS=93U
M10 P W=100U L=2U AD=650P AS=650P PD=213U PS=213U
M11 N W=40U L=2U AD=260P AS=260P PD=93U PS=93U
M12 N W=40U L=2U AD=260P AS=260P PD=93U PS=93U
M13 N W=40U L=2U AD=260P AS=260P PD=93U PS=93U

A.17 Transistor dimensions of OA2

M1 N W=20U L=2U AD=130P AS=130P PD=53U PS=53U
M2 N W=20U L=2U AD=130P AS=130P PD=53U PS=53U
M3 P W=50U L=2U AD=325P AS=325P PD=113U PS=113U
M4 P W=50U L=2U AD=325P AS=325P PD=113U PS=113U
M5 N W=40U L=2U AD=260P AS=260P PD=93U PS=93U
M6 P W=100U L=2U AD=650P AS=650P PD=213U PS=213U
M7 P W=100U L=2U AD=650P AS=650P PD=213U PS=213U
M8 N W=40U L=2U AD=260P AS=260P PD=93U PS=93U
M9 N W=40U L=2U AD=260P AS=260P PD=93U PS=93U
M10 P W=100U L=2U AD=650P AS=650P PD=213U PS=213U
M11 N W=40U L=2U AD=260P AS=260P PD=93U PS=93U
M12 N W=40U L=2U AD=260P AS=260P PD=93U PS=93U

BIOGRAPHY

The author was born in İzmit, Turkey, in 1968. She graduated from Erenköy Girls High School. In 1985, she entered the Electronics and Communications Engineering Department of İstanbul Technical University, and received her B.Sc. degree in 1989. The same year, she started her M.Sc. studies majoring in Electronics and Communications Engineering at the Institute of Science and Technology of İstanbul Technical University. In 1990, she joined the Electronics and Communications Department as a research assistant, of which she is still working. In 1992, she received her M.Sc. degree and started her Ph.D. studies at the same place. Her research interests include analog circuit design, modeling of electron devices and microprocessors.